

Biocatalytic synthesis of taste-modifying flavonoids

Dissertation

zur Erlangung des

Doktorgrades der Naturwissenschaften (Dr. rer. nat.)

der

Naturwissenschaftlichen Fakultät II – Chemie, Physik und Mathematik

der Martin-Luther-Universität

Halle-Wittenberg

vorgelegt von

Frau Diplom-Lebensmittelchemikerin

Anne-Katrin Bauer

geboren am 17.02.1984 in Halle (Saale)

Die vorliegende Arbeit wurde im Zeitraum Oktober 2010 bis März 2014 am Leibniz-Institut für Pflanzenbiochemie in der Abteilung für Natur-und Wirkstoffchemie (Abteilungsleiter Professor Dr. Ludger A. Wessjohann) angefertigt.



Tag der Verteidigung: 04.11.2016

1. Gutachter: Professor Dr. Ludger A. Wessjohann

2. Gutachter: Professor Dr. Wolf-Dieter Fessner

*“Man muss viel gelernt haben, um nach dem, was man nicht weiß,
fragen zu können.”*

Jean-Jacques Rousseau (1712 - 1778)

Acknowledgement

At this point I would like to emphasize my sincerely thanks to a few people: First of all, I would like to thank Prof. Dr. Ludger A. Wessjohann for the opportunity to work in an application-oriented project, for supervision and for the opportunity to attend international conferences and to join different external working groups.

Thanks to Prof. Dr. Rita Bernhardt from the ZHMB in Saarbrücken, Prof. Dr. Bernhard Hauer and Prof. Dr. Jürgen Pleiß from the ITB in Stuttgart for the opportunity to work in their laboratories and for providing their library of P450 enzymes. Special thanks to the BMBF and to the Symrise AG for funding and cooperation.

Many thanks to Prof. David B. Collinge from Copenhagen for providing the CHS2, to M.Sc. Bartłomiej Tomaszewski from Dortmund for the 2-HBP and Dr. Martin Dippe for the 4HPA3H variants;

In particular, I would like to thank Dr. Thomas Vogt for cooperation, discussion and fruitful collaboration; Dr. Danilo Meyer for critically questioning, vivid discussions and for friendship;

Dr. Andrea Porzel and Dr. Jürgen Schmidt for analytical support, Christine Kuhnt, Martina Lerbs and Anja Ehrlich for excellent technical assistance;

PD Dr. Wolfgang Brandt and Eva Schulze for support in computer-modeling and docking, Artem Kamaev and Julia Christke for laboratory assistance.

Special thanks to Sebastian Stark, Dr. Jeanette Keim, Steve Ludwig, Benjamin Weigel, Robert Berger, Rainer and Julia Kufka for a pleasant working atmosphere and a great time.

My warmest thanks to my family, without their mental support and several hours of babysitting this work would not have been finished.

Abstract

Consumption of food and eating habits of humans are guided by the sensory perception. Bitter taste suppresses the regular consumption of beneficial phytonutrients. Hence, in products of the food and pharmaceutical industry these bitter effects are often masked with unhealthy additives like sugar, fat or alcohol. Eriodictyol (ED) and homoeriodictyol (HED) are natural, tasteless, bitter-masking compounds and feature additionally healthy effects like antioxidant activities that are common for flavonoids. However, their availability is strongly limited. In this study, the microbial production of ED and HED was investigated basing on two different strategies.

The first approach focusses on the precursor-directed chalcone biosynthesis starting from the corresponding hydroxycinnamic acid (HCA). The target flavonoids ED and HED were formed in two consecutive enzymatic steps: in the first step the formation of an active coenzyme A thioester from caffeic acid or ferulic acid was catalyzed by the ligase *At4CL2*. The respective substrates already contain the desired modifications at ring B making the subsequent hydroxylation- and methylation-steps unnecessary. Secondly, the corresponding chalcone is formed by the specific chalcone synthase *HvCHS2* and finally a non-enzymatic step is used for the ring closure to convert the chalcone into a flavonoid. Both enzymes were heterologously expressed in *Escherichia coli*, purified and investigated. The single steps have been established for *in vitro* conversion of inexpensive HCA into the desired flavanones.

The second strategy is based on the specific modification of the cheap and readily available flavanone naringenin (Nar). After screening of over 30 oxygenating biocatalysts, the bacterial monooxygenase variant BM3-GVQ was discovered to catalyze the 3'-hydroxylation step without further oxidation of the product. In the second step of this strategy, the plant *O*-methyltransferase (OMT) PFOMT was applied acting selectively with high catalytic potential on ring B of ED forming 3'-*O*-methylated ED (HED). This strategy was established for successful *in vitro* biosynthesis of ED and HED. Moreover, the whole enzyme-cascade was developed as a proof of concept for *in vivo* biotransformation in *E. coli* yielding already 36 % of HED ($\approx 20 \text{ mg l}^{-1}$) after 25 h of incubation for the first generation without time-consuming enzyme purification steps or the addition of cost-intensive cofactors. This fundamental system offers the

basis for a time-saving biotechnological process that is already registered for patenting (EP14187583.1 - 1501).

Zusammenfassung

Der Lebensmittelkonsum und die Eßgewohnheiten des Menschen richten sich nach seiner geschmacklichen Wahrnehmung. Der bittere Geschmack von wirksamen Phytonährstoffen verhindert ihren regelmäßigen Verzehr. In industriellen Produkten werden bittere Stoffe häufig durch den Einsatz von Zucker, Fett und Alkohol maskiert. Eriodictyol (ED) und Homoeriodictyol (HED) sind natürlich vorkommende, selbst geschmacklose, bitter-maskierende Stoffe und liefern zusätzlich gesundheitsfördernde Effekte aufgrund ihrer Zugehörigkeit zu den Flavonoiden. Allerdings sind sie in ihrer Verfügbarkeit bisher begrenzt. In dieser Arbeit wurden zwei Wege zur enzymatisch katalysierten Herstellung von ED und HED entwickelt.

Die erste Strategie basiert auf der natürlichen Biosynthese der Flavonoide unter der Verwendung ausgewählter Hydroxyzimtsäuren (HCAs), die als Vorstufen bereits die entsprechenden Modifikationen des Grundgerüsts enthalten. Die entsprechenden Chalkone von ED und HED werden dabei über zwei enzymatisch katalysierte Reaktionsschritte aufgebaut: die Ligase *At4CL2* katalysiert die essentielle Aktivierung der HCAs Kaffeesäure und Ferulasäure zu den entsprechenden Coenzym A-thioestern. Im zweiten Schritt katalysiert die Chalkonsynthase *HvCHS2* den Aufbau des Chalkongerüsts aus den entsprechenden Vorstufen und abschließend wird das Chalkon durch eine Basen-katalysierte Zyklisierung zum Flavanon geschlossen. Beide Enzyme wurden heterolog in *Escherichia coli* exprimiert, gereinigt und untersucht. Die einzelnen Schritte wurden als *in vitro* Umsetzung zur Herstellung von ED und HED aus preiswerten HCAs etabliert.

Die zweite Strategie basiert auf der gezielten Modifikation des günstigen und weitverbreiteten Flavanons Naringenin (Nar). Nach dem Screening von über 30 Oxidoreduktasen wurde die bakterielle Monooxygenase BM3-GVQ als potentielle 3'-Hydroxylase zur Erzeugung von ED identifiziert, ohne dabei das Produkt weiter zu oxidieren. Im zweiten Schritt dieser Strategie katalysiert eine pflanzliche O-Methyltransferase (PFOMT) ED zum 3'-Methylether (HED). Die Einzelschritte dieser Strategie wurden in *in vitro* Experimenten optimiert.

Darüber hinaus wurde die gesamte Enzymkaskade als *proof of concept* zur *in vivo* Biotransformation in *E. coli* entwickelt. In der ersten Generation wurden dabei bereits 36 % HED ($\pm \sim 20 \text{ mg l}^{-1}$) nach 25 h Inkubationszeit direkt aus Naringenin ohne Reinigungsschritte von Enzymen oder der Zugabe von preisintensiven Cofaktoren ge-

VI

wonnen. Dieses System liefert die Basis für einen zeitsparenden biotechnologischen Prozess, welcher bereits zum Patent (EP14187583.1 - 1501) angemeldet wurde.

Table of contents

Acknowledgement.....	III
Abstract.....	IV
Zusammenfassung.....	VI
Abbreviations	XII
List of Figures.....	XVI
List of Tables.....	XX
1 Theoretical principles	1
1.1 Gustatory modifiers.....	1
1.2 Eriodictyol and Homoeriodictyol – bitter masking flavonoids from <i>Eriodictyon californicum</i>	6
1.3 Chemical engineering and green biotechnology	8
2 Materials and methods	14
2.1 Materials	14
2.1.1 Consumables and Chemicals.....	14
2.1.2 Substrates and reference substances	16
2.1.3 Enzymes	17
2.1.4 Media	18
2.1.5 Buffers and stock solutions	19
2.1.6 Bacterial strains	20
2.1.7 Plasmids	20
2.1.8 Synthetic oligonucleotides.....	22
2.2 Methods in molecular biology	23
2.2.1 Determination of DNA concentration	23
2.2.2 Polymerase chain reaction (PCR)	23
2.2.3 Plasmid DNA isolation.....	24
2.2.4 Restriction of plasmid DNA	24
2.2.5 Isolation, purification and verification of DNA fragments.....	24

2.2.6	DNA ligation reaction	25
2.2.7	Gateway® cloning system.....	25
2.2.8	Agarose gel electrophoresis.....	25
2.3	Microbiological methods.....	26
2.3.1	Cultivation of <i>E. coli</i> cells.....	26
2.3.2	Preparation of chemically competent cells.....	26
2.3.3	Transformation of plasmid DNA into chemically competent <i>Escherichia coli</i> cells	26
2.4	Protein methods.....	27
2.4.1	Gene expression.....	27
2.4.2	Cell lysis by sonication	27
2.4.3	Enzyme purification.....	27
2.5	Enzymatic reactions and preparative approaches	28
2.5.1	Enzymatic activity assays.....	28
2.5.2	Preparative substrate conversion	30
2.5.3	Living whole-cell biotransformation	30
2.6	Analytics	31
2.6.1	H ₂ O ₂ determination (HRP <i>o</i> -dianisidine assay).....	31
2.6.2	Protein detection	31
2.6.3	Analytics of substances.....	32
2.6.4	Computer modeling and docking.....	35
3	Chapter I: Precursor-directed biosynthesis of flavonoids	36
3.1	Introduction	36
3.2	Objectives	39
3.3	Results.....	40
3.3.1	Ligase reaction – At4CL2	40
3.3.2	Chalcone synthase reaction – HvCHS2	45
3.3.3	Enzyme cascade.....	49

3.4	Discussion.....	50
3.5	Outlook	52
4	Chapter II: Hydroxylation of flavonoids	53
4.1	Introduction	53
4.2	Objectives	57
4.3	Results.....	58
4.3.1	Screening for a specific flavonoid 3'-oxygenase.....	58
4.3.2	Investigation of BM3-GVQ for optimized ED formation.....	61
4.3.3	Design and screening of new BM3 variants.....	78
4.3.4	<i>In vivo</i> biotransformation of Naringenin	81
4.4	Discussion.....	83
4.5	Outlook	85
5	Chapter III: Methylation of ED – the final step of HED biosynthesis.....	87
5.1	Introduction	87
5.2	Objectives	90
5.3	Results.....	91
5.3.1	Regiospecificity and substrate spectrum of PFOMT	91
5.3.2	PFOMT – <i>in vivo</i> biotransformation	97
5.3.3	Enzyme cascade: oxidation and methylation.....	98
5.4	Discussion.....	100
5.5	Outlook	101
6	Final discussion.....	102
	Appendix A.....	107
	Appendix B.....	120
	Appendix C	130
	References.....	133
	Presentations and Proceedings.....	XXII
	Curriculum vitae	XXIV
	X	

Eidesstattliche Erklärung.....XXVI

Abbreviations

AdR	adrenodoxin reductase
Adx	adrenodoxin
ATP	adenosine 5'-triphosphate
AtTSM1	<i>Arabidopsis thaliana</i> tapetum-specific methyltransferase 1
At4CL2	<i>Arabidopsis thaliana</i> 4-coumarate:coenzyme A ligase 2
AUC	area under the curve
BM3	CYP102A1 from <i>Bacillus megaterium</i>
BM3-F87V	BM3 mutant: F87V
BM3-GAQ	BM3 mutant: A74G/F87A/L188Q
BM3-GV	BM3 mutant: A74G/F87V
BM3-GVQ	BM3 mutant: A74G/F87V/L188Q
BM3-GVQS	BM3 mutant: A74G/F87V/L188Q/A330S
BM3-GNVQ	BM3 mutant: A74G/L75N/F87V/ L188Q
BM3-GSVQ	BM3 mutant: A74G/L75S/F87V/ L188Q
BM3-NVQ	BM3 mutant: L75N/F87V/ L188Q
BM3-SVQ	BM3 mutant: L75S/F87V/ L188Q
BM3-VQ	BM3 mutant: F87V/L188Q
CCoAOMT	caffeoyl coenzyme A- <i>O</i> -methyltransferases
CHI	chalcone isomerase
CHS2	chalcone synthase 2
4CL	4-coumarate:coenzyme A ligase
CoA	coenzyme A
COMT	catechol <i>O</i> -methyltransferases
CRP	NADPH-cytochrome P450 reductase
<i>C. testosteroni</i>	<i>Comamonas testosteroni</i>

CYP	cytochrome P450
DHFA	dihydroxyfumaric acid
DMSO	dimethyl sulfoxid
DNA	desoxyribonucleic acid
DQF-COSY	double quantum filtered correlation spectroscopy
<i>E. californicum</i>	<i>Eriodictyon californicum</i>
<i>E. coli</i>	<i>Escherichia coli</i>
EIC	Extracted-ion chromatogram
ED	eriodictyol
EDCh	eriodictyol chalcone
ENaC	epithelial Na Channel
f3'h	flavonoid 3'-hydroxylase (CYP75B)
FAD	Flavin adenine dinucleotide
FdR	FAD-containing ferredoxin reductase
Fdx	ferredoxin
fwd.	forward
Glc-6-P	glucose-6-phosphate
Glc-6-P-DH	glucose-6-phosphate dehydrogenase
GP(C)R	G-protein coupled receptor
2-HBP	2-hydroxybiphenyl 3-monooxygenase
HCA	hydroxycinnamic acid
HED	homoeriodictyol
HEDCh	homoeriodictyol chalcone
HEPES	4-(2-hydroxyethyl)-1-piperazineethanesulfonic acid
Hesp	hesperetin
6xHis-tag	hexa histidine-tag
HMBC	heteronuclear multiple-bond correlation spectroscopy

4HPA3H	4-hydroxyphenylacetate 3-hydroxylase
HRP	horseradish peroxidase
HSQC	heteronuclear single-quantum correlation spectroscopy
HvCHS2	<i>Hordeum vulgare</i> chalcone synthase 2
IPB	Leibniz Institute of Plant Biochemistry (Halle)
IPTG	Isopropyl β -D-1-thiogalactopyranoside
ITB	Institute of Technical Biochemistry (Stuttgart)
KP _i	potassium phosphate
LB	lysogeny broth
MBP	maltose-binding protein
MBP-At4CL2	maltose-binding protein-At4CL2 fusion protein
MobA	<i>m</i> -hydroxy-benzoate hydroxylase
MT	methyltransferase
NAD ⁺	nicotinamide adenine dinucleotide, oxidized form
NADH	nicotinamide adenine dinucleotide, reduced form
NADP ⁺	nicotinamide adenine dinucleotide phosphate, oxidized form
NADPH	nicotinamide adenine dinucleotide phosphate, reduced form
OMT	O-methyltransferase
PAGE	polyacrylamide gel electrophoresis
<i>P. azeleica</i>	<i>Pseudomonas azeleica</i>
PFOMT	phenylpropanoid and flavonoid O-methyltransferase
PMSF	phenylmethylsulfonyl fluoride
PPO	polyphenol oxidase
rev.	reverse
<i>R. ruber</i>	<i>Rhodococcus ruber</i>
ROESY	rotating frame nuclear Overhauser effect spectroscopy
ROS	reactive oxygen species
XIV	

SAH	S-adenosyl-L-homocystein
SAM	S-adenosyl-L-methionine
<i>S. cerevisiae</i>	<i>Saccharomyces cerevisiae</i>
SDS	sodium dodecylsulfate
S.O.C.	super optimal broth with catabolite repression
TAIR	the arabidopsis information resource
TRC	taste receptor cell
TEMED	<i>N,N,N',N'</i> -tetramethylethylenediamine
TOCSY	total correlation spectroscopy
Tris	tris(hydroxymethyl)aminomethane
UV	ultraviolet (light)
Vis	visible (light)
WT	wild type

List of Figures

Fig. 1.1: Two examples for bitter tasting active agents used as orally applied pharmaceuticals	1
Fig. 1.2: Taste bud of the human tongue	2
Fig. 1.3: Signal transduction in a TRC.	3
Fig. 1.4: Chemical structures of eriodictyol (ED) and homoeriodictyol (HED).....	6
Fig. 1.5: (A) Plant and single leaf of <i>Eriodictyon californicum</i> . (B) Leaf cross-section of <i>Eriodictyon californicum</i> after PEG-embedding showing excretory cells for the resin exudation on the surface of the epidermis.	7
Fig. 1.6: Chemical synthesis of ED and HED according to Kulkarni (2012) [51].....	9
Fig. 1.7: Biocatalytic synthesis of ED and HED. Naringenin (Nar) offers a suitable precursor for the synthesis of ED and HED due to minor modifications at position 3' at ring B (green).	10
Fig. 1.8: Approach for biocatalytic synthesis of (S)-naringenin starting from L-phenylalanine (A) and precursor-directed biosynthesis of further flavonoids (B).....	12
Fig. 2.1: Reaction of H ₂ O ₂ and <i>o</i> -dianisidine catalyzed by HRP forming a pink chromophore.	31
Fig. 3.1: Phenylpropanoid pathway	36
Fig. 3.2: Scheme of the CHS-catalyzed condensation reaction. The hydroxycinnamoyl-CoA used determines the substitution pattern of ring B (blue), the elongating acetyl units of malonyl-CoA build ring-A (red) after cyclization and aromatization.....	37
Fig. 3.3: Schematic proposal of a modified biocatalytic pathway for the synthesis of (H)ED (framed).....	38
Fig. 3.4: Base-catalyzed Michael addition forming the racemic flavanone from the chalcone skeleton.....	39
Fig. 3.5: Activity measurement of the crude extracts of At4CL2 and MBP-At4CL2 compared to a control.....	41
Fig. 3.6: SDS-PAGE of MBP-At4CL2 purification	42
Fig. 3.7: Absorption difference spectra for the conversion of HCAs and derivatives tested <i>in vitro</i> with MBP-At4CL2	43
Fig. 3.8: SDS-PAGE of CHS2 purification.	46
Fig. 3.9: CHS2 catalyzed formation of chalcones (B) from <i>p</i> -coumaroyl-CoA (A: R=H), caffeoyl-CoA (A: R=OH) and feruloyl-CoA (A: R=OCH ₃)	47
Fig. 3.10: Retention time and MS ² fragmentation pattern of the CHS2 product (A) compared to EDCh (B) and ED (C) as references.	48
Fig. 3.11: Strategy for the one-pot synthesis of ED and HED starting from HCA. Caffeic acid (R ₁ = H) or ferulic acid (R ₂ = CH ₃) are accepted by MBP-At4CL2 as starting material (A) for the synthesis of the corresponding CoA esters (B)	49
Fig. 3.12: A: Colony PCR after cotransformation	50
Fig. 4.1: Main classification of CYPs according to the topology of the P450 and the used electron transfer system	53

Fig. 4.2: Selective aromatic hydroxylation in flavonoid metabolism catalyzed by flavonoid 3'-hydroxylase (f3'h).....	54
Fig. 4.3: Catalytic cycle of CYPs [112].....	55
Fig. 4.4: EIC of UHPLC/MS runs of the extracts of oxidative biotransformations compared to a reference and a control.....	60
Fig. 4.5: Quantification of ED formation by different oxidating enzymes.	61
Fig. 4.6: SDS-PAGE picture of BM3-GVQ expression (A), CO difference spectrum of the BM3-GVQ lysate (B).....	62
Fig. 4.7: Expected reaction of Nar catalyzed by BM3-GVQ. The inserted hydroxyl group at position 3' is highlighted in dark green.....	64
Fig. 4.8: Chromatogram of chiral HPLC run.....	65
Fig. 4.9: Conversion of flavanone by BM3-GVQ.....	67
Fig. 4.10: Structural model of naringenin docked in BM3_GVQ.....	68
Fig. 4.11: Compound formation of the created BM3 double mutants and BM3-GVQ in the enzyme activity assay using Nar as a substrate.	69
Fig. 4.12: Time course of the conversion of Nar to ED by BM3-GVQ.	70
Fig. 4.13: Correlation of the applied GVQ enzyme concentration to the ED yield and to the resulting total turnover number (TTN).....	71
Fig. 4.14: Variation of the initial concentration of Nar.....	72
Fig. 4.15: Evaluation of the BM3-GVQ assay buffer	73
Fig. 4.16: A: Oxidation of NADPH by BM3-GVQ in presence of the regeneration system.....	74
Fig. 4.17: A: NADPH consumption of a standard BM3-GVQ assay incomplete conversion of Nar into ED at the beginning of the reaction. B: Extra supply of NADPH and regeneration system after 8 h incubation compared to a standard BM3-GVQ assay.....	75
Fig. 4.18: Influence of the initial concentration of NADPH on the formation of eriodictyol.....	76
Fig. 4.19: A: External calibration line of the H ₂ O ₂ concentration. B: H ₂ O ₂ production within the BM3-GVQ assay measured via HRP α -dianisidine assay.....	77
Fig. 4.20: Effects of catalase addition.....	78
Fig. 4.21: Docking studies of Nar (green) in the active site of a BM3 GVQ model based on BM3 wild type (pdb-code: 1bu7)	79
Fig. 4.22: CO difference spectra of BM3- variants based on BM3-GVQ or BM3-VQ containing a further mutation at position L75	80
Fig. 4.23: Product distribution and total conversion of Nar catalyzed by different BM3 variants	81
Fig. 4.24: <i>In vivo</i> conversion of Nar by BM3-GVQ in two different media.....	82
Fig. 4.25: SDS-PAGE of BM3-GVQ variant (1) and an empty vector as a control (0) after <i>in vivo</i> biotransformation of Nar in AI medium at different time points of incubation.....	82
Fig. 5.1: Reaction scheme of the 3'-OMT-catalyzed transfer of the methyl group from S-adenosyl-L-methionine (SAM) to ED forming HED.....	87
Fig. 5.2: O-Methylation steps in the biosynthesis of lignin precursor.....	88
Fig. 5.3: Selective conversion of ED into HED catalyzed by PFOMT	91

Fig. 5.4: Examples for the assayed flavonoids with sp ² - (A) and sp ³ -hybridised (B) pyran ring C.....	95
Fig. 5.5: Alignment of the 3D structure of the homology model of AtTSM1 (gray) and the 3D protein structure of PFOMT (pdb-code: 3C3Y) (green).....	95
Fig. 5.6: Taxifolin docked in the active site of PFOMT (green) (pdb-code: 3C3Y)....	96
Fig. 5.7: Chemical structure of oleuropein.	97
Fig. 5.8: Comparison of the <i>in vivo</i> conversion of ED catalyzed by PFOMT in two different growth media.....	98
Fig. 5.9: SDS-PAGE from the coexpression of PFOMT and BM3-GVQ in different media after 25 h incubation.	99
Fig. 5.10: Comparison of the <i>in vivo</i> conversion of Nar in the coexpression <i>E. coli</i> strain GVQ+PFOMT in two different induction media: LB/IPTG (A) and AI medium (B).....	99
Fig. 6.1: Two strategies investigated for the microbial biosynthesis of HED.	102
Fig. 6.2: Malonyl-CoA biosynthesis	104
Fig. 6.3: Biosynthesis of SAM.....	105

List of Appendix Figures

Fig. A 1: Purification steps of CoA ester synthesis exemplified for caffeoyl-CoA. Crude extract (c) was loaded on a SPE cartridge.	107
Fig. A 2: HPLC run of <i>p</i> -coumaroyl-CoA formed by enzymatic ligase reaction and purified using SPE.....	107
Fig. A 3: HPLC run of caffeoyl-CoA formed by enzymatic ligase reaction and purified using SPE.	108
Fig. A 4: HPLC run of feruloyl-CoA formed by enzymatic ligase reaction and purified using SPE.	108
Fig. A 5: HPLC run of isoferuloyl-CoA formed by enzymatic ligase reaction and purified using SPE.....	109
Fig. A 6: HPLC run of 4-ethoxy-3-hydroxycinnamoyl-CoA formed by enzymatic ligase reaction and purified using SPE.	109
Fig. A 7: HPLC run of 4-propoxy-3-hydroxycinnamoyl-CoA formed by enzymatic ligase reaction and purified using SPE.	110
Fig. A 8: ¹ H-NMR of <i>p</i> -coumaroyl-CoA.	115
Fig. A 9: Double quantum filtered correlation spectroscopy (DQF-COSY) plot of <i>p</i> -coumaroyl-CoA.	115
Fig. A 10: Total correlation spectrum (TOCSY) of <i>p</i> -coumaroyl-CoA.	116
Fig. A 11: Heteronuclear single-quantum correlation spectrum (HSQC) of <i>p</i> -coumaroyl-CoA.	116
Fig. A 12: Heteronuclear multiple-bond correlation spectroscopy (HMBC) plot of <i>p</i> -coumaroyl-CoA.	117

Fig. A 13: Rotating frame nuclear Overhauser effect spectroscopy (ROESY) plot of <i>p</i> -coumaroyl-CoA.	117
Fig. A 14: Wavelength shift during the ligase reaction using caffeic acid under time control	118
Fig. A 15: Retention time and MS ² fragmentation pattern of the CHS2 product (A) compared to HED (B) and Hesp (C) as references.....	119
Fig. B 1: UHPLC and MS/MS fragmentation patterns of the products of a BM3-GVQ assay using Nar as a substrate	120
Fig. B 2: UHPLC and MS/MS fragmentation pattern of the products of a BM3-GVQ assay using phloretin as a substrate	121
Fig. B 3: UHPLC and MS/MS fragmentation pattern of the products of a BM3-GVQ assay using Hesp as a substrate.....	122
Fig. B 4: Proposed reaction, UHPLC and MS/MS fragmentation pattern of the products of a BM3-GVQ assay using HED as a substrate.	123
Fig. B 5: Achiral GC-MS chromatogram and fragmentation pattern of a BM3-GVQ assay using flavanone.....	124
Fig. B 6:(A) ¹ H-NMR plot of the main product from the BM3-GVQ assay and (B) relevant section zoomed in the range of 5 and 9 ppm.	125
Fig. B 7 : ¹ H-NMR plot of a ED reference.	126
Fig. B 8: SDS-PAGE of the newly designed BM3 variants.....	127
Fig. B 9: CO difference spectra of BM3- variants based on BM3-F87V for BM3-GV and BM3-VQ, and BM3-GVQ for BM3-GVQS containing a further mutation A330S, respectively	127
Fig. B 10: SDS-PAGE of <i>in vivo</i> biotransformation of Nar in LB/IPTG.....	128
Fig. B 11: UV spectrum of references (A) and external calibration curve of relevant products measured at 280 nm (B) within the BM3-GVQ assay.....	128
Fig. C 1: SDS-PAGE of the purification of PFOMT	130
Fig. C 2: SDS-PAGE of the purification of AtTSM1.....	130
Fig. C 3: Sequence alignment of PFOMT and AtTSM1	131
Fig. C 4: HPLC Chromatogram of a product mixture of a standard PFOMT assay using 1,5-dicaffeoylquinic acid as a substrate after 600 min incubation.....	131
Fig. C 5: UHPLC and MS/MS fragmentation pattern of the products of the PFOMT assay using 1,5-dicaffeoylquinic acid as a substrate	132

List of Tables

Table 1.1: Traditional bitter masking compounds.	4
Table 2.1: List of reagents.	14
Table 2.2: Substrates and reference substances for analytics and enzymatic assays.	16
Table 2.3: Applied enzymes and the corresponding provider.	17
Table 2.4: Composition of mixing solutions for auto-inducing media.....	18
Table 2.5: Composition of buffers and stock solutions used.	19
Table 2.6: <i>E. coli</i> strains used for gene cloning and expression.....	20
Table 2.7: Plasmids for gene cloning and expression.....	20
Table 2.8: Primer sequences of applied oligonucleotides for DNA amplification and sequencing.....	22
Table 2.9: Oligonucleotides designed for mutagenesis.....	23
Table 2.10: Composition and incubation conditions of enzymatic activity assays. ...	29
Table 2.11: Assay conditions of inactive oxidation systems for the substrate Nar....	29
Table 2.12: Columns and conditions and (U)HPLC techniques applied.	33
Table 3.1: Natural and synthetic HCAs as substrates for MBP-At4CL2 activity.	42
Table 3.2: Percentage yield (amount of product) of the enzymatic synthesized CoA ester after purification.....	44
Table 3.3: HPLC and ESI-MS data from the products of the ligase reaction.	44
Table 3.4: FT-ICR HR-MS analysis of the biocatalytically synthesized CoA thioester.	45
Table 3.5: HPLC-,ESI-MS and HR-MS analysis products formed in the CHS2.....	47
Table 4.1: Commercially available enzymes used to test selective hydroxylation reactions on aromatic compounds.....	56
Table 4.2: Purified recombinant bacterial monooxygenases tested for the conversion of Nar.	58
Table 4.3: Recombinant bacterial monooxygenases applied for the biotransformation of Nar <i>in vivo</i> or <i>in vitro</i> with crude enzyme extracts.	59
Table 4.4: Results of the MS measurements compared to the calculated exact mass of ED.....	63
Table 4.5: ¹ H NMR (600 MHz) spectral assignments of the substrate Nar (A) and the isolated product (B) of a BM3-GVQ assay compared to the data from a reference of ED (C).....	64
Table 4.6: Substrate promiscuity of BM3-GVQ.....	66
Table 5.1: Tested OMT substrates consisting of at least one catechol group (bold) in the scaffold.....	92

List of Appendix Tables

Table A 1: FT-ICR HR-MS data of the CoA thioester compared to the calculated mass.	111
Table A 2: NMR data and spectral assignments for caffeoyl- and feruloyl-CoA	112
Table A 3: NMR spectra of <i>p</i> -coumaroyl-CoA.....	114
Table B 1: BM3 variants with no conversion of Nar and ED after 24 h <i>in vivo</i> biotransformation.	129

1 Theoretical principles

1.1 Gustatory modifiers

Consumption of food and eating habits of humans are guided by the sensory perception. In detail the gustation, olfaction and the oral perception like the texture of nutrients or other compounds are crucial for their rate of consumption [1]. Especially children are highly influenced by gustation preferring a sweet perception and disliking a bitter taste. This evolutionary given situation increases the consume of sweet tasting food that is often connected to unhealthy effects like diabetes and obesity with the risk of various diseases [2, 3]. In contrast, bitter tasting ingredients are often beneficial phytonutrients like glycosinolates, terpenes or polyphenols, but their gustation hinders the regular consumption of these compounds [4–6]. Moreover, bitter tasting molecules are often active agents and accordingly they are applied in pharmaceuticals, e.g.: ambroxol which is used in the treatment of respiratory diseases and paracetamol used as analgesic and antipyretic (Fig. 1.1).

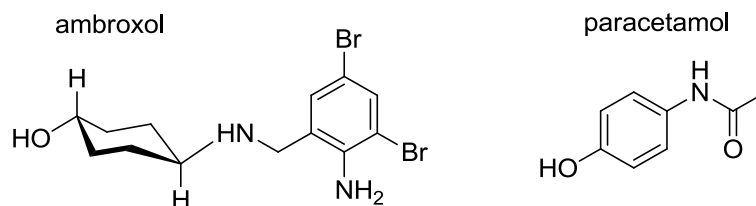


Fig. 1.1: Two examples for bitter tasting active agents used as orally applied pharmaceuticals. Ambroxol is applied for the treatment of respiratory diseases and paracetamol used analgesic and antipyretic are common drugs with bitter sensory perception. To avoid their bitterness oral applied pharmaceuticals for children are mostly added with bitter masking compounds especially sugar and aroma additives to facilitate the incorporation [7, 8].

To enhance the acceptance of children for oral medicine, especially bitter tasting compounds, industry tries to cover the bitterness by different methods of masking, e.g.: cognitive illusion by the addition of sweeteners and strong flavors, decreasing the concentration on free active molecules by the use of scavenging molecules like cyclodextrine or chitosan, or the reduction of the contact time of the molecule to the corresponding receptor e.g. by application of lipophilic vehicles [7, 9]. However, the most common and economic way is still the addition of sugar, salt, alcohol or fat as these additives are low-priced [10]. Therefore, alternatives for the modification of undesired taste are demanded to improve health promotion policy, consumer protection, and improve the responsibility of the industry.

To influence gustation, it is essential to know, how the gustation perception is realized in mammals. In general, the gustation or taste of a compound is a complex process and is acti-

vated by the taste-receptor cells (TRCs) of the taste buds in the epithelia of the oral cavity [1] (Fig. 1.2). Taste buds are predominantly comprised in different forms of papillae distributed on the tongue [11], but were also discovered in the non-bony palate in front of the uvula (soft palate) as well as in the back of the throat (pharynx) [1]. Papillae differ in their occurrence, location and the concentration of taste buds.

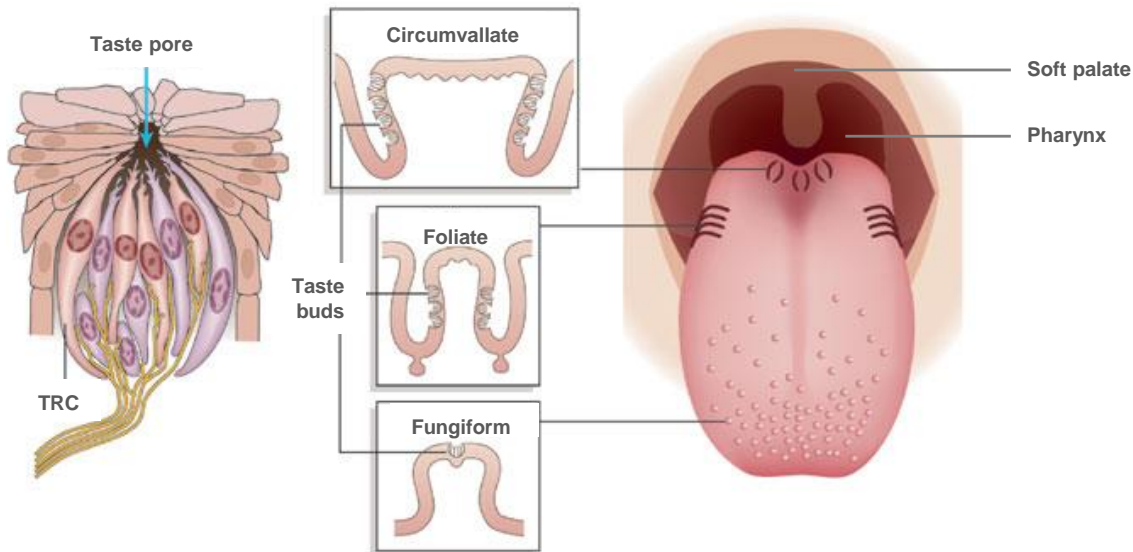


Fig. 1.2: Taste bud of the human tongue. The taste bud (left) contains the crucial taste-receptor cells (TRCs) and is element of different types of papillae located on the human tongue: circumvallate, foliate and fungiform with type-dependent number of taste buds. A taste pore emerging at the apical surface of the taste bud concentrates the TRCs receiving the sensory perception of the five basic qualities of taste – salty, sour, sweet, umami and bitter – without any taste-specific location on the tongue. Taste buds were also discovered in the soft palate and the pharynx on the epithelium without papillary structures [1]. Figure is modified according to Chandrashekar *et al.*(2006) [12].

A taste bud concentrates three different types of taste cells: until now, type I cells were shown to have a supporting function. Cells of type II (TRCs) contain **G**-protein coupled receptors (GPR or GPCR) that are responsible for sweet, bitter and umami taste perception. Cells of type III are so-called “synaptic cells”, containing synapsis with afferent nerve fibers detecting amongst others acidity that results in sour taste perception [13]. TRCs lead into a taste pore which allows the transduction of different taste qualities by chemoreception of fluid compounds on the apical surface [11]. In contrast to a widely distributed myth, a specific location for each taste at the tongue is unconfirmed [12].

Five basic qualities of taste are distinguished: sour, salty, sweet, umami and bitter [12]. However, there are additional qualities like fatty or metallic that cannot be explained by the five basic tastes, but the knowledge about potential receptors is marginal [11]. Previously, the fat taste was believed to be based on trigeminal and olfactory perception, but this consideration

could be countered after the discovery of two GP(C)Rs. GPR40 and GPR120 are activated by medium and long chain fatty acids and could be found in rodent in 2010 [14] and in human tongue tissue in 2012 [15]. In general, GP(C)Rs are complex proteins with seven transmembrane domains expressed in the taste buds [16]. Depending on the GP(C)R types different neurotransmitters, hormones or other stimulating compounds are bound by the G protein called gustducin which initializes the chemoreception of umami, sweet and bitter taste by a multiple signal transduction pathway (Fig. 1.3) [11].

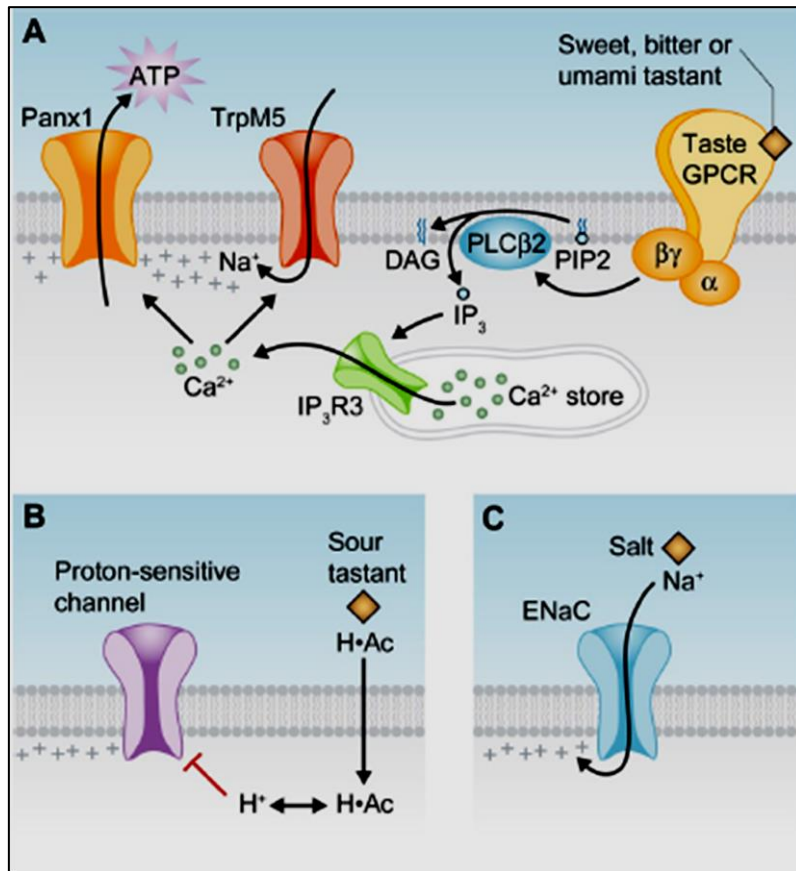


Fig. 1.3: Signal transduction in a TRC. The five basic taste qualities are perceived by chemoreception: **(A)** Umami, sweet and bitter taste are activated by GP(C)Rs which initialize a multiple signal transduction pathway starting with the production of the second messengers inositol triphosphate (IP $_3$) and diacylglycerol (DAG) followed by the intracellular increase of Ca $^{2+}$. Na $^{+}$ influxes by a cation channel called TrpM5. **(B)** Sour tastants permeate through the membrane and increase the H $^{+}$ level in the cytoplasm. **(C)** Salty taste is directly coupled to an ion channel (ENaC – Epithelial Na Channel). After the binding of active ligands, the concentration of the cations in the cytoplasm changes and the cell is depolarized. ATP is released and initializes signal transduction. According to Chaudhari *et al.* (2010) [11].

Activated gustducin triggers the production of the second messengers inositol triphosphate and diacylglycerol that initializes the intracellular Ca $^{2+}$ release and allows the influx of Na $^{+}$ via the cation channel TrpM5 depolarizing the cell membrane [11]. ATP is effused and Ca $^{2+}$ is

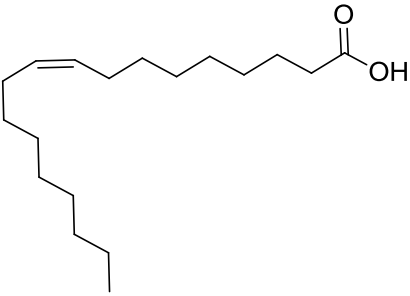
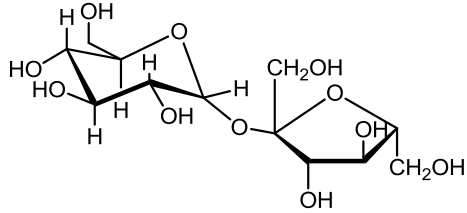

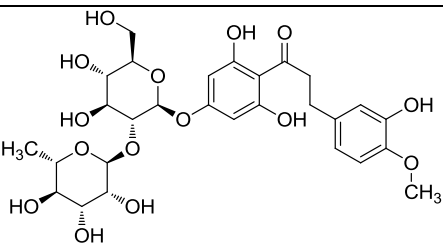
deported by exocytosis releasing neurotransmitter and forming action potentials that are sent to the brain as a taste perception [1].

Except from the salty and sour quality, the remaining basic taste perceptions – bitter, sweet and umami – are activated by such GP(C)Rs. Sour quality is based on proton acidity and salty taste on sodium ions. Both tastes are based on cations which simply activate ion channels by changing the activation potential and therefore do not require GP(C)Rs [16]. For umami, sweet and bitter taste perception, homo- or heterodimeric receptor complexes of TR subunits (T1R and T2R family) are coupled to the G protein gustducin. Depending on the assembling of the dimers, GP(C)Rs are activated by binding the responsible compounds and different taste qualities are transmitted to the brain. T1R subunits form the pairs of GP(C)Rs for sweet (T1R2/T1R3) and for umami (T1R1/T1R3) taste; for bitter perception, two subunits of the T2Rs family build the receptor [11]. Up to know, more than 25 different T2R subunits were identified in humans [1]. Hence, the appearance of the bitter receptors is highly differentiated and allows a multitude of variations in activating and blocking compounds followed by the corresponding taste perception [17].

Bitter taste is based on the most structurally diverse receptor family of the five basic tastes [1]. Due to the complex activation mechanism of bitter reception and the high similarity to umami and sweet taste transduction, the structure-activity relationship of compounds that activate or block the bitter taste are not exhaustively clarified [18, 19]. The tastants vary a lot in their features and are still under research [9]. Table 1.1 summarizes a few typical examples for different classes of compounds with bitter masking effects and their additional feature.

Table 1.1: Traditional bitter masking compounds.

substance	structure	class	additional feature
sodium chloride	$\text{Na}^+ \text{Cl}^-$	salt	addition of strong salty taste by activation of ENaC

substance	structure	class	additional feature
oleic acid		fatty acid	decreases concentration of free bitter molecules
sucrose		carbohydrate	addition of a strong sweet taste by activation of sweet receptors (T1R2/T1R3)
thaumatin I	 ¹	protein	low-calorie sweet protein with high potency in micromolar concentration
neohesperidin dihydrochalcone		artificial phenylglycoside	artificial sweetener, 340 times sweeter than sugar (weight to weight)

All listed compounds have in common that their application is connected to a disadvantage: they mask bitterness by modifying the flavor, for example: neohesperidin dihydrochalcone and thaumatin are themselves sweeteners, thus disturbing in non-sweet applications. Moreover, a few of these examples bear unhealthy side effects at higher doses of consumption that are required for their bitter masking effects, e.g.: sodium chloride, oleic acid and sucrose. Even artificial sweeteners with low-calories and high potency in micromolar concentrations were recently discovered to induce glucose-intolerance and dysbiosis [20]. Hence, discovering new compounds with bitter masking effects which are tasteless, odorless and uncritical in their consumption are very important in future food processing and pharmacology [8].

¹ Pdb-code: 1RQW

1.2 Eriodictyol and Homoeriodictyol – bitter masking flavonoids from *Eriodictyon californicum*

Eriodictyol (ED) and homoeriodictyol (HED) are flavonoids discovered in *Eriodictyon californicum* [8, 21]. Both compounds impress due to their remarkable bitter masking effect of about 10-40 %, for example: a strong bitter tasting solution of 500 ppm caffeine is masked remarkably by the addition of 200 ppm HED sodium salt (~ 40 % bitter reduction) [8]. Several chemical classes of bitter compounds are masked by ED and HED, e.g.: caffeine and amarogentin, but also quinine, paracetamol and salicin while both flavonoids being themselves neutral in taste [8]. Hence, they are variable in applications as food or pharmaceutical additives without any noxious or texture effects like they are exhibited by salt, fat or sugar [3]. ED and HED are structurally related and differ only in a methyl group at position 3' at ring B (Fig. 1.4).

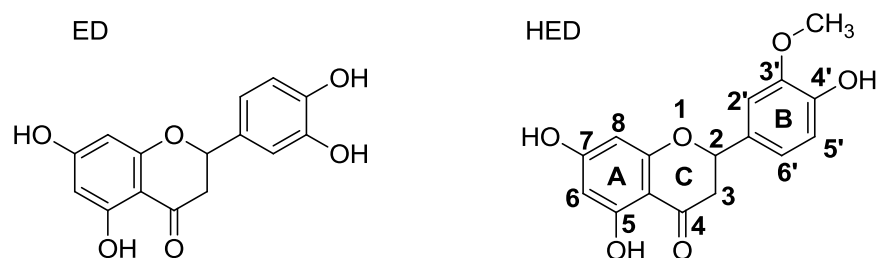


Fig. 1.4: Chemical structures of eriodictyol (ED) and homoeriodictyol (HED). The aglycones were predominantly found on the leaf surface of *Eriodictyon californicum* and feature a neutral masking effect on several bitter compounds [8].

These compounds belong to the flavanones – a subgroup of flavonoids widely distributed in plant secondary metabolism – which contain a carbonyl group of their pyran ring (C). Generally, flavonoids are a class of phenolic compounds with over 10,000 different structures [22]. Their simplest structures occur already in evolutionary old photosynthetic plants e.g.: in mosses [23]. The nomenclature of flavonoids is oriented towards the degree of the oxidation on the central pyran ring (C) at their C₆-C₃-C₆ tricyclic framework as well as on the functionalization by diverse modifications like hydroxylation, methoxylation and prenylation at the skeleton [24, 25]. The variations are manifold due to the number and localization of substituents and in addition due to the glycosylation, esterification and the possible di-, oligo- and polymerization of the flavonoids [24, 26]. The general biosynthesis of flavonoids in plants is realized by the phenylpropanoid pathway which is further described in section 3.1.

Originally, the term “flavonoid” arises from the Latin word “flavus” meaning “yellow” due to their natural color and their historical usage for the dyeing of wool [24]. Along with carotenoids and betalains, this colorful compounds are responsible for flower pigmentation which is

not only essential to attract pollinators but also to protect the plant against photooxidative damage, ultraviolet (UV) radiation and phytopathogens [27, 28]. Moreover, flavonoids are involved in intra- and intercellular signal transduction like the auxin transport and extracellularly for plant communication with insects and microbes like for the root nodulation [28–30]. Their properties and effects on human health are also diverse and allow a huge range of application. In addition to a more generally antioxidative potential [31, 32], some flavonoids provide anti-inflammatory, -atherosclerotic, -thrombogenic, -osteoporotic, -tumor and antiviral effects [33]. Especially flavonols like quercetin and kaempferol offer potential as radical scavengers and metal chelators [29, 30].

Flavonoids were found in different plant tissues like in stems, barks, seeds and flowers [34]. Therefore, they are also present in various food and food products, e.g.: in fruits, vegetables, nuts, tea, wine and honey [25, 26]. Glycosylated flavonoids as hydrophilic compounds accumulate primarily in the vacuoles of plants and in the cell wall where they are often esterified with aliphatic or phenolic acids like malonic acid or caffeic acid [24, 35]. Non O-glycosylated flavonoids – so-called aglycones – occur mainly in wood-parenchyma or are excreted on the epidermis (cuticula) of the plant [24, 36, 37]. The flavonoids ED and HED are such aglycones and were mainly found in the exudate (resin) on the leaf surface of herba santa – *Eriodictyon californicum* (Hook. & Arn.) Torr. (Fig. 1.5) [8, 21].

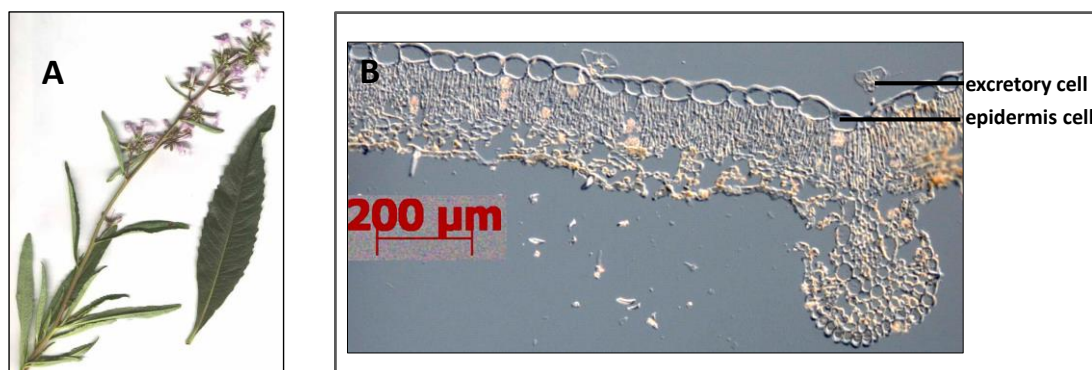


Fig. 1.5: (A) Plant and single leaf of *Eriodictyon californicum*². (B) Leaf cross-section of *Eriodictyon californicum* after PEG-embedding showing excretory cells for the resin exudation on the surface of the epidermis.

This plant is native in the Baja California Desert – a region in the north of Mexico and in the south of California – as well as in Oregon [21] and has an application in traditional medicine [8]. In general, *E. californicum* is a member of the Waterleaf family (Hydrophyllaceae) adapted to the desert conditions of low water level and high solar radiation [21, 38]. Thus, the

² Source: http://calphotos.berkeley.edu/imgs/128x192/0000_0000/0102/0270.jpeg

exudative sedimentation of resin including phytochemicals on the leaf surface is common and indispensable in desert environment to avoid evaporation and repel herbivores [39]. The resin contains mainly phenolic compounds especially flavonoids as well as terpenoids mainly sesqui- and diterpenes. Members of the former group are non-volatile compounds that are structurally similar to one another featuring UV absorption, deterrent to predators and act as antimicrobial agent [40]; the latter group is essential for a glutinous and gleaming texture of the resin [38].

1.3 Chemical engineering and green biotechnology

The synthesis of natural compounds is a traditional line of business for the chemical and pharmaceutical industry. The early production processes of synthetic purple and blue pigments for the dyeing of textiles were a mile stone for the chemical industry. For example, the production of synthetic indigo led to a commercial feasible manufacturing process [41]. The chemical industry started in the beginning of the 19th century but its development exploded during the industrial revolution before the turn of last century offering the commercial application of advanced materials like artificial silk or rubber, drugs such as insulin or morphine for a wide medicinal application, dyes, flavors and fragrances for perfume and cosmetic industry as well as the paper production which was also revolutionized [42, 43]. However, the current scope of customer's demands further development of industrial products, ingredients and additives which are produced to be resource-saving and eco-friendly. Moreover, food, cosmetic and pharmaceutical additives should derive from natural sources but should also be sustainable in their commercial application. Hence, a shift from fossil to bio-based raw material is a long term trend for energy and feedstock. These requirements on commercial products lead industry to evolve innovative strategies in white biotechnology to optimize biological systems and thus to develop highly efficient biocatalysts like enzymes, whole-cells and even eukaryotic organisms.

In fact, most biocatalysts feature economic and ecologic advantages because of mild reaction conditions, selectivity and sustainability. In the last decades, several approaches for the biotechnological production of industrially relevant compounds were published and some were also applied in industry, e.g.: the application of amylases from plants and fungi in food processing to produce high fructose-corn syrup from starch [44] or fermentation-produced chymosin, that allows expansive industrial cheese production for commercial applications [45].

However, up to know ED and HED are industrially produced by the extraction from *E. californicum*. Although there are different isolation techniques published since the first one

appeared from Geissman in 1940 [46], the efficiency is still limited to 2.5 % yield related to the dry weight of the plant [8, 47]. Due to lack of sustainability of current harvesting of the plants and their agriculture in a politically critical area of Mexico, the production of high amounts of the bitter masking compounds by isolation is rather difficult. Another strategy for the production of ED and HED is the chemical synthesis: previously in 1929, Shinoda and Sato synthesized ED and HED using phloroglucinol and carbethoxyferuloyl chloride [48] that was improved in 1959 by Farooq *et al.* [49] using the same precursors. In 2003, Shetgiri and Rege modified the first synthesis by a four step route to achieve ED and HED starting from phloroglucinol [50]. Kulkarni improved this method in 2012 by developing a three step total synthesis [51] (Fig. 1.6.).

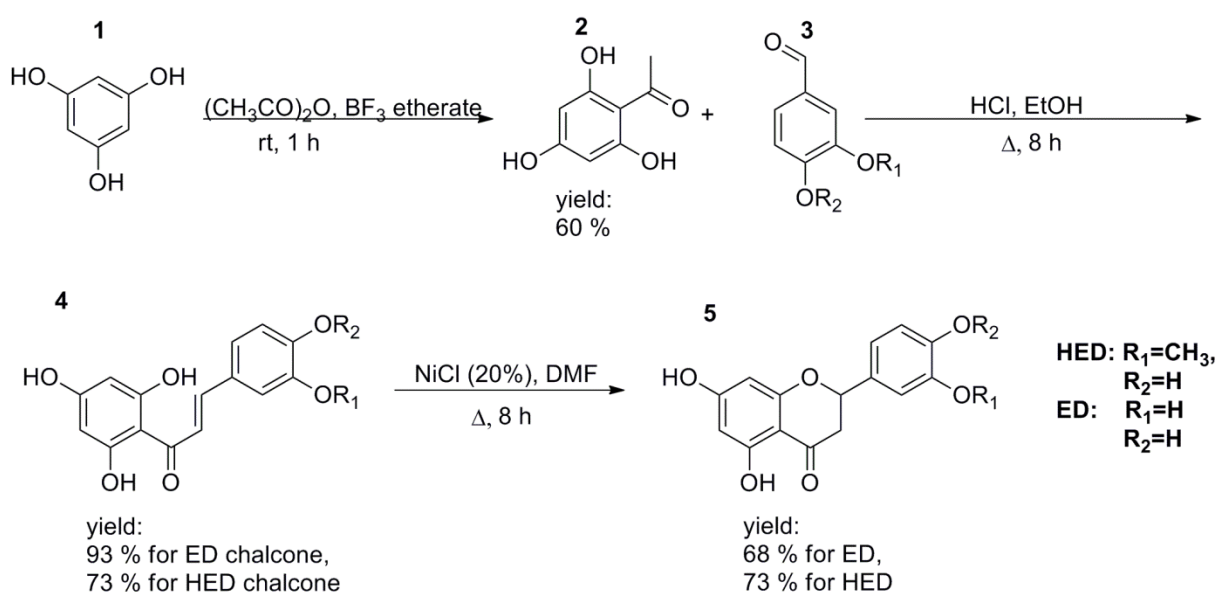


Fig. 1.6: Chemical synthesis of ED and HED according to Kulkarni (2012) [51]. The flavonoids are achieved by a three step total synthesis. Phloroglucinol (1) is used as the precursor for the synthesis of 2,4,6-trihydroxy acetophenone using acetic anhydride and Boron trifluoride etherate at room temperature. The resulting phloroacetophenone (2) was condensed either with 2,3-dihydroxybenzaldehyde (3) to achieve the chalcone precursor for ED or with 2-hydroxy-3-methoxy benzaldehyde (3) to synthesize the precursor for HED by using HCl in ethanol with heating. The chalcones (4) were cyclized to the corresponding flavanones (5) in the environment of 20 % NiCl in DMF with heating.

However, all strategies of chemical synthesis require more than two reaction steps and the application of solvents and reagents is associated with economic and toxicological hazards. Therefore, new appropriate methods are necessary to enable the economically and ecologically rational utilization of ED and HED as bitter masking compounds.

In addition, the biocatalyzed production of rare flavonoids like ED and HED were already proposed by a few working groups in different organisms, for example: the hydroxylation of naringenin (Nar) to obtain ED by a co-expression system of P450s in white-rot fungus *Phan-*

erochaete chrysosporium and the NADPH-reductase in *Saccharomyces cerevisiae* [52]. The functional expression of a flavonoid 3'-hydroxylase from *Gerbera hybrid* in *S. cerevisiae* obtained even 200 mg l⁻¹ ED from Nar in selective media [53]. In general, Nar is the biological precursor and chemical lead for the natural biosynthesis of flavonoids. Nar is sourced in high amounts from the peel of citrus fruits especially grapefruit, orange and mandarin, but it also occurs in low concentrations in the skin of tomato [54]. Moreover, O-glycosidically linked esters like naringin (naringenin-7-neohesperoside) and narirutin (naringenin-7-rutinoside) are found in high amounts in the juice of citrus fruits and can be easily converted by saponification into Nar. In comparison to ED and HED, Nar is low-priced due to the high availability: the consumer price of Nar averages 26 € g⁻¹ (Sigma Aldrich, catalogue from November 21, 2014) and naringin is even available for 1.96 € g⁻¹ (Sigma Aldrich, catalogue from November 21, 2014), in contrast to ED and HED which are sold for 6500 € g⁻¹ (Extrasynthese, catalogue from November 21, 2014). Nar is structurally similar to ED as well as HED and they differ just in a minor modification at ring B (Fig. 1.7).

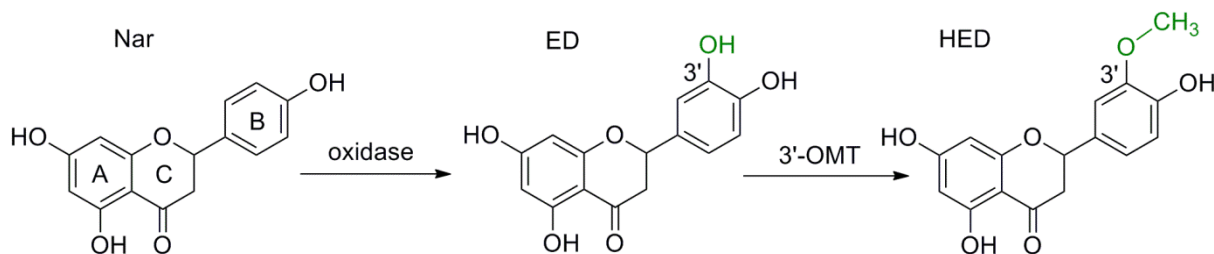


Fig. 1.7: Biocatalytic synthesis of ED and HED. Naringenin (Nar) offers a suitable precursor for the synthesis of ED and HED due to minor modifications at position 3' at ring B (green). A selective oxidase catalyzing the hydroxylation to form ED and a specific 3'-OMT catalyzing the regioselective methylation are required to form HED.

However, these slightly modifications offer mainly different features for the taste modifying properties of the flavonoids: Nar shows no significant influence on bitter taste, while ED and HED exhibit remarkable bitter masking effects. However, these flavanones have one feature in common: their taste profile shows no additional (own) strong taste or flavor [8]. Therefore, Nar is a suitable starting material for the selective hydroxylation into ED by an oxidase and subsequently the 3'-O-methylation into HED (Fig. 1.7). HED was previously supposed to be produced by selective methylation of ED using a specific 3'-OMT, e.g.: flavone 3'-O-methyltransferase ROMT-9 expressed in the recombinant *Yarrowia lipolytica*. Thereby 110 mg l⁻¹ HED were obtained by a conversion rate of 52.4 %. [55].

However, the production of ED and HED in an easy biotechnological system to obtain high amounts suitable for commercial application is still a challenge, because the investigation of

enzymes for selective oxidation and methylation in industrial biotechnology applications is still in its infancy and has to be optimized with regard to cofactor dependence, controllability, activity and stability.

For example, selective hydroxylation of aromatic compounds is one of the most challenging processes for the synthetic production of fine chemicals [56] as non-activated C-H bonds have to be attacked. In nature hydroxylation is realized by different types of oxidoreductases especially by oxygenases, peroxidases and oxidases. They are classified either according to their cofactor requirement or to the utilized electron acceptor and the generated product [57]. Oxygenases – named by Hayashi in 1955 [58] – catalyze the oxidation of a substrate by providing an oxygen atom from molecular oxygen (O_2). These enzymes commonly feature high regio- and stereoselectivity and are widely distributed in all kingdoms of life [59]. Such oxidative biocatalysts might be an alternative for metal catalyzed reactions in industrial application.

Methylation is also a ubiquitous process in all living organisms. It is realized by specialized enzymes called methyltransferases (MTs). Based on the chemical nature of the substrates, MTs are classified into major groups based on the atom type which is methylated: C-, O-, N-, S- and As-MTs, and methyl halide transferases acting on halide ions as nucleophilic substrates [67]. However, the enzymatic addition of (at least) one methyl group to natural compounds does not only modify their solubility, lipophilicity or pKs but also their intracellular compartmentalization and interaction with target proteins resulting in modifications of odor, taste and also pharmaceutical effects [60–62]. Because of this high biological impact, all cellular methylation processes must be strictly regulated with respect to chemo-, regio-, and stereoselectivity. So far, the use of MTs which have been investigated and engineered for biocatalytic production of selectively methylated (natural) compounds is still negligible compared to the number of methylated products on the market [63, 64]. They still offer significant potential but also pose challenges, the latter mostly connected to the sufficient accessibility of the crucial cofactor SAM [60].

However, enzymatic reactions can be superior to classical chemical methods due to substrate specificity and a usually excellent selectivity. In addition, enzymatic synthesis mostly allows mild reaction conditions with regard to temperature, pressure, pH value, and solvent. Usually, it is performed in aqueous environment [65]. For industrial applications, enzymes can additionally be tailored to improve availability, stability, selectivity, conversion rate, and substrate promiscuity [66, 67]. Once a suitable biocatalyst is found or developed, disadvantages

can emerge primarily from long term stability, cofactor supply or regeneration, substrate or product inhibition, low substrate concentrations and conversion/turnover rates, and downstream processing problems. Thus, industry is interested in the development of biocatalysts especially for difficult chemical processes like oxidation or selective methylation to replace metal-catalyzed reactions and avoid non-economical reaction steps like protecting group introduction and removal to obtain chemoselectivity.

In addition, even the five-step biosynthetic pathway to Nar starting directly from the phenylpropanoic acids was already achieved in different microorganism like *E. coli* [61], yeast like *S. cerevisiae* [68] or in combination of procaryotes and eucaryotes [69]. This approach offers simple and low-priced substrates like *p*-coumaric acid or even L-phenylalanine to achieve costly and rare flavonoids (Fig. 1.8A). Furthermore, the choice of the precursor defines the synthesized structure of the flavanone offering a multitude of natural and unnatural flavonoids in approach (Fig. 1.8B) [69].

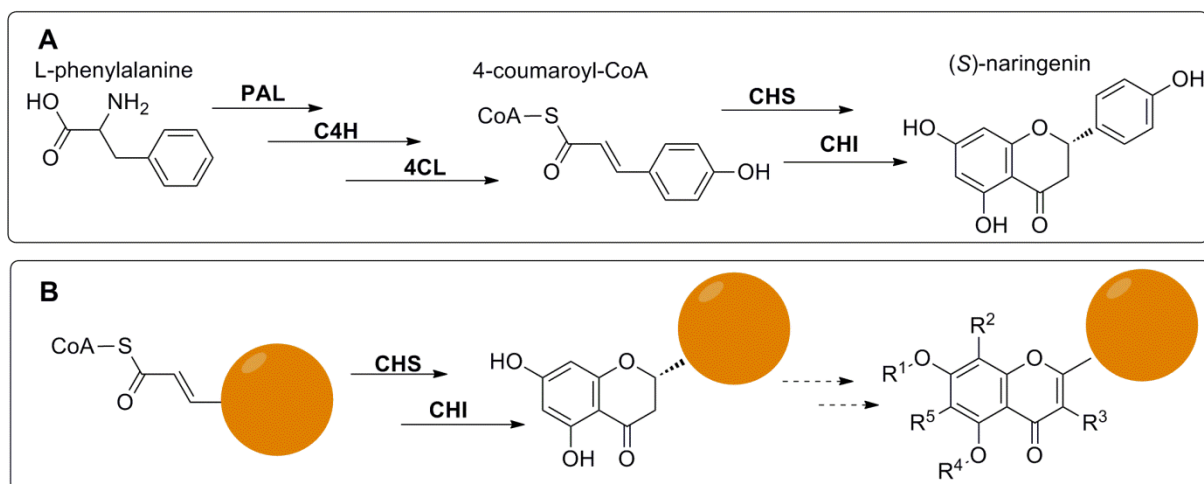


Fig. 1.8: Approach for biocatalytic synthesis of (S)-naringenin starting from L-phenylalanine (A) and precursor-directed biosynthesis of further flavonoids (B). A: L-phenylalanine is the natural precursor for the five-step biosynthesis of flavonoids. B: Modification at the aromatic ring of the CoA ester by for example oxidation, methylation and/or prenylation are shown schematically and lead to modified flavanones by an artificial pathway. Further modifications (dashed arrows) result in various natural and unnatural flavonoids.

Although there are a few strategies and proposals for the biocatalytic synthesis of flavonoids like ED and HED, the biotechnological production of high amounts in an efficient and simple-cultivating host like *E. coli* for commercial applications is still in the initial state.

Hence, this study concerns two strategies to obtain the desired flavonoids ED and HED in *E. coli*. Chapter I focuses the precursor-directed biosynthesis of ED and HED starting from caffeic acid and ferulic acid, wherein plant enzymes are heterologously expressed in *E. coli*

and investigated according to their substrate spectrum. Finally, a first approach of the enzyme cascade for *in vivo* biotransformation is presented. Chapter II centers the oxidation of Nar into ED and targets the screening for a suitable biocatalyst of selective 3'-hydroxylation from microorganisms and plants. The appropriate candidate – a triple mutant of CYP102A1 from *Bacillus megaterium* (BM3-GVQ) – is further investigated and optimized for the ED production. The system is first applied as *in vivo* biotransformation feeding Nar. The last chapter III concerns the methylation of ED forming HED using the appropriate OMT of *Mesembryanthemum crystallinum* (PFOMT) heterologous expressed in *E. coli* based on the diploma thesis of 2010 [70]. The substrate spectrum of PFOMT is further investigated and first steps of *in vivo* biotransformation are presented. This chapter concludes the linkage of oxidation and methylation by an enzyme-cascade that is first applied as *in vivo* whole-cell biotransformation.

2 Materials and methods

2.1 Materials

2.1.1 Consumables and Chemicals

Reagents and consumables were purchased as listed in table 2.1. Bidistilled water for buffers and solutions was achieved using a MilliQ-biocel apparatus from Millipore (Billerica, USA); methanol and ethyl acetate were applied after in house distillation.

Table 2.1: List of reagents.

reagents and consumables	purchaser
Acetic acid, Rotipuran® 100% (AcOH)	Roth, Karlsruhe
Aceton-D6 (C ₃ D ₆ O)	VWR, Darmstadt
Acetonitrile, HPLC grade (MeCN)	Merck, Darmstadt
Acrylamide:Bis-acrylamide (37.5:1), 30% solution	Merck, Darmstadt
Agar	Roth, Karlsruhe
Agarose	Roth, Karlsruhe
Ammonium acetate (NH ₄ OAc)	Sigma-Aldrich, Munich
Ammonium peroxydisulfate (APS)	Roth, Karlsruhe
Ampicillin, sodium salt	Roth, Karlsruhe
10x BamHI buffer	Thermo Scientific, Darmstadt
2x B-PER™ Bacterial Protein Extraction Reagent (B-PER II reagent)	Thermo Scientific, Darmstadt
Bromophenol blue	Roth, Karlsruhe
Carbenicillin	Roth, Karlsruhe
Chloroform EMPLURA®	Merck, Darmstadt
Coomassie brilliant blue G-250	Roth, Karlsruhe
Diethyl ether EMSURE®, p.a.	VWR, Darmstadt
Dimethyl sulfoxide (DMSO), ≥99.5% (GC)	Sigma-Aldrich, Munich
6x DNA Loading Dye	Thermo Scientific, Darmstadt
10x DreamTaq buffer	Thermo Scientific, Darmstadt
Ethanol, 96% (EtOH)	Merck, Darmstadt
Ethidium bromide (10 mg ml ⁻¹)	VWR, Darmstadt
Ethyl acetate EMSURE® (EtOAc)	Merck, Darmstadt
Flavin adenine dinucleotide (FAD)	Roth, Karlsruhe
Formic acid, > 98% (HCOOH)	Roth, Karlsruhe
Gene-Ruler™ 1 kb DNA Ladder	Thermo Scientific, Darmstadt

Materials and methods

reagents and consumables	purchaser
α -D(+)- Glucose	Roth, Karlsruhe
D-Glucose 6-phosphate sodium salt (glc-6-P)	Sigma-Aldrich, Munich
Glycerol	Roth, Karlsruhe
Hydrochloric acid (37%) (HCl)	Roth, Karlsruhe
4-(2-Hydroxyethyl)-1-piperazineethanesulfonic acid (HEPES)	Roth, Karlsruhe
Imidazole	Roth, Karlsruhe
Isopropyl alcohol	Merck, Darmstadt
Isopropyl β -D-1-thiogalactopyranoside (IPTG)	Roth, Karlsruhe
Kanamycin sulfate	Roth, Karlsruhe
K_2HPO_4	Merck, Darmstadt
KCl	Sigma-Aldrich, Munich
KH_2PO_4	Sigma-Aldrich, Munich
Lactose	Sigma-Aldrich, Munich
β -mercaptoethanol	Roth, Karlsruhe
Methanol NORMAPUR®, p. a. (MeOH)	VWR, Darmstadt
$MgCl_2 \times 6 H_2O$	Roth, Karlsruhe
$MgSO_4$	VEB Laborchemie, Apolda (GDR)
N_2	Air Liquide, Düsseldorf
NaCl	Roth, Karlsruhe
NaOAc	Merck, Darmstadt
$Na_2S_2O_4$	Fisher Scientific, Schwerte
NaOH	Roth, Karlsruhe
Nicotinamide adenine dinucleotide (NADH)	Roth, Karlsruhe
Nicotinamide adenine dinucleotide phosphate (NADPH)	Appli Chem, Darmstadt
$(NH_4)_2SO_4$	VEB Laborchemie, Apolda (GDR)
dNTP-Mix (10 mM per desoxynucleotide triphosphate)	Thermo Scientific, Darmstadt
PageRuler™ Plus Prestained Protein Ladder	Thermo Scientific, Darmstadt
10x Pfu buffer	Thermo Scientific, Darmstadt
Phenylmethylsulfonyl fluoride (PMSF)	Sigma-Aldrich, Munich
Potassium acetate (KOAc)	Merck, Darmstadt
Roti®-Phenol/Chloroform/Isoamyl alcohol	Roth, Karlsruhe
Roti®-Quant (Bradford reagent)	Roth, Karlsruhe
S-(5'-Adenosyl)-L-methionine p-toluenesulfonate salt (SAM)	Sigma-Aldrich, Munich
Sodium dodecylsulfate (SDS)	Roth, Karlsruhe

reagents and consumables	purchaser
10x T4 DNA ligase buffer	Thermo Scientific, Darmstadt
Tetramethylethylenediamine (TEMED)	Roth, Karlsruhe
Trichloroacetic acid (TCA)	Alfa Aesar, Karlsruhe
Tris(hydroxymethyl)aminomethane (Tris)	Roth, Karlsruhe
Tris-Hydrochloride (Tris-HCl)	Roth, Karlsruhe
Tryptone / peptone ex casein (tryptone)	Roth, Karlsruhe
Yeast extract	Roth, Karlsruhe

2.1.2 Substrates and reference substances

Substrates and reference substances used for enzymatic assays and as analytical standards are shown in table 2.2. Each compound was ordered in its highest available quality. Synthetic derivatives of hydroxycinnamic acid (HCAs) and isoferulic acid were synthesized in house (Dr. Martin Dippe). Unless otherwise noted, 10 mM stock solutions, dissolved in MeOH, were prepared.

Table 2.2: Substrates and reference substances for analytics and enzymatic assays.

compound	purchaser
Adenosine 5'-triphosphate (ATP) disodium salt hydrate	Sigma-Aldrich, Munich
Caffeic acid	Sigma-Aldrich, Munich
Cichoric acid	Symrise, Holzminden
Coenzyme A trilithium salt dehydrate (coenzyme A)	AppliChem, Darmstadt
1,5-Dicaffeoyl-quinic acid	Symrise, Holzminden
3,4-Dicaffeoyl-quinic acid	Symrise, Holzminden
3,5-Dicaffeoyl-quinic acid	Symrise, Holzminden
4,5-Dicaffeoyl-quinic acid	Symrise, Holzminden
Dihydroxyfumaric acid hydrate (DHFA)	Sigma-Aldrich, Munich
Flavanone	Acros Organics, Thermo Fisher Scientific, Geel, Belgium
Flavone	Sigma-Aldrich, Munich
Ferulic acid	Sigma-Aldrich, Munich
Fisetin	Symrise, Holzminden
(-)-Epicatechin	Symrise, Holzminden
Eriodictyol (ED)	Symrise, Holzminden
Eriodictyol chalcone (EDch)	Extrasynthese, Genay Cedey, France

compound	purchaser
Hesperetin (Hesp)	Symrise, Holzminden
Homoeriodictyol (HED)	Extrasynthese, Genay Cedey, France
2-Hydroxyflavanone	Sigma-Aldrich, Munich
6-Hydroxyflavanone	Sigma-Aldrich, Munich
7-Hydroxyflavanone	Acros Organics, Thermo Fisher Scientific, Geel, Belgium
3-Hydroxyflavone	Sigma-Aldrich, Munich
3'-Hydroxyflavone	Sigma-Aldrich, Munich
Luteolin	Sigma-Aldrich, Munich
Malonyl-CoA	Santa Cruz, Dallas, U.S.A.
Methoxyflavone	Sigma-Aldrich, Munich
Myricetin	Symrise, Holzminden
Naringenin (Nar)	Sigma-Aldrich, Munich
Oleuropein	Symrise, Holzminden
<i>p</i> -Coumaric acid	Sigma-Aldrich, Munich
Phloretin	Extrasynthese, Genay Cedey, France
Sterubin	Symrise, Holzminden
Rosmarinic acid	Symrise, Holzminden
Taxifolin	Sigma-Aldrich, Munich

2.1.3 Enzymes

Enzymes were purchased as listed in table 2.3 and stored as described in manufacturer's instructions.

Table 2.3: Applied enzymes and the corresponding provider.

type	enzyme	source
oxidoreductase	<ul style="list-style-type: none"> catalase from bovine liver ($\geq 11,700 \text{ U mg}^{-1}$ solid) horseradish peroxidase (HRP) ($\geq 250 \text{ U mg}^{-1}$ solid) tyrosinase from mushroom ($\geq 1,000 \text{ U mg}^{-1}$ solid) 2-hydroxybiphenyl 3-monooxygenase (2-HBP), recombinantly expressed in <i>E. coli</i>, purified and freeze-dried (1.2 U mg^{-1}) 	Roth; Karlsruhe Iris Biotech GmbH, Marktredwitz Sigma-Aldrich, Munich Bartłomiej Tomaszewski (TU Dortmund)
dehydrogenase	glucose-6-phosphate dehydrogenase, grade II, from yeast (glc-6-P-DHG) (140 U ml^{-1})	Roche, Indianapolis, U.S.A.
DNase	DNase I ($3,000 \text{ U mg}^{-1}$)	AppliChem, Darmstadt

type	enzyme	source
ligase	T4 DNA ligase (5 U μl^{-1})	Thermo Scientific, Darmstadt
glycosidase	lysozyme (20,000 U mg^{-1})	Roth, Karlsruhe
polymerase	DreamTaq DNA polymerase (5 U μl^{-1}) PfuUltra HF DNA polymerase (2.5 U μl^{-1})	Thermo Scientific, Darmstadt
restriction enzyme	BamHI (10 U μl^{-1}) DpnI (10 U μl^{-1}) HindIII (10 U μl^{-1})	Thermo Scientific, Darmstadt

2.1.4 Media

Escherichia coli (*E. coli*) cells were grown in auto-inducing media and in Luria-Bertani (LB) broth. Super Optimal broth with Catabolite repression (S.O.C.) was used to cultivate bacteria competent cells after plasmid DNA transformation. Before application, medium was autoclaved at 121 °C with excess pressure for 20 min according to GenTSV §12. Sterile filtered additives were added after autoclaving as designated. 0.1 % (v/v) of the appropriate sterile filtered antibiotic (table 2.4) was generally added to LB and auto-inducing medium before usage. For whole-cell biotransformation, ampicillin was replaced with carbenicillin.

Auto-inducing medium

1 l auto-inducing medium is composed of 928 ml autoclaved ZY medium (10 g tryptone, 5 g yeast extract mixed with 925 ml H₂O), 1 mM MgSO₄ (sterile filtered), 1 ml trace metal mix (1000x), 20 ml 5052 solution (50x) and 50 ml NPS (20x). The compositions of mixed solutions are shown in table 2.4.

Table 2.4: Composition of mixing solutions for auto-inducing media.

trace metal mix (1000x)	5052 solution (50x)	NPS (20x)
50 ml 0.1 M FeCl ₃ in 0.1 M HCl (sterile filtered)	25 % (w/v) glycerol	0.5 M (NH ₄) ₂ SO ₄
	2.5 % (w/v) glucose	1 M KH ₄ PO ₄
20 mM CaCl ₂	10 % (w/v) α -lactose	1 M Na ₂ HPO ₄
10 mM ZnSO ₄		
2 mM CoCl ₂		
2 mM CuCl ₂		
2 mM NiCl ₂		
2 mM Na ₂ MoO ₄		
2 mM Na ₂ SeO ₃		
2 mM H ₃ BO ₃		
ad 100 ml H ₂ O		

LB medium

LB medium contained 10 g l⁻¹ tryptone, 10 g l⁻¹ NaCl and 5 g l⁻¹ yeast extract. For preparation of LB agar plates, 15 g l⁻¹ agar was added before autoclaving.

S.O.C. medium

S.O.C. medium was prepared with 20 g l⁻¹ trypton, 5 g l⁻¹ yeast extract and 0.5 g l⁻¹ NaCl. After autoclaving, sterile filtered salt solutions were added to achieve the final concentrations of 10 mM MgSO₄, 10 mM MgCl₂ and 2.5 mM KCl. After addition of sterile filtered 20 mM glucose, S.O.C. medium was aliquoted and stored at -20 °C.

2.1.5 Buffers and stock solutions

Compositions of used buffers and stock solutions are listed in table 2.5.

Table 2.5: Composition of buffers and stock solutions used.

buffer and stock solutions		composition
50x TAE running buffer (pH 8.0)		2 M Tris, 1 M AcOH, 100 mM EDTA
10x SDS-PAGE running buffer		250 mM Tris, 2 M glycine, 10g l ⁻¹ SDS
5x SDS-PAGE loading dye		10% (w/v) SDS , 10 mM β-mercaptoethanol, 200 mM Tris-HCl, 0.05% (w/v) bromphenol blue, 20% (v/v) glycerol
KP _i buffer (pH 7.5)		50 mM potassium phosphate buffer (K ₂ HPO ₄ + KH ₂ PO ₄)
ampicillin, sterile filtered		100 mg ml ⁻¹
carbenicillin, sterile filtered		50 mg ml ⁻¹
DNase I solution		1 mg ml ⁻¹ DNase I, 20 mM Tris-HCl (pH 7.5), 1 mM MgCl ₂ , 50 % glycerol
kanamycin, sterile filtered		50 mg ml ⁻¹
IPTG, sterile filtered		1 M
Coomassie staining solution		10 % AcOH (v/v), 50 % MeOH (v/v), 40 % H ₂ O (v/v), 0.25 % Coomassie brilliant blue G-250 (w/v)
Coomassie decolorizing solution		30 % MeOH (v/v), 10 % AcOH, ad 1 l H ₂ O
lysis and binding buffer	BM3	50 mM KP _i buffer, 300 mM KCl, 0.1 mM PMSF, pH 7.5
	PFOMT	50 mM KP _i buffer, 10 % glycerol, pH 7.5
	MBP-At4CL2, CHS2	50 mM KP _i buffer, 10 % glycerol, 10 mM imidazole, pH 7.5
elution buffer	MBP-At4CL2, CHS2, PFOMT, AtTSM1	50 mM KP _i buffer, 10 % glycerol, 300 mM imidazole, pH 7.5
dialysis buffer	At4CL2-B, CHS2	50 mM HEPES, 5 % glycerol, 100 mM NaCl, 100 μM EDTA, pH 7.5

2.1.6 Bacterial strains

Different chemically competent *E. coli* strains were used for gene cloning and expression listed in table 2.6. Strains were cultivated according to section 2.3.1. Streaked on agar plates, *E. coli* strains were stored at 4 °C for several weeks. For long-time storage at -80 °C, glycerol stocks were prepared by addition of 20 % glycerol to an *E. coli* starter preculture (section 2.3.1).

Table 2.6: *E. coli* strains used for gene cloning and expression.

application	<i>E. coli</i> strain	provider
gene cloning	DH5α	Life technologies, Darmstadt
	DH10B	Life technologies, Darmstadt
gene expression	BL21 (DE3)	Life technologies, Darmstadt
	BL21 (DE3) star	Life technologies, Darmstadt
	T7 Express Competent (High Efficiency)	New England Biolabs, Ipswich (UK)
	M15[pRep4]	Qiagen, Hilden

2.1.7 Plasmids

Plasmids for gene cloning and expression are shown in table 2.7. For testing transformation efficiency (section 2.3.3), pUC19 plasmid ordered from New England Biolabs (Ipswich, UK) was used.

Table 2.7: Plasmids for gene cloning and expression.

variants	gene / donor organism	vector	resistance, features	source
BM3: F87V; F87A/A328V (AV); A74G/F87A/L188Q (GAQ); A74G/F87V/L188Q (GVQ)	<i>CYP102A1</i> mutants / <i>Bacillus megaterium</i>	pET-28a(+)	kanamycin resistance, N-terminal 6xHis-tag, T7 promoter, pBR322 origin	plasmid DNA from Jürgen Pleiß, ITB, Stuttgart
origin: BM3-F87V BM3: A74G/F87V (GV); F87V/L188Q (VQ); L75S/F87V/L188Q (SVQ); L75S/F87V/L188Q (NVQ)	<i>CYP102A1</i> mutant / <i>Bacillus megaterium</i>	pET-28a(+)	kanamycin resistance, N-terminal 6xHis-tag, T7 promoter, pBR322 origin	section 4.3.3

Materials and methods

variants	gene / donor organism	vector	resistance, features	source
origin: BM3-GVQ BM3: A74G/L75S/F87V/ L188Q (GSVQ); A74G/L75N/F87V/L188Q (GNVQ); A74G/F87V/L188Q/A330S (GVQS)	<i>CYP102A1</i> mutant / <i>Bacillus megaterium</i>	pET-28a(+)	kanamycin resistance, N-terminal 6xHis-tag, T7 promoter, pBR322 origin	section 4.3.3
PFOMT	<i>PFOMT</i> / <i>Mesembryanthemum crystallinum</i>	pQE30	ampicillin resistance, N-terminal 6xHis-tag, T5 promoter, ColE1 origin	clone from Thomas Vogt, IPB, Halle
4HPA3H	4HPA3H / <i>Escherichia coli</i>	pET-28a(+)	kanamycin resistance, N-terminal 6xHis-tag, T7 promoter, pBR322 origin	clones from Martin Dippe, IPB, Halle
AtTSM1	<i>at1g67990</i> / <i>Arabidopsis thaliana</i>	pQE30	ampicillin resistance, N-terminal 6xHis-tag, T5 promoter, ColE1 origin	clone from Thomas Vogt, IPB, Halle
no promotor for expression	<i>at3g21240</i> / <i>Arabidopsis thaliana</i>	pENTR™/SD/D-TOPO®	kanamycin resistance, pUC origin	Arabidopsis Biological Resource Center, Columbus, (U.S.A.)
At4CL2	<i>at3g21240</i> / <i>Arabidopsis thaliana</i>	pDEST-N110	ampicillin resistance, N-terminal 6xHis-tag, T7 promoter, pUC origin	section 3.3.1.1
MBP-At4CL2	<i>at3g21240</i> / <i>Arabidopsis thaliana</i>	pDEST-N112-MBP	ampicillin resistance, N-terminal 6xHis-tag, T7 promoter, maltose-binding protein (MBP), pUC origin	section 3.3.1.1

variants	gene / donor organism	vector	resistance, features	source
HvCHS2	<i>HvCHS2</i> / <i>Hordeum vulgare</i>	pBluescript SK(-)	ampicillin resistance, T7 promoter ColE1 origin	clone from David Collinge, university of Copenhagen (DK)
CHS2	<i>HvCHS2</i> / <i>Hordeum vulgare</i>	pET-28a(+)	kanamycin resistance, N-terminal 8xHis-tag, T7 promoter, pBR322 origin	section 3.3.2.1

2.1.8 Synthetic oligonucleotides

Oligonucleotides were specifically designed for partial DNA amplification (section 2.2.2), sequencing or mutagenesis. Primer synthesis and gene sequencing was performed by MWG Eurofins Operon (Ebersberg, <http://www.eurofinsgenomics.de>).

Designed primers were examined using “Sequence Manipulation Suite”. (http://www.bioinformatics.org/sms2/pcr_primer_stats.html). Primer designations and their corresponding sequences are listed in the following tables. For amplification and sequencing, primers are shown in table 2.8.

Table 2.8: Primer sequences of applied oligonucleotides for DNA amplification and sequencing.

primer	sequence of synthetic oligonucleotide: 5'-3'
At4CL2_1fwd	GCCTCCGCGGCGAAACTCAT
At4CL2_2fwd	CCCTTCACCATGACGACACA
At4CL2_1rev	CATACTTCTCCGTCTCCGGC
At4CL2_2rev	ACCCGTCTGTCGGGATGAGA
BM3_1fwd	AAGCGGTGAACAAAGCGATG
HvCHS2_1fwd	ACGGTCAAACGCCTGATGAT
HvCHS2_2fwd	ATCGGCGCTGACCCTGACCA
HvCHS2_1rev	TCCGTA CTCCGACAGAACCT
pENTattL1for	TCGCGTTAACGCTAGCATGGATCTC
pENTattL2rev	ACATCAGAGATTTTGAGACACGGGC
PFOMT_fwd	CATATGGATTTTGCTGTGATGAAGCAGGTC
PFOMT_rev	GAATTCAATAAAGACGCCTGCAGAAAGTG
T7_fwd	TAATACGACTCACTATAGGG
T7_rev	CTAGTTATTGCTCAGCGGT
T7 TOPO_His8fwd	CGAAATTAATACGACTCACTATAG
T7 TOPO_rev	TAGTTATTGCTCAGCGGTGG

Designed oligonucleotides for mutagenesis are given in table 2.9. Already existing modifications of the plasmid are printed in blue. Red colored nucleotides represent desired modifications for the preparation of BM3-variants. Unless otherwise noted, primer concentration was 10 pmol μl^{-1} .

Table 2.9: Oligonucleotides designed for mutagenesis. Red colored nucleotides represent desired modifications for the preparation of BM3-variants. Already existing modifications of the plasmid are printed in blue.

primer	sequence of synthetic oligonucleotide: 5'-3'	mutation
HisTag+2_fwd	GATATACCATGGGCAG- CAGCCATCATCATCATCATCACA	2x HisTag elongation of HvCHS2
HisTag+2_rev	TGTGATGATGATGATGATGATGATGATGGCTGCTGCC CATGGTATATC	
BM3_74G_fwd	TTGATAAAACTTAAGTCAAGGTCTTAAATTT- GTACGTGATTT	A74G of BM3-F87V
BM3_74G_rev	AAATCACGTACAAATTTAAGACCTT- GACTTAAGTTTTTATCAA	
BM3_188Q_fwd	TGGATGAAGCAATGAACAAGCAGCAGCGAG- CAAATCCAGACGA	L188Q of BM3-F87V
BM3_188Q_rev	TCGTCTGGATTTGCTCGCTGCTGCTTGTTCATT- GCTTCATCCA	
BM3_L75N_fwd	CTTAAGTCAAGCGAATAAATTTGTACGTGA	L75N of BM3-F87V
BM3_L75N_rev	TCACGTACAAATTTATTCGCTTGACTTAAG	
BM3_74G+L75N_fwd	CTTAAGTCAAGGTAATAAATTTGTACGTGA	L75N of BM3-GVQ
BM3_74G+L75N_rev	TCACGTACAAATTTATTACCTTGACTTAAG	
BM3_L75S_fwd	CTTAAGTCAAGCGTCTAAATTTGTACGTGA	L75S of BM3-F87V
BM3_L75S_rev	TCACGTACAAATTTAGACGCTTGACTTAAG	
BM3_74G+L75S_fwd	CTTAAGTCAAGGTTCTAAATTTGTACGTGA	L75S of BM3-GVQ
BM3_74G+L75S_rev	TCACGTACAAATTTAGAACCCTTGACTTAAG	
BM3_330S_fwd	TATGGCCAAGTCTCCTTCGTTTTCCCTAT	A330S of BM3-GVQ
BM3_330S_rev	ATAGGGAAAAAGAAGGAGCAGTTGGCCATA	

2.2 Methods in molecular biology

2.2.1 Determination of DNA concentration

DNA concentration was measured by spectrophotometric estimation using Eppendorf Bio Photometer Plus (Hamburg). Difference spectra of 2 μl plasmid DNA dissolved in 58 μl H_2O were measured in comparison to a cuvette containing 60 μl H_2O (blank). Concentration and purity of the nucleic acid was determined according to the instruction manual.

2.2.2 Polymerase chain reaction (PCR)

PCR was used for partial amplification of DNA to verify the success of plasmid transformation in chemical competent *E. coli* cells (section 2.3.3) and for site-directed mutagenesis of genes

and plasmids (section 2.2.2.2). Primers were designed and synthesized as described in section 2.1.8.

2.2.2.1 Colony PCR

After plasmid transformation (section 2.3.3), a single colony was picked by a pipette tip and used as a template for colony PCR. Water was used as a control. 20 μ l reaction mixture contained 0.2 mM dNTPs mix, 4 pmol of forward and reverse primer, 0.5 U DreamTaq DNA polymerase and DreamTaq buffer.

Amplification was achieved after initial denaturation (3 min at 95 °C) within 25 repetitions of the following cycle: denaturation for 30 s at 94 °C, annealing for 30 s at 60 °C and elongation at 72 °C. Depending on plasmid length, elongation time was modified for the corresponding genes: 1:40 min (*At4CL2* and *HvCHS2*), 3:30 min (*BM3*), 1:30 min (*PFOMT*). Final elongation for 10 min at 72 °C completed the colony PCR reaction.

2.2.2.2 PCR site-directed mutagenesis

QuikChange II Site-Directed Mutagenesis Kit (Agilent, Waldbronn) was used according to the instruction manual and designed oligonucleotides (table 2.9) were used for site-directed mutagenesis of the corresponding gene or plasmid.

2.2.3 Plasmid DNA isolation

Plasmid DNA was isolated from *E. coli* preculture (section 2.3.1) according to manufacturer's instructions of the QIAGEN Plasmid Mini Prep Kit (Qiagen, Hilden).

2.2.4 Restriction of plasmid DNA

For selective cleavage of the *HvCHS2* gene out of the pBluescript SK(-) plasmid or for linearization of the pET-28a(+) vector, 0.15 μ g μ l⁻¹ plasmid DNA, a double digest reaction was achieved using 0.5 U μ l⁻¹ BamHI and 1 U μ l⁻¹ HindIII. The restriction assay was performed in BamHI buffer and incubated at 37 °C for 14 h. Subsequently, the enzymes were inactivated by incubation of the whole mixture at 80 °C for 15 min. Double digestion mixture were analyzed by agarose gel electrophoresis (section 2.2.8).

2.2.5 Isolation, purification and verification of DNA fragments

After agarose gel electrophoresis, plasmid DNA fragments were isolated and purified according to manufacturer's instructions of the Invisorb® Fragment CleanUp Kit (STRATEC Molecular GmbH, Berlin). DNA was verified by sequencing using the appropriate primers (section 2.1.8).

Linearized vector was selectively precipitated after double digest mixture. An equal volume of phenol/ chloroform/ isoamyl alcohol solution was directly added to the restriction mixture, intensely mixed for 20 s and centrifuged at room temperature for 5 min at 14,000 x g. The aqueous supernatant was added to an equal volume of chloroform, subsequent mixed and centrifuged as described above. For precipitation, 100 μ l of the aqueous supernatant was added to 800 μ l isopropyl alcohol and 100 μ l 3 M of KOAc solution. The mixture was incubated for 10 min on ice and then centrifuged for 15 min at 8,000 x g and 4 °C. The supernatant was carefully removed and the resulting cell pellet was washed twice with 200 μ l 70 % ice-cold EtOH and centrifuged as above. The remaining solvent was removed using a speed vac.

2.2.6 DNA ligation reaction

The ligation of the *HvCHS2* gene into the linearized vector pET-28a(+) (section 2.2.4) was achieved with a T4 DNA ligase reaction. A 20 μ l reaction mixture contained 0.15 U μ l⁻¹ T4 DNA ligase, T4 DNA ligase buffer and 5 ng μ l⁻¹ *HvCHS2* gene fragment and linearized vector, respectively, and was incubated at 4 °C overnight. 5 μ l of ligation assay were directly used for transformation into chemically competent DH5 α cells as described in section 2.3.3.

2.2.7 Gateway® cloning system

For restriction and cloning the provided *At4CL2* gene fragment from the entry-vector pENTR™/SD/D-TOPO® into the Gateway™ destination vector pDEST-N112-MBP, Gateway® LR Clonase® II enzyme mix (Invitrogen, Life technologies, Darmstadt) was used according to the instruction manual.

2.2.8 Agarose gel electrophoresis

Agarose gels were used to visualize gene fragments and to analyze the success of digestion and transformation. Depending on the length of the DNA fragment, the concentration of agarose in 1x TAE running buffer varied from 0.8 % to 1.5 %. The resulting suspension was boiled up for dissolving by using a microwave. After cooling down to 40 °C, ethidium bromide (0.5 μ g ml⁻¹) was added to visualize DNA fragments by UV light. The mixed solution was poured in a chamber with comb for polymerization. The agarose gel was loaded with samples containing DNA Loading Dye and with 5 μ l Gene-Ruler™ 1 kb DNA Ladder as a molecular weight marker. Separation of DNA fragments was achieved by running the gel at 100 V in a horizontal gel chamber (Biometra Compact XS/S, Göttingen) in 1xTAE buffer. A BioDocAnalyze (BDA) live system including BDA analysis software (Biometra, Göttingen) was used for documentation.

2.3 Microbiological methods

2.3.1 Cultivation of *E. coli* cells

E. coli strains (section 2.1.6) were streaked onto LB agar plates containing the appropriate antibiotic and incubated overnight (14 h) at 37 °C. One single colony was used to inoculate 5 ml LB medium (section 2.1.4). The culture was incubated overnight at 37 °C and was shaken at 200 rpm. The resulting preculture was used for long term storage at -80 °C (section 2.1.6), plasmid preparation (section 2.2.3) or to inoculate growth media (section 2.4.1) in case of strains applied for gene expression.

2.3.2 Preparation of chemically competent cells

Chemically competent *E. coli* cells were prepared according to the method of Inoue (1990) [71]. 50 ml of LB medium was inoculated with the preculture and incubated at 160 rpm and 37 °C until an optical density at 600 nm of 0.4-0.6 was reached. The culture was centrifuged for 10 min at 5,000 x g and 4 °C. Supernatant was removed. Cell pellet was resuspended in 20 ml 0.1 M CaCl₂ solution and stored on ice for 30 min. The suspension was again centrifuged as described above and then resuspended in 5 ml 0.1 M CaCl₂ solution and 900 µl of 87% sterile filtered glycerol. Suspension of chemically competent *E. coli* cells was aliquoted (50 µl) and stored at -80 °C. Transformation efficiency was tested using 10 pg test plasmid (pUC19) for transformation into one aliquot according to section 2.3.3. Depending on the *E. coli* strain, transformation efficiency reached 1-3 x 10⁷ cfu µg⁻¹.

2.3.3 Transformation of plasmid DNA into chemically competent

***Escherichia coli* cells**

50 µl aliquots of chemical competent *E. coli* cells (section 2.3.2), were incubated for 5 min on ice. After addition of 100 ng plasmid DNA (unless otherwise noted), the suspension was carefully mixed with a pipette tip and incubated for 10 min on ice. Heat shock transformation was achieved by incubation of the mixture for 30 s at 42 °C in a water bath and subsequently fast ice water quenching for 5 min. 250 µl S.O.C. medium (section 2.1.4) was added and incubated at 37 °C at 200 rpm for 1 h. Subsequently, 200 µl of the culture was streaked on a LB agar plate containing the appropriate antibiotic for selection of successfully transformed cells. The plate was incubated at 37 °C for 14 h.

2.4 Protein methods

2.4.1 Gene expression

Using auto-inducing medium (section 2.1.4), 5 % preculture (v/v) (section 2.3.1) was used to inoculate the main culture. Gene expression was achieved by incubation at 37 °C and 200 rpm for 24 h.

For expression in LB medium (section 2.1.4), 1 % starter culture (v/v) (section 2.3.1) was used for inoculation of the main culture. Cells were grown at 37 °C and shaken at 200 rpm until an optical density at 600 nm of 0.8-1.0 was reached.

BM3 gene expression was induced by adding IPTG in a final concentration of 0.35 mM to the culture medium. Subsequently, the culture was incubated at 25 °C and 160 rpm for 14 h. OMTs, At4CL2 and CHS, expression was induced with a final concentration of 1 mM IPTG at 25 °C for 14 h and shaking at 180 rpm.

2.4.2 Cell lysis by sonication

After gene expression (section 2.4.1), the culture was centrifuged at 4 °C and 8,000 x g for 20 min. The supernatant was removed and the cell pellet was resuspended in 5 ml g⁻¹ lysis buffer containing 100 µg ml⁻¹ lysozyme and 10 µg ml⁻¹ DNase I solution (section 2.1.5). After 30 min incubation on ice, the cell lysis was supported by sonication using a Bandelin electronic SonoPuls HD 3200 for 8 x 15 s at 70 % amplitude (approximately 2200 kJ) under ice cooling. The lysate was centrifuged at 10,000 x g and 4 °C for 30 min. The supernatant was used for purification of the enzyme (section 2.4.3) and/or for *in vitro* enzymatic reaction (section 2.5). Insoluble fraction were tested for inclusion bodies of the expressed proteins by resuspending 100 mg cell pellet in 1 ml urea solution (8 M) and heating at 95 °C for 10 min. The suspension was centrifuged at 14,000 x g for 1 min and the supernatant was used for SDS-PAGE (section 2.6.2.3).

2.4.3 Enzyme purification

The applied expression vectors (section 2.1.7) exhibit a N-terminal histidine tag fused to the synthesized proteins which allows Immobilized Metal Ion Affinity Chromatography (IMAC) for purification. The supernatant of cell lysis (section 2.4.2) was loaded onto a previously equilibrated HisTrap column (HisTrapTM HP, 1 ml, 7 x 25 mm, GE Healthcare, Buckinghamshire, UK) according to instruction manual with a flow rate of 0.3 ml min using a peristaltic pump. The loaded column was initially washed with 5 ml lysis buffer followed by a washing step with

10 ml washing buffer (10 % elution buffer + 90 % lysis buffer (v/v)). For elution, 15 ml of a buffer mixture containing 90 % elution buffer and 10 % lysis buffer (v/v) was used. The eluate was collected in 1 ml fractions and analyzed via protein detection methods (section 2.6.2). Appropriate protein fractions were pooled and dialyzed under stirring in 1.5 l of the respective dialysis buffer at 4 °C overnight using a dialysis membrane (ZelluTrans/Roth (Roth, Karlsruhe)) according to the instruction manual. Resulting enzyme solution was aliquoted and stored at -80 °C.

2.5 Enzymatic reactions and preparative approaches

Enzymatic reactions were performed *in vitro* for activity measurement and for characterization of catalytic activity. Substrate conversion was analyzed by two-times extraction of 1 ml of the assay using 500 µl of EtOAc. EtOAc fractions were pooled and the extraction solvent was removed *in vacuo* using Eppendorf Speed Vac Concentrator Plus 5305 (Hamburg). After re-suspension in 200 µl MeCN, extracts were measured via HPLC and UHPLC-MS/MS. *In vivo* biotransformations were performed in living whole-cells of *E. coli* as described in section 2.5.3.

2.5.1 Enzymatic activity assays

Compositions and conditions for small scale (up to 1 ml) activity assays are given in table 2.10. Crude extracts were prepared from lysed cell pellet according to section 2.4.2 and purified enzyme (section 2.4.3) was used for the assay. For prescreening, protein extraction was achieved using 150 µl B-PerII reagent mixed with 50 µl DNase for 1.5 ml bacterial culture following manufacturer's instruction. In table 2.10, the assay conditions for the most relevant enzymes are listed.

Table 2.10: Composition and incubation conditions of enzymatic activity assays.

	At4CL2	BM3	CHS2	OMT
buffer system	100 mM Tris-HCl buffer (pH 7.5), 2 mM MgCl ₂	50 mM Tris-HCl buffer (pH 7.5)	100 mM HEPES buffer (pH 7.0)	50 mM KPi buffer (pH 7.5), 250 μM MgCl ₂
enzyme concentration	10 μg At4CL2	0.4-1.0 μM BM3	10 μg CHS	1.0 μM PFOMT, AtTSM1
substrate (most relevant)	200 μM caffeic acid	200 μM Nar	20 μM caffeoyl-CoA	20 μM ED
co-substrates and cofactors	200 μM CoA, 2.5 mM ATP	100 μM NADPH	15 μM malonyl-CoA	1 mM SAM
cofactor regeneration system	no regeneration	14 U ml ⁻¹ glc-6-P DHG, 5 mM glc-6-P	no regeneration	no regeneration
final volume	200 μl	1000 μl	1000 μl	50 μl
incubation conditions	25 °C, 90 min	25 °C, 200 rpm, 1000 min	30 min, 37 °C, addition of 200 μl Tris-HCl pH 8,0 (1M), incubation for further 15 min	37 °C, 10 min

Further oxidation systems of purified enzymes were not able to convert Nar into ED (table 2.11). Enzyme activity assays were performed *in vitro* with a separate reductase system of either FAD or bovine adrenodoxin (Adx) and adrenodoxin reductase (AdR) to provide the electron transfer.

Table 2.11: Assay conditions of inactive oxidation systems for the substrate Nar.

	CYP106A2 (<i>B. megaterium</i>)	CYP109D1, CYP264A1, CYP260A1, CYP260B1 (<i>S. cellulosum</i>)	2-HBP (<i>P. azeleica</i>)
buffer system	20 mM KPi buffer (pH 7.5)		20 mM KPi buffer (pH 7.5)
enzyme concentration	1 μM CYP		10 μg 2-HBP
substrates	100 μM substrate		200 μM substrate
co substrates and cofactors	100 μM NADPH, 1 mM MgCl ₂		300 μM NADH
cofactor regeneration system	5 mM glc-6-P, 1 U glc-6-P DHG		no regeneration system
electron transfer system	3 μM AdR, 20 μM Adx		8 μM FAD
final volume	250 μl		1000 μl
incubation conditions	30 °C, 300 rpm, 60 min		30 °C, 30 min

2.5.2 Preparative substrate conversion

For a preparative scale of 20 μmol expected product, standard assays, described in section 2.5.1, were scaled up to an assay volume of 10 ml and were performed in a 100 ml flask and incubated overnight. Enzymatic product of preparative conversion by BM3-GVQ was isolated using semi-preparative HPLC (section 2.6.3.1).

For a preparative scale of expected 10 μmol CoA ester, At4Cl2 standard assay was scaled up to an assay volume of 20 ml, performed in a 100 ml flask and incubated overnight: 40 μmol HCA was preincubated with 5.1 μmol CoA, 2.5 μmol ATP and 500 μg ligase. Fresh CoA (5.1 μmol), ATP (2.5 μmol) and protein (500 μg ligase) were added to the mixture after 5 h preincubation and further incubated overnight. Unconverted acids were extracted from the mixture using 2 times 10 ml diethyl ether. CoA esters were isolated by purification over Solid Phase Extraction (SPE) cartridge (CHROMABOND® C₁₈ ec, 1 g, 60 Å, 45 μm , Macherey-Nagel, Düren). The cartridge was previously conditioned with 10 ml of MeOH, following by H₂O and finally 4 % NH₄OAc solution. 400 mg NH₄OAc were added to the extracted mixture and loaded onto a cartridge. After washing with 10 ml 4 % NH₄OAc solution, CoA esters were eluted using 10 ml water under spectrometric control (section 2.6.3.4). The solvent was removed by freeze-drying and the product was stored at -20 °C.

2.5.3 Living whole-cell biotransformation

Living whole-cell biotransformation was performed in LB medium or AI medium (section 2.1.4). The AI medium was inoculated with 5 % (v/v) preculture (section 2.3.1) and substrate (100 mM dissolved in DMSO) was added to a final concentration of 200 μM . Culture medium was incubated at 37 °C and 200 rpm for 25 h. For conversion in LB medium, the cells were grown at 37 °C and 180 rpm until an OD₆₀₀ of 0.8-1.0 was reached. Afterwards gene expression was induced with 1 mM IPTG. After 3 h incubation time at the same conditions, substrate was added to the medium to a final concentration of 200 μM and the mixture was further incubated for 16 h. The alteration of cell density, gene expression and substrate conversion were analyzed at defined time points. Therefore, samples were taken from the main culture. Optical density was determined at 600 nm. For the analysis of protein biosynthesis, 1 ml of culture broth was centrifuged at 14,000 x g for 10 minutes. The resulting cell pellet was used for analyzing protein expression via SDS-PAGE (section 2.6.2.3) by using 150 μl B-PerII reagent mixed with 50 μl DNase following manufacturer's instruction.

Substrate conversion was analyzed by two-times extraction of 1 ml supernatant of the centrifuged culture with 500 μl of EtOAc containing 1 % HCOOH. EtOAc fractions were pooled and

the extraction solvent was removed *in vacuo*. After resuspending in 200 μl MeCN, the extracts were measured via HPLC and UHPLC-MS/MS (section 2.6.3).

2.6 Analytics

2.6.1 H_2O_2 determination (HRP *o*-dianisidine assay)

Horseshoe peroxidase (HRP) catalyzes the reaction of H_2O_2 with the chromogenic *o*-dianisidine under acidic conditions (Fig. 2.1). The resulting pink-colored chromophore was detected at 540 nm.

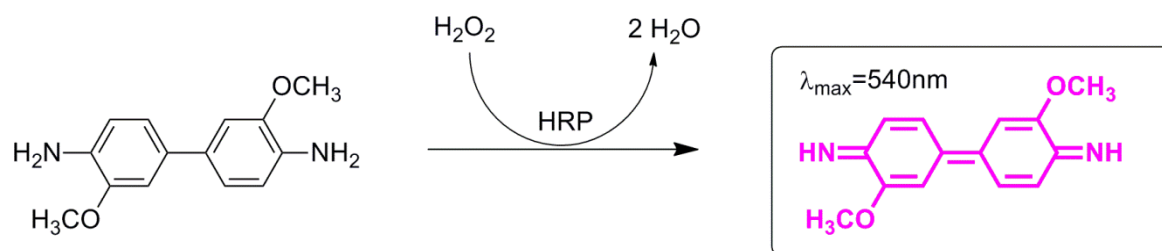


Fig. 2.1: Reaction of H_2O_2 and *o*-dianisidine catalyzed by HRP forming a pink chromophore.

100 μl reagent solution containing 2.5 U ml^{-1} HRP and 0.1 mg ml^{-1} *o*-dianisidine hydrochloride dissolved in 50 mM NaOAc were added to 50 μl assay or calibration solution and incubated for 5 min at 25 $^\circ\text{C}$. The enzymatic reaction was stopped by adding 100 μl of 12 N H_2SO_4 solution. The whole mixture was centrifuged for 2 min at 14,000 $\times g$. 125 μl of the supernatant were measured at 540 nm. Quantification of H_2O_2 was calculated using an external calibration curve in the range of 60 μM and 600 μM . For determination of H_2O_2 within the assay, triplicates of the HRP *o*-dianisidine assay were performed.

2.6.2 Protein detection

Protein was detected via UV spectroscopy and quantified by Bradford assay [72] or CO difference spectra for CYPs [73]. SDS-PAGE was used for qualitative characterization of the protein composition in solution.

2.6.2.1 Protein concentration determination (Bradford assay)

Protein concentration was determined photometrically using Roti®-Quant as described in instructors manual and the mixture was measured at 595 nm. An external BSA calibration curve between 0 and 2 mg ml^{-1} was used for estimation of protein content according to linear regression: $\text{abs} = 0.049 \times [\text{protein}] \times \text{Df}$.

abs = absorption; Df = Dilution factor

2.6.2.2 P450 concentration determination from CO difference spectra

For calculating the active cytochrome P450 concentration of the lysate, CO difference spectra were recorded on a UV/Vis spectrometer (Jasco V-560): 100 µl cell lysate was added to 1500 µl 50 mM KPi buffer containing 300 mM KCl (pH 7.5) und mixed carefully. Diluted lysate was reduced by adding 3 mg sodium dithionite and was mixed carefully by tube inverting. Mixture was separated into two cuvettes (700 µl) and a base line at 400 nm to 500 nm was measured. One of the cuvette was aerated with CO under the fume hood for 30 s and sealed. Immediately, a difference spectrum of the aerated and the non-aerated solution was measured and used for calculation of active P450 enzyme according to the law of Lambert-Beer:

$$c(\text{P450}) = \frac{\Delta A_{450-490} \times Df}{\epsilon \times d}$$

d= 1 cm, ϵ = 91 (mM cm⁻¹)

2.6.2.3 Sodium dodecyl sulfate-polyacrylamide gel electrophoresis (SDS-PAGE)

SDS-PAGE was used to visualize proteins and to analyze the success of overexpression and purification. The standard procedure was performed according to Laemmli [74]. 5 µl PageRuler™ Plus Prestained Protein Ladder was used as a molecular weight marker. Depending on the molecular weight of the expected proteins, polyacrylamide content in the running gel differed in the range of 10 - 14 %. In the stacking gel, 4 % polyacrylamide was polymerized. Samples were prepared in a final volume of 20 µl containing 5 µg protein of soluble protein fraction after cell lysis (section 2.4.2) and SDS-PAGE loading dye. Sample mixture was heated for 5 min at 95 °C for denaturation before running SDS-PAGE at 30 mA in the stacking gel and at 60 mA for separation in the running gel in a vertical gel chamber Eco-Mini (Biometra Göttingen). A BioDocAnalyze (BDA) live system including BDA analysis software (Biometra, Göttingen) was used for documentation.

2.6.3 Analytics of substances

Full range UV/Vis spectra of all compounds used were scanned on a Jasco V-560 spectrometer. Reference substances were used as standards for analytics (Fig. B 11).

2.6.3.1 Chromatography (HPLC)

HPLC was performed for quantification and preparative separation of the product after enzymatic conversion visualized via photodiode array detector in the range of 200 and 400 nm.

Column and conditions depending on the substance class and application are summarized in table 2.12. For quantification calibration curves using defined concentrations of standards were prepared (Fig. B 11). The area under the curve (AUC) of HPLC at 280 nm was compared to a similarly treated control with an empty vector and the relative compound formation was calculated. For chiral HPLC measurement, the samples and references were dissolved in isopropyl alcohol. UHPLC-MS/MS technique, realizing higher resolution of chromatography and targeted fragmentation of selected compounds, was used for identification of the products. The positive ion electrospray ionization (ESI) mass spectra and the collision-induced dissociation (CID) mass spectra were obtained from a TSQ Quantum Ultra AM system equipped with a hot ESI source (electrospray voltage 3.0 kV, sheath gas: nitrogen; vaporizer temperature: 100 °C; capillary, temperature: 300 °C). The MS system is coupled with a UHPLC-system Accela 1250 (ThermoFisher Scientific). The CID mass spectra were measured with a collision energy of 15 eV (collision gas: argon; collision pressure: 1.5 mTorr). Semi-preparative HPLC was applied to purify the product from the reaction mixture after preparative substrate conversion (section 2.5.2). The solvent was removed by freeze-drying and the product was analyzed according to section 2.6.3.

Table 2.12: Columns and conditions and (U)HPLC techniques applied.

application	analysis of flavonoids	analysis of chiral flavonoids	analysis of CoA esters	UHPLC-MS/MS analysis	semi-preparative purification
column	YMC-Pack B&D, ODS-A, 150 x4.6 mm, 5 µM	Daicel column Chiralpak, AS-H, 250 x 4.6 mm, 5 µM	YMC-Pack B&D, ODS-A, 150 x 4.6 mm, 5 µM	Synchronis C18, RP18 50 x 2.1 mm, 1,7 µm,	YMC-Pack B&D, ODS-A, 150 x 10 mm, 5 µM, 12 nm
method	gradient	isocratic	gradient	gradient	gradient
mobile phase	95:5 (H ₂ O:MeCN each containing 0.2 % HCOOH) to 5:95 within 20 min to 0:100 stayed for 5 min	60 % hexane/ 40 % isopropyl alcohol, 30 min, 25 °C	95:5 (H ₂ O containing 0.5 % H ₃ PO ₄ :MeCN) to 5:95 within 20 min to 0:100 stayed for 5 min	85:15 (H ₂ O:MeCN each containing 0.2 % HCOOH) to 60:40 within 30 min to 0:100 stayed for 10 min	95:5 (H ₂ O:MeCN each containing 0.2 % HCOOH) to 5:95 within 20 min to 0:100 stayed for 5 min
flow	0.5 ml/min	0.5 ml/min	0.5 ml/min	150 µl/min	3.8 ml/min
injection volume	5 µl	10 µl	5 µl	1 µl	20 µl

For flavonoids bearing less than three hydroxyl groups, GC-MS was used instead of UHPLC-MS. GC/EI mass spectra were obtained from a GCMS-QP2010 (High-End Gas Chromatograph-Mass Spectrometer) equipped with a 70 eV electron-impact ionization, a source temperature of 200 °C, and a ZB-5MS column (Zebron, 30 m x 0.25 mm x 0.25 µm). Injector

temperature was 220 °C by applying an injection volume of 1 µl and a splittless injection. A temperature program was established starting from 60 °C for 1 min, ramping at 10 K min⁻¹ till 300 °C and finally heating for 5 min with a helium flow rate of 1 ml min⁻¹. The scan rate for mass spectra in the range of 40-500 u was 1000 u s⁻¹. For compound identification, authentic standards, if available, were compared with the samples to verify compound identity.

2.6.3.2 MS spectrometry

FINNIGAN MAT TSQ 7000 using ESI voltage of 70 eV was used for MS analysis.

High resolution mass spectrometry (HR-MS) was performed using Bio Apex 70eV with ESI injection technique and Fourier transformation of ion cyclotron resonance (FT-ICR) MS. The positive and negative ion high resolution ESI mass spectra were obtained from a Bruker Apex III Fourier transform ion cyclotron resonance (FT-ICR) mass spectrometer (Bruker Daltonics, Billerica, USA) equipped with an Infinity™ cell, a 7.0 Tesla superconducting magnet (Bruker, Karlsruhe, Germany), an RF-only hexapole ion guide and an APOLLO electrospray ion source (Agilent, off axis spray). Nitrogen was used as drying gas at 150 °C. The sample solutions were introduced continuously via a syringe pump with a flow rate of 120 µl h⁻¹. All data were acquired with 512 k data points and zero filled to 2048 k by averaging 32 scans.

2.6.3.3 NMR spectroscopy

VARIAN UNITY 400 (¹H: 399.94 MHz, ¹³C: 100.57 MHz) and a VARIAN VNMRs 600 (¹H: 599.83 MHz, ¹³C: 150.84 MHz) were used for measurement of a ¹H-NMR and ¹³C-NMR, ³¹P-NMR and 2d-NMR (COSY, TOCSY, HSQC, HMBC, ROESY) spectra of substrates, products and available references. Flavonoids were dissolved in deuterated acetone (¹H: 2.057 ppm) including tetramethylsilane (¹H: 0 ppm) as internal standard. CoA esters were dissolved in deuterated water (¹H: 1.55 ppm).

2.6.3.4 UV-Vis Spectroscopy

CoA ester formation was determined by a wave length shift using absorbance difference measurement and for product verification of CoA esters at selected wave length according to Meng *et al.* [75] via SpectraMax M5 Multi-Mode Microplate Reader.

2.6.4 Computer modeling and docking

2.6.4.1 BM3-GVQ

The three dimensional protein model of the BM3 variant GVQ was created using MOE (Molecular Operating Environment) [76]. Based on the X-ray structure of the wild-type enzyme (protein data bank-code: 1bu7), mutations were introduced and crystallized water molecules removed. A short (475 ps) molecular dynamic (MD) simulation with YASARA 2 force field [77] was done using the MD refinement function of YASARA (Yet Another Scientific Artificial Reality Application) [78]. The quality of the model was validated via Ramachandran plot of MOE and PROCHECK [79]. Heme was bound to oxygen in SYBYL [80] to create a transition state of the reaction. The model was energy minimized by MOE (Amber12:EHT[81], born solvation [82]).

Nar structures of both configurations and their conformers were constructed in MOE and minimized with the MMFF94x force field [83].

GOLD Suite v5.1 (Genetic Optimization for Ligand Docking) [84, 85] docking studies were performed at a radius of 20 Å to the binding pocket (center: backbone oxygen of A264) with 5 flexible side chains (rotamer library) in the active site: S72, L75, V87, Q188 and L437. 20 protein-ligand complexes were created and valued using GOLDScore.

2.6.4.2 AtTSM1

Analogous to the three-dimensional structure of BM3-GVQ (section 2.6.4.1), a homology model of AtTSM1 was created based on the x-ray structure of PFOMT (pdb-code: 3C3Y [86]) as a template using YASARA [77, 78]. The quality of the model was proved via PROCHECK [79]. The docking of the ligands within the active site of the model was realized using PLANTS [87, 88]. 10 docking poses were generated with flexible side chains (rotamer library) in the active site of the appropriate protein: for PFOMT S72, Y51, M52, W184 and F198; and Lys17, Glu49, M50, W180, F181 and His194 for AtTSM1. Generated docking poses were elected due to the lowest distance of the methyl group of SAM to the receptor hydroxyl group of the substrate.

3 Chapter I: Precursor-directed biosynthesis of flavonoids

3.1 Introduction

The biosynthesis of flavonoids in plant secondary metabolism of plants is well-investigated since several decades [89–92]. This phenylpropanoid pathway is starting from L-phenylalanine – a product from the shikimate pathway. The amino acid is converted over three different enzymatic steps into 4-coumaroyl-CoA (Fig. 3.1).

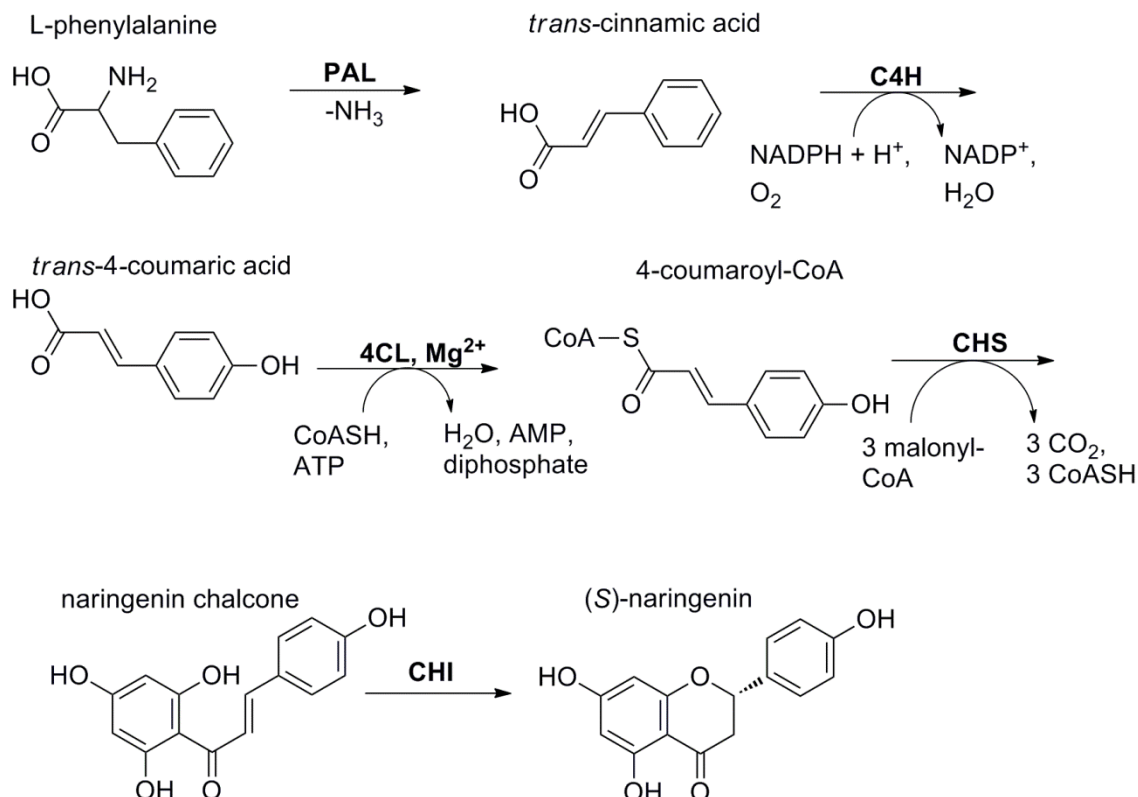


Fig. 3.1: Phenylpropanoid pathway. The conversion starts with L-phenylalanine that is produced in the shikimate pathway. L-phenylalanine ammonia lyase (**PAL**) catalyzes the conversion into ammonia and *trans*-cinnamic acid which is subsequently hydroxylated to *trans*-4-coumaric acid catalyzed by *trans*-cinnamic acid 4-hydroxylase (**C4H**). The activation into the thioester is catalyzed by 4-coumarate:CoA ligase (**4CL**) and requires coenzyme A (CoASH) and ATP. The resulting ester is elongated with three units of malonyl-CoA and cyclized into naringenin chalcone by a chalcone synthase (**CHS**). The final stereospecific ring closure is catalyzed by the chalcone isomerase (**CHI**) forming the (2S)-flavanone naringenin.

The thioester formation from hydroxycinnamic acid (HCA) and coenzyme A (CoASH or CoA) depends on ATP, Mg^{2+} and is catalyzed by the 4-coumarate: CoA ligase (4CL). The common flavonoid skeleton consisting of three rings is constructed by the elongation of 4-coumaroyl-CoA with three units of malonyl-CoA, following by the cyclization and the aromatization into the chalcone catalyzed by the chalcone synthase (CHS). Finally, the stereospecific ring-closure into the (2S)-flavanone is obtained by a chalcone isomerase (CHI). The basic struc-

ture of (*S*)-naringenin is decorated afterwards by hydroxylation, prenylation, methylation or glycosylation catalyzed by further enzymatic reactions forming the enormous variety of flavonoids with diverse features. Typical products of this biosynthetic pathway are for example catechines, which are prominent for their astringent taste. They are found in unfermented green tea but occur also in red wine and cacao [4], or anthocyanins which are responsible for flower pigmentation next to betalains and carotenoids [27].

Within the CHS reaction (Fig. 3.2), the condensed malonyl-CoA units are converted into acetyl extender units by decarboxylation, yielding the trihydroxybenzene structure of ring A. Depending on the substitution of the starter unit hydroxycinnamoyl-CoA (HCA-CoA), different chalcones can be produced. The required malonyl-CoA is synthesized from acetyl-CoA by carboxylation catalyzed by acetyl-CoA carboxylase (ACC). It is also the initializing step of the fatty acid biosynthesis that is ubiquitous within biological systems.

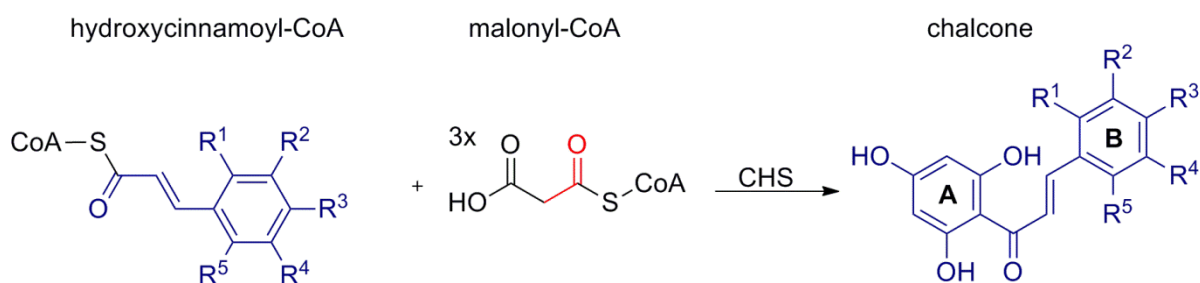


Fig. 3.2: Scheme of the CHS-catalyzed condensation reaction. The hydroxycinnamoyl-CoA used determines the substitution pattern of ring B (blue), the elongating acetyl units of malonyl-CoA build ring-A (red) after cyclization and aromatization.

4-Coumaroyl-CoA is the major substrate for most CHS which form naringenin chalcone. However, some of the CHS enzymes are able to accept other HCA-CoA esters such as caffeoyl-CoA or feruloyl-CoA [93], forming the corresponding eriodictyol chalcone (EDCh) and homoeriodictyol chalcone (HEDCh), respectively, e.g.: CHS2 from *Hordeum vulgare*. The gene is expressed in response to UV light and pathogene attack [94]. Moreover, this enzyme reveals a substrate preference for caffeoyl-CoA or feruloyl-CoA ($K_m = 0.001$ mM) over the common substrate 4-coumaroyl-CoA ($K_m = 0.002$ mM) [94]. Thus, further decoration steps like 3'-hydroxylation of Nar to achieve ED catalyzed by the membrane-bound flavonoid-3' hydroxylase and consequently the 3'-O-methylation forming HED catalyzed by 3'OMT can be replaced by the corresponding precursor caffeoyl-CoA and feruloyl-CoA (Fig. 3.3). Hence, the difficult biocatalytic steps of the pathway to achieve ED and HED from Nar are dispensable.

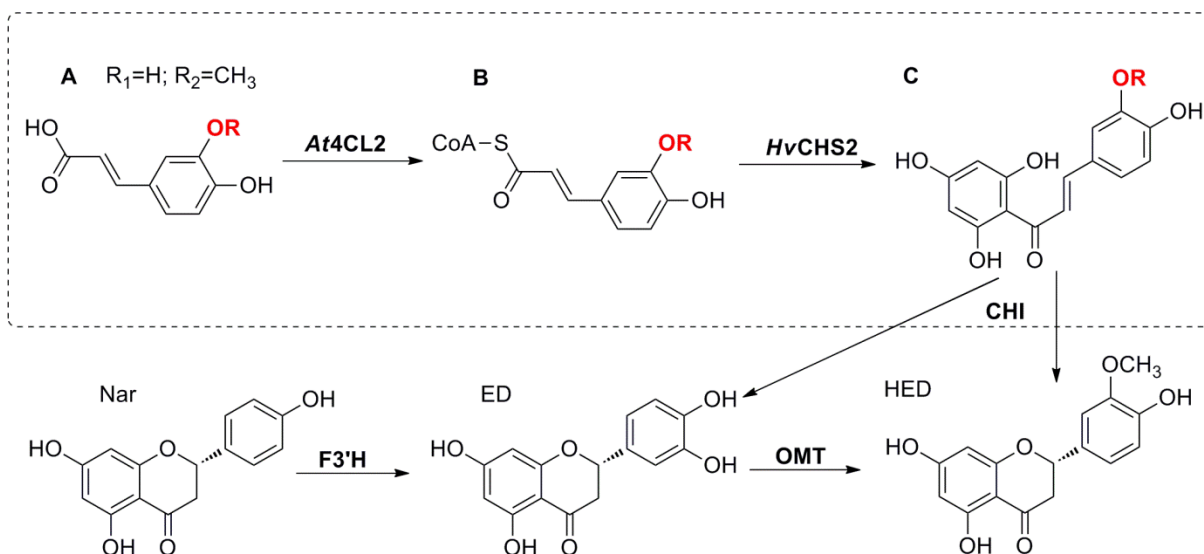


Fig. 3.3: Schematic proposal of a modified biocatalytic pathway for the synthesis of (H)ED (framed). (A) Caffeic acid (R=H) and ferulic acid (R=CH₃) are used as precursor for the enzymatically catalyzed synthesis of ED and HED, respectively. 4-Coumarate:coenzyme A ligase from *Arabidopsis thaliana* (At4CL2) catalyzes the activation of the HCA precursor (A) forming the thioester caffeoyl-CoA and feruloyl-CoA (B). A chalcone synthase from *Hordeum vulgare* (HvCHS2) accepts both thioesters as substrates for the biocatalytic synthesis of EDCh and HEDCh (C), respectively [94]. This modified biocatalytic pathway to HED could replace the hydroxylation step of Nar which is naturally catalyzed by a flavonoid 3' hydroxylase (F3'H) and the methylation step catalyzed by an O-methyltransferase (OMT).

Caffeic acid and ferulic acid are suitable starting materials for the production of ED and HED: the purchasing price of caffeic acid averages 2.8 € g⁻¹ (Sigma Aldrich catalogue from October 21, 2014) and ferulic acid even is available for 1.16 € g⁻¹ (Sigma Aldrich catalogue from October 21, 2014). These inexpensive precursors can be used to form initially the CoA ester from the HCA and in the second step to synthesize the chalcone. The first step, which is essential for the CHS reaction, is catalyzed by the ligase 4-coumarate:coenzyme A ligase from *Arabidopsis thaliana* (At4CL2) is a well-investigated enzyme and features the appropriate substrate promiscuity: it accepts caffeic acid (K_m=0.024 mM) and ferulic acid (K_m=0.003 mM) forming the corresponding CoA ester [95, 96].

The last step on the route to (S)-configured flavonoids is the stereoselective formation of the chalcone that is naturally catalyzed by CHI [97]. In general, the isomerization of chalcones into flavanones can be catalyzed chemically under acidic or basic conditions, yielding a racemic compound unless chiral catalysts are used [98]. If the configuration is not crucial, usually soft-basic conditions are applied to achieve the Michael addition of the chalcone for the chemoenzymatic synthesis of flavanones [97] (Fig. 3.4).

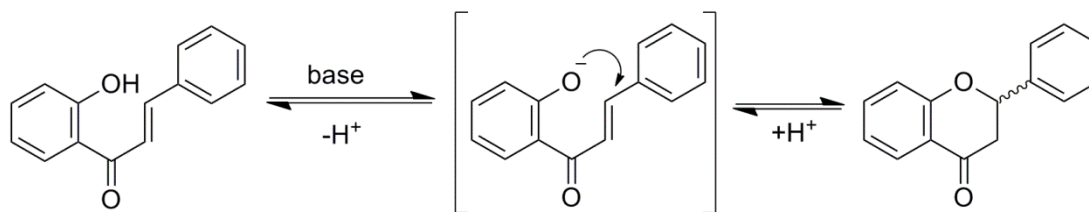


Fig. 3.4: Base-catalyzed Michael addition forming the racemic flavanone from the chalcone skeleton.

Due to the fact that HED shall be applied as a food additive passing through environments of different pH values. Racemization cannot be avoided. Therefore the selective synthesis of the (S)-configuration is dispensable. Hence, mild basic conditions are a simple alternative to replace the more costly CHI-catalyzed cyclization.

3.2 Objectives

The natural biosynthesis of flavonoids is realized in plants by the phenylpropanoid pathway. To bypass naringenin oxidation (4 chapter II) and eriodictyol methylation (5 chapter III), the aim of this chapter was to imitate the flavonoid biosynthesis starting from modified HCA structures that feature already a catecholic frame (caffeic acid) or the vanillyl motif (ferulic acid) to achieve directly the desired flavonoids ED and HED, respectively. The crucial plant enzymes 4CL and CHS are characterized as cytosolic, soluble proteins [99] and therefore they might be appropriate for the recombinant overexpression in *E. coli*.

At4CL2 was already investigated for the thioester formation of caffeic acid and is also able to convert ferulic acid into feruloyl-CoA [95]. *HvCHS2* showed to catalyze the conversion of caffeoyl-CoA into ED and feruloyl-CoA into HED [94].

In this approach the combination of both recombinant enzymes was targeted to convert low-priced HCA structures directly into ED and HED. The enzyme cascade should be applicable for whole-cell biotransformation to avoid the application of costly cosubstrates and cofactors.

3.3 Results

3.3.1 Ligase reaction – At4CL2

At4CL2 initiates the enzyme cascade for the modified biosynthetic pathway forming the active CoA ester of HCAs. The investigation concentrated on the heterologous expression of the gene, measurement of the enzyme activity, the substrate promiscuity and the final product elucidation.

3.3.1.1 Cloning and transformation

At4CL2 was cloned in two different expression vectors using the Gateway® cloning system. The gene was cloned into pDEST-N110 (*At4CL2*) and into pDEST-N112-MBP (MBP-*At4CL2*) expression vector. Both constructs contain a decahistidin tag sequence for the enhanced affinity to nickel resins for purification of the synthesized enzyme. To increase the cytosolic solubility of the recombinant eukaryotic proteins, pDEST-N112-MBP contains a maltose-binding protein (MBP) sequence that is fused to the N-terminal of the *At4CL2* protein [100]. *At4CL2* and MBP-*At4CL2* were subsequently transformed in two different *E. coli* BL21 (DE3) star strains for recombinant protein expression.

3.3.1.2 Expression and enzyme activity assay

Both strains containing the plasmids of *At4CL2* and MBP-*At4CL2* were used for recombinant expression. The enzyme activity assay was performed with crude lysate prepared as described in section 2.5.1 for a prescreening of activity.

A spectrophotometric assay system according to Meng *et al.* [75] was applied to determine the activity of *At4CL2*. As HCAs and their corresponding thioesters differ in their absorption spectra, the absorption is significantly increased upon the formation of e.g. caffeoyl-CoA. This change in absorbance at 346 nm was used to measure the activity of the crude extracts compared to a similarly treated control – an empty vector of pDEST-N110 transformed into the same *E. coli* T7 express strain (Fig. 3.5).

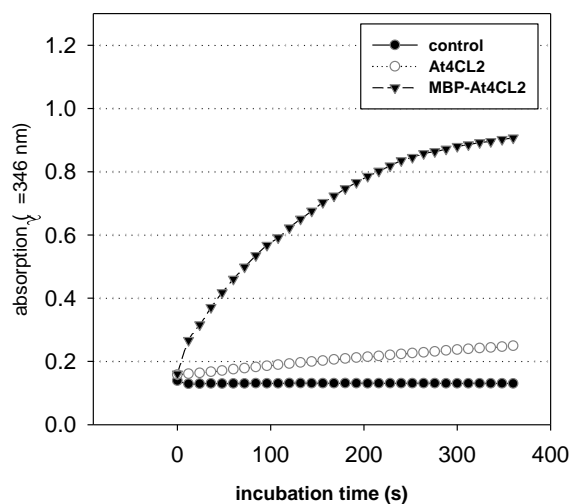


Fig. 3.5: Activity measurement of the crude extracts of At4CL2 and MBP-At4CL2 compared to a control. According to Meng *et al.* [75], absorption difference spectra at $\lambda=346$ nm were used to measure the caffeoyl-CoA formation of 10 μ l crude extract of At4CL2. MBP-At4CL2 expressed in pDEST-N112 is fused to a maltose-binding protein (MBP) enhancing the solubility of the recombinant protein and shows a higher activity of CoA thioester formation than At4CL2 expressed in pDEST-N110 without a fusion partner. A similar treated control (empty vector of pDEST-N110 transformed into an *E. coli* T7 express strain) showed only marginal activity.

The MBP-At4CL2 fusion protein showed the highest enzyme activity of the tested crude extracts. With regard to whole-cell biotransformation, MBP-At4CL2 was used for further investigations.

3.3.1.3 Substrate promiscuity

To examine the substrate promiscuity of the ligase, MBP-At4CL2 was purified using the fused decahistidin tag for separation via affinity chromatography, and pure fractions containing homogeneous protein were dialyzed to remove the eluent imidazole (Fig. 3.6).

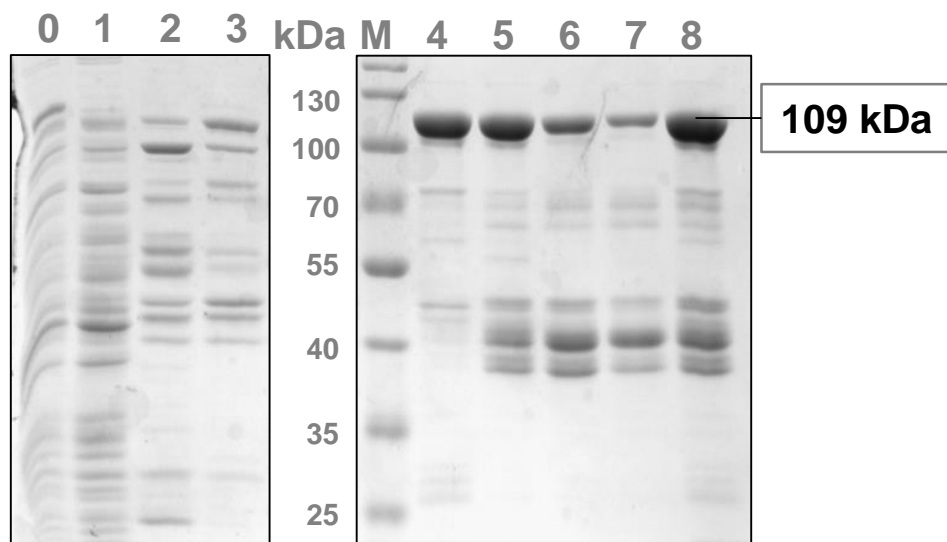
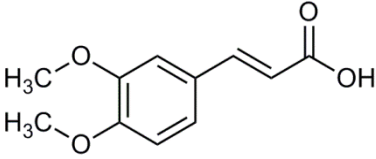
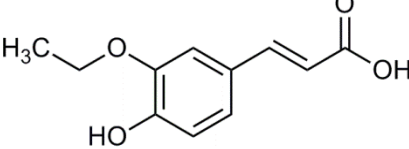
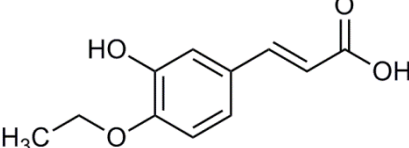
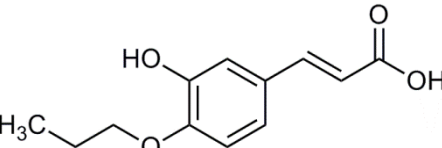


Fig. 3.6: SDS-PAGE of MBP-At4CL2 purification. The 10 % SDS-PAGE gel shows the steps of purification after cell lysis of the crude extract (0): the flow-through (1), washing steps (2, 3), elution of MBP-At4CL2 (109 kDa) (4 – 7) and the dialyzed concentrate (8). The marker (M) was used to identify the molecular weight. Fused to an MBP bearing a molecular weight of 42.5 kDa, the full-length protein (At4CL2+MBP) is characterized by a molecular weight of ~109 kDa.

MBP-At4CL2 was tested for *in vitro* conversion of different natural and synthetic HCAs to evaluate its substrate spectrum (table 3.1).

Table 3.1: Natural and synthetic HCAs as substrates for MBP-At4CL2 activity. Different hydroxycinnamic acids were used to evaluate the substrate promiscuity of the ligase forming the corresponding CoA thioester.

	hydroxycinnamic acid	structure
natural compounds	<i>p</i> -coumaric acid	<chem>Oc1ccc(cc1)/C=C/C(=O)O</chem>
	caffeic acid	<chem>Oc1cc(O)ccc1/C=C/C(=O)O</chem>
	ferulic acid	<chem>COc1cc(O)ccc1/C=C/C(=O)O</chem>
	isoferulic acid	<chem>COc1ccc(O)cc1/C=C/C(=O)O</chem>

	hydroxycinnamic acid	structure
natural compounds	3,4-dimethoxycinnamic acid	
synthetic derivatives	3-ethoxy-4-hydroxycinnamic acid	
	4-ethoxy-3-hydroxycinnamic acid	
	4-propoxy-3-hydroxycinnamic acid	

Before and after incubation, the absorption difference spectra of each hydroxycinnamic acid assay were measured to examine the CoA thioester formation (Fig. 3.7).

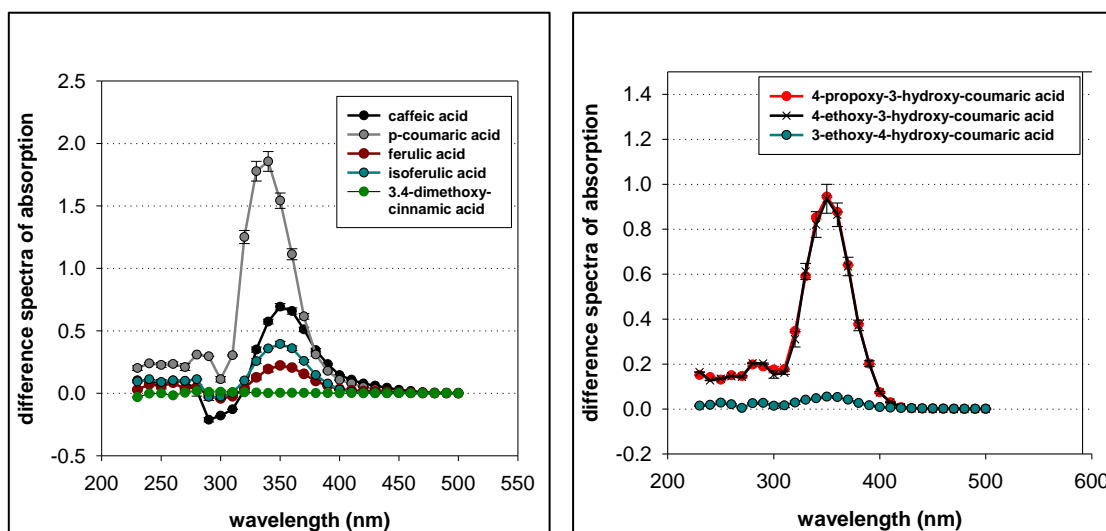


Fig. 3.7: Absorption difference spectra for the conversion of HCAs and derivatives tested *in vitro* with MBP-At4CL2. After reaction, a significant wavelength shift in the range of 300-400 nm was measured indicating a CoA thioester bond formation. 500 μ M of natural (left graph) or synthetic HCA (right graph) each were incubated with 3.75 ng of purified enzyme in a standard assay system (200 μ l) and incubated for 65 min.

With exception of 3,4-dimethoxycinnamic acid, all tested substrates show a wavelength shift indicating CoA thioester bond formation. Caffeic acid, *p*-coumaric acid and ferulic acid were

confirmed as substrates. Isoferulic acid and the synthetic derivatives with longer side chains are new potential substrates for the At4CL2. The formation of the corresponding thioester has to be verified by structure elucidation of the products.

3.3.1.4 Structure elucidation of the products

To verify the structure of the formed CoA esters, a preparative scale reaction was performed to conduct selected analyses. The purification over SPE cartridge was followed via absorption of the elution fractions (Fig. A 1) and reaction yields were calculated (table 3.1).

Table 3.2: Percentage yield (amount of product) of the enzymatic synthesized CoA ester after purification.

	hydroxycinnamic CoA ester	yield
natural compounds	<i>p</i> -coumaroyl-CoA	91 % (\pm 8.62 mg)
	caffeoyl-CoA	36 % (\pm 3.50 mg)
	feruloyl-CoA	59 % (\pm 5.78 mg)
	isoferuloyl-CoA	72 % (\pm 7.01 mg)
synthetic derivatives	3-ethoxy-4-hydroxycinnamoyl-CoA	57 % (\pm 5.67 mg)
	4-ethoxy-3-hydroxycinnamoyl-CoA	61 % (\pm 6.40 mg)
	4-propoxy-3-hydroxycinnamoyl-CoA	76 % (\pm 7.49 mg)

The retention times in HPLC (analytics of CoA ester, section 2.6.3.1) and ESI-MS data of the products were measured (table 3.2, Fig. A 2-Fig. A 7).

Table 3.3: HPLC and ESI-MS data from the products of the ligase reaction.

	CoA ester	calculated mass	<i>m/z</i> of ESI-MS [M-2H] ²⁻	retention time (min)
natural compounds	caffeoyl-CoA	929	463.8	21.3
	feruloyl-CoA	943	470.6	24.6
	<i>p</i> -coumaroyl-CoA	913	455.8	21.7
	isoferuloyl-CoA	943	471.1	24.8
synthetic derivatives	3-ethoxy-4-hydroxycinnamoyl-CoA	957	477.3	28.2
	4-ethoxy-3-hydroxycinnamoyl-CoA	957	447.9	28.1
	4-propoxy-3-hydroxycinnamoyl-CoA	971	484.8	28.1

The CoA thioester formation was verified using NMR and HR-MS technique. In all cases, the exact mass of the CoA thioester was found. Exemplarily, the exact mass of the CoA ester relevant for precursor-directed biosynthesis of ED and HED are shown in table 3.3. For all others CoA thioester, this information is shown in the appendix (table A 1).

Table 3.4: FT-ICR HR-MS analysis of the biocatalytically synthesized CoA thioester.

CoA thioester	mode	calculated mass		<i>m/z</i> (FT-ICR HR-MS)
		[M]		
caffeoyl-CoA (C ₃₀ H ₄₂ O ₁₉ N ₇ P ₃ S)	positive mode	[M+H] ⁺	930.1543	930.1542
		[M]	929.147	--
	negative mode	[M-H] ⁻	928.1396	928.1395
		[M-2H] ²⁻	463.5662	463.5659
feruloyl-CoA (C ₃₁ H ₄₄ O ₁₉ N ₇ P ₃ S)	positive mode	[M+H] ⁺	944.1703	--
		[M]	943.163	--
	negative mode	[M-H] ⁻	942.1553	942.1552
		[M-2H] ²⁻	470.5734	470.5740

To allocate the NMR signals of the CoA thioester, structure numbering based on D'Ordine *et al.* (1995) [101] was modified for analyses of the different HCAs. ¹H-NMR, ¹³C-NMR, ³¹P-NMR and 2D-NMR (DQF-COSY, HSQC, HMBC, ROESY, TOCSY) correlation spectra were measured to confirm exemplarily the structure of the CoA thioester for caffeoyl-CoA, feruloyl-CoA (table A 2) and *p*-coumaroyl-CoA (table A 3, Fig. A 8-Fig. A 13). The spectral assignment confirmed the structure of the synthesized CoA ester and thus the success of the MBP-At4CL2 catalyzed reactions.

3.3.2 Chalcone synthase reaction – HvCHS2

HvCHS2, known to convert caffeoyl-CoA and feruloyl-CoA forming ED and HED respectively [94], was chosen to realize the second step for the modified biosynthesis of flavonoids.

3.3.2.1 Plasmid construction and transformation

A pBluescript SK(-) plasmid containing the *HvCHS2* gene was provided by David B. Collinge from the University of Copenhagen (DK) [94]. The *HvCHS2* gene was amplified from the vector pBluescript SK(-) and cloned into pET-28a(+) bearing a kanamycin resistance and an N-terminal His₆-Tag for purification via affinity chromatography (section 0). The constructed plasmid was transformed into *E. coli* DH5α for storage and into *E. coli* BL21 (DE3) star for expression.

First experiments of purification failed because of an insufficient binding of the hexa-histidine tagged protein to the HisTrap column despite a N-terminal location of the tag. Therefore, the

plasmid was mutated (section 2.2.2.2) using the designed HisTag+2 primers to obtain an extension of the N-terminal 6xHis-tag. The modified pET-28a(+) vector translating the octahistidine tag fused to *HvCHS2* was transformed into *E. coli* DH5 α for storage and into *E. coli* BL21 (DE3) star for expression. The new clones were designated as CHS2.

3.3.2.2 Expression and purification

After successful gene expression and cell lysis of CHS2, the protein was isolated using Immobilized Metal Ion Affinity Chromatography (IMAC) (section 2.4). The success of expression, purification, concentration and dialysis of the CHS2 protein (43 kDa) was visualized by SDS-PAGE (Fig. 3.8).

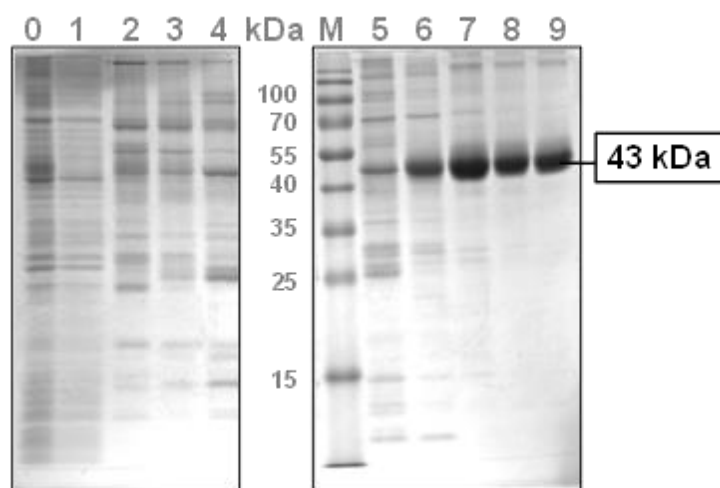


Fig. 3.8: SDS-PAGE of CHS2 purification. The 12 % SDS-PAGE gel shows the steps of purification after cell lysis of the crude extract (0): the flow-through (1), washing steps (2 – 4), elution of CHS2 (43 kDa) (5 – 8) and the dialyzed concentrate (9). The marker (M) was used to identify the molecular weight.

3.3.2.3 Enzyme activity assay

After purification, the ability of the enzyme to form the corresponding chalcones by cyclizing three units of malonyl-CoA with one unit of the natural CoA ester was tested (Fig. 3.9). The conversion into the resultant chalcones was confirmed for *p*-coumaroyl-CoA (A: R=H), caffeoyl-CoA (A: R=OH) and feruloyl-CoA (A: R=OCH₃) (table 3.5). Isoferuloyl-CoA was not accepted as a substrate.

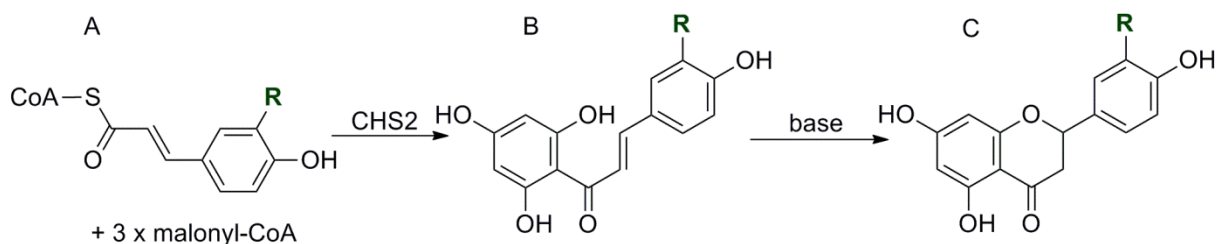


Fig. 3.9: CHS2 catalyzed formation of chalcones (B) from *p*-coumaroyl-CoA (A: R=H), caffeoyl-CoA (A: R=OH) and feruloyl-CoA (A: R=OCH₃). The final ring closure to the corresponding flavonoid (C) could be achieved by incubation under mild basic conditions (pH=8.0).

The isomerization of the chalcone (B) forming the flavonoid (C) was achieved by adding base (pH = 8.0) after reaction. The ring closure was followed by the decrease of the absorption spectra at $\lambda = 350$ nm due to the flavonoid formation [102]. ED chalcone was used as a reference.

Table 3.5: HPLC-,ESI-MS and HR-MS analysis products formed in the CHS2.

substrate (CoA ester)	flavonoid formed	calculated mass of flavonoid – negative mode [M-H] ⁻	<i>m/z</i> of ESI-MS: [M-H] ⁻	<i>m/z</i> (HR-MS) [M-H] ⁻	ret. time
caffeoyl-CoA	ED	287.0561	287.1	287.0562	12.7
<i>p</i> -coumaroyl-CoA	Nar	271.0612	271.0	271.0613	13.7
feruloyl-CoA	HED	301.0718	300.9	301.0719	13.8
isoferuloyl-CoA	no conversion	301.0718	n.d.	n.d.	n.d.

Flavonoid formation was analyzed by retention time and mass (table 3.5). The fragmentation pattern) in UHPLC-MS/MS measurements confirmed the products compared to the references of ED and HED respectively (Fig. A 15). As exemplified for caffeoyl-CoA conversion, the fragmentation pattern from the references of ED and EDCh compared to the CHS2 assay is shown in Fig. 3.10.

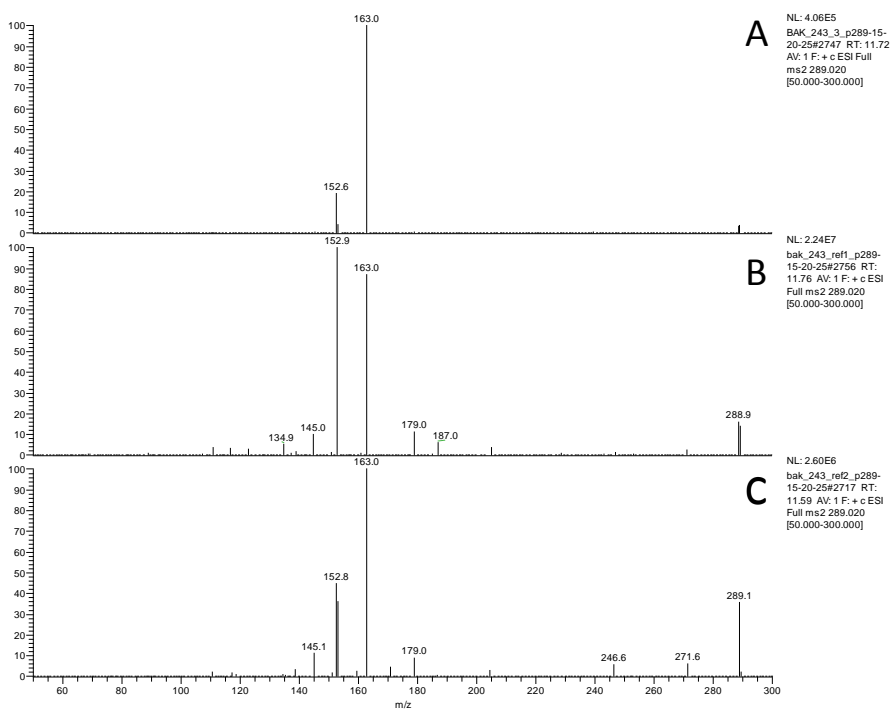
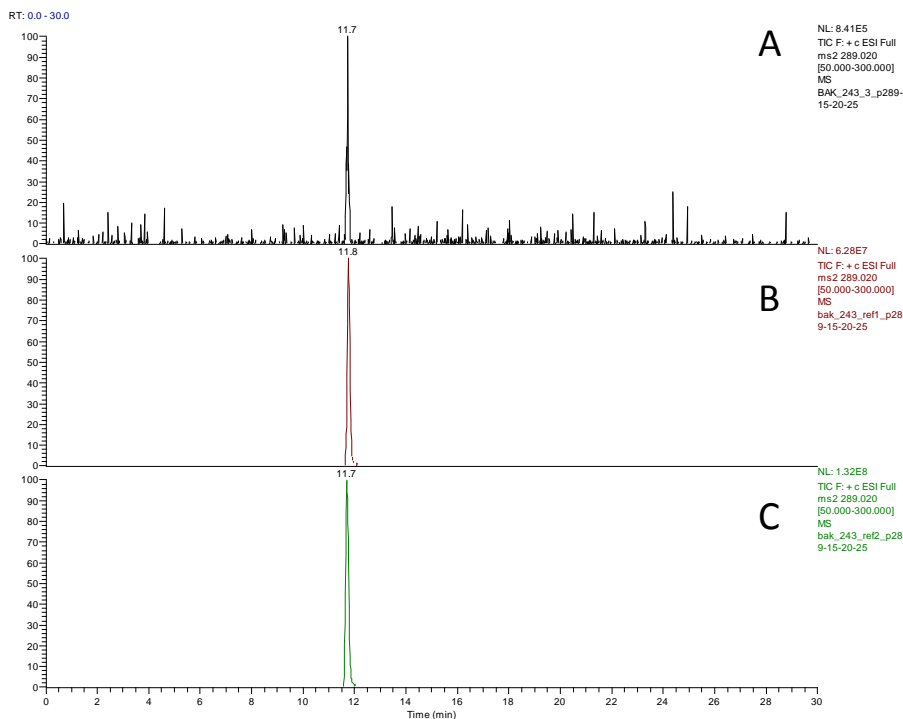


Fig. 3.10: Retention time and MS² fragmentation pattern of the CHS2 product (A) compared to EDCh (B) and ED (C) as references. The retention time and the relative intensity of the fragments of the MS² measurement using 20 eV for ionization from the reference ED accord to the data from the product formation of the CHS2 assay using caffeoyl-CoA as a substrate. The chalcone (EDCh) gave a different fragmentation pattern at 20 eV and was not obtained in the assay.

ED formation from caffeoyl-CoA and HED formation from feruloyl-CoA could be confirmed using enzymatic catalysis by CHS2.

3.3.3 Enzyme cascade

To omit the purification of the CoA esters produced by MBP-At4CL2, the two-step pathway combining this enzyme with CHS2 a cascade was investigated next (Fig. 3.11).

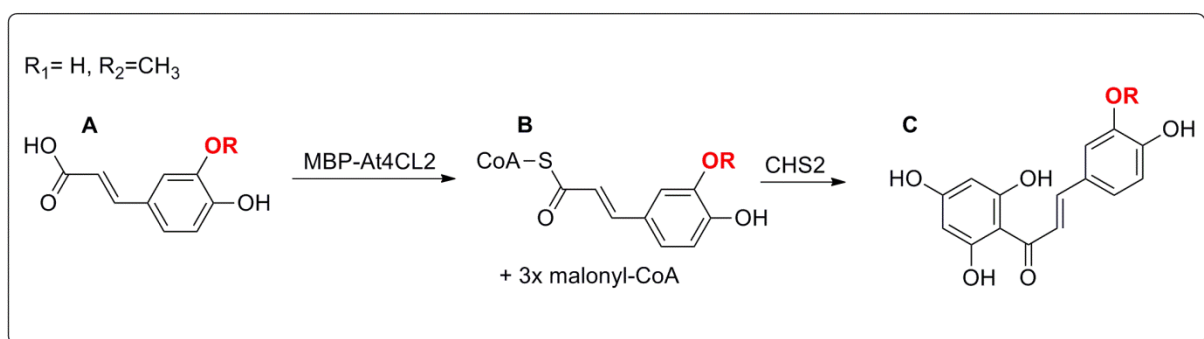


Fig. 3.11: Strategy for the one-pot synthesis of ED and HED starting from HCA. Caffeic acid ($R_1 = H$) or ferulic acid ($R_2 = CH_3$) are accepted by MBP-At4CL2 as starting material (A) for the synthesis of the corresponding CoA esters (B). In the second step the CoA esters are converted into the appropriate chalcones (C) catalyzed by CHS2. Both enzymatic steps are investigated separately *in vitro*. The application as an enzyme cascade has to be proven.

MBP-At4CL2 and CHS2 were combined *in vitro*. After incubation of the ligase with its substrates for 90 min at pH = 7.0, the CoA ester formation was successful (wavelength shift at $\lambda=346$ nm, Fig. A 14). At this time point, CHS2 and three equivalents of malonyl-CoA were added to the system. After incubation for 24 h, the product mixture was analyzed by HPLC. However, no formation of flavonoids ED and HED was detected but the educts CA and FA were still present in the assay. Direct simple coupling of MBP-At4CL2 and CHS2 seems to be unsuccessful via *in vitro* one-pot synthesis. However, the production of ED or even HED from HCA by a simply two-enzyme cascade will only be cost-efficient if the expensive cosubstrates CoA, ATP and malonyl-CoA can be provided by cells and if the time consuming purification steps of the enzymes and the CoA esters can be omitted.

Thus, living whole-cell biosynthesis was performed to supply a suitable reaction environment and the required cosubstrates for the biosynthesis of ED and HED from caffeic acid and ferulic acid, respectively. The pET28a-(+) vector-which contains the *HvCHS2* gene and a kanamycin resistance gene - and the pDEST-N112 vector containing the *At2CL4* gene and an ampicillin resistance gene - were cotransformed into chemically competent *E. coli* BL21 (DE3) cells for coexpression (Fig. 3.12A).

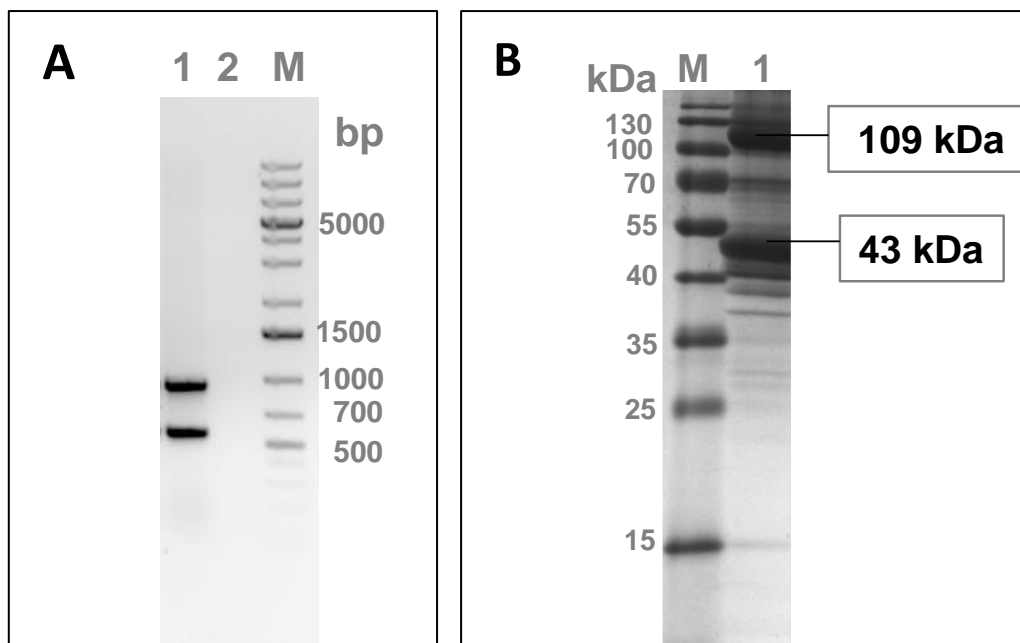


Fig. 3.12: A: Colony PCR after cotransformation. The 1 % agarose gel shows (1) a ~500 bp fragment originated from specific amplification of pET28a(+)-*HvCHS2* and a ~1000 bp fragment originating from pDEST-N112-*At2CL4*. The water control (2) shows no gene fragments after PCR. **B: SDS-PAGE of the crude extract from cells after coexpression in LB medium.** The two extensive protein bands (1) result from successful production of MBP-At4CL2 protein (~109 kDa) and CHS2 (~43 kDa). Molecular masses were estimated by comparison with molecular markers (M).

The success of recombinant overexpression of both genes in one *E. coli* strain was confirmed by SDS-PAGE of crude cell lysates (Fig. 3.12B). However, after 24 h whole-cell biotransformation of CA and FA in LB medium, the analysis of the phenylpropanoid profile of the coexpression culture was similar to that of a control (empty vector). No conversion of the HCAs into ED or HED could be achieved using this *in vivo* biotransformation. In contrast, the HCAs were degraded in both reactions after 24 hours of incubation.

3.4 Discussion

The flavonoids can be available in two steps by application of the inexpensive precursor caffeic acid and ferulic acid. The modified biosynthetic pathway to HED (and intermediate ED) starts with precursors that already bear the desired B-ring substitution patterns. Two enzymes – At4CL2 as ligase and HvCHS2 as chalcone synthase – are naturally occurring in plants and were published to catalyze the favored reactions [94, 95]. In this work MBP-At4CL2 was shown to catalyze further reactions resulting in the formation of new CoA esters from natural compounds and synthetic derivatives except from 3,4-dimethoxycinnamic acid. No shift of the wavelength after incubation was detected for 3,4-dimethoxycinnamic acid, however CoA thi-

oester formation from 3,4-dimethoxycinnamic acid cannot be excluded due to lack in reference compound and has to be proven in future. A possible perspective might be to quantify the free thiol group of the non-reacted coenzyme-A by for example Ellman's reagent (5,5'-dithiobis-(2-nitrobenzoic acid) [103]. This method can also be applied to investigate the enzyme kinetics of the substrates.

The indicated high substrate promiscuity was utilized for preparative scale and, thereby, for verification of the structures of the resulting thioesters. The natural CoA esters were also proved to be substrates for the second step conversion by CHS2. Caffeoyl-CoA, *p*-coumaroyl-CoA and feruloyl-CoA were accepted by this enzyme. Isoferuloyl-CoA was not transformed into Hesp despite its structural similarity to feruloyl-CoA, indicating high selectivity and a small substrate spectrum. Although the CHS2 was limited due to the accepted substrates, probably this enzymatic pathway can be used for the biocatalytic synthesis of further flavanones like Hesp from isoferulic acid applying mutagenesis methods on HvCHS2.

The enzyme cascade was not successful as *in vitro* one-pot synthesis, although the successive two-step chemoenzymatic reaction to the flavonoids ED and HED was confirmed. A reason might be the mixture of CoA and CoA esters as potential substrates for both enzymes, while fitting into both binding pockets of the proteins due to their structural similarity. The yield of the thioester synthesized *in situ* was estimated as a total conversion of the corresponding HCA. Hence, a threefold amount of malonyl-CoA was present in the buffer system for the second reaction. Malonyl-CoA potentially inhibits the first reaction due to the high similarity to CoA. To avoid this, malonyl-CoA was added after detection of CoA ester formation (90 min) although the reaction was not yet complete at this time (stagnation of the wavelength shift at 900 min incubation time, Fig. A 14). Analogously, the substrates of the first reaction (free HCAs, CoA) may inhibit the second reaction step by seizing the enzyme CHS2. However, the chemoenzymatic approach is not feasible for the economical and sustainable production of flavonoids because of the addition of expensive cosubstrates like CoA, ATP and malonyl-CoA. Thus, it was not further optimized for conversion.

In fact, the modified pathway was inserted into a single *E. coli* strain that might be able to provide the required cosubstrates and cofactors. The coexpression of both plasmids bearing the corresponding gene for the ligase and the synthase could be achieved. Also protein synthesis of MBP-At4CL2 and CHS2 in LB medium was confirmed. However, the *in vivo* whole-cell biotransformation of the precursors CA or FA to ED or HED, respectively, was investigated as a first approach using the simplest methods like the coexpression of both plasmids into

one *E. coli* strain without optimization techniques. This proof of concept was not successful according to the designated methods.

3.5 Outlook

The separate *in vitro* conversion of each step was confirmed to produce ED and HED from caffeic acid and ferulic acid, respectively. The method uses inexpensive precursors, soluble enzymes and a well-established host organism for expression of the genes that are interesting due to sustainability of the biocatalytic synthesis of the flavanones. However, this approach is only reasonable, if the whole-cell biosynthesis will successfully provided the crucial and expensive cosubstrates.

Several improving strategies like plasmid choice, culture media and ACC coexpression were presented in similar metabolic engineered organism to produce flavonoids [61, 104, 105] and is potentially also successful for the *in vivo* biosynthesis of natural ED and HED.

Therefore, this approach is an additional example for the utility of this fundamental strategy for the inexpensive and sustainable production of the rare flavonoids ED and HED by a two steps enzyme-cascade. However, this work represents single-acting enzymes that potentially work constitutively *in vivo* as modified biosynthetic pathway, if the system will be adapted and optimized. In addition, this enzyme-cascade might be applied for synthesis of further flavonoids due to the high substrate promiscuity of the ligase and perspectives to mutational studies of the CHS enzyme.

4 Chapter II: Hydroxylation of flavonoids

4.1 Introduction

Hydroxylation of flavonoids is realized in nature by the catalytic activity of cytochrome P450 oxygenases (CYPs) [106]. This superfamily of enzymes bears a heme as prosthetic group and is termed for the characteristic wavelength of maximum absorption at 450 nm of the reduced carbon-monoxide-bound-form [107]. CYPs are often responsible for detoxification processes as they increase the hydrophilicity of compounds and hence facilitate their excretion [108]. In general, CYPs belong to the external monooxygenases, thus they depend on an external electron donor transferring the electrons for oxygen activation and in consequence for the substrate hydroxylation [109].

CYPs are designated according to their structural homology and classified due to the structural organization of the CYP and their electron transfer proteins [107]. In general, two main classes can be specified (Fig. 4.1), although there are many further variations and subclasses reported [107].

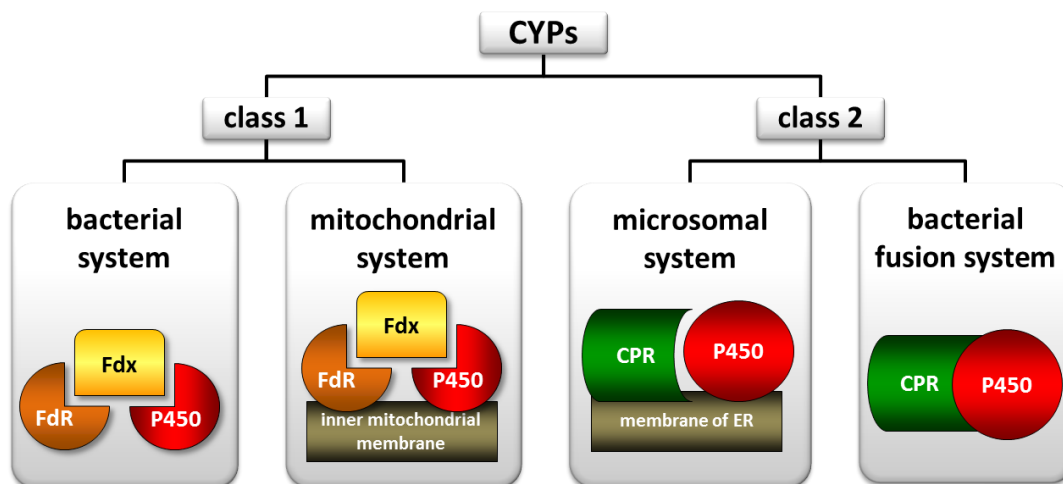


Fig. 4.1: Main classification of CYPs according to the topology of the P450 and the used electron transfer system. Class 1 consists of a P450 protein depending on a reductase system that contains a soluble ferredoxin (Fdx) and a FAD-containing ferredoxin reductase (FdR). In the bacterial type all three components are cytosolic and soluble. In the mitochondrial system, P450 and FdR are bound to the inner mitochondrial membrane. In CYPs of class 2, a specific NADPH- cytochrome P450 reductase (CPR) provides the electrons for the P450 enzyme instead of FdR and Fdx. CPR and P450 protein are associated to the membrane of the ER in the microsomal type. In the bacterial fusion system like P450-BM3 (CYP102A1), both activities are organized in a single, cytosolic soluble polypeptide chain offering a catalytically self-sufficient oxidation system.

The class 1 of CYPs is characterized by a three-membered system that consists of the P450 protein including a heme prosthetic group (P450) and a FAD-containing reductase (FdR) transferring the reduction equivalents from NADPH or NADH to the third component: the soluble iron-sulfur cluster ([Fe-S]) protein called ferredoxin (Fdx) that reduces the heme of the P450. This class can be subdivided into mitochondrial and bacterial type CYPs. The mitochondrial system has a P450 protein bound to the inner mitochondrial membrane, a cytosolic soluble Fdx and a FdR that is associated to the membrane. In bacteria reduction of NAD(P)H (FdR), heme-reduction (Fdx) and oxidation of the substrate (P450) are localized at three different proteins. However, in contrast to the mitochondrial type, they are cytosolic and soluble proteins [109].

Class 2 – microsomal type CYPs – are the most prominent cytochrome P450 enzymes in eukaryotic cells and are characterized by a P450 and NADPH-cytochrome P450 reductase (CPR) which provides the electrons for the reduction of the P450. Both enzymes are attached to the endoplasmic reticulum (ER) membrane [110]. CYPs of this class preferably use NADPH for their respective oxygenation reaction, e.g.: the selective 3' hydroxylation of the flavonoid naringenin (Nar) into eriodictyol (ED) is catalyzed by CYP75B in plant metabolism [106] (Fig. 4.2).

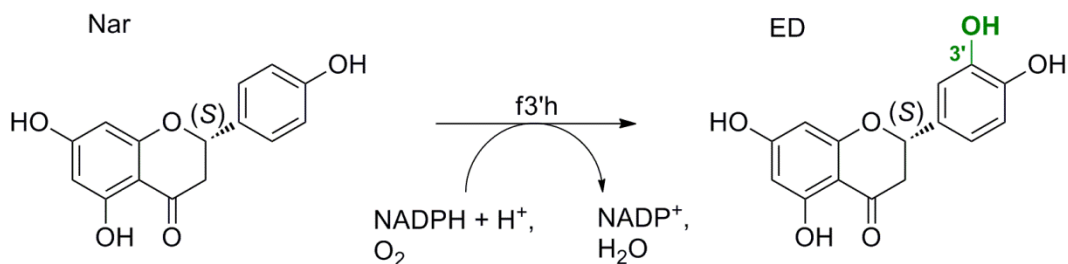


Fig. 4.2: Selective aromatic hydroxylation in flavonoid metabolism catalyzed by flavonoid 3'-hydroxylase (f3'h). The regioselective hydroxylation at the 3' position (bold green) of naringenin (Nar) yielding eriodictyol (ED) is catalyzed by the membrane-bound enzyme CYP75B called flavonoid 3'-hydroxylase (f3'h) in plants [106].

The bacterial fusion protein P450-BM3 from *Bacillus megaterium* (CYP102A1) constitutes an interesting member of this class as it combines the CYP and the FAD-reductase in a single polypeptide chain [109]. This catalytically self-sufficient CYP BM3 draws perspectives for industrial applications due to the high catalytic activity e.g.: the oxidation of arachidonate accomplishes a K_M of 4.7 μM and a turnover number over 15 mM^{-1} for the wild type enzyme [111]. This results from the topology and the solubility of this oxygenase [112]. Almost all of the other soluble CYPs of bacteria belong also to this type and catalyze selective hydroxylations of different compounds like fatty acids or (polycyclic) aromatic hydrocarbons for instance

the self-sufficient monooxygenases from *Rhodococcus ruber* [113] or the *m*-hydroxybenzoate hydroxylase MobA from *Comamonas testosteroni* [114]. However, most of them depend on cost intensive cofactors, are complex proteins with a limited substrate spectrum and in many cases they are instable and exhibit low activities which are insufficient properties for application as industrial biocatalysts [109]. The reaction mechanism of CYPs is very complex including several “shunt” pathways (Fig. 4.3). In brief, the overall reaction of CYPs can be summarized as:



Although oxidation processes are highly concerted, side products like H_2O_2 or superoxide can be produced within the catalytic reaction mechanism (Fig. 4.3).

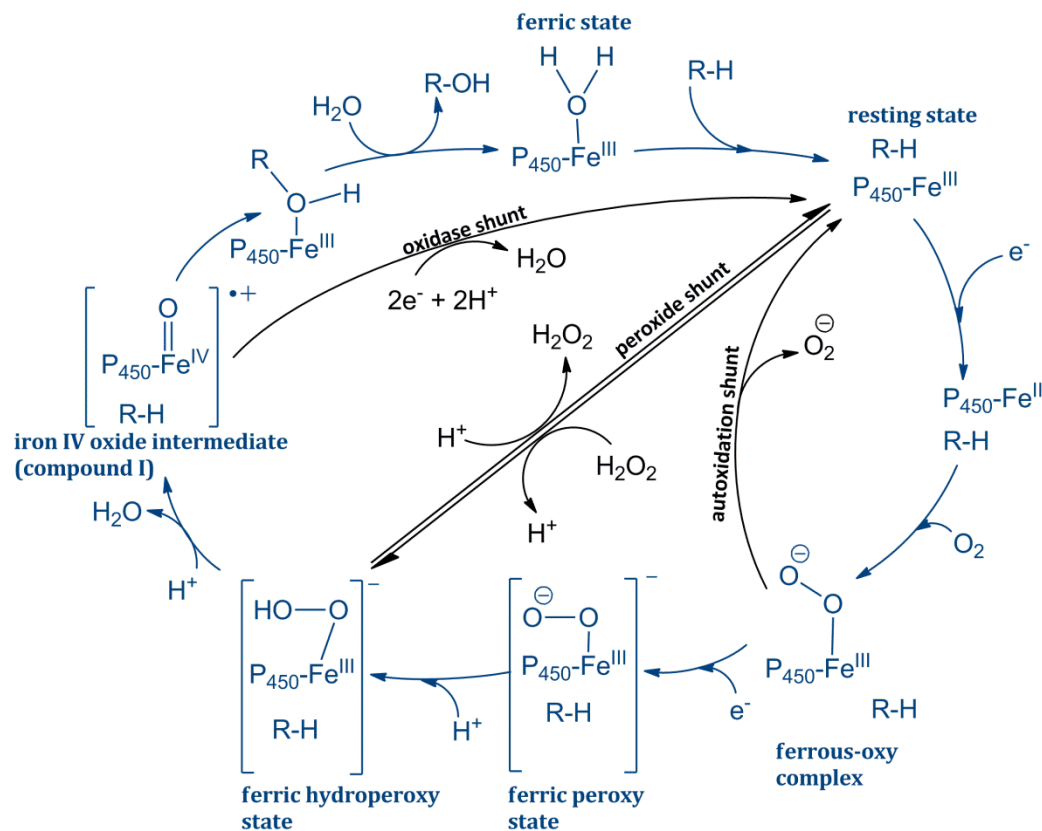


Fig. 4.3: Catalytic cycle of CYPs [112]. Starting from the ferric state ($\text{P}_{450}\text{-Fe}^{3+}$) with a distal bound water, the resting state is formed after the binding of a substrate (R-H) displacing the water. After reduction by one electron, the resulting ferric (II) ($\text{P}_{450}\text{-Fe}^{2+}$) is able to bind the dioxygen (O_2) forming a ferrous-oxy complex. The ferric peroxy state is generated after a further addition of an electron and then converted into the ferric hydroperoxy state by protonation. The crucial compound I (drawn as a radical cation) is responsible for the hydroxylation of inactive C-H bonds and formed after delivery of a further proton under release of water. The monooxygenase mechanism is completed by the release of the hydroxylated product and the binding of a water molecule – the ferric state is regenerated. Possible shunt pathways are shown in black forming the resting state from different starting points under release of superoxide from the ferrous-oxy complex (autoxidation shunt), hydrogen peroxide from ferric hydroperoxy state (peroxide shunt) and water from iron (IV) oxide (oxidase shunt).

In living cells these undesired, harmful products of the shunt pathways are removed by endogenous detoxification systems like catalase or superoxide dismutase. The control of these side reactions which can become dominant during *in vitro* applications is often a challenge. Hence, CYPs can act as monooxygenases, oxidases but also as peroxidases [109]. In the latter case they do not require oxygen or electrons from NAD(P)H as they can use inorganic or organic peroxides for dealkylation or hydroxylation [110, 115].

Also other oxidases and peroxidases offer hydroxylase activities on aromatic compounds using peroxides or molecular oxygen [56, 116, 117]. For example, the commercially available horseradish peroxidase (HRP) was shown to catalyze the hydroxylation of *p*-coumaric acid [118] and the polyphenol oxidase (PPO) can catalyze the hydroxylation of phenolic compounds [119] (table 4.1). In the present thesis this observation was one attempt to investigate the hydroxylation of flavonoids like Nar.

Table 4.1: Commercially available enzymes used to test selective hydroxylation reactions on aromatic compounds. HRP = horseradish peroxidase, PPO = polyphenol oxidase, DHFA = dihydroxyfumaric acid, Asc=ascorbic acid, DHAsc= dehydro ascorbic acid

enzyme	catalyzed reaction	reference
HRP	<p>Reaction scheme for HRP: <i>p</i>-coumaric acid (HOOC-CH=CH-C₆H₄-OH) reacts with HRP, DHFA, and O₂ to form 3,4-dihydroxycoumaric acid (HOOC-CH=CH-C₆H₃(OH)₂) in 100% yield.</p>	[118]
PPO	<p>Reaction scheme for PPO: Phenol (C₆H₅OH) reacts with PPO and 1/2 O₂ to form catechol (C₆H₄(OH)₂). Catechol then reacts with PPO and 1/2 O₂ to form o-quinone (C₆H₄(=O)₂) in 71% yield. This reaction is coupled with the oxidation of ascorbic acid (Asc) to dehydroascorbic acid (DHAsc).</p>	[119]

Both enzymes are already industrially relevant and are applied for analytical diagnostics (HRP) [120] and browning processes in food industry (PPO) [57]. Amongst others, the advantages of (per)oxidases are their particular stability, accessibility, their independence of expensive cosubstrates/cofactors and their acceptance of numerous substrates [57]. However, (per)oxidase reactions commonly suffer from the production of reactive intermediates [57]. This is often accompanied by the formation of unspecific products which is undesired for industrial biosynthetic applications.

4.2 Objectives

Herein the development and optimization of a biocatalyst for the selective hydroxylation of Nar to form ED – the precursor of HED is reported. First, upscaling attempts were conducted to proof a potential biotechnological application. In plants this reaction is catalyzed by the membrane-associated f3'h, an enzyme that is difficult to be functionally expressed in prokaryotic systems [121]. Thus, alternative enzymes that can catalyze this reaction had to be identified. Therefore, different enzymes were investigated for this purpose and were chosen according to their published substrate and product range as well as their stability. The selected oxidoreductases were screened for their capability to catalyze selectively the hydroxylation at 3' positions of flavonoids.

The investigations focus on one hand on easily accessible and biotechnologically or immunohistochemically already applied enzymes: PPO and HRP. On the other hand the studies focus on soluble monooxygenases from different bacteria. They were heterologously expressed in *E. coli* and are characterized by low costs, easy transformation and fermentation, and high protein yields. A few of the screened bacterial monooxygenases like 2-HBP or BM3 were previously being considered as potential biocatalysts for biotechnological processes [122]. Others are known for selective hydroxylation of bulky and aromatic structures.

4.3 Results

4.3.1 Screening for a specific flavonoid 3'-oxygenase

With focus to selective hydroxylation of Nar at position 3', different available oxidoreductases were tested regarding their activity and regioselectivity to form ED.

Screening started using the commercially available oxidases HRP and PPO that are able to catalyze hydroxylation of phenolic structures to form a catechol scaffold [118, 119]. Nar was converted by both enzymes, but was mainly degraded by HRP [123]. PPO catalyzes the hydroxylation of Nar but the product is further oxidized to eriodictyol-*o*-quinone which rapidly polymerizes to polyphenolic structures determined by HPLC at $\lambda=475$ nm according to Jiménez-Atiéndzar *et al.*, additionally, masses of 557 m/z and 859 m/z were found using esi-ms supporting this assumption. Attempts were made to immobilize both enzymes. This should increase the stability of the catalysts and allow their use in organic solvents. As Azevedo and coworkers published, performing the reaction in organic solvents might suppress the observed polymerization to polyphenols [125]. Even though the immobilized enzymes were indeed active and allowed the conversion of their natural substrate, the selective hydroxylation of Nar yielding ED in EtOAc could still not be obtained using HRP or PPO.

The performed screening for a biocatalyst for conversion of Nar to ED focused on different types of recombinant bacterial monooxygenases, usually acting on fatty acids, aromatic compounds or a steroid skeleton. The respective enzymes were heterologously overexpressed in *E. coli* and assayed for the conversion of Nar. The first subset of enzymes was tested in purified form under addition of a separate reductase system to provide electrons (table 4.2). None of these *in vitro* enzyme systems allowed conversion of Nar.

Table 4.2: Purified recombinant bacterial monooxygenases tested for the conversion of Nar. The listed monooxygenases catalyze enzymatic hydroxylation reactions of different substrates. Enzyme activity assays were performed *in vitro* using Nar as a substrate and a separate reductase system of either bovine adrenodoxin (Adx) and adrenodoxin reductase (AdR) or FAD to provide the electron transfer. None of these enzymes were able to catalyze the hydroxylation of Nar.

enzymes	accepted substrate(s)	electron provider, cofactor and co-substrate	ref.	conversion of Nar
CYP106A2 (<i>B. megaterium</i>)	ketosteroids	heterologous reductase system from bovine (Adx/AdR), NADPH, O ₂	[126]	no
CYP109D1, CYP264A1, CYP260A1, CYP260B1 (<i>Sorangium cellulosum</i>)	fatty acids		[127]	no
2-HBP (<i>Pseudomonas azelaica</i>)	2-hydroxy-biphenyl	FAD, NADH, O ₂	[128]	no

A second subset of recombinant monooxygenases was investigated either using growing cells (biotransformation “*in vivo*”) or they were applied as crude enzyme extracts (“*in vitro*”). Table 4.3 summarizes the accepted substrate(s) or substrate classes, the required cofactors and cosubstrates of the enzymes and the results of the assay with Nar as a substrate.

Table 4.3: Recombinant bacterial monooxygenases applied for the biotransformation of Nar *in vivo* or *in vitro* with crude enzyme extracts. The enzymes catalyze the hydroxylation of different substrates and substrate classes. The conversion of Nar was achieved by two variants of CYP102A1 from *B. megaterium*: BM3-F87V and BM3-GVQ (A74G/F87V/L188Q) and by the wild type (WT) and the Y301F variant of 4-hydroxyphenylacetate 3-hydroxylase (4HPA3H) from *E. coli*.

enzymes	reported substrate(s)	cofactors and cosubstrates	ref.	biotransformation	conversion of Nar
CYP102A1 (BM3), wild type and 25 variants (<i>B. megaterium</i>)	fatty acids	NADPH, O ₂	[129]	<i>in vitro</i>	variants: F87V, GVQ
CYP116B3 (<i>R. ruber</i>)	polycyclic aromatic hydrocarbons	NADPH, O ₂	[113]	<i>in vitro</i>	no conversion
4HPA3H, wild type and Y301F variant (<i>E. coli</i>)	<i>p</i> -coumaric acid	NADH, FAD, O ₂	[130]	<i>in vivo</i>	WT, variant: Y301F
MobA (<i>C. testosteroni</i>)	<i>m</i> -hydroxy-benzoate	NADH, FAD, O ₂	[114]	<i>in vitro</i>	no conversion

The *m*-hydroxy-benzoate hydroxylase (MobA) and CYP116B3 showed no conversion of Nar. 4-hydroxyphenylacetate 3-hydroxylase (4HPA3H) wild type enzyme and the variant Y301F from *E. coli* as well as BM3-variants F87V and A74G/F87V/L188Q (GVQ) from *B. megaterium* were identified to convert Nar into ED. Product formation was determined by the use of UHPLC/MS in comparison to the reference (Fig. 4.4).

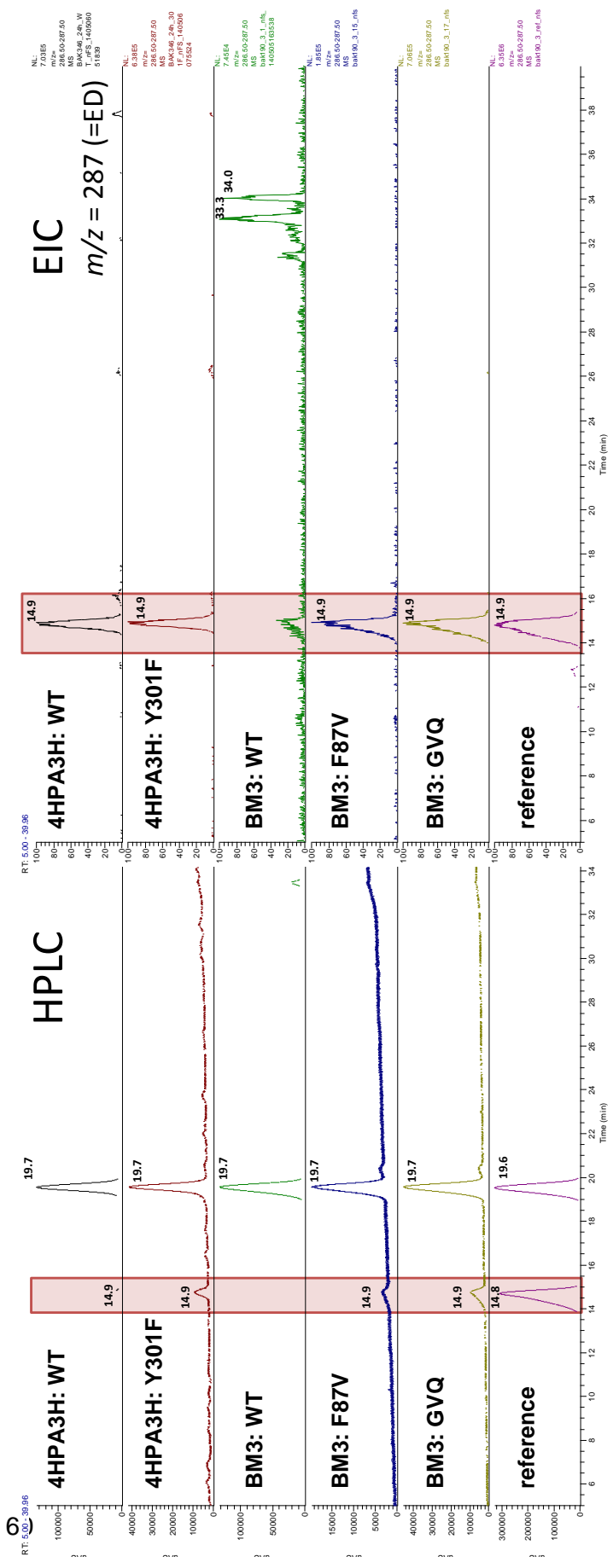


Fig. 4.4: EIC of UHPLC/MS runs of the extracts of oxidative biotransformations compared to a reference and a control. Left: The chromatograms show two main peaks for all *in vivo* biotransformations except for the wild type of BM3 (BM3: WT). The extracted-ion chromatogram (EIC) in the negative mode confirms peaks of compounds showing the same mass (m/z : 287, retention time 14.8-14.9) compared to the reference, indicating the desired product formation by the variant Y301F and the wild type of 4HPA3H and by the variants BM3-F87V and BM3-GVQ of the BM3. In contrast, no product peak was observed at EIC-extracted mass m/z 287 with BM3-WT (except for poor quality signals mainly at 33-34 min). The substrate Nar (retention time 19.6-19.7) was recovered in all assay measurements of the UHPLC. The red area shows the expected product area (cf. reference).

MS/MS fragmentation pattern of the product compared to the ED reference confirmed the hydroxylation of ring B of Nar catalyzed by the enzymes (Fig. B 1). Enzymes which accept Nar as a substrate and produce ED were further analyzed due to the highest conversion of Nar by *in vivo* biotransformation (Fig. 4.5).

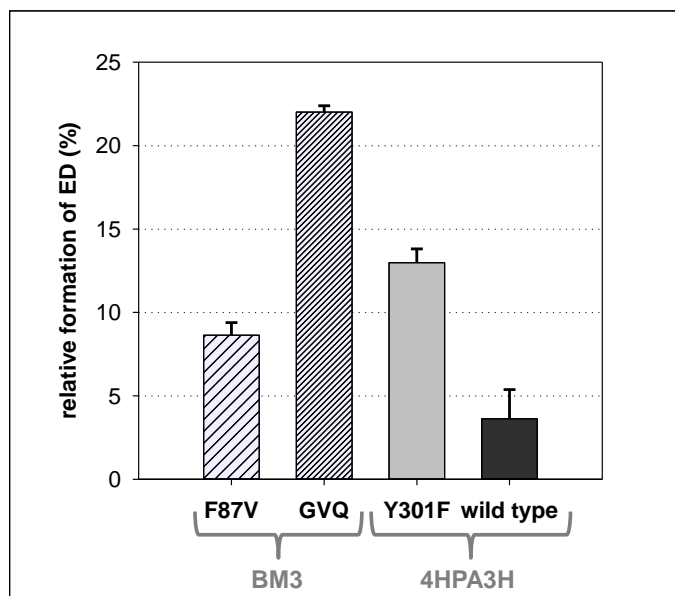


Fig. 4.5: Quantification of ED formation by different oxidating enzymes. BM3 variants F87V and GVQ, as well as the 4HPA3H variant Y301F and its wild type were compared quantitatively due to the ED formation after 24 h *in vivo* biotransformation in AI medium. BM3-GVQ under the conditions applied showed the highest conversion of Nar to ED and was used for further investigations.

Although complete conversion of Nar could not be observed, BM3-GVQ catalyzes the conversion of over 20 % Nar into ED. As BM3: F87V and 4HPA3H-variants show less conversion of Nar (3 %-13 %), BM3-GVQ was selected for the subsequent optimization of the reaction conditions.

4.3.2 Investigation of BM3-GVQ for optimized ED formation

BM3-GVQ was identified as a suitable enzyme to convert Nar into ED (LC-MS/MS detection). Although this variant was the most successful oxidoreductase of more than 30 analyzed biocatalysts, the conversion of Nar was incomplete and depends on the costly electron provider NADPH. Therefore, Nar conversion by BM3-GVQ was further analyzed and the assay conditions were optimized to increase the yield of ED. Furthermore, the structure of the product was elucidated using HR-MS and NMR to verify ED formation.

4.3.2.1 Expression and activity measurement of BM3-GVQ

BM3-GVQ was heterologously expressed in *E. coli* BL21 (DE3) and cells were lysed. The crude extract was analyzed by SDS-PAGE to prove the overexpression of BM3: GVQ (Fig. 4.6A, line 1) compared to an empty vector-control without BM3-GVQ coding sequence (Fig. 4.6A, line 0). Determination of P450 enzyme activity and calculation of the protein concentration was achieved by CO difference measurements (Fig. 4.6B).

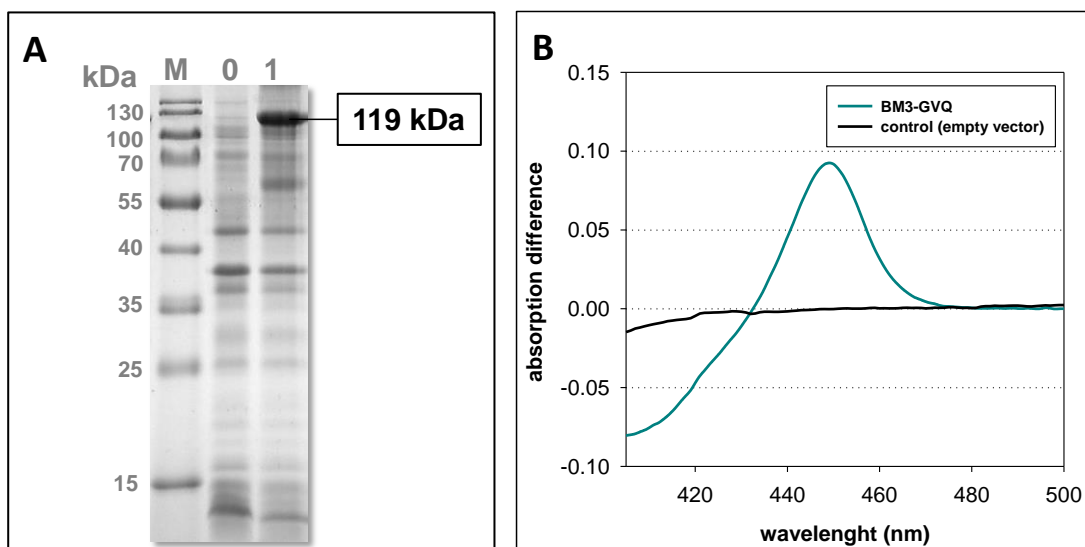


Fig. 4.6: SDS-PAGE picture of BM3-GVQ expression (A), CO difference spectrum of the BM3-GVQ lysate (B). A: A 10 % SDS-PAGE gel was loaded with crude extract of the soluble fraction of BM3-GVQ (1), with a similar induced and lysed empty vector in *E. coli* strain BL21 as a control (0) and with a protein standard marker (M) for determination of the molecular weight. BM3-GVQ (119 kDa) is only present in line 1 and not in the control (line 0). B: A CO difference spectrum was performed to determine the correct folding of the enzyme and to calculate the BM3-GVQ protein concentration of the lysate. The difference spectrum of BM3-GVQ shows an absorption maximum at 450 nm in consequence of a wavelength shift under CO-fumigation indicating the correct folding of an active P450 enzyme.

An enzyme activity assay confirmed the catalytic activity of the lysate by conversion of Nar into ED (LC-MS detection).

4.3.2.2 Structure elucidation of the product eriodictyol

HPLC and UHPLC/MS of the product formed from Nar by BM3-GVQ revealed the same retention time, mass and fragmentation pattern as the authentic standard eriodictyol (Fig. B 1). However, this information does not allow an exact discrimination between different hydroxylated naringenin derivatives (regioisomers). Thus, the product was separated on a semi-preparative HPLC system from a preparative reaction mixture and analyzed by high resolution MS and NMR in order to verify the exact structure of the main product.

To determine the exact mass of the obtained compound, FT-ICR HR-MS was used. There-with, the exact mass of 287.05611 for $C_{15}H_{12}O_6$ species in the negative ion mode was observed (table 4.4) which is in accordance to the calculated mass of ED (287.0561).

Table 4.4: Results of the MS measurements compared to the calculated exact mass of ED.

calculated mass of ED ($C_{15}H_{12}O_6$) [M]		m/z (ESI-MS)	m/z (FT-ICR HR-MS)
$[M+H]^+$	289.0707	-	-
[M]	288.0634	-	-
$[M-H]^-$	287.0561	287.2	287.05611

The exact position of the inserted hydroxyl group of the product was determined by NMR: 1H NMR experiments (Fig. B 6) were performed and compared to a ED-reference (Fig. B 7) and to the substrate to prove the success of the conversion of Nar into ED catalyzed by BM3-GVQ (table 4.5). The atom numbering of the flavonoids is exemplified on ED (Fig. 4.7).

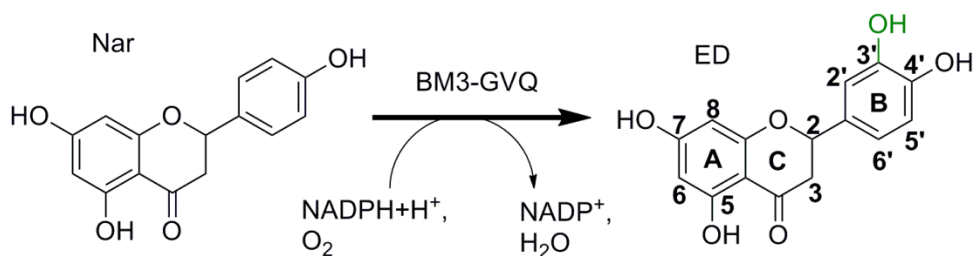


Fig. 4.7: Expected reaction of Nar catalyzed by BM3-GVQ. The inserted hydroxyl group at position 3' is highlighted in dark green.

^1H NMR (600 MHz) data of the isolated product (table 4.5, C) correlate with the measurement of an ED reference (table 4.5, B). The substrate Nar was also isolated and analyzed by ^1H NMR (table 4.5, A). The chemical shifts of the substrate and product differ substantially at ring B. Nar shows a signal for the proton of H3' in contrast to the product, where no signal was observed. Due to the 3'-hydroxylation, the chemical shifts of the neighbor protons at position 5', 6' and especially 2' of ring B become unequally deshielded by the OH-group(s) and differ therefore also in substrate and product. The functional OH groups of ring B are not visible in substrate, product and reference with the exception of the H-bridged proton from OH-5 in the educt Nar.

Table 4.5: ^1H NMR (600 MHz) spectral assignments of the substrate Nar (A) and the isolated product (B) of a BM3-GVQ assay compared to the data from a reference of ED (C). The substrate shows a significant signal for the proton of the unsubstituted position 3' that is missing in the product and the reference (highlighted in green). Protons of ring B (2', 5' and 6') of the BM3_GVQ product are identical to the chemical shifts for ED reference. The functional OH groups were not visible in the spectra with the exception of the proton from OH-5. Proton positions are assigned according to the convention for flavonoids. *chemical shifts of HSQC and HMBC correlation peaks

ring	position	reference naringenin	reference eriodictyol	BM3_GVQ product
		(A) δ_{H} ($J_{\text{H,H}}$ /Hz)	(B) δ_{H} ($J_{\text{H,H}}$ /Hz)	(C) δ_{H} ($J_{\text{H,H}}$ /Hz)
ring C	2	5.461 (13.0, 3.1)	5.40 (12.7, 3.1)	5.400 (12.9, 3.7)
	3a*	3.188 (17.2, 13.0)	3.15 (17.1, 12.7)	3.142 (17.2, 12.8)
	3b*	2.734 (17.2, 3.1)	2.73 (17.1, 3.1)	2.792 (17.2, 3.1)
ring A	6*	5.966 (2.1)	5.95 (2.2)	5.965 (2.2)
	8*	5.955 (2.1)	5.96 (2.2)	5.947 (2.2)
ring B	2'	7.400 (8.7)	7.038 (1.8)	7.032 (1.8)
	3'	7.400 (8.7)	no signal	no signal
	5'*	6.902 (8.7)	6.875 (8.2)	6.864 (8.2)
	6'*	6.902 (8.7)	6.875(8.2, 1.8)	6.874 (8.2, 1.8)
ring A/B	5-OH	12.184 (s)	12.175 (s)	12.179 (s)
	7,3',4'-OH	not visible	not visible	not visible

Nar and ED occur in both enantiomeric forms due to the stereocenter at C2 of ring C. To elucidate, if the conversion of Nar into ED is stereoselective, the reaction mixture containing substrate (Nar) and product (ED) was analyzed by chiral HPLC. References of the respective racemate gave two signals of equal intensity in the chromatograms of the authentic naringenin (15.5 min; 16.9 min) and of eriodictyol (20.3 min, 24.9 min). Samples from conversion by BM3-GVQ gave the same profile of signals and retention times as the references with equal intensity for each enantiomer (Fig. 4.8).

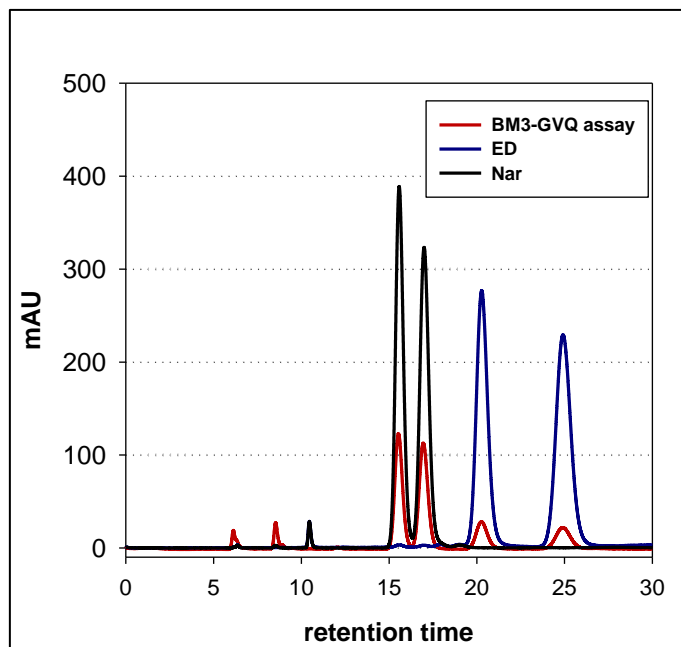


Fig. 4.8: Chromatogram of chiral HPLC run. Samples from conversion by BM3-GVQ (red) give the same profile of signals and retention times as the references Nar (15.5 min; 16.9 min; black) and of ED (20.3 min, 24.9 min; blue) with equal intensity for each enantiomer. The minor product apigenin gives a signal at 8.6 min. A further signal at 6.1 min likely is a product from substrate impurities (10.6 min) of the compound Nar with no relevance.

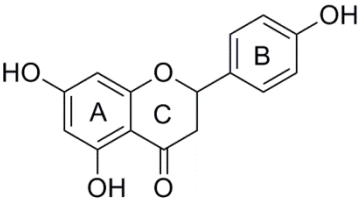
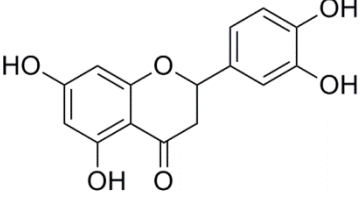
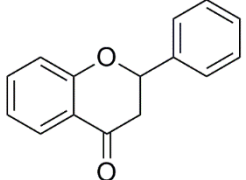
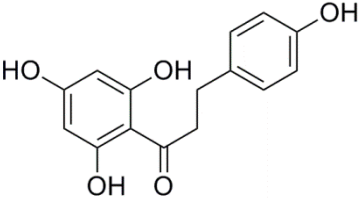
This finding can either be explained by no preference of the enzyme for one of the enantiomers (no stereoselective conversion) or a potentially existing stereoselective conversion that is covered by a spontaneous, fast racemization of the potential single enantiomer of the substrate Nar or the product ED. Non-enzymatic conversion of Nar into ED can be excluded as a control with lysate of an empty vector-control without BM3-GVQ coding sequence was checked.

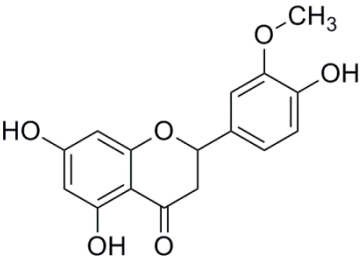
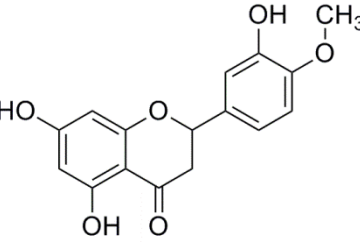
4.3.2.3 Elucidation of the substrate profile of BM3-GVQ

The final goal of this work is the establishment of an enzyme cascade containing an oxidase and a methyltransferase that allows formation of HED from Nar (Theoretical principles 1.3). As the substrate (Nar), the final product (HED) as well as the intermediate (ED) are very simi-

lar compounds, an enzyme acting on one of these substances might also possess activity towards the other. Especially, overoxidation of ED or oxidation of the methylated product HED by the applied oxidase might result in a loss of product yield in the final biocatalytic process. Thus, the substrate profile of the variant BM3-GVQ regarding the conversion of a set of related flavonoids was tested. Besides ED and HED also flavanone, the flavanone scaffold, was assayed. This compound bears no hydroxyl group and is more hydrophobic than Nar. Hesperetin (4'-O-methyl ED) - the constitutional isomer of HED - might act as an alternative substrate for BM3-GVQ. The demethylation of hesperetin would also result in the formation of ED. Phloretin, the dihydrochalcone related to Nar, might be more flexible for binding within the active site. Except ED, all substrates were accepted and converted by BM3-GVQ (table 4.6).

Table 4.6: Substrate promiscuity of BM3-GVQ. Different flavonoids were tested for their *in vitro* conversion using 500 nM of BM3-GVQ. Highest conversion showed the frame flavanone. Phloretin was degraded. HED and hesperetin were both slightly demethylated, the former flavonoid was also hydroxylated in position 3 of ring C. Nar was hydroxylated at ring B in position 3' resulting in ED formation and gave also a minor product by hydroxylation in position 3 of ring C resulting in apigenin (LC-MS/MS detection). ED was not accepted as a substrate.

substrate	structure	substrate conversion (%)	reaction
Nar		22.0±0.4	hydroxylation (3'-OH at ring B and 3-OH at ring C)
ED		no conversion (as desired)	no reaction
flavanone		75.9±3.1	hydroxylation (3-OH at ring C and ring A)
phloretin		31.7±6.5	hydroxylation and degradation

substrate	structure	substrate conversion (%)	reaction
HED		< 5	hydroxylation (3-OH at ring C)
hesperetin		9.2±1.0	demethylation

Phloretin conversion was over 30 %, but only ~10 % gave a hydroxylated product. The residual conversion showed nearly complete degradation under cleavage of the structure into fragments by the enzyme. Flavanone achieved the highest conversion (over 75 %) and yielded different products. Based on the identified products a reaction mechanism for flavanone conversion by BM3-GVQ is proposed (Fig. 4.9).

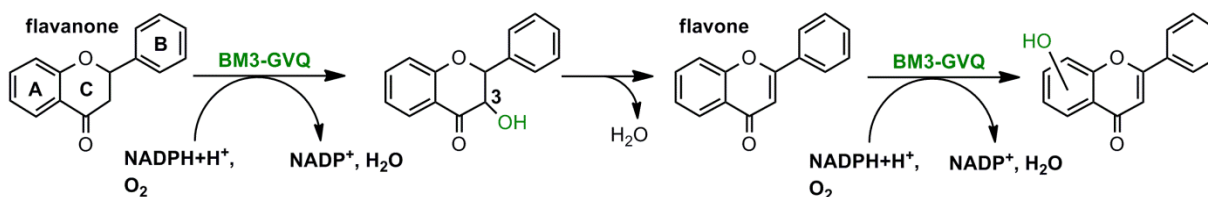


Fig. 4.9: Conversion of flavanone by BM3-GVQ. BM3-GVQ catalyzes the hydroxylation of position 3 (ring C). Water is eliminated and the unsaturated flavone is formed. This acts as a substrate and is further hydroxylated at ring A (undefined position).

Initially, position 3 of ring C of flavanone is selectively hydroxylated by BM3-GVQ yielding 3-OH flavanone. Subsequently, water is eliminated forming the unsaturated flavone that acts as a further substrate and is hydroxylated in the ring A at a hitherto undefined position. All products were detected via GC-MS in different amounts within the assay (Fig. B 5). HED and hesperetin are only marginally converted (< 10%) by BM3-GVQ. Hesperetin was demethylated forming ED in low yields. HED was hydroxylated at position 3 (ring C) as also observed for flavanone (Fig. B 4). The *in vitro* conversion of HED was under 5 % with no relevance for the *in vivo* enzyme cascade.

4.3.2.4 Importance of the triple mutant BM3-GVQ

BM3-GVQ shows highest activity of the screened variants (section 4.3.1). The mutations are located at the entrance of the mainly hydrophobic channel leading to the heme cofactor, which control entry to the active site (Fig. 4.10).

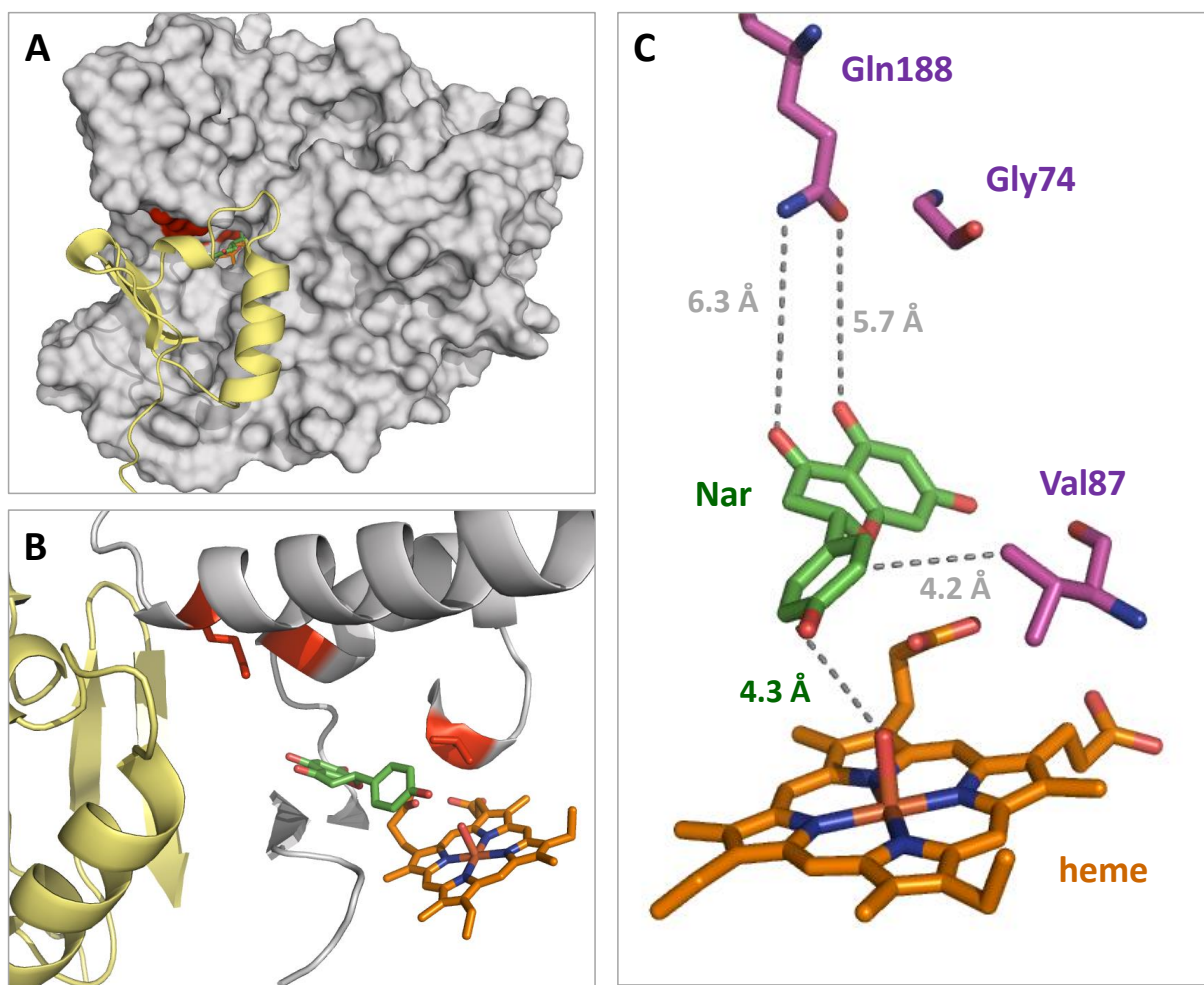


Fig. 4.10: Structural model of naringenin docked in BM3_GVQ. A) Overall view of the BM3 heme domain (gray). The substrate binding channel is closest by the flexible N-terminal part (yellow) of the heme domain. B) Closeview of the substrate binding channel. The mutated residues in BM3_GVQ (red) are flanking one site of the channel. C) Active site and closest atom-to-atom distances between the docked substrate naringenin and the mutated residues (indicated as gray lines). The distance between the substrates reacting 3' and the activated heme-oxygen is 4.3Å in this docking mode. The model of BM3_GVQ was generated using PDB-code 1BU7.

The exchange of Phe87 by valine seems to be of particular importance, because BM3-GAQ (A74G/**F87A**/L188Q) was not active using Nar as a substrate, while both – BM3-GVQ (A74G/**F87V**/L188Q) and BM3-F87V possess activity towards Nar. To dissect the individual effects of mutations at position 74 and 188, double variants A74G/F87V (BM3-GV) and F87V/L188Q (BM3-VQ) were prepared and transformed into *E. coli* BL21 (DE3). After suc-

68

Successful expression of BM3-GV and BM3-VQ the new variants were verified for correct folding via CO difference spectra measurement (Fig. B 9) and tested for conversion of Nar. Both variants catalyze the formation of ED (3'-OH Nar) but also the formation of apigenin (3-OH Nar) that was determined by LC-MS/MS measurements. In the GVQ assay, apigenin occurs only as a byproduct in minor ratio to the main product ED (approximately 1:4) compared to the conversion of Nar in the activity assays of the other BM3 variants (Fig. 4.11).

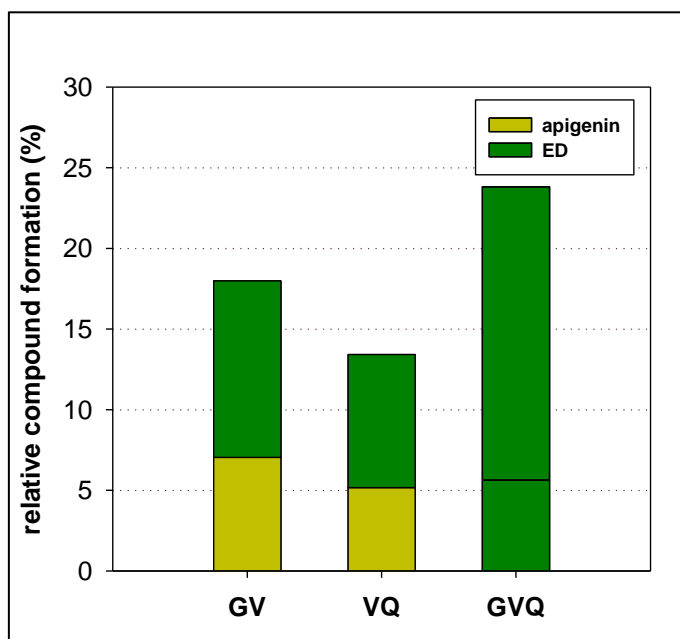


Fig. 4.11: Compound formation of the created BM3 double mutants and BM3-GVQ in the enzyme activity assay using Nar as a substrate. Conversion was analyzed in a standard in vitro assay system using 200 μM of substrate (Nar) and 500 nM of enzyme of the respective BM3 variant. BM3-GVQ catalyzes the highest conversion of Nar and the lowest percentage of the side product apigenin (3-OH Nar).

BM3-GVQ was still the most active enzyme catalyzing the formation of ED (3'-OH Nar) and also shows the lowest percentage of the side product apigenin (3-OH Nar).

4.3.2.5 Optimization of the assay conditions for naringenin conversion

The BM3-GVQ/Nar system shows only a moderate substrate conversion of ~ 25 %. To increase the yield of ED the BM3-GVQ *in vitro* assay was investigated regarding different factors: incubation time, enzyme concentration, buffer system, substrate concentration, product inhibition, initial NADPH concentration and activity of the NADPH regeneration system.

a) Time dependence of ED-formation

The dependence of the conversion of Nar into ED from the incubation time was analyzed in a standard *in vitro* assay system using 200 μM of the substrate Nar and 820 nM BM3-GVQ (Fig. 4.12).

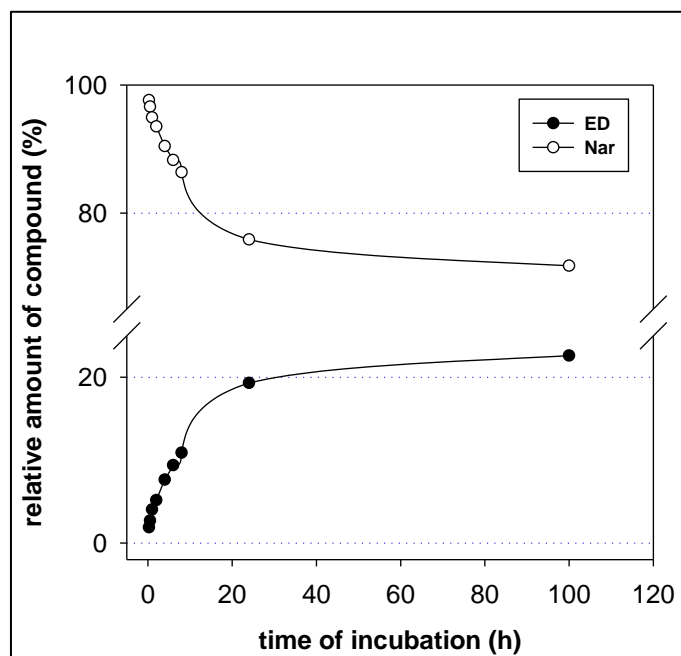


Fig. 4.12: Time course of the conversion of Nar to ED by BM3-GVQ. The assay was performed under standard conditions using 820 nM of BM3-GVQ and 200 μM of the substrate Nar.

Upon an initial fast depletion of Nar within the first two hours (~ 4 % product formation) the reaction proceeds for 24 h with a final yield of ~20 % ED. Addition of fresh enzyme at this time-point does not lead to higher product yield. This indicates that after 24 h the assay is in a non-productive state. This might be either due to depleted cofactor-regeneration system or the accumulation of inhibitory factors that inactivates the enzyme (e.g.: product inhibition).

b) Influence of enzyme concentration

The dependence of Nar conversion from the initial concentrations of active enzyme was analyzed in the range of 35 to 1733 nM catalyst. ED yield and the total turnover number (TTN) calculated as the molar ratio of product formation to the catalyst was correlated to the enzyme concentration (Fig. 4.13).

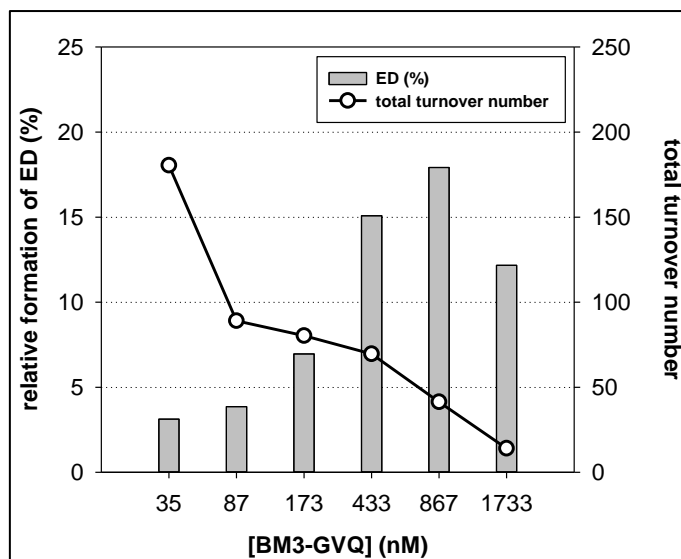


Fig. 4.13: Correlation of the applied GVQ enzyme concentration to the ED yield and to the resulting total turnover number (TTN). Increasing the enzyme concentration within the BM3-GVQ assay, the relative formation of ED was enhanced until an applied enzyme concentration of 867 nM. The highest TTN is achieved by the lowest enzyme concentration and decreases strongly by the addition of more enzyme.

Increasing the concentration of BM3-GVQ up to 867 nM leads to an enhanced product formation while the yield decreases at higher concentrations. In contrast, the TTN shows the highest value at the lowest GVQ concentration (35 nM) and gradually decreases at higher enzyme concentrations. This behavior could be explained by the presence of an enzyme-dependent-inhibitory-process. This inhibitory process might be the decoupling reactions in the GVQ assay (“shunt” pathway) producing toxic substances like H_2O_2 that poisons the enzyme and therefore decreases the conversion of Nar.

c) Initial substrate concentration and product inhibition

Enzymes can be altered in their activity by substances that influence the binding of the substrate [131]. Especially, flavonoids can inhibit enzyme activity of CYPs [132]. To clarify if the initial concentration of the substrate or the formation of ED has an inhibitory effect on the conversion of Nar by BM3-GVQ, two approaches were used.

To examine the optimal substrate concentration and to identify a potential enzyme inhibition by the substrate, initial concentration of Nar was modified in the range of 10 to 200 μ M within a standard BM3-GVQ assay system using 870 nM of enzyme. Percentage formation of ED was analyzed and compared to the initial Nar concentration (Fig. 4.14). Nar concentration has no influence on the conversion as the relative product outcome (ED) is constant with increasing Nar concentration.

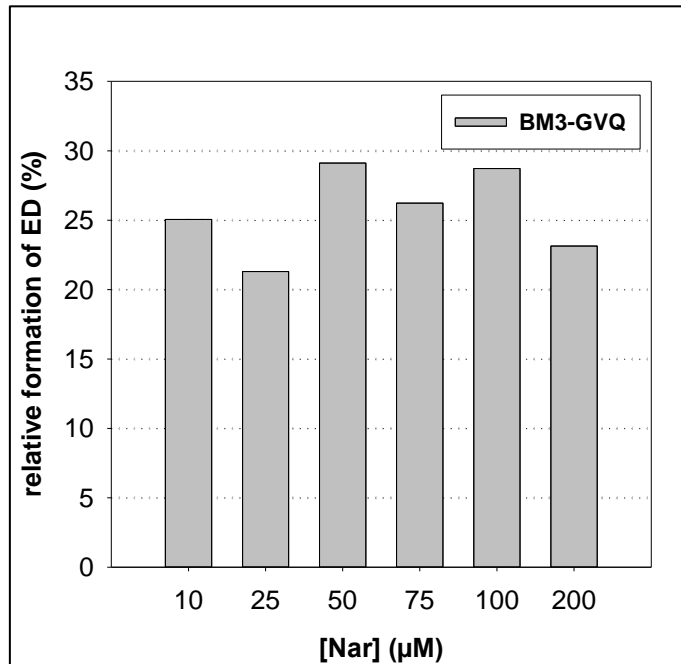


Fig. 4.14: Variation of the initial concentration of Nar. A standard BM3-GVQ assay (870 nM BM3-GVQ) was performed and relative formation of ED was analyzed. Relative ED formation is constant (21-29 %) with increasing Nar concentrations.

Product formation can also cause inhibitory effects. To determine if increasing ED concentration suppresses the conversion of the substrate by toxification or inhibiting the biocatalyst, a BM3-GVQ assay was performed using 25 % initial ED concentration (50 µM) and 150 µM Nar. These concentrations reflect the situation at the end of a standard conversion of 200 µM Naringenin. After 1000 min incubation of this substrate/product mixture, 46.2 % ± 5.0 % ED was detected in the assay containing BM3-GVQ and 22.6 % ED in the control without the enzyme (empty vector control). Hence no inhibitory effect of ED for the BM3 catalyzed conversion of naringenin was observed. The yield of ED neither depends on the substrate concentration, nor on the product concentration, indicating the presence of another inhibitory effect.

d) Influence of the buffer system

Enzymes are sensitive to pH value. Within their narrow range of accepted values, the pH can influence the ionization and the binding of the substrate(s) to the enzyme and hence affect their catalytic activity [133].

Standard BM3-GVQ assay was performed in 50 mM Tris-HCl buffer at a pH value of 7.5. To optimize and increase the conversion rate, the buffer system was modified and pH value was

varied in the range of 6.5 and 8.5. The relative formation of ED was compared to the different buffer systems at two different time points of incubation (Fig. 4.15).

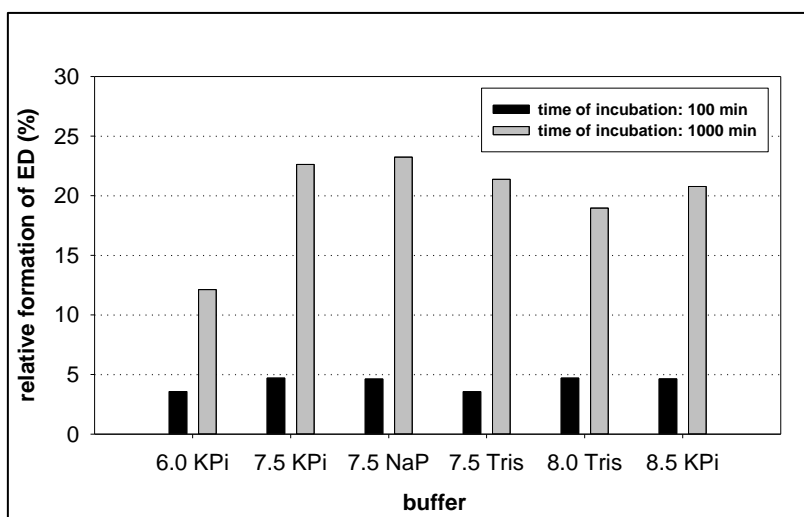


Fig. 4.15: Evaluation of the BM3-GVQ assay buffer. Standard BM3-GVQ assay was performed in Tris-HCl buffer at a pH value of 7.5. Buffer system was modified and the tested pH value ranged from 6.5 to 8.5. Modification of the standard assay buffer conditions did not increase the formation of ED at two different time points of incubation. As a consequence, the standard assay buffer (Tris-HCl, pH 7.5) for BM3-GVQ was not changed.

The variation of the buffer substance only slightly influences the formation of ED. The yield of ED is around 20 % independent from the buffer compound (potassium phosphate, sodium phosphate, Tris-HCl) in the pH range between 7.5 and 8.5. At pH 6.0 the yield decreases to 12 % after 1000 min reaction time, while the amount of ED after 100 min incubation is similar to the other conditions (4 %). That hints to a faster inactivation of the enzyme at lower pH value. Concluding, no significant improvement of ED formation could be achieved by the modification of the buffer substance and the standard buffer (Tris-HCl, pH 7.5) was used for further investigations.

e) Influence of cofactor concentration and regeneration system

NADPH supplies electrons and hydrogen ions for the hydroxylation process of Nar. Reduction equivalents are very expensive (NADPH: ~1400 € mmol⁻¹, Sigma Aldrich) and would constitute a major cost factor in an industrial process. Within the BM3-GVQ assay system, costly NADPH is regenerated from NADP⁺ by glucose-6-phosphate-dehydrogenase (glc-6-P) consuming less expensive glucose-6-phosphate (glc-6-P: ~13 € mmol⁻¹, Sigma Aldrich). A standard assay contains 200 μM of substrate, 100 μM of cofactor and 5 mM of glc-6-P and thus allows the 50fold regeneration of NADPH in theory.

NADPH consumption was analyzed in a BM3-GVQ assay system without the substrate Nar (Fig. 4.16). Fig. 4.16A illustrates that NADPH ($\lambda=340$ nm) is expended also in the absence of Nar. This indicates a separate pathway like so called shunt pathway that forms H_2O from oxygen or a decoupling process producing H_2O_2 from oxygen. To verify NADPH consumption of a BM3-GVQ assay in the absence of Nar and to prove the functioning of the NADPH regeneration system, same assay conditions were applied without adding glc-6-P-DHG and glc-6-P (Fig. 4.16B).

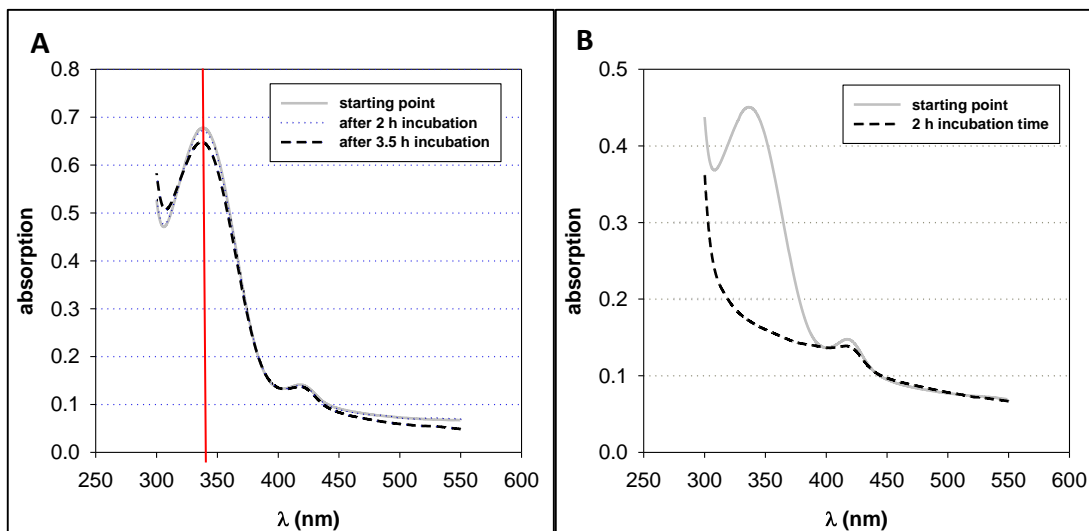


Fig. 4.16: A: Oxidation of NADPH by BM3-GVQ in presence of the regeneration system. NADPH is oxidized by BM3 only to a minor extent after 3.5 h incubation time. **B: Oxidation of 100 μ M NADPH ($\lambda=340$ nm) by BM3-GVQ in absence of the regeneration system.**

After 2 h incubation time, NADPH was almost completely consumed. This indicates a high activity for the separate uncoupled pathway and also highlights the strong dependence of the BM3-GVQ assay system from the NADPH regeneration system.

A spectrum of a standard BM3-GVQ assay including the NADPH regeneration system and Nar as a substrate was analyzed to evaluate the efficiency of the regeneration system (Fig. 4.17A). Even after 3.5 h of incubation the amount of NADPH is only slightly decreased.

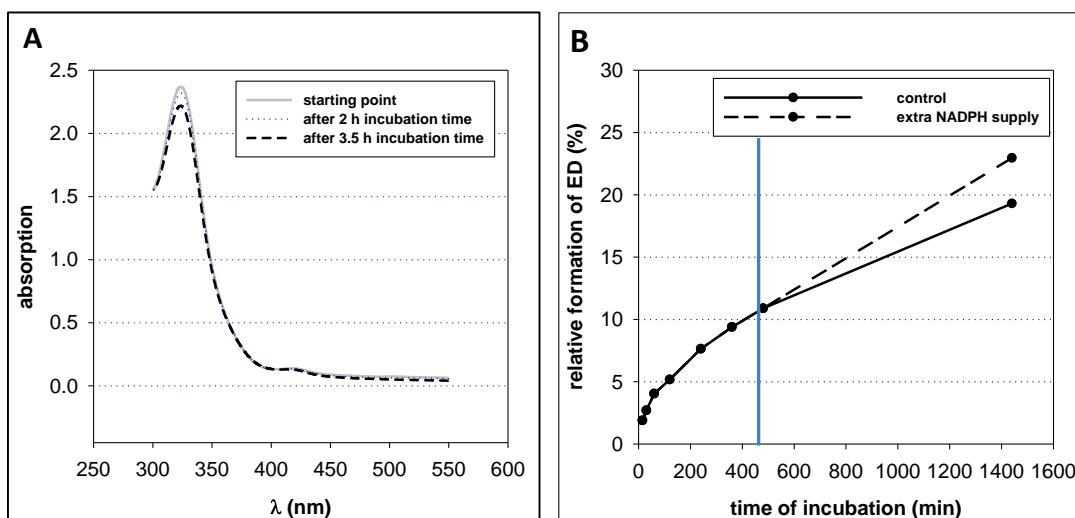


Fig. 4.17: A: NADPH consumption of a standard BM3-GVQ assay. After 3.5 h (dashed line), NADPH slowly decreased, but is still available in the assay. The regeneration system is efficient, thus NADPH is not the limiting factor of the incomplete conversion of Nar into ED at the beginning of the reaction. **B: Extra supply of NADPH and regeneration system after 8 h incubation compared to a standard BM3-GVQ assay.** The addition of fresh NADPH and regeneration system increases the formation of ED slightly (up to 20 %, dashed line) compared to a standard BM3-GVQ assay under equal conditions (control: solid line). The assay was performed in a 2 ml scale under standard conditions using 0.8 μM BM3-GVQ.

Thus, the regeneration system is highly efficient and NADPH concentration is still available for the conversion of Nar into ED after 3.5 h incubation. However, the extra supply of NADPH after 8 h preincubation enhances the formation of ED by some 20 % in comparison to a control (Fig. 4.17B) indicating that the NADPH level is a limiting factor in a later state of incubation.

A further experiment was performed to examine the required initial NADPH concentration for conversion of Nar into ED. A standard BM3-GVQ assay was performed for two different enzyme concentrations to analyze the formation of ED at varying initial NADPH concentrations in a range of 10 μM to 200 μM (Fig. 4.18).

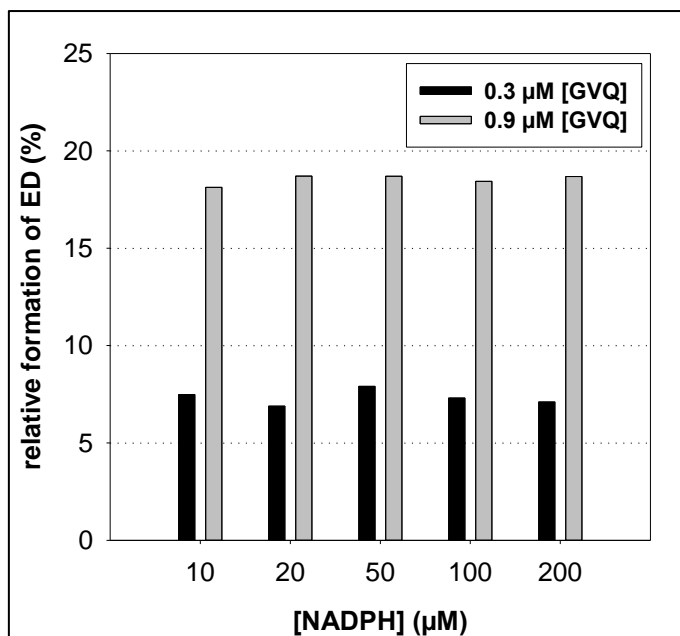


Fig. 4.18: Influence of the initial concentration of NADPH on the formation of eriodictyol. For two different enzyme concentrations no effect was obtained in the NADPH range of 10 μM to 200 μM.

The conversion of Nar into ED is independent of the initial NADPH concentration in this concentration range. The regeneration system is efficient and provides sufficient NADPH for the formation of ED. Strikingly, only 10 % of the standard NADPH concentration (100 μM) is required to generate the same ED amount in the BM3-GVQ assay. Additionally, this setup also allows the exchange of NADPH by NADP⁺ (~ 300 € mmol⁻¹), as the regeneration system for the latter will readily reduce the cofactor costs. Thus, an exchange of 100 μM NADPH by 10 μM NADP⁺ yields the same amount of ED while decreasing the cost for cofactor by a factor of ~45.

4.3.2.6 Influence of H₂O₂ formation on naringenin conversion

The decrease of the total turnover number for the BM3-GVQ catalyzed conversion of Nar at increasing enzyme concentrations as well as the NADPH consumption in the absence of Nar hint to an uncoupled consumption of O₂ by BM3-GVQ. According to the known shunt processes, H₂O₂ might be an expected product.

a) H₂O₂ level of the BM3-GVQ assay

An HRP o-dianisidine assay was used to determine the production of H₂O₂. An external calibration curve (Fig. 4.19A) was measured to calculate the produced H₂O₂ level of the BM3-GVQ *in vitro* assay after linear regression:

$\text{abs} = 3.228 \times 10^{-4} [\text{H}_2\text{O}_2] + 0.0618$. Fig. 4.19B visualizes the H_2O_2 concentration in dependence of the incubation time of a standard BM3-GVQ assay. After 1 h incubation time, H_2O_2 production was detectable and increased rapidly by further incubation. After 2.5 h incubation time, over 1 mM H_2O_2 could be measured.

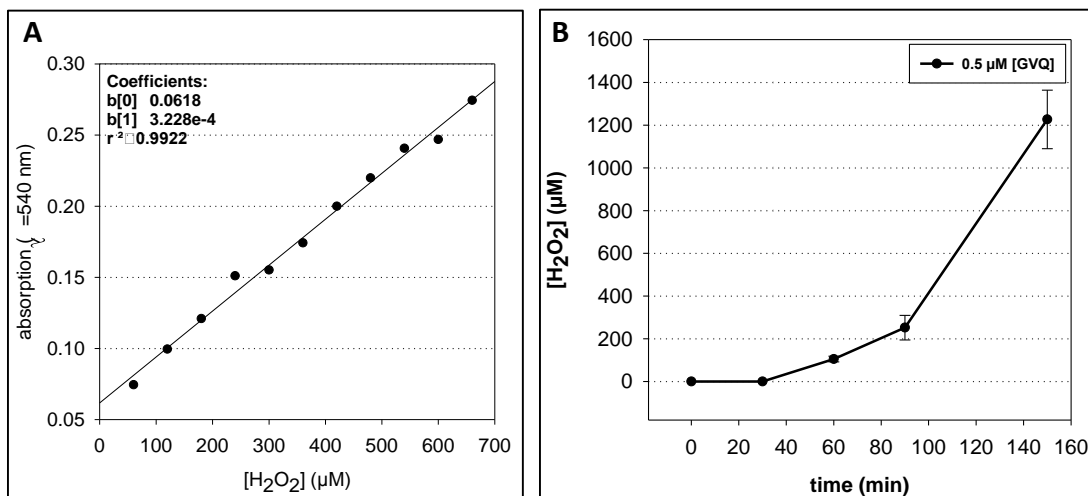
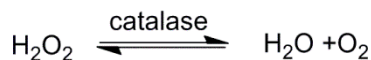


Fig. 4.19: A: External calibration line of the H_2O_2 concentration. B: H_2O_2 production within the BM3-GVQ assay measured via HRP o-dianisidine assay. After 2.5 h incubation time, more than 1 mM H_2O_2 was produced by BM3-GVQ consuming O_2 and NADPH of the system.

Shunt pathways require also NADPH and O_2 , hence these consumed (co)-substrates are no longer available for the hydroxylation of Nar. Additionally, the formation of H_2O_2 can lead to inactivation of the catalyst, or abiotic oxidation of substrate or product.

b) Catalase addition for H_2O_2 reduction

Catalase, an ubiquitous heme protein, constitutes a common defense strategy of cells to protect themselves from cell damage induced by H_2O_2 . The enzyme catalyzes the reaction of H_2O_2 into water and molecular O_2 [134]:



6 U catalase were applied in the BM3-GVQ assay to degrade the produced H_2O_2 (Fig. 4.20) and, as a consequence, to avoid the possible inactivation of the biocatalyst and to restore the consumed cosubstrate O_2 .

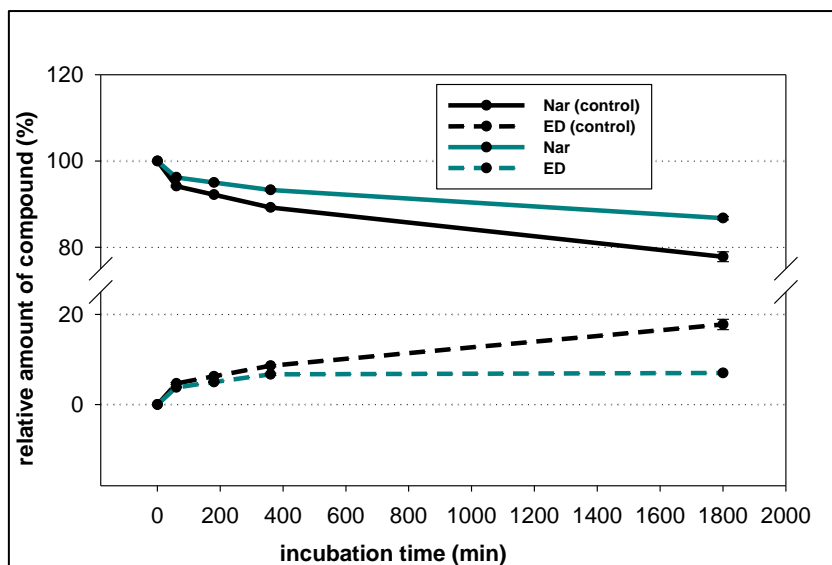


Fig. 4.20: Effects of catalase addition. Conversion of 200 μ M Nar by BM3-GVQ in a standard reaction using 500 nM BM3-GVQ was investigated in absence (control, black) or presence of 6 U catalase (dark cyan). After 400 min incubation time, the formation of ED stopped within the catalase assay, but Nar was further converted into other products. A standard BM3-GVQ assay was used as a control.

After 360 min incubation time, no further ED formation was observed in the catalase assay, but Nar was still consumed. After incubation overnight, more ED was formed in a standard BM3-GVQ assay than in the assay containing catalase. Furthermore, the assay containing catalase produced byproducts. Thus, the addition of catalase was not successful to optimize the reaction *in vitro* and to increase the formation of ED.

4.3.3 Design and screening of new BM3 variants

As all attempts to improve the conversion of Nar into ED by BM3-GVQ failed, new BM3 variants obtaining better ED yields should be generated. To increase the conversion of Nar bioinformatics techniques were applied (section 2.6.4.1). A protein model (Fig. 4.21) of BM3-GVQ was built based on the X-ray structure of BM3 wild type (pdb-code: 1bu7). Nar was docked into the active site. The resulting structure was used to identify positions for the insertion of stabilizing hydrogen bonds that potentially increase affinity and catalytic activity of BM3 for Nar (Fig. 4.21). Two amino acids were suggested for mutations: Leu75 and Ala330. The mutations were suggested to increase the interaction of hydrogen bonds within the binding pocket and thus to improve substrate recognition and to influence the substrate saturation.

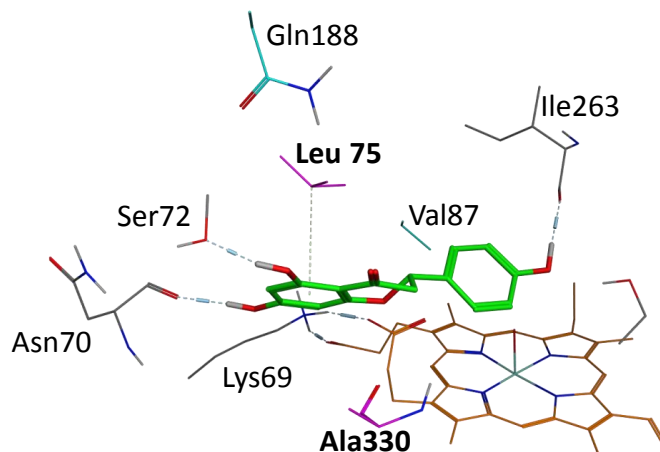


Fig. 4.21: Docking studies of Nar (green) in the active site of a BM3 GVQ model based on BM3 wild type (pdb-code: 1bu7). Suggested mutations at selective amino acids are highlighted in pink. The light blue amino acids visualize the mutations F87V and L188Q in BM3-GVQ. A74G is not shown.

For mutation at position 75 (L75S and L75N), plasmids of BM3-VQ and BM3-GVQ were used as a template to prove an influence of the adjacent position 74 (A74 or G74) on the new enzyme variants (L75S or L75N). The four resulting mutants were heterologously expressed in *E. coli* BL21 and analyzed by SDS-PAGE for successful overexpression (Fig. B 8). CO difference spectra measurements showed a characteristic absorbance maximum at $\lambda = 450$ nm but also a further signal at $\lambda = 420$ nm (Fig. 4.22); the latter is a typical signal for inactive species resulting from incorrectly folded active center of P450 enzymes or from partial denaturation [135]. Indeed, no activity with Nar was found for all four variants.

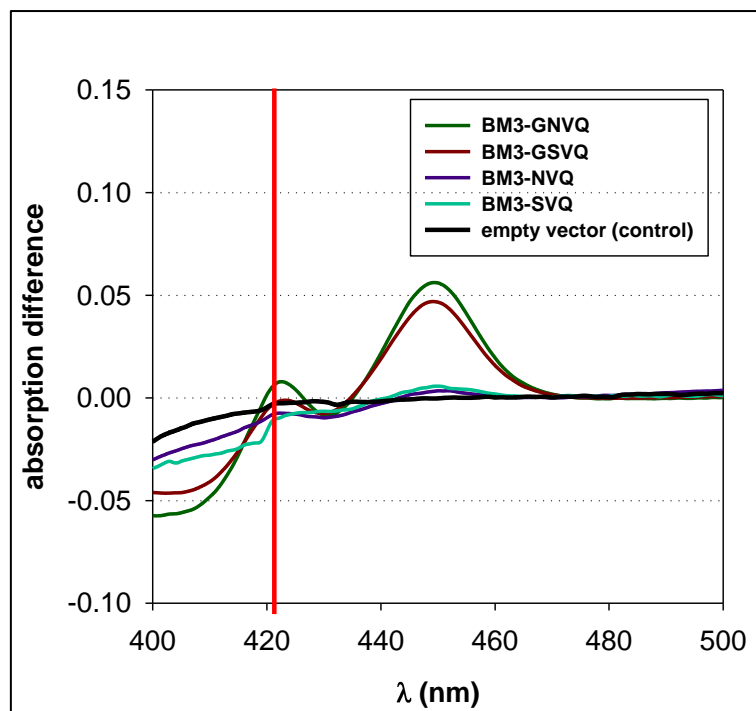


Fig. 4.22: CO difference spectra of BM3- variants based on BM3-GVQ or BM3-VQ containing a further mutation at position L75. In addition to the typical Soret band at 450 nm, a further maximum was detected at ~ 420 nm which is characteristic for incorrectly folded P450 enzymes or partial denaturation [135].

For the second predicted, relevant amino acid position that might increase the activity of the BM3-GVQ, a quadruple variant GVQS (A74G/F87V/L188Q/A330S) was created, transformed and overexpressed in *E. coli* BL21. CO difference spectra showed a typical spectrum of correctly folded P450 enzymes with a single Soret band at 450 nm (Fig. B 9). In the enzyme activity assay, BM3-GVQS converted Nar into ED but also into apigenin. To compare all active variants regarding their product formation, the enzymes were tested under equal conditions (0.42 μM enzyme, 200 μM substrate incubated for 1000 min at 25° C) for the conversions of Nar (Fig. 4.23).

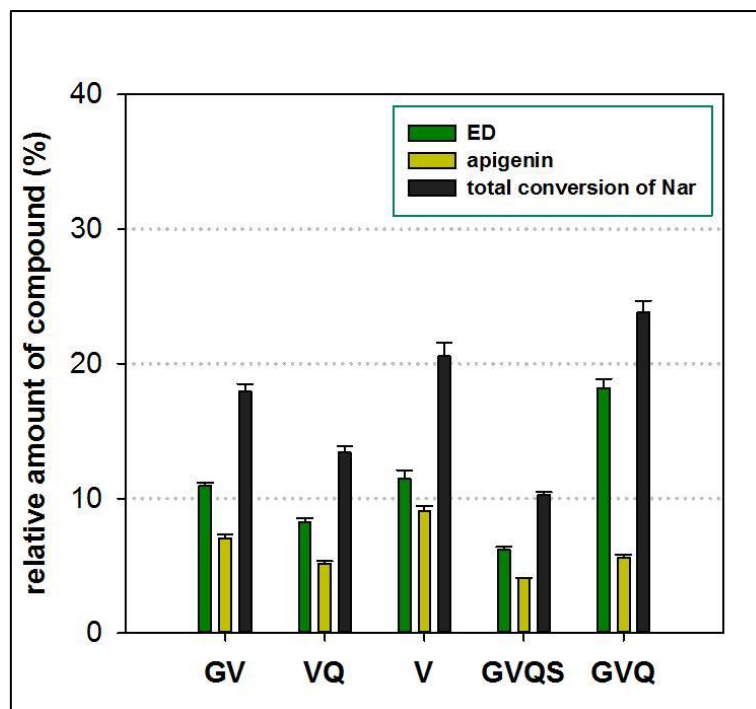


Fig. 4.23: Product distribution and total conversion of Nar catalyzed by different BM3 variants. The enzyme activity assay was performed under equal conditions using 420 nM enzyme of each variant and 200 μ M Nar in a BM3 standard assay that was incubated for 1000 min at 25° C. The GVQ enzyme is the most active variant for the conversion of Nar.

The highest conversion of Nar was still achieved by the BM3-GVQ variant. Also the content of the byproduct apigenin is lower compared to the other active variants. BM3-GVQ was still the most active enzyme to convert Nar into ED.

4.3.4 *In vivo* biotransformation of Naringenin

For industrial applications in multistep, cofactor-dependent processes, *in vivo* conversions are usually preferred, as thereby steps like cell lysis and protein purification can be avoided. Furthermore, *in vivo* transformations do not require the addition of expensive cosubstrates, cofactors or regeneration systems as all the respective compounds are provided by the growing cell. In addition, cells contain detoxification systems against reactive oxygen species (ROS), e.g.: catalase and glutathione peroxidase that catalyze the degradation of potential toxic by-products like H_2O_2 [131].

Biotransformation of Nar was performed *in vivo* with BM3-GVQ. Two different media were analyzed: LB medium and IPTG-induced overexpression of BM3-GVQ as well as auto-inducing (AI) medium (Fig. 4.24). An *E. coli* BL21 strain bearing an empty vector was used as a control.

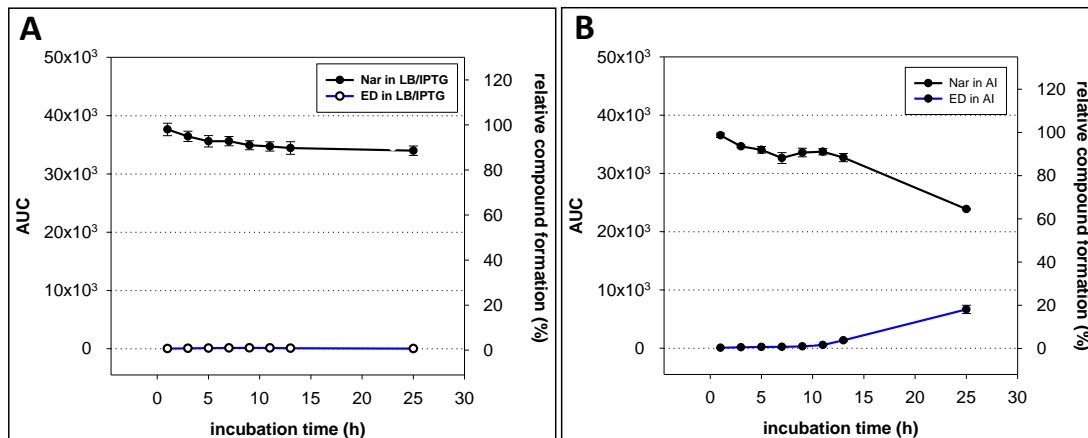


Fig. 4.24: *In vivo* conversion of Nar by BM3-GVQ in two different media. A: The area under the curve of the signal in the HPLC chromatogram ($\lambda=325$ nm) was used to estimate the amount of the compounds. An empty pET-28a(+) vector transformed into *E. coli* BL21 (DE) cells was used as a control for conversion. After 25 h, no conversion of Nar into ED could be achieved in the LB/IPTG medium (A) in contrast to the AI medium (B). However, product formation and substrate conversion was first detected in AI-medium after 12 h.

After 25 h, no formation of ED was detected for the biotransformation in LB medium even though distinct expression of the variant was detected by SDS-PAGE (Fig. B 10). In AI medium, ED formation could not be observed until 12 h incubation time, although the enzyme was previously already detectable after 4 h of incubation (Fig. 4.25).

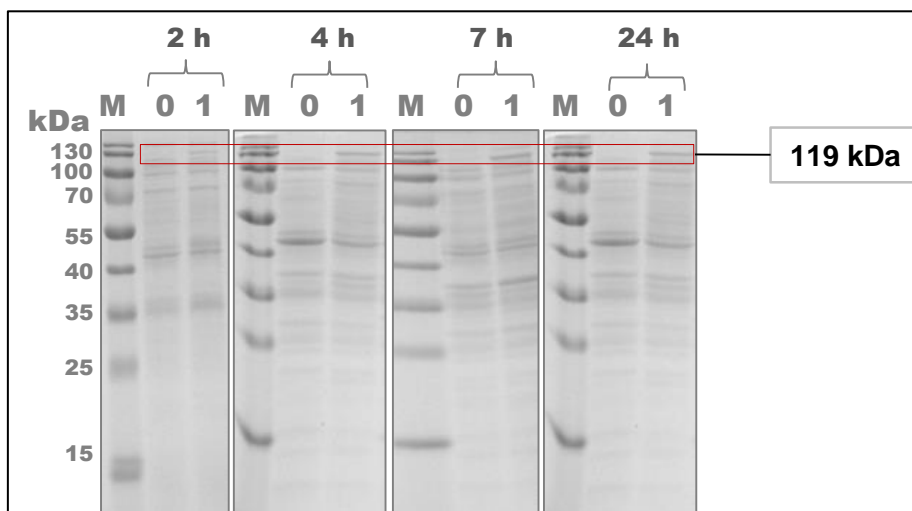


Fig. 4.25: SDS-PAGE of BM3-GVQ variant (1) and an empty vector as a control (0) after *in vivo* biotransformation of Nar in AI medium at different time points of incubation. After 2 h no significant protein band was detected in the BM3-GVQ variant (1). A slight band at the expected molecular weight of the BM3-GVQ protein (119 kDa) was initially observed after 4 h incubation. Although ED formation was initially detected after 12 h of incubation the BM3-GVQ show a similar protein band with low expression after 4 h, 7 h and 24 h of incubation.

In addition, with a maximal yield of 18 % ED after 25 h, the conversion was less efficient as the *in vitro* BM3-GVQ system (up to 25 % ED).

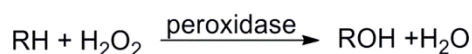
4.4 Discussion

Three enzymes were investigated for the selective 3' hydroxylation of Nar to form ED after a screening of more than 30 different oxygenating biocatalysts. The variant GVQ (A74G/F87V/L188Q) of the self-sufficient P450 enzyme BM3 showed the highest conversion of the initial three candidates and can be easily expressed in *E. coli* as a soluble protein. However, even with this variant the reaction was still incomplete. Therefore, the *in vitro* enzyme activity assay was analyzed regarding the parameters incubation time, enzyme concentration, substrate and product inhibition, cofactor and cosubstrate availability and the influence of buffer and pH value. Finally, the BM3-GVQ assay system was tested in an *in vivo* biotransformation.

A maximum of around 25 % Nar consumption and therefore ED formation was achieved by increasing the initial enzyme concentration. Indeed, the highest TTN (ca. 180) of BM3-GVQ was achieved with the lowest enzyme concentration (35 nM, section 4.3.2.5) and gradually decreases to ~10 % with enzyme concentrations up to 1733 nM. These observations hint to a possible inhibition of the enzyme by the product or to undesired shunt pathways producing inhibitory or toxic compounds. The presence of product inhibition was tested using an initial concentration of 25 % ED in the standard assay. The conversion of Nar was still about 25 %. Hence ED does not inhibit the reaction. However, the *in vitro* conversion using crude extract was under 5 % with no relevance for *in vivo* biotransformation.

Investigation of the cofactor NADPH-dependency of the assay highlighted the indispensability of the regeneration system (section 4.3.2.5) for the conversion of Nar into ED. NADPH provides electrons for the activation of iron and consequently for the hydroxylation of the substrate Nar. Though, NADPH is rapidly consumed in the BM3-GVQ assay also in absence of Nar (Fig. 4.16). Hence, NADPH must be consumed in shunt pathways. Highly active CYPs like BM3 can catalyze such decoupling reactions that produce ROS, primarily superoxide and peroxide [136]. The production of up to 1 mM H₂O₂ within the first hour of *in vitro* enzyme reaction was shown (section 4.3.2.6). ROS like superoxide and H₂O₂ causes enzyme inactivation by poisoning the active site of the biocatalyst and might explain the decreased TTN of the BM3-GVQ – Nar assay at higher enzyme concentrations. Beside the potential inactivation, this reaction also leads to the depletion of molecular oxygen which is thus less available for the desired oxidation of Nar. The concentration of solved O₂ is around 250 μM under the applied conditions and might be much lower in an assay containing high NADPH-oxidizing activities.

To prove if H₂O₂ causes the ED formation by a spontaneous non-enzymatic hydroxylation, catalase was applied to remove the H₂O₂ formed in the BM3-GVQ assay. Furthermore, catalase should protect the protein itself from inactivation due to the reactive H₂O₂. Additionally, catalase might restore molecular oxygen for the conversion of Nar. Both facts should have a positive effect on the ED formation. However, until 400 min incubation time the catalase addition leads to a similar time-dependent ED formation compared to the control (without catalase). H₂O₂ is rapidly degraded by catalase as it is formed slowly. Therefore, no H₂O₂ is available in the beginning of the reaction, thus hydroxylation of Nar is independent from this peroxide. After 400 min incubation time, the ED formation stagnated in the catalase assay whereas ~20 % ED was formed in the control. In addition, Nar was still converted but into undesired products. Probably these side products are formed due to the peroxidase-activity of catalase. It has been shown that catalase can oxidase aromatic substrates at high H₂O₂ concentration [134]:



The stereoselectivity of the ED formation was investigated since incomplete conversion of Nar could be caused by an enantioselective conversion by BM3. As typical for flavanones, Nar and ED bear a stereogenic center at atom C-2 of the ring C [137]. This ring system can easily be cleaved to the chalcone form and re-closed to the flavonoid by a slight change in the pH value resulting in a racemate [138]. Nar was applied as a racemate in the assay and was analyzed by chiral HPLC. Racemization due to chalcone formation on re-cyclization was investigated at different pH-values of the reaction buffer. Nar and ED was always a racemate in the assay and pH variation in the range of 6.0 until 8.5 could not increase the ED formation. Hence, the incomplete substrate conversion was not caused by enantioselective catalysis.

Another approach focused on protein engineering by site-directed mutagenesis. With the help of bioinformatics, BM3-variants were proposed and tested for ED formation. Variants bearing a mutation at position L75 showed altered CO difference spectra compared to BM3-GVQ and were inactive most likely due to a wrong protein folding. Mutation at position A330 leads to an active variant, but the conversion of Nar into ED was lower than with BM3-GVQ. The mutation A330S was inserted to increase the binding of the substrate Nar due to the formation of hydrogen bonds of serine in contrast to the non-polar amino acid alanine. The lower activity of the new variant BM3-GVQS can be reasoned by the hindrance of the product released from the active site: the substrate was calculated to interact with the amino acid 330, but the

product ED bearing a further hydroxyl group might also interact with the new hydrogen bond. Hence, the stronger binding of the product might reduce the rate of reaction due to a slowly release of the product. Furthermore, the substrate also binds to the active site by further interactions like hydrophobic or van der Waals interactions which were not included in the calculation. The exchange of alanine to serine enhances the polar character of the active site and might decrease hydrophobic interaction with the substrate. However, to verify this assumption further investigations are necessary.

Finally, the most active variant, BM3-GVQ was applied in an *in vivo* biotransformation. This enables cofactor-supply by *E.coli* and *in vivo* removal of toxic side products like reactive oxygen species (ROS), superoxide and H₂O₂. In addition, the system was tested as a proof of concept for the biotechnological application. The conversion was successful but still incomplete (under 20 % ED formation). Thus, *in vivo* biotransformation could not increase the conversion of Nar to ED. In addition, after 24 h the substrate was further metabolized, but the ED formation has stopped. A surprising observation was, that no direct correlation between protein synthesis and substrate conversion was detected. For example, no product formation was detected in LB/IPTG medium although good expression of the BM3-GVQ variant was observed. Additionally, the formation of ED under autoinducing conditions started after 12 h incubation time, although the protein was already present after 4 h. A reason might be the problem of accessibility of the substrate. The time delay between expression of the protein and ED formation could hint to the involvement of a carrier protein and/or a transporter for the substrate Nar which might be expressed in a later stage of growing. It has been shown before that accumulation of high amount of indole in *E. coli* induces the expression of multidrug exporter genes [139]. Indole formation was also detected in the *in vivo* biotransformation after expression of BM3-GVQ [140]. A similar system might act to import the substrate Nar into the *E. coli* cells.

Another problem could be the availability of cofactors and cosubstrates. *In vivo* biotransformation was performed in flasks shaken in an incubator at high rpm to provide enough oxygen for the hydroxylation process. NADPH is provided and can be regenerated by the cells but it is unknown whether these capacities can meet anticipated demand for industrial ED production.

4.5 Outlook

Selective hydroxylation of Nar is the initial step in the enzyme cascade; additionally it is the bottleneck for the production of HED. The enzyme BM3-GVQ was identified to catalyze the

biotransformation of Nar into ED *in vitro* and *in vivo*. *In vivo* conversion of Nar was confirmed as a proof of concept. Hence, the enzyme has not to be purified and/or external addition of expensive cosubstrates and cofactors for the conversion of Nar is not necessary. The substrate is directly added to the culture and ED is available after 24 h incubation time. Although the conversion was incomplete, the system can be further optimized using, e.g., insertion of a coexpressed NADPH regeneration system. Modification of the culture media composition can also regulate product formation as well as other bioprocess conditions like temperature or glucose level [141]. Process optimization might lead to a higher efficiency of the substrate conversion. Finally, the two-enzyme cascade could be performed in a proper host by coexpression of BM3-GVQ with a suitable OMT.

BM3 is already commonly used as biocatalyst for industrial applications and process efficiency has been investigated since several years. The selective hydroxylation of Nar to produce ED of a selective BM3-variant, i.e. GVQ, in laboratory scale constitutes the basis for efficient bioprocess design.

5 Chapter III: Methylation of ED – the final step of HED biosynthesis

5.1 Introduction

O-methyltransferases (OMTs) catalyze the transfer of a methyl group from a methyl donor to, e.g., hydroxyl or carboxyl groups [142]. HED is formed by the selective 3'-O-methylation of ED catalyzed by a specific 3'-OMT in the phenylpropanoid pathway in plants (Fig. 5.1). S-adenosyl-L-methionine (SAM or AdoMet) acts as the methyl donor and is itself converted to S-adenosyl-L-homocysteine (SAH).

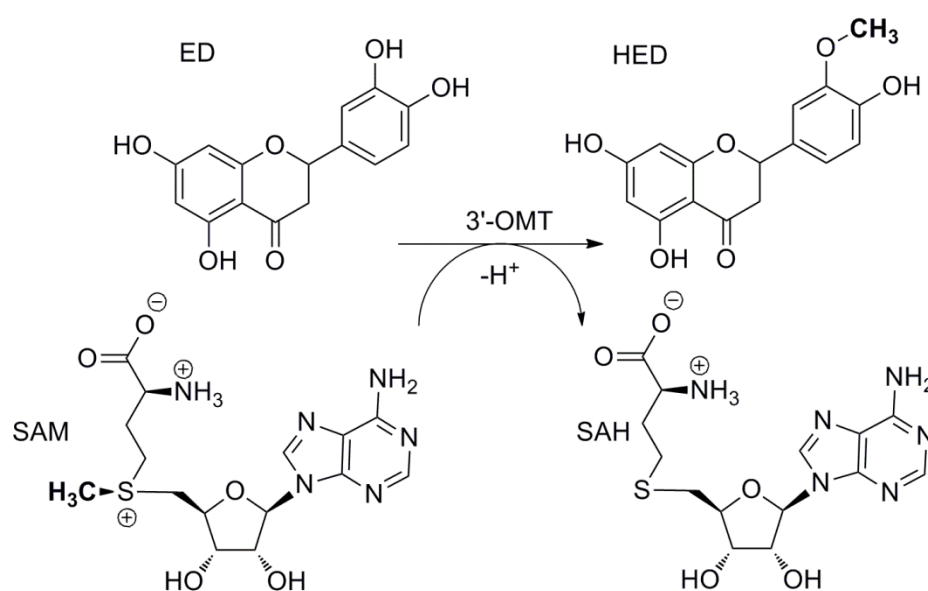


Fig. 5.1: Reaction scheme of the 3'-OMT-catalyzed transfer of the methyl group from S-adenosyl-L-methionine (SAM) to ED forming HED. SAM acts as the methyl donor and is itself converted to S-adenosyl-L-homocysteine (SAH). The transferred methyl group is drawn in boldface type.

SAM is the most relevant methyl donor in nature and was already discovered in 1953 by Cantoni [143]. The mechanism of these methyl group transfer reactions is well investigated since several decades, and was shown to proceed by a nucleophilic substitution process [144]. Due to the strong electron-withdrawing effect of the positively charged sulfur atom, the methyl group of SAM is activated as electrophile and attacked by the phenolic hydroxyl group of ring B in ED. As both of the hydroxyl groups have comparable acidities, the regioselectivity is mainly governed by the correct positioning of the hydroxyl. As evidence for a S_N2 process, the mechanism involves an inversion of the configuration of the reacting carbon of SAM [144]. (For radical mechanisms of methyl transfer from SAM see ref. [145].)

In animals, some of the most essential O-methylations are performed by catechol O-methyltransferases (COMTs), which were first discovered in 1957 by Julius Axelrod [146]. COMTs are involved in the metabolism of catecholic amines, including neurotransmitters such as dopamine and the hormone melatonin. COMTs also initiate deactivation and biological detoxification of catechols like epinephrine. The accepted substrates for COMTs are highly diverse, albeit the consensus substructure of their substrates is specific as these enzymes are strictly limited to catechol moieties and proved to be inefficient for the modification of simple phenols [147]. Two isoforms of COMTs occur in humans: membrane-bound and cytosolic COMTs [148].

In plants, most of the OMTs occur as cytosolic proteins in soluble form [99], albeit there are also some examples of membrane-associated enzymes like the sequential orcinol O-methyltransferase, which catalyzes the last two steps in the biosynthesis of the volatile compound 3,5-dimethoxytoluene - a major scent in many rose varieties [149]. Plant OMTs are not only involved in the biosynthesis of compounds that play a key role in biological interactions, such as flower scents [150], pigments [151], or phytoalexins, the latter being involved in the defense against phytopathogens [152]. In general, they catalyze the O-methylation of a broad spectrum of plant metabolites, commonly phenolic moieties of alkaloids and phenylpropanoids. Thus, O-methylation is influencing a variety of processes such as plant growth, signaling and development [152]. Of particular importance is their participation in the production of certain lignin precursors, such as coniferyl and sinapyl alcohol [99] (Fig. 5.2).

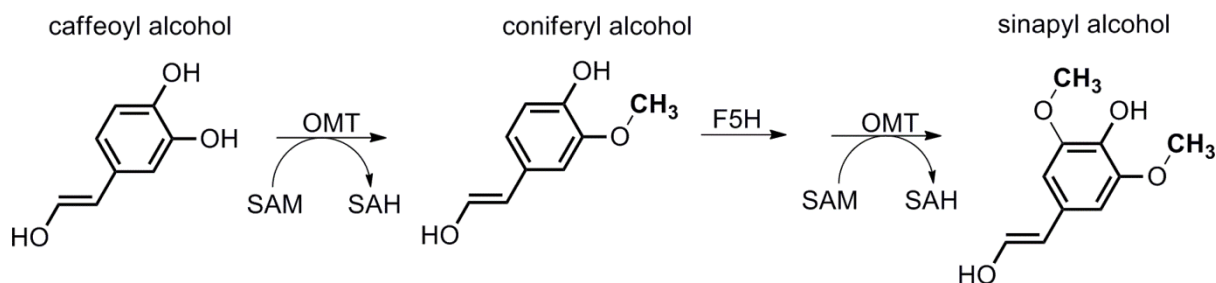


Fig. 5.2: O-Methylation steps in the biosynthesis of lignin precursor. OMTs catalyze the essential methylation steps for the production of coniferyl alcohol from caffeoyl alcohol and after hydroxylation catalyzed by a ferulate 5-hydroxylase (F5H) the further methylation to sinapyl alcohol – the precursor structures of lignin [153]. The introduced methyl groups are highlighted in boldface type.

OMTs of plants can be grouped in three main classes based on amino acid sequence alignments and structural studies [154]: type 1 is characterized by a high sequence similarity, and do not require bivalent cations for activity. These enzymes usually accept a broad range of substrates like flavonoids, hydroxycinnamic acids (HCAs) or alkaloids. Type 2 OMTs require

cations and all occur typically in lignin-producing plants. These enzymes are specific for coenzyme A-derivatized compounds and therefore they are specified as caffeoyl coenzyme A-O-methyltransferases (CCoAOMT). These proteins exhibit a high sequence similarity to mammalian COMTs [154]. The third group, called SABATH (Salicylic Acid, Benzoic Acid, Theobromine synthase) enzymes, acts only on carboxyl groups forming the corresponding methyl esters [151, 154]. Depending on amino acid sequence similarities, members of this group are more closely related to *N*-methyltransferases (NMTs) than to the other OMT classes [155]. Typical products resulting from SABATH enzymes are methylsalicylate or methylbenzoate, essential compounds of floral scents attracting insect pollinators [155].³

The Mg²⁺-dependent phenylpropanoid and flavonoid *O*-methyltransferase (PFOMT) from ice plant (*Mesembryanthemum crystallinum*) is characterized by significant sequence similarities to CCoAOMTs and therefore it is subgrouped to CCoAOMT-like enzymes. This enzyme accepts a broad spectrum of compounds that consist of a catecholic frame and prefers caffeoyl-CoA as well as flavonoids [156]. PFOMT can be heterologously expressed as soluble enzyme in *E. coli* as a cytosolic soluble enzyme [156] and it can catalyze the selective 3'-*O*-methylation of ED forming HED with a catalytic efficiency of 5178.4 M⁻¹s⁻¹ [70] (Fig. 5.3). The gene sequence expressing the native 3'-OMT enzyme that catalyzes this enzymatic step in the origin *Eriodictyon californicum* is still unknown. Hence, PFOMT offers an appropriate candidate for the biocatalytic synthesis of HED.

AtTSM1 (*Arabidopsis thaliana* tapetum-specific methyltransferase 1) belongs also to the CCoAOMT-like family and has a high sequence similarity of 54.5 % to PFOMT [157]. It was verified to convert flavonoids like quercetin regiospecific in 3'-position [158], but does not accept 3,4-dihydroxy benzoic acid as a substrate. Hence, AtTSM1 was considered as a suitable candidate for the conversion of ED due to tighter substrate specificity than PFOMT. The gene is specifically expressed in flower buds of *A. thaliana* but was shown to be also recombinantly expressible as a soluble protein in *E. coli* [158].

³ partially extracted from L. Wessjohann, A.-K. Bauer, M. Dippe, J. Ley, T. Geissler: *Biocatalytic synthesis of natural products by O-methyltransferases*, Book-Chapter in „Applied Biocatalysis - From Fundamental Signs To Industrial Applications“. Weinheim, Germany: Wiley-VCH Verlag GmbH & Co. KGaA, ISBN: 9783527336692; *in print*

5.2 Objectives

An enzyme cascade reaction combining the initial oxidation and the final methylation step should be investigated to achieve HED directly from Nar. The system ought to be appropriate for *in vivo* biotransformation to save cost-intensive cofactors and complex enzyme purification steps.

Therefore, a suitable OMT should be identified that catalyzes the *O*-methylation of the 3'-position of the substrate ED to form HED. Within the preceding diploma thesis[70], PFOMT was heterologously expressed in *E. coli* and confirmed for the selective *O*-methylation of ED forming HED. Finally, the success of *in vivo* biotransformation of ED was shown as a proof of concept to produce HED in *E. coli* cells by heterologous expression of PFOMT under feeding of ED [70].

The aim of this chapter concentrates on the investigation of the substrate specificity of PFOMT and the bio-based production of HED directly from Nar. The whole enzyme cascade (first 3'-oxidation and second 3'-*O*-methylation) should be developed as a proof of concept for biotechnological application.

5.3 Results

5.3.1 Regiospecificity and substrate spectrum of PFOMT

PFOMT was investigated for *in vitro* and *in vivo* conversion of ED in a preceding diploma thesis in 2010 [70]. The gene was heterologously expressed in *E. coli* and the synthesized enzyme was confirmed for the selective *O*-methylation of ED forming HED (Fig. 5.3). It was discovered, that PFOMT catalyzes the complete conversion of ED into HED *in vitro* using an excess of SAM as methyl donor. The product formation was verified by FT-ICR HR-MS and NMR analysis.

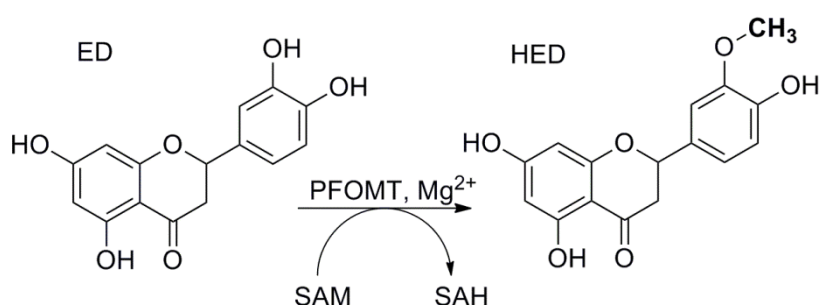


Fig. 5.3: Selective conversion of ED into HED catalyzed by PFOMT. The transferred methyl group is highlighted in boldface type. In previous studies, the enzyme was investigated and *in vitro* showed complete conversion of ED. HED could be obtained in 22 % yield by *in vivo* biotransformation [70].

Due to the regiospecificity on ED, this enzyme was further investigated for activity and stability. Investigation of the kinetic data in the *in vitro* assay determined the catalytic parameters: the apparent K_M value of 0.87 μM and a maximum rate of 4.5 pM s^{-1} that result in a catalytic efficiency of 5178 $\text{M}^{-1}\text{s}^{-1}$. Finally, the success of *in vivo* biotransformation of ED was shown as a proof of concept to produce HED in *E. coli* cells by heterologous expression of PFOMT under feeding of ED in LB media [70]. However, HED formation could be observed, but the conversion of ED was below 25 % [70]. It was discussed that the availability of the methyl donor SAM, the low solubility or membrane permeability of the substrate or the higher affinity of other compounds as a substrate could be the reason for the observed incomplete conversion in whole-cell biotransformation.

PFOMT was characterized concerning chemospecificity, regioselectivity, enzyme activity and stability [70]. Based on this study, PFOMT was further analyzed according to the substrate spectrum and compared to AtTSM1. Both recombinant enzymes were tested after expression and purification for *in vitro* conversion of different types of substrates containing of at least one catecholic moiety (table 5.1).

Table 5.1: Tested OMT substrates consisting of at least one catechol group (bold) in the scaffold. PFOMT and AtTSM1 show different substrate spectra. AtTSM1 is distinguished by higher substrate specificity than PFOMT. AtTSM1 only accepts the flavonols that are sp² hybridised at the C2 and C3 atom. Hence ED (highlighted in blue) was not converted by AtTSM1. PFOMT catalyzes the transmethylation of a broad spectrum of substrates independent of a double bond at the pyran ring C. Both enzymes catalyze the O-methylation of position 3(′) with 100 % regioselectivity (red). Substrate conversion (X) is defined as product formation over 5 % yield under OMT assay conditions.

substrates	chemical structure	substrate conversion	
		PFOMT	AtTSM1
ED (5, 7, 3′, 4′-tetrahydroxy-flavanone)		X	no conversion
(-)-epicatechin (3′,4′,5,7-tetrahydroxy-flavanole)		X	no conversion
sterubin (7-methoxy-3′,4′,5-trihydroxy-flavanone)		X	no conversion
taxifolin (5, 7, 3′, 4′-tetrahydroxy-flavanonole)		X	no conversion
fisetin (3′, 4′, 7-trihydroxy-flavonole)		X	X
caffeic acid (3,4-dihydroxy-cinnamic acid)		X	X

substrates	chemical structure	substrate conversion	
		PFOMT	AtTSM1
myricetin (3',4',5,5',7-pentahydroxyflavonole)		X	X
oleuropein		no conversion	
1,5-dicaffeoylquinic acid		X	X
3,5-dicaffeoylquinic acid		X	X
4,5-dicaffeoylquinic acid		X	X

substrates	chemical structure	substrate conversion	
		PFOMT	AtTSM1
3,4-dicaffeoyl-quinic acid		X	X
rosmarinic acid (<i>(R)</i> - <i>O</i> -(3,4-dihydroxycinnamoyl)-3-(3,4-dihydroxyphenyl) lactic acid)		X	X
cichoric acid (<i>(2R,3R)</i> - <i>O</i> -dicaffeoyl-tartaric acid)		X	X

Aromatic vicinal dihydroxyl groups are essential for the catalysis of the transmethylation mechanism by CCoAOMTs. PFOMT and AtTSM1 catalyze the *O*-methylation at the 3⁽ⁱ⁾-position with 100 % regioselectivity. However, there are differences between the accepted substrate spectra within this OMT subgroup. AtTSM1 only accepts substrates that are sp² hybridised at the C2 and C3 atom on the pyran ring C (Fig. 5.4). Thus, AtTSM1 does not catalyze the *O*-methylation of ED.

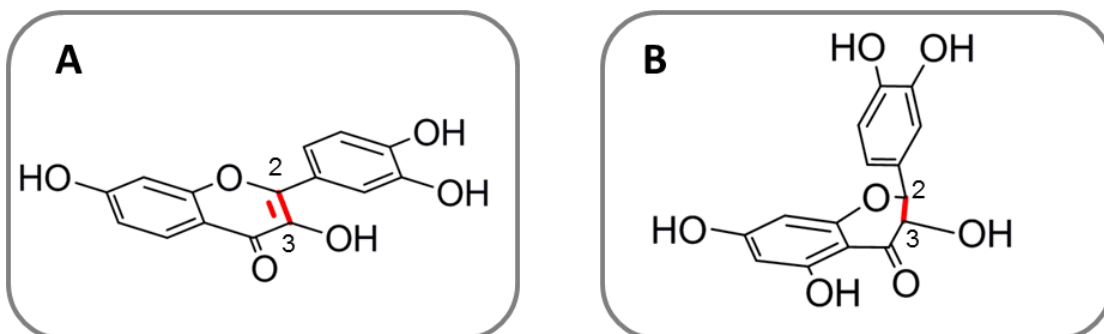


Fig. 5.4: Examples for the assayed flavonoids with sp^2 - (A) and sp^3 -hybridised (B) pyran ring C. The crucial bond of the C2 and C3 atom are highlighted in bold red. The hybridization of ring C influences enormously the spatial arrangement of the flavonoids. A: fisetin, B: taxifolin

To investigate the potential reasons for the observed different substrate specificities, AtTSM1 and PFOMT were analyzed due to their structural differences of the active site using docking studies. Therefore, a protein model of AtTSM1 based on the crystallized protein structure of PFOMT was constructed and the applied substrates were docked into the active site. Alterations in the tertiary structure within the active site visualized the potential source of non-acceptance of sp^3 -hybridised flavonoids. Mainly the Tyr51 of PFOMT corresponding to the Glu49 of AtTSM1 was determined as necessary for the structural stabilization of ring C in flavonoids and as crucial for the substrate recognition (Fig. 5.5).

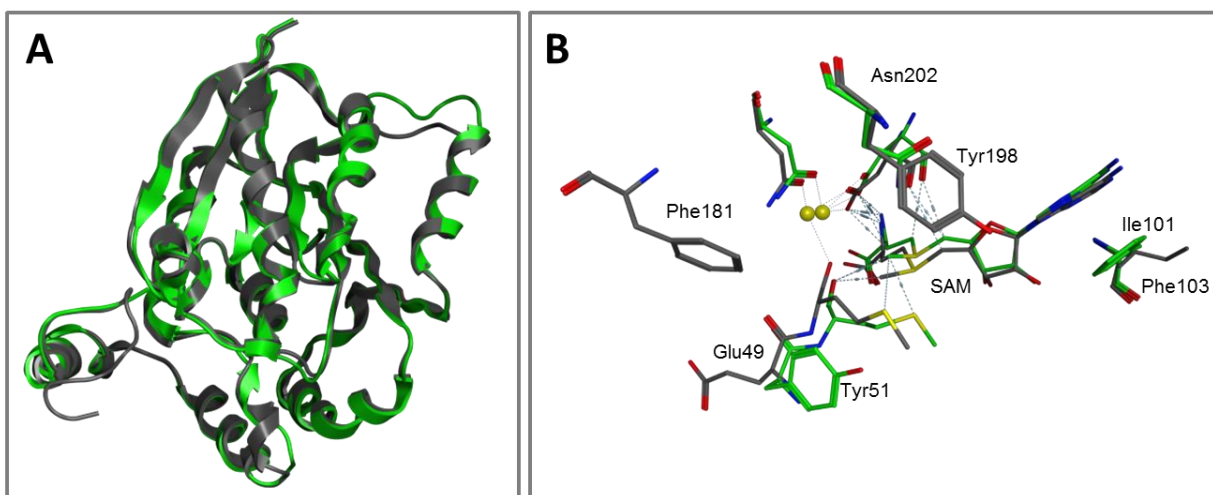


Fig. 5.5: Alignment of the 3D structure of the homology model of AtTSM1 (gray) and the 3D protein structure of PFOMT (pdb-code: 3C3Y (green)). A) Overall view of the alignment of AtTSM1 (gray) and PFOMT (green). B) Closeview of the active sites with SAM: The highlighted and designated aa residues are potentially involved in the (non-)acceptance of sp^3 -hybridised flavonoids.

Sp^3 -hybridised flavonoids offer a flexible conformation of ring C and are only accepted by the PFOMT stabilizing the ring because of π - π interaction with the Tyr51 missing in AtTSM1.

Both enzymes accept the sp^2 -hybridised flavonoids fisetin (flavonol) resulting from a fixed planar C-ring within their structure. Asn202 was assessed as the putatively critical aa for activity of PFOMT on flavanonols like taxifolin. The corresponding aa of AtTSM1 (Tyr198) is not able to develop hydrogen bonds to the hydroxyl group at 3 -position in contrast to the Asn202 of PFOMT (Fig. 5.6).

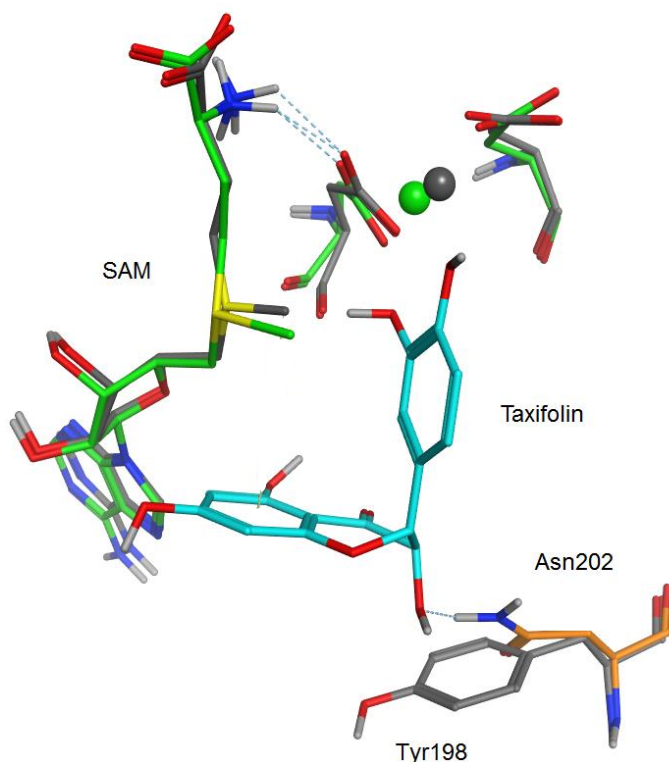


Fig. 5.6: Taxifolin docked in the active site of PFOMT (green) (pdb-code: 3C3Y). PFOMT is able to develop hydrogen bonds to the hydroxyl group at 3-position of taxifolin (cyan) by Asn202 (orange) in contrast to the corresponding bulky Tyr198 of AtTSM1 (gray). AtTSM1 does not accept sp^3 -hybridised flavonoids which have a conformationally flexible ring C.

In addition, bulky side chains in AtTSM1 like Lys17 and Phe181 located in the entrance of the active site are exchanged in PFOMT for more compact aa: Cys21 and Gly185, respectively. Other aa exchanges result in the same function of the side chains, e.g.: Phe103 of PFOMT and the corresponding Ile101 in AtTSM1 for the binding of SAM. Finally, AtTSM1 was found to be more substrate specific than PFOMT, but exactly therefore unable to convert ED into HED.

Oleuropein was not accepted by PFOMT or AtTSM1, although the docking calculations gave good positions for binding of the substrate and enough room for conversion (Fig. 5.7). A rea-

son for this could be the very low $\log K_{OW}$ value of oleuropein (-0.86) indicating a much too hydrophilic substance for the conversion in the hydrophobic substrate pocket of PFOMT. Typical substrates of PFOMT are considerably more lipophilic than oleuropein, e.g.: quercetin ($\log K_{OW}=1.82$) or luteolin ($\log K_{OW}=2.36$) [156, 159].

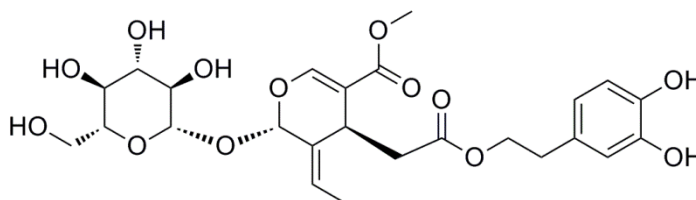


Fig. 5.7: Chemical structure of oleuropein.

PFOMT accepts a broad range of substrates of different size and polarity like CoA ester, aglycones and hydroxycinnamic acids due to its large and flexible active site [156], but the glycosylated phenylethanoid oleuropein was not accepted as a substrate.

5.3.2 PFOMT – *in vivo* biotransformation

In the previous studies, PFOMT was heterologously expressed in *E. coli* M15[pRep4] cells [70]. To compare and to combine the oxidation of Nar (chapter II) with the methylation step of ED, the plasmid bearing the *PFOMT* gene was transformed in the similar strain *E. coli* BL21 (DE) used for the oxidation. The *in vivo* biotransformation of ED was performed analogously to the *in vivo* biotransformation of Nar using the BM3-GVQ strain.

Two different media were used for cultivation: LB and AI medium. Their efficiency was determined comparing the area of the signal in the HPL chromatogram ($\lambda=280$ nm) of the substrate and the product (Fig. 5.8). An empty pET-28a(+) vector transformed into *E. coli* BL21 (DE) cells was used as a control for conversion.

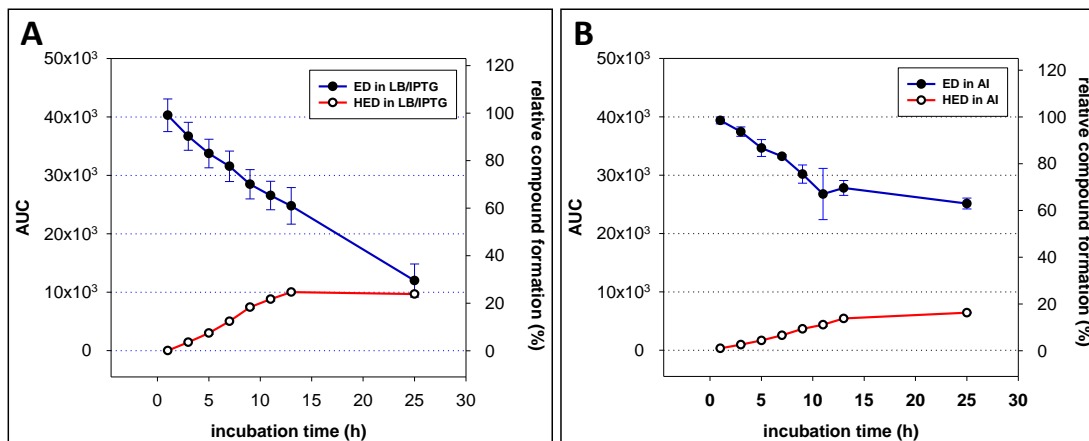


Fig. 5.8: Comparison of the *in vivo* conversion of ED catalyzed by PFOMT in two different growth media.

The area under the curve of the signal in the HPL chromatogram ($\lambda=325$ nm) was used to estimate the amount of the compounds. An empty pET-28a(+) vector transformed into *E. coli* BL21 (DE) cells was used as a control for conversion. After 25 h, ED conversion into HED achieved higher amounts in the LB/IPTG medium (A) than in the AI medium (B). However, while product formation and substrate conversion decreases in AI-medium after 12 h, a further metabolization of ED without product formation is observed in LB-medium.

Indeed, after 25 h the formation of HED achieved 24 % in the LB/IPTG medium and 16,3 % in AI medium. However, in LB medium the substrate ED was more intensively metabolized into further compounds and also HED degradation started already after 13 h (HED yield 24.9 %) in contrast to the AI medium. In both cases, the conversion of ED started at an early stage (after 3 h) but no complete conversion to HED could be observed even after 25 h of conversion. After 25 h the flavonoids were strongly metabolized in both media.

5.3.3 Enzyme cascade: oxidation and methylation

The catalytic cascade for the biosynthesis of HED starting from the selective oxidation step of Nar to form ED and the further conversion into HED by selective O-methylation was proved as one-pot synthesis by *in vivo* biotransformation of Nar.

Therefore, both plasmids bearing the respective genes for BM3 GVQ or PFOMT were co-transformed into one *E. coli* BL21 (DE) strain (GVQ+PFOMT). According to the preceding studies (section 4.3.4, 5.3.2) two different media were used for coexpression of the BM3-GVQ and PFOMT: LB/IPTG and AI medium. An *E. coli* BL21 (DE) strain including an empty vector was used as a control. In LB medium, no conversion of Nar into ED or HED could be determined after 25 h incubation time although PFOMT and BM3-GVQ were expressed in the media (Fig. 5.9).

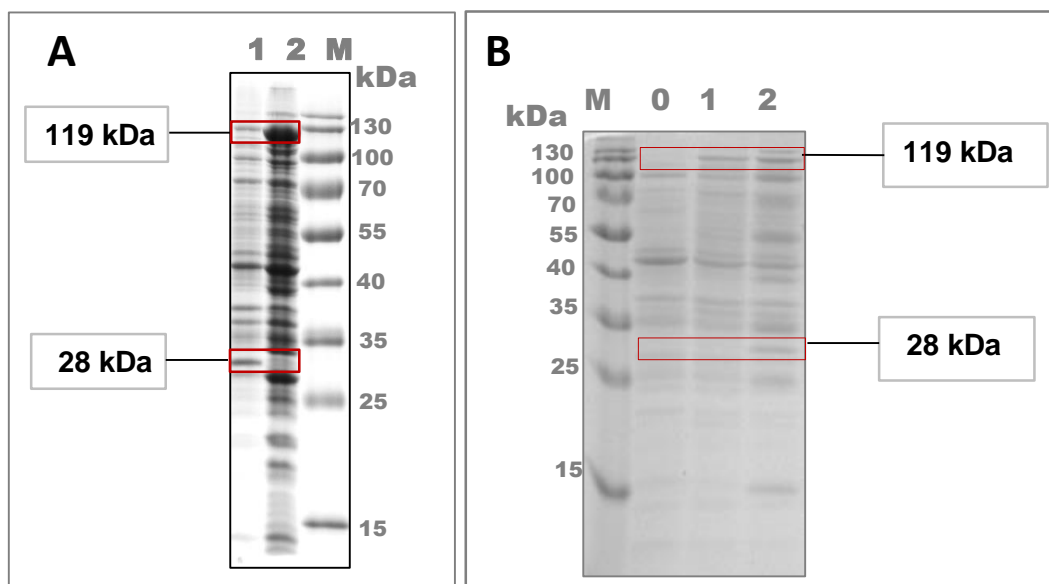


Fig. 5.9: SDS-PAGE from the coexpression of PFOMT and BM3-GVQ in different media after 25 h incubation. A: In LB medium the coexpression (1) of PFOMT (28 kDa) and BM3-GVQ (119 kDa) is slightly compared to the single BM3-GVQ (2) expression shown in the SDS-PAGE. B: In AI medium the single expression of BM3-GVQ (1) and the coexpression (2) of both genes show similarly weak protein bands. An *E. coli* BL21 (DE) strain, including an empty vector was used as a control (0).

In the AI medium, the product HED could be obtained after incubation over 12 h, but no ED formation was detected (Fig. 5.10).

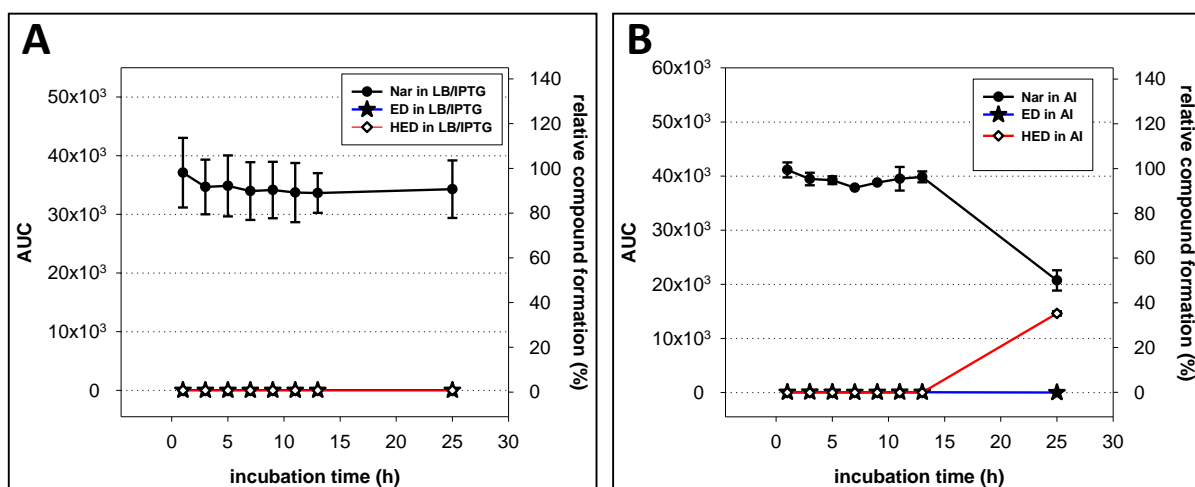


Fig. 5.10: Comparison of the *in vivo* conversion of Nar in the coexpression *E. coli* strain GVQ+PFOMT in two different induction media: LB/IPTG (A) and AI medium (B). The efficiency was determined comparing the area under the curve (AUC) of the signal in the HPLC chromatogram ($\lambda=325$ nm) of the compounds. After 12 h incubation time, HED formation was obtained using AI medium. ED was not detected at any time. The conversion of Nar started in principal after 12 h incubation time. In LB/IPTG medium, neither HED nor ED was determined after 25 h. After 25 h substrate and product were metabolized into further compounds by the strains and by the control.

This indicates, that during coexpression of BM3-GVQ and PFOMT the hydroxylation of Nar is the rate limiting step and the subsequent methylation of ED yielding HED is fast. As the highest conversion over 30 % yield of HED produced from Nar could be obtained after 25 h incubation time. In both media and in the control, the compounds were readily consumed after 48 h incubation time.

5.4 Discussion

PFOMT is a suitable OMT for the *in vitro* synthesis of HED. The enzyme catalyzes regio-specific the 3⁽⁴⁾-O-methylation of substrates bearing a catecholic frame – a specific structural motif consisting of an aromatic system with a vicinal dihydroxyl group. A further requirement on the substrate is that the compound must be hydrophobic enough to be accepted in the active site. PFOMT features the catalysis of 100 % regioselectivity in 3⁽⁴⁾-position for all tested substances in comparison to further representatives of the CCoAOMT-like enzyme family that differ in their regioselectivity in dependence of the substrate, e.g.: the OMT encoded by the gene of *at4g21220* from *Arabidopsis thaliana* [160].

However, PFOMT has a broad substrate spectrum in comparison to AtTSM1 (section 5.3.1) that is undesirable for *in vivo* conversion. Although PFOMT obtains a high catalytic efficiency of $5178 \text{ s}^{-1} \text{ M}^{-1}$ for ED *in vitro*, the conversion of smaller molecules like caffeic acid show a considerable higher efficiency ($k_{\text{cat}}/K_{\text{M app}} = 22900$) [70]. Due to this fact, other substrates can competitively inhibit the *in vivo* conversion of ED and might be responsible for the uncompleted conversion of ED during *in vivo* biotransformation. In contrast to the single step of *in vivo* biooxidation and to the *in vivo* enzyme cascade, HED is already detected in an early stage (3 h) of growing and expression. However, independent of the applied media, ED is also metabolized to further products by the cells. The consumption of ED is higher in LB/IPTG medium than in AI medium. Using terrific broth medium, the formation of HED could be increased but conversion was still uncompleted (< 40 %) [70]. Moreover, indole was formed in high amounts [70] indicating an environmental response [161] of the cells that can result *inter alia* in the expression of multidrug exporter genes [139]. Such multidrug exporters can act as efflux pumps to aid the bacterial cells to expel hydrophobic, toxic compounds and to allow their survival. In addition, the methyl donor SAM can be limited. SAM was used in an excess amount for the *in vitro* assay. Therefore, the calculated catalytic efficiency is only an apparent value of ED conversion where SAM is not limited in contrast to the *in vivo* conversion. The heterologous host *E. coli* provides SAM by its endogenous metabolism, but this might be in-

sufficient for (living) whole-cell biotransformation. Coexpression of a SAM regeneration system or of a SAM synthase could yield an increased product formation.

The whole enzyme cascade was only successfully realizable in AI medium. The high influence of the media used for the bioconversion yield was already shown for the oxidation and also affects the enzyme cascade. Media like terrific-broth or M9 minimal medium can increase the membrane permeability and the conversion rate [162]. Although both reactions depend on cofactors and cosubstrates that must be provided by the hosts endogenous metabolism, an overall conversion of Nar of over 30 % HED was achieved after 25 h incubation time. ED was not detected at all, indicating that the first step (oxidation of Nar) limits the reaction velocity for the formation of HED from Nar. In addition, both plasmids were cotransformed and coexpressed in one strain. For successful biotransformation, one optimized plasmid bearing both genes could adjust the protein synthesis and probably improve the bioconversion of Nar forming HED. Furthermore, the applied plasmids are not compatible due to the same origin of replication. Though this was adequate for a first trial if this two-step *in vivo* biotransformation works at all, it causes the inhibition of replication for one plasmid and plasmid segregation [163] that can be optimized.

In summary, with this first generation *in vivo* enzyme cascade a successful conversion of Nar to HED was achieved. The (living) whole-cell biotransformation was developed as a proof of concept that needs to be further optimized for production and upscaling.

5.5 Outlook

Selective O-methylation of ED to form HED is the final step in the enzyme cascade starting from Nar. The investigations that are described in this chapter show that PFOMT is a suitable enzyme for *in vitro* and *in vivo* bioconversion of ED to form HED including the O-methylation of ED produced from Nar *in situ* by oxidation using BM3-GVQ in *E. coli*. The enzyme cascade was developed as a proof of concept that can be further optimized regarding the culture media, plasmid selection, expression and incubation conditions and of course according to cofactor coexpression systems.

The biotechnological system of oxidation and methylation in one enzyme-cascade was successfully established for a suitable host in a laboratory scale applicable for system biology and biotechnology [164]. The advanced system generates the foundation for an industrial bio-process that now can be optimized and scaled up for the microbiological production of natural HED from Nar.

6 Final discussion

The microbial production of ED and HED was investigated based on two different starting points (Fig. 6.1). Both approaches need two enzymatically catalyzed steps to obtain the desired product HED.

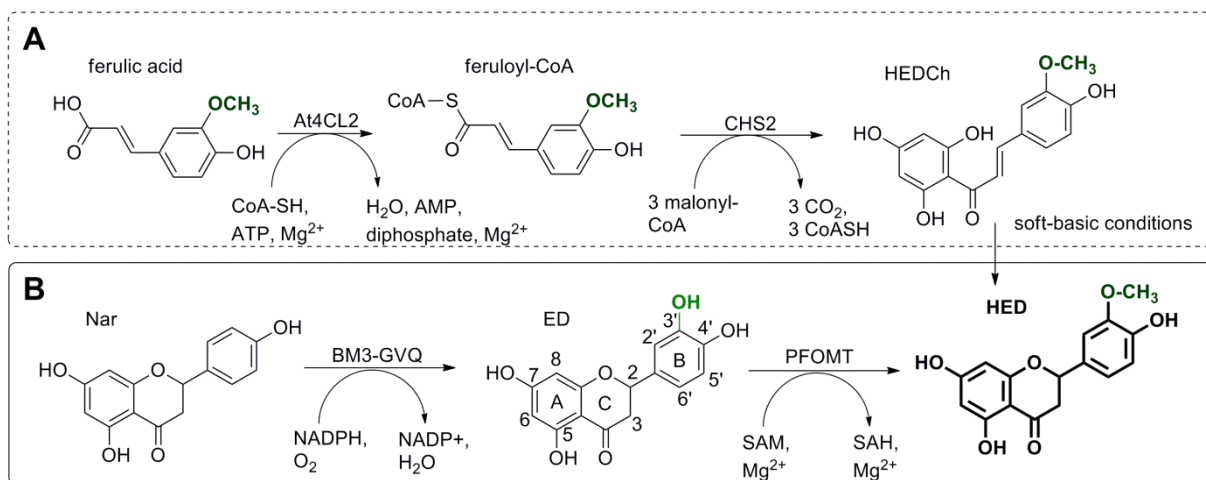


Fig. 6.1: Two strategies investigated for the microbial biosynthesis of HED. A: The dashed line covers a precursor-directed approach by a modified biosynthetic pathway. The chalcone (HEDCh) is synthesized via two enzymatically catalyzed steps: at first ferulic acid is activated by At4CL2 catalyzing the CoA ester formation and secondly CHS2 catalyzes the polyketide formation and aromatization into the HEDCh that closes the ring forming the desired flavonoid HED under soft-basic conditions. B: The solid line comprises an approach adapted to the natural biosynthesis of HED: Nar is used as a substrate for selective hydroxylation forming ED catalyzed by BM3-GVQ in the first step and secondly HED is formed by 3'-O-methylation of ED catalyzed by a selective 3'OMT called PFOMT.

The first approach of microbial biosynthesis focusses the precursor-directed chalcone biosynthesis starting from the HCAs within the phenylpropanoid pathway (Fig. 6.1A). The target flavonoid HED is formed in two enzymatically catalyzed steps: at first, the ligase At4CL2 catalyzes the formation of an active ester from ferulic acid which already consists of the desired modifications at ring B. Secondly the chalcone HEDCh is formed catalyzed by a specific CHS2 using three units of malonyl-CoA to construct the typical skeleton C6-C3-C6 of the polyketide. Finally a chemical step is used for the ring closure instead of a CHI to convert the chalcone into a flavonoid. The single steps were proved for the conversion of inexpensive hydroxycinnamic acids into the desired flavanones. Modifications of the hydroxycinnamic acid determine the skeleton of the ring B of the flavanones and avoid the use of enzymes that are difficult to handle like *trans*-cinnamic acid 4-hydroxylase (class 2 – microsomal type CYPs, 4.1 Introduction, chapter II).

The second strategy based on the modification of the flavonoid Nar derived from the natural HED biosynthesis in plants (Fig. 6.1B). For this purpose a 3'-hydroxylase was required, cata-

lyzing selectively the conversion of Nar into ED. After screening a multitude of oxygenating biocatalysts, the microbial monooxygenase BM3-GVQ was discovered realizing this hydroxylation step. Moreover, the triple mutant offers a high potential for industrial application [122, 129]. In the second step, an OMT acting selectively on ring B forming 3'-O-methylated ED (HED) was necessary. Therefore, a plant OMT with high catalytic potential for conversion of ED called PFOMT was applied. The enzyme was already investigated for conversion of ED and for the *in vivo* biotransformation within the diploma thesis of 2010 [70]. However, the combination of both steps realizing an enzyme cascade for *in vivo* biotransformation was crucial and could be achieved within this study.

Both strategies were extensively investigated and separate *in vitro* conversion for each step was confirmed to produce ED and HED. Moreover, strategy B was also established as enzyme cascade for *in vivo* biotransformation in *E. coli*. Nar can be fed as a substrate to the culture and HED is directly yielded after 24 h incubation in AI medium without the addition of expensive cofactors and cosubstrates. Hence, this approach (B) offers an appropriate foundation for the industrial biocatalytic synthesis of natural HED from the cheap precursor Nar.

However, the system is limited in its formation of HED (yield up to 36 % \pm 19.6 mg l⁻¹ after 24 h incubation). A few reasons are possible: For this first approach of *in vivo* biotransformation, the plasmid of hydroxylation bearing the gene *BM3-GVQ* (pET-28a(+)) and the plasmid for 3'-O-methylation (pQE30) translating the *PFOMT* gene were cotransformed and co-expressed in one *E. coli* strain. The biotransformation of Nar in this strain was performed as a proof of concept. However, due to the low expression levels, both plasmids have the same origin of replicons resulting in incompatibility [165, 166]. However, several research groups already investigated such microbial flavonoid biosynthesis and presented a successful methodology for the production of flavonoids basing on inexpensive precursors [69, 167–172]. With a look to the methods, the researchers used on the one hand appropriate Duet-plasmids like pACYCDuet-1 (Novagen) bearing sets of the target genes according to one flavonoid metabolon. In general, such a flavonoid metabolon unites enzymes of the plant phenylpropanoid pathway that are cytosolic soluble and organizes them as weak association to the cytoplasmic face of the endoplasmic reticulum [173]. Thus, the expression levels are attuned for temporization and localization of the synthesized proteins and can be optimized for an enzyme cascade using one plasmid. In addition, duet-plasmids feature compatible replicons that are essential to avoid the RNA antisense mechanism suppressing the replication of one plasmid and causing plasmid segregation [163]. For the first approach of cotransformation the

already tested plasmids bearing the crucial genes were applied although they bear the same origin of replication that is incompatible.

Another difference within the designated method was the applied culture medium for the feeding experiments. The overall reaction requires high levels of cosubstrates and cofactors like NADPH and SAM for strategy B and for the first approach, CoA, ATP and especially malonyl-CoA that are limited in *E. coli* [172]. For example, a nutrient medium with high amounts of glucose as a carbon source is essential to provide the cosubstrate malonyl-CoA which is mainly used in the fatty acid pathway [174]. This strategy significantly enhances the yield of produced flavanones in microbes [169]. In addition, the pathway can be further engineered by expression of the genes of the key enzyme acetyl-CoA carboxylase (ACC) to increase the malonyl-CoA level [167] (Fig. 6.2).

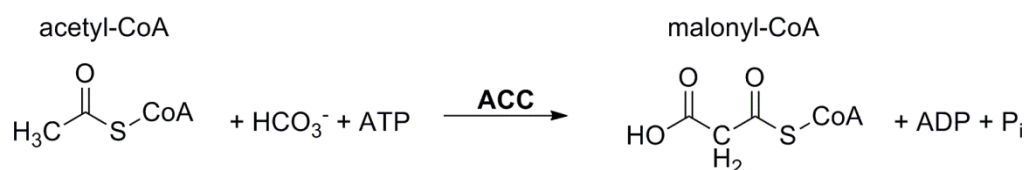


Fig. 6.2: Malonyl-CoA biosynthesis. Acetyl-CoA carboxylase (ACC) catalyzes the carboxylation of acetyl-CoA forming malonyl-CoA and is essential in the fatty acid biosynthetic pathway.

Although the approach for a precursor-directed, biosynthetic enzyme-cascade was not successful, this modified biosynthetic pathway using the recombinant genes *At4CL2* and *HvCHS2* might be successful after engineering recombinant coexpression and cultivation conditions. Watts and coworkers (2004) explored recombinant flavonoid biosynthesis in metabolically engineered *Escherichia coli* and described the blockage of the whole system by the initial enzymatic step (ligase) due to simultaneous coexpression. Variation in feeding conditions of *p*-coumaric-acid and cultivation methods established the production of Nar, but ED and HED could not be obtained from caffeic acid and ferulic acid within this system [175].

Similar, for strategy B starting from Nar, NADPH and SAM are limited and might be one reason amongst others for the incomplete conversion of Nar into HED. Under *in vivo* conditions, the low cellular concentration of produced SAM is rate-limiting for subsequent OMT reactions. The biosynthesis of SAM is strongly regulated and requires a methionine adenosyltransferase (MAT) that is also called SAM synthase (SAMS). The amino acid L-methionine (Met) and ATP act as substrates for SAM synthesis [176]. In the first step of the reaction, SAM and triphosphate is formed, whereby the latter is subsequently converted into monophosphate and

diphosphate by hydrolysis within MAT (Fig. 6.3). SAM synthesis also represents the initial step in the biodegradation of Met [177].

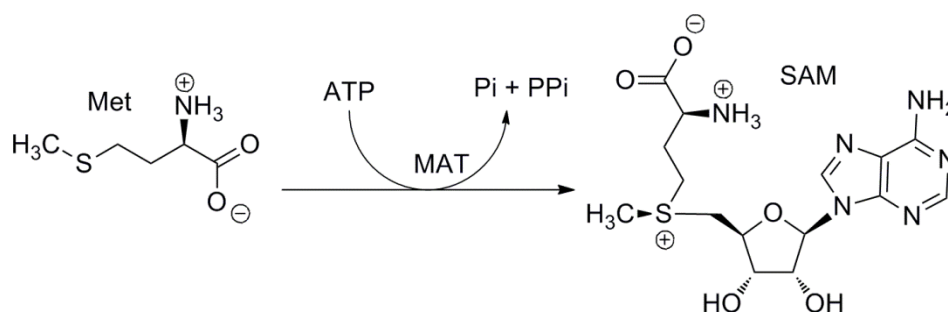


Fig. 6.3: Biosynthesis of SAM. L-methionine (Met) and ATP act as substrates for MAT (SAMS) under the driving force of the hydrolysis of the inorganic triphosphate anhydride. SAM, phosphate (Pi) and diphosphate (PPi) result as products.⁴

Two types of SAM MATs (MAT1 and MAT2) are known from *Saccharomyces cerevisiae*. The latter is the important one for SAM synthesis [178] allowing high gene expression during growth [179]. Therefore, MAT2 is used in several heterologous expression systems to increase the SAM levels and might be an alternative by coexpression to improve the HED yield in strategy B. A further problem is caused by the antimicrobial effect of some flavonoids against *E. coli* amongst others, in particular if the compounds bear a ring B hydroxylation [34] that is given in case of Nar, ED, HED and apigenin. All these reasons can suppress the conversion of Nar into ED within the *in vivo* biotransformation. A further reason for low conversion might be the problem of accessibility of the substrate. Nar and ED are aglycones and not well soluble in water or media. Therefore, the substrate was dissolved in DMSO (stock solution) to increase the membrane penetration of the *E. coli* cells. However, DMSO possesses also poisonous effects and can constitute its greatest toxic potential to organism in a combination of toxic agents [180]. To avoid such effects, DMSO can be replaced by other penetration enhancers to increase the bioavailability of the flavonoids within the cytoplasm, and the excretion of product in the ideal case.

In conclusion, strategy A established two enzymatic steps to form ED and HED from the low-priced substrates caffeic acid and ferulic acid, respectively. The system is still limited to the single steps and for *in vitro* conversion, but opens the door to *in vivo* biotransformation and the production of further natural and unnatural flavonoids due to the precursor-directed bio-

⁴ extracted from L. Wessjohann, A.-K. Bauer, M. Dippe, J. Ley, T. Geissler: *Biocatalytic synthesis of natural products by O-methyltransferases*, Book-Chapter in „Applied Biocatalysis - From Fundamental Signs To Industrial Applications“. Weinheim, Germany: Wiley-VCH Verlag GmbH & Co. KGaA, ISBN: 9783527336692; *in print*

synthesis. Strategy B was established as the successful *in vitro* formation of ED and HED. Moreover, the whole enzyme-cascade was developed as a proof of concept for *in vivo* bio-transformation yielding $\sim 20 \text{ mg l}^{-1}$ of HED after 24 h of incubation for a first generation proof of concept. This fundamental system offers a biotechnological process that is already registered for patent (EP14187583) due to the successful foundation.

Appendix A

Supplementary information to Chapter I: Precursor-directed biosynthesis of flavonoids

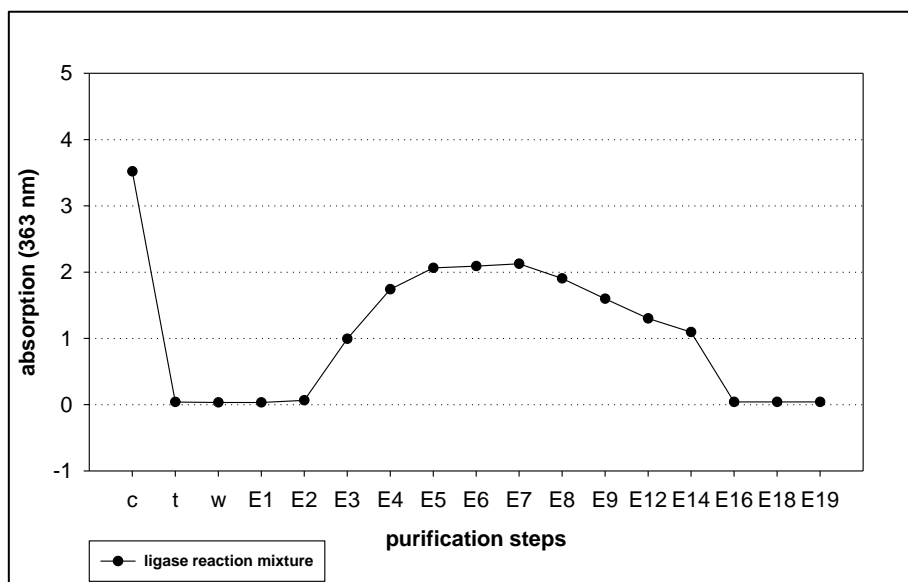


Fig. A 1: Purification steps of CoA ester synthesis exemplified for caffeoyl-CoA. Crude extract (c) was loaded on a SPE cartridge. The throughput (t), washing step (w) and elution (E1-E2) show no absorption indicating complete and successful binding of the CoA ester on the solid phase material. The purified CoA ester is then liberated by water, eluted fractions (E3-E14) are pooled and freeze dried.

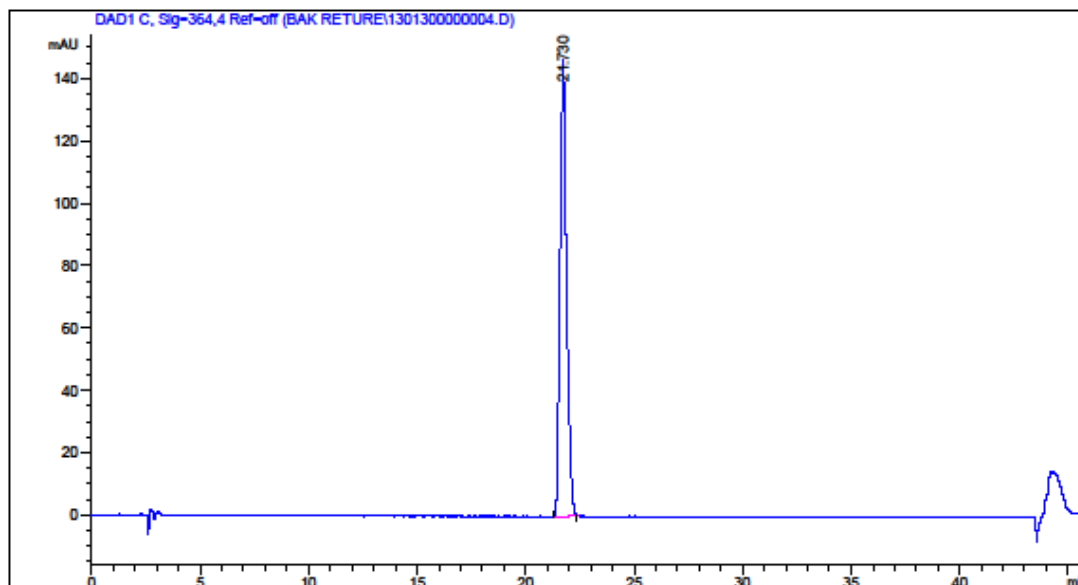


Fig. A 2: HPLC run of *p*-coumaroyl-CoA formed by enzymatic ligase reaction and purified using SPE.

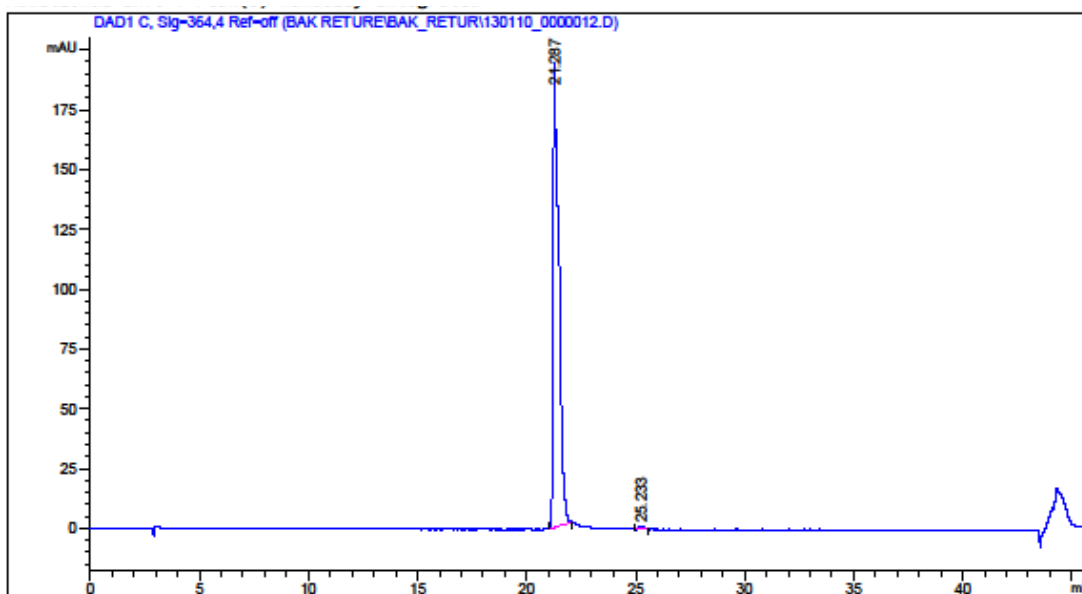


Fig. A 3: HPLC run of caffeoyl-CoA formed by enzymatic ligase reaction and purified using SPE.

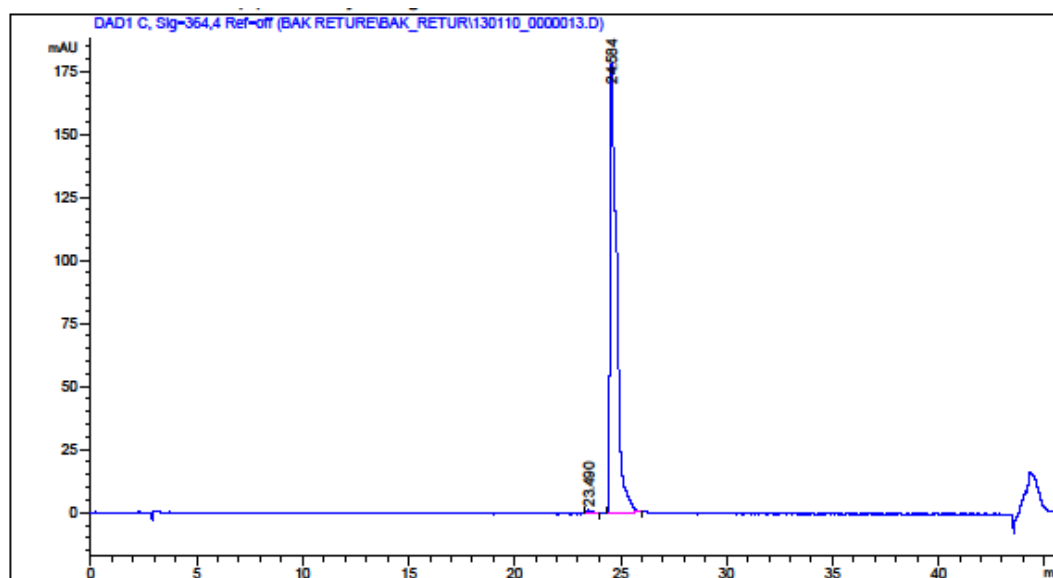


Fig. A 4: HPLC run of feruloyl-CoA formed by enzymatic ligase reaction and purified using SPE.

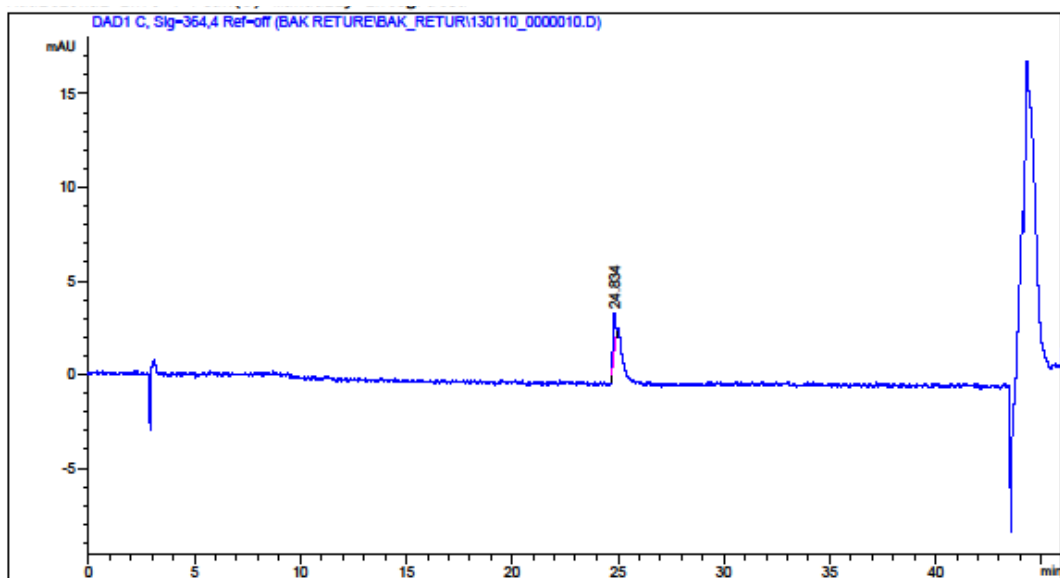


Fig. A 5: HPLC run of isoferuloyl-CoA formed by enzymatic ligase reaction and purified using SPE.

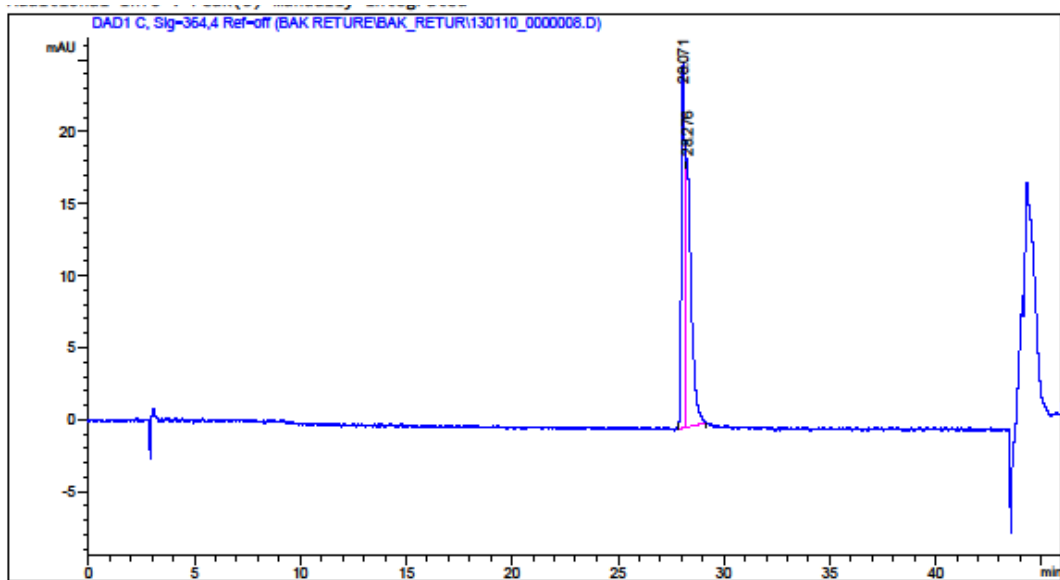


Fig. A 6: HPLC run of 4-ethoxy-3-hydroxycinnamoyl-CoA formed by enzymatic ligase reaction and purified using SPE.

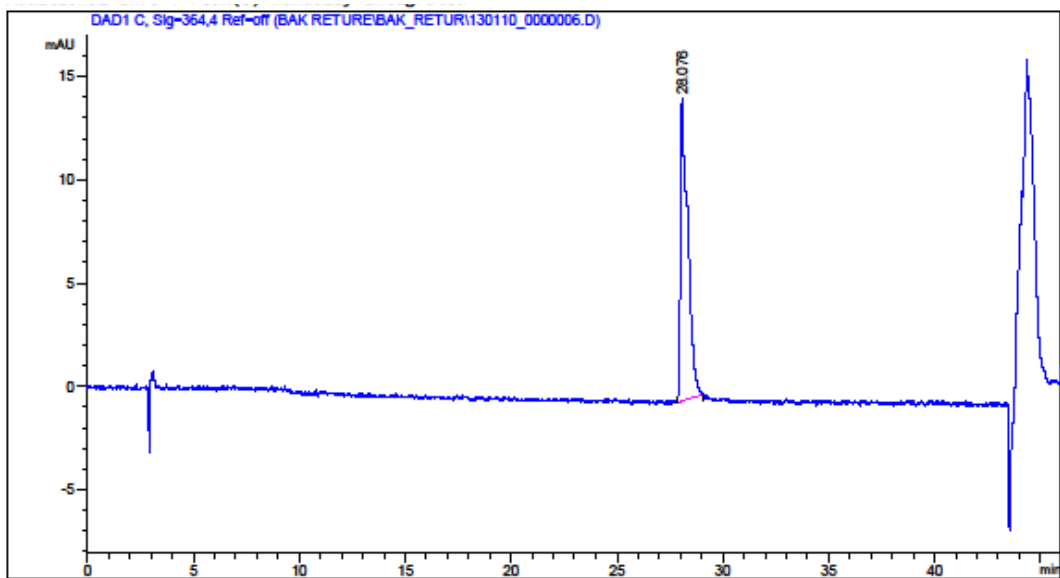


Fig. A 7: HPLC run of 4-propoxy-3-hydroxycinnamoyl-CoA formed by enzymatic ligase reaction and purified using SPE.

Table A 1: FT-ICR HR-MS data of the CoA thioester compared to the calculated mass.

CoA thioester (M)	mode	calculated mass [M]		m/z (FT-ICR HR-MS)
<i>p</i> -coumaroyl-CoA (C ₃₀ H ₄₁ O ₁₈ N ₇ P ₃ S)	positive mode	[M+H] ⁺	914.1593	-
		[M]	913.152	-
	negative mode	[M-H] ⁻	912.1447	912.1443
		[M-2H] ²⁻	455.4587	455.5690
isoferuloyl-CoA (C ₃₁ H ₄₄ O ₁₉ N ₇ P ₃ S)	positive mode	[M+H] ⁺	944.1703	-
		[M]	943.163	-
	negative mode	[M-H] ⁻	942.1553	942.1550
		[M-2H] ²⁻	470.574	470.5732
3-ethoxy-4-hydroxycinnamoyl-CoA (C ₃₂ H ₄₆ O ₁₉ N ₇ P ₃ S)	positive mode	[M+H] ⁺	958.1855	-
		[M]	957.1782	-
	negative mode	[M-H] ⁻	956.1709	956.1699
		[M-2H] ²⁻	477.5818	477.5811
4-ethoxy-3-hydroxycinnamoyl-CoA (C ₃₂ H ₄₆ O ₁₉ N ₇ P ₃ S)	positive mode	[M+H] ⁺	958.1855	-
		[M]	957.1782	-
	negative mode	[M-H] ⁻	956.1709	956.1708
		[M-2H] ²⁻	477.5818	477.5812
4-propoxy-3-hydroxycinnamoyl-CoA (C ₃₃ H ₄₈ O ₁₉ N ₇ P ₃ S)	positive mode	[M+H] ⁺	972,1973	-
		[M]	971.1939	-
	negative mode	[M-H] ⁻	970,1866	970.1856
		[M-2H] ²⁻	484.5896	484.4896

Table A 2: NMR data and spectral assignments for caffeoyl- and feruloyl-CoA (over 2 pages). NMR measurements were performed in D₂O at 600 MHz. ¹H-NMR, ¹³C-NMR and 2D-NMR correlation spectra (HMBC, HSQC) were measured to confirm the structure of caffeoyl-CoA (R = H) and feruloyl-CoA (R = CH₃). ³¹P-NMR was measured exemplarily for caffeoyl-CoA (highlighted in green). To allocate the relevant positions, NMR signals for the CoA thioester follow the numbering convention of the synthesized CoA thioester and was modified according to D'Ordine et al. (1995) [103]. a) Chemical shift of HSQC and HMBC correlation peaks. b) Chemical shift of DQF-COSY correlation peaks. c) May be interchanged.

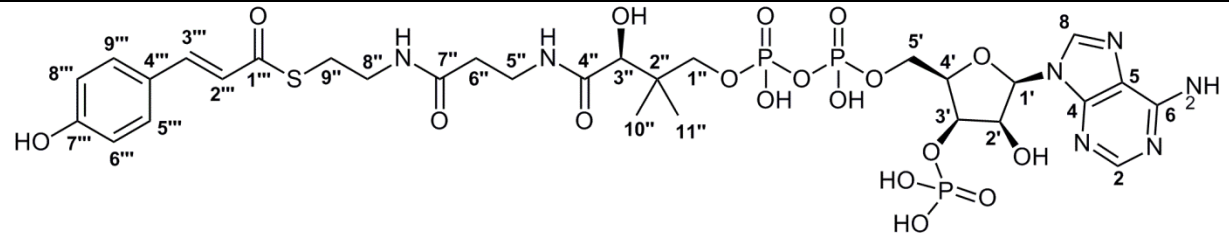
caffeoyl-CoA: R=H
feruloyl-CoA: R=CH₃

caffeoyl-CoA (R=H)				feruloyl-CoA (R=CH ₃)		
Pos.	¹³ C: δ [ppm]	¹ H δ [ppm] (J[Hz])	³¹ P δ [ppm] (J[Hz])	Pos.	¹³ C ^a : δ [ppm]	¹ H: δ [ppm] (J[Hz])
2	152.3	8.099 s		2	152.3	8.064 s
4	148.9	---		4	148.8	---
5	118.5	---		5	118.4	---
6	155.2	---		6	155.1	---
8	139.5	8.441 s		8	139.3	8.428 s
1'	86.2	6.044 d (6.4)		1'	86.4	6.020 d (6.6)
2'	74	4.79 ^b		2'	74	4.79 ^b
3'	73.9	4.82 ^b		3'	74	4.77 ^b
4'	83.2	4.571 m		4'	83.4	4.558 m
5'	65.2	4.267 m		5'	65.2	4.247 m
1''	71.8	3.781 dd (9.8/4.8) / 3.585 dd (9.8/4.7)		1''	71.8	3.853 dd (9.9/5.0) / 3.576 dd (9.9/5.0)
2''	38.3	---		2''	38.3	---
3''	74.2	4.052 s		3''	74.1	4.046 s
4''	174.7	---		4''	174.7	---
5''	35.4 ^a	3.51 ^b / 3.45 ^b		5''	35.4	3.50 ^b /3.47 ^b
6''	35.3 ^a	2.474 t (6.5)		6''	35.3	2.472 t (6.6)
7''	174.1	---		7''	174	---

Appendix A

caffeoyl-CoA (R=H)				feruloyl-CoA (R=CH ₃)		
Pos.	¹³ C: δ [ppm]	¹ H δ [ppm] (J[Hz])	³¹ P δ [ppm] (J[Hz])	Pos.	¹³ C ^a : δ [ppm]	¹ H: δ [ppm] (J[Hz])
8 ^{''}	38.7	3.444 t (6.4)		8 ^{''}	38.7	3.437 t (6.3)
9 ^{''}	28.1	3.167 dt (14.1/6.4) / 3.118 dt (14.1 / 6.4)		9 ^{''}	28	3.159 dt (14.1/6.3) / 3.121 dt (14.1/6.3)
10 ^{''}	20.8	0.921 s		10 ^{''}	21	0.920 s
11 ^{''}	18.2	0.790 s		11 ^{''}	18.2	0.790 s
1 ^{'''}	193.2	---		1 ^{'''}	193.1	---
2 ^{'''}	121.7	6.554 d (15.9)		2 ^{'''}	121.8	6.591 d (15.9)
3 ^{'''}	141.6	7.319 d (15.9)		3 ^{'''}	141.7	7.361 d (15.9)
4 ^{'''}	126.2	---		4 ^{'''}	126.1	---
5 ^{'''}	114.8	7.010 d (2.1)		5 ^{'''}	110.8	7.032 d (1.9)
6 ^{'''}	144.6	---		6 ^{'''}	147.4	---
7 ^{'''}	147.2	---		7 ^{'''}	147.8	---
8 ^{'''}	116	6.836 d (8.4)		8 ^{'''}	115.4	6.830 d (8.3)
9 ^{'''}	123	6.929 dd (8.4/2.1)		9 ^{'''}	123.7	6.985 dd (8.3/1.9)
3 ⁱ -O- P			1.0 s	7 ^{'''} - OMe	55.6	3.858 s
5 ⁱ -O- P ^c			-10.1 d (20.7)			
1 ⁱ -O- P ^c			-10.6 d (20.7)			

Table A 3: NMR spectra of *p*-coumaroyl-CoA. (D₂O, 600 MHz). ^a NMR measurements were performed in D₂O at 600 MHz. ¹H-NMR, ¹³C-NMR and 2d-NMR correlation spectra (HMBC, HSQC) were measured to confirm the structure of *p*-coumaroyl-CoA. To allocate the relevant positions NMR signals for the CoA thioester the numbering convention of the synthesized CoA thioester was modified according as D'Ordine *et al.* (1995) [101]. a) chemical shift of HSQC and HMBC correlation peaks



Pos.	¹³ C ^a : δ [ppm]	¹ H: δ [ppm] (J [Hz])
2	152.7	8.130 s
4	149.1	---
5	118.5	---
6	155.4	---
8	139.6	8.497 s
1'	86.5	6.096 d (6.3)
2'	74.3	4.81 ^a
3'	73.9	4.81 ^a
4'	83.8	4.594 m
5'	65.6	4.278 m
1''	71.9	3.877 dd (9.9/4.9) / 3.592 dd (9.9/4.9)
2''	38.4	---
3''	74.1	4.064 s
4''	174.8	---
5''	35.4	3.504 m
6''	35.4	2.499 t (6.5)
7''	174.1	---
8''	38.8	3.468 m
9''	28.2	3.179 dt (14.0/6.3) / 3.157 dt (14.0/6.3)
10''	21.0	0.931 s
11''	18.2	0.790 s
1'''	193.4	---
2'''	121.6	6.633 d (16.0)
3'''	141.7	7.454 d (16.0)
4'''	125.7	---
5'''/9'''	130.7	7.451 d-like (8.7)
6'''/8'''	115.9	6.889 d-like (8.7)
7'''	158.5	---

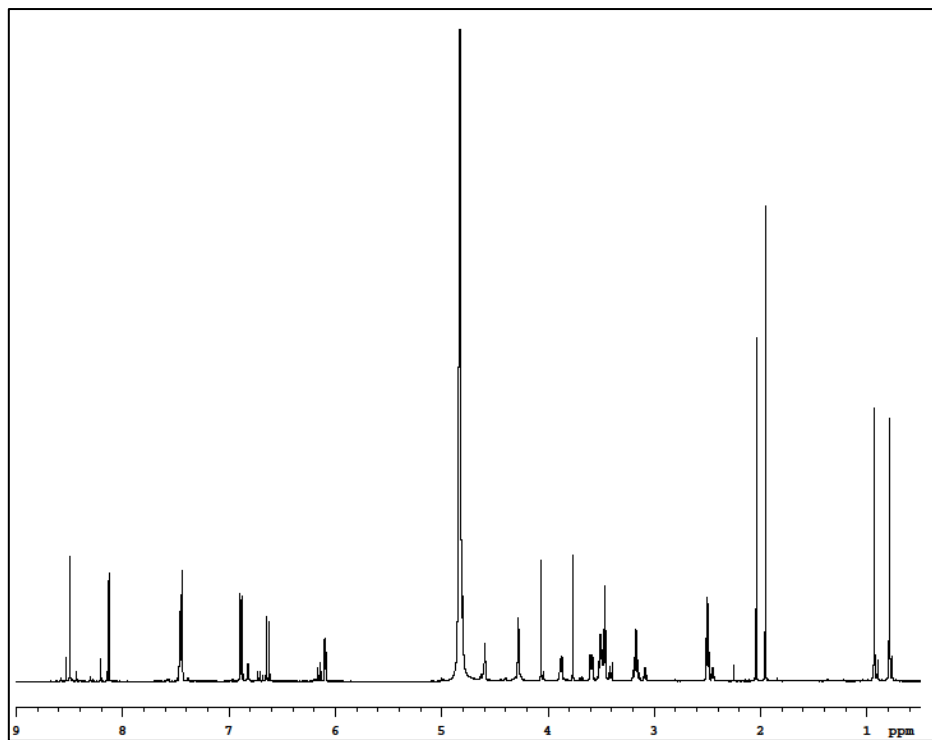


Fig. A 8: $^1\text{H-NMR}$ of *p*-coumaroyl-CoA.

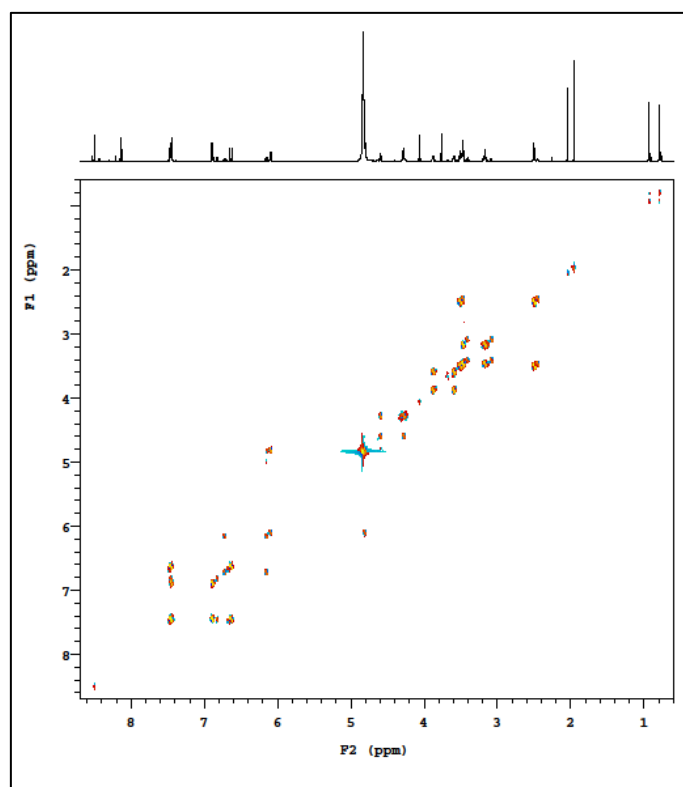


Fig. A 9: Double quantum filtered correlation spectroscopy (DQF-COSY) plot of *p*-coumaroyl-CoA.

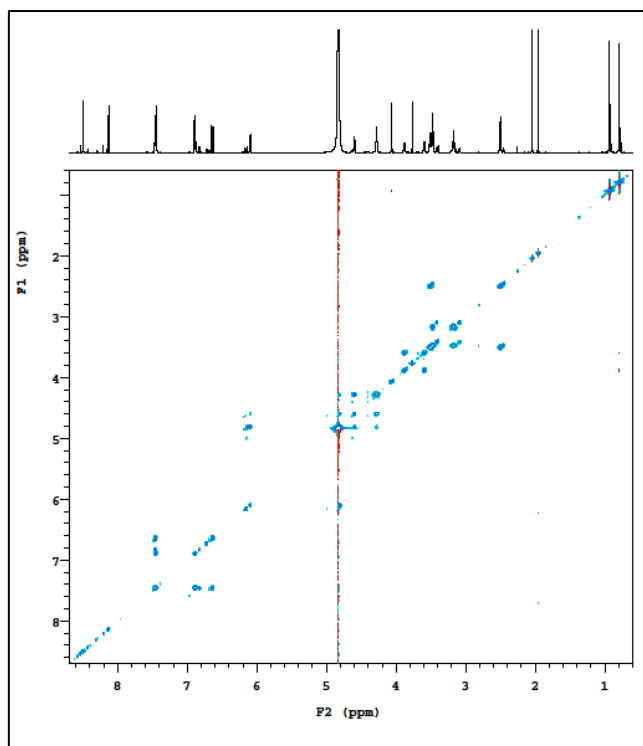


Fig. A 10: Total correlation spectrum (TOCSY) of *p*-coumaroyl-CoA.

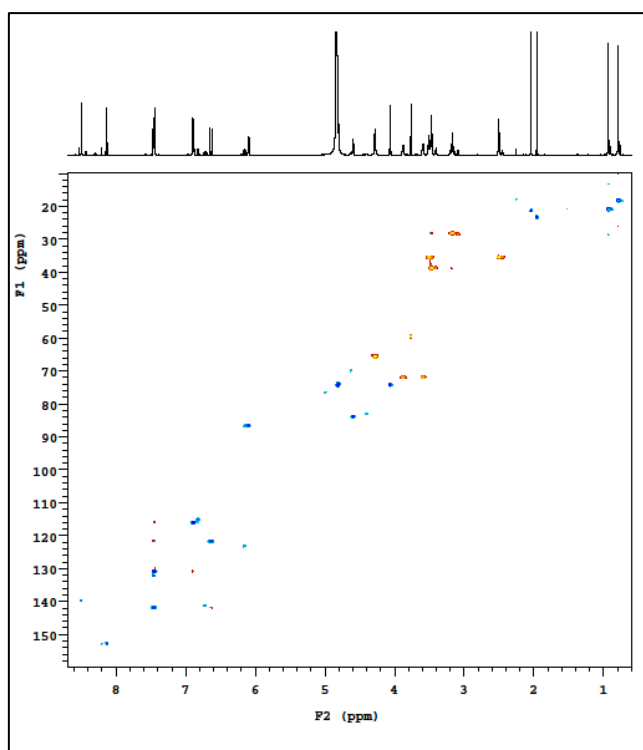


Fig. A 11: Heteronuclear single-quantum correlation spectrum (HSQC) of *p*-coumaroyl-CoA.

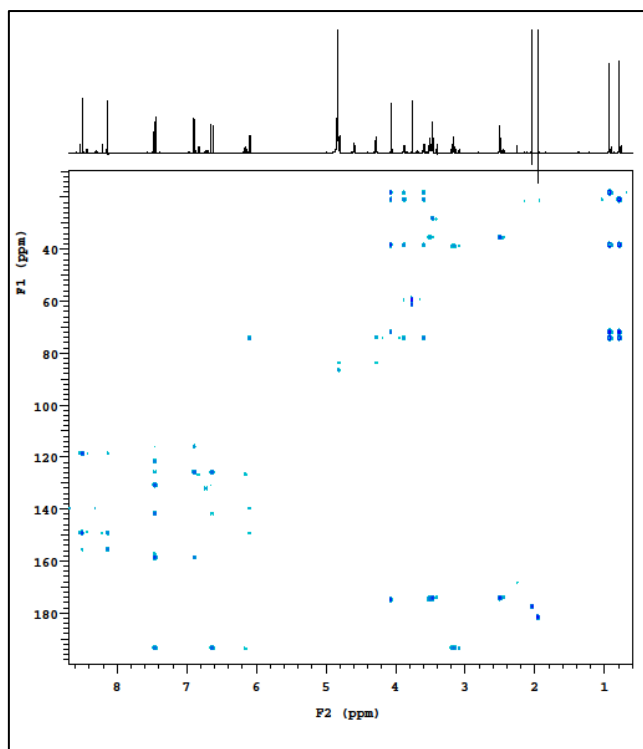


Fig. A 12: Heteronuclear multiple-bond correlation spectroscopy (HMBC) plot of *p*-coumaroyl-CoA.

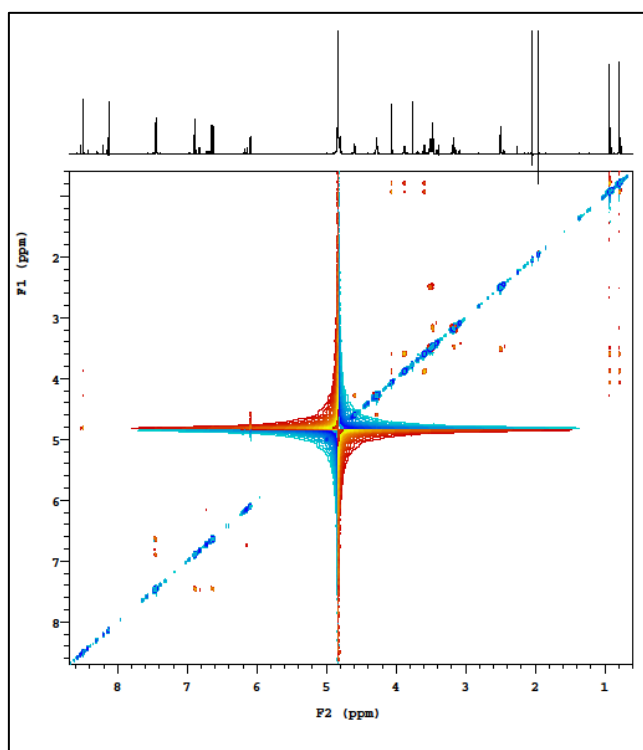


Fig. A 13: Rotating frame nuclear Overhauser effect spectroscopy (ROESY) plot of *p*-coumaroyl-CoA.

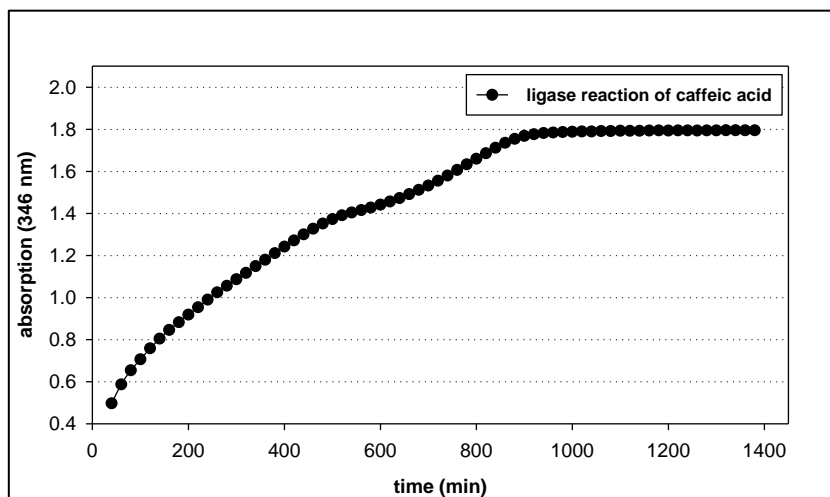


Fig. A 14: Wavelength shift during the ligase reaction using caffeic acid under time control. The CoA thioester gives a specific absorption at 346 nm indicating product formation.

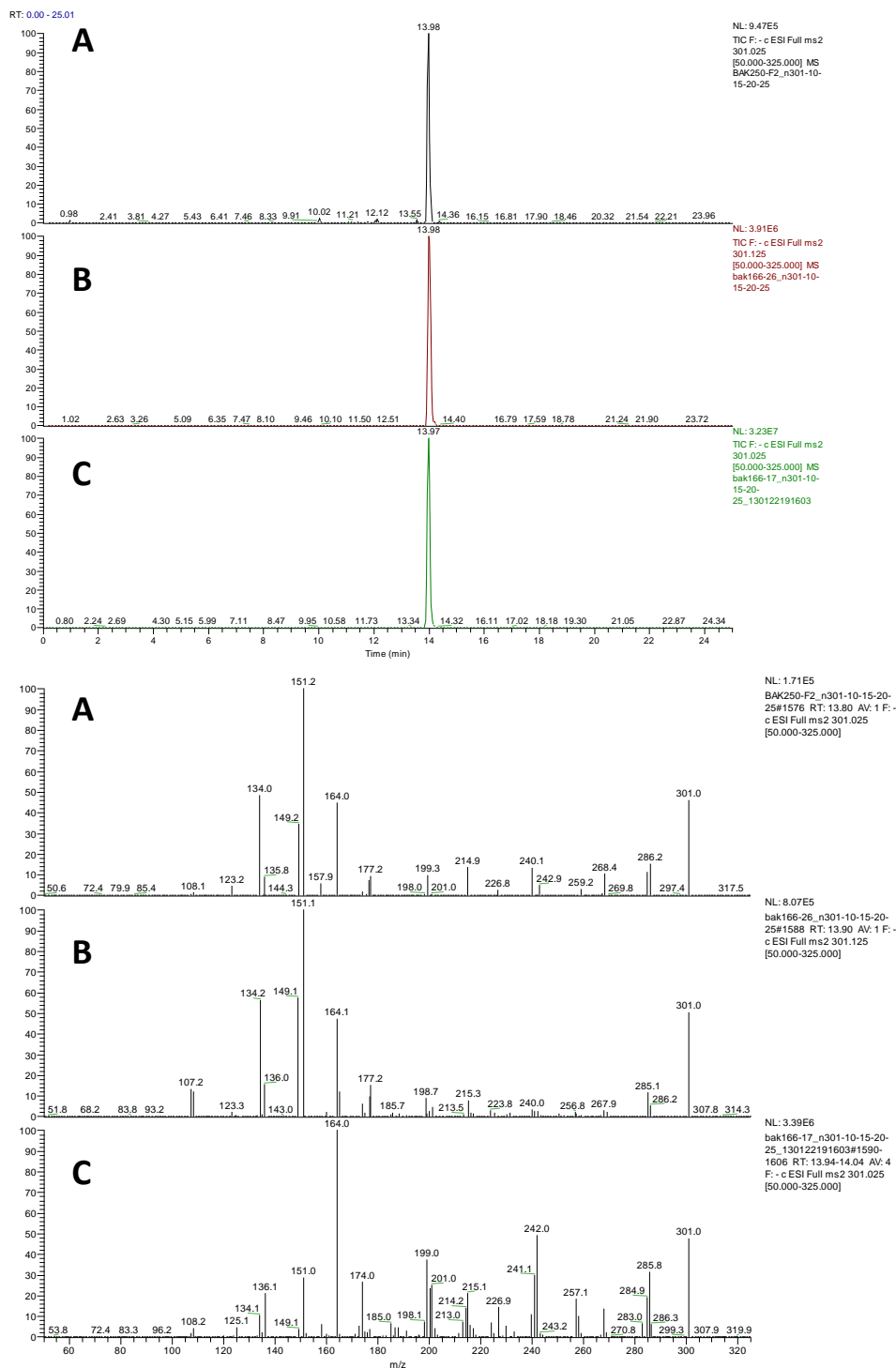


Fig. A 15: Retention time and MS² fragmentation pattern of the CHS2 product (A) compared to HED (B) and Hesp (C) as references. The retention time and the relative intensity of the fragments of the MS² measurement using 20 eV for ionization from the reference HED (3'-O-methoxy-eriodictyol) accord to the data from the product formation of the CHS2 assay using feruloyl-CoA as a substrate. The regioisomer Hesp (4'-O-methoxy-eriodictyol) gave the same retention time but a distinctly different fragmentation pattern at 20 eV and was not formed in the assay.

Appendix B

Supplementary information to Chapter II: Hydroxylation of flavonoids

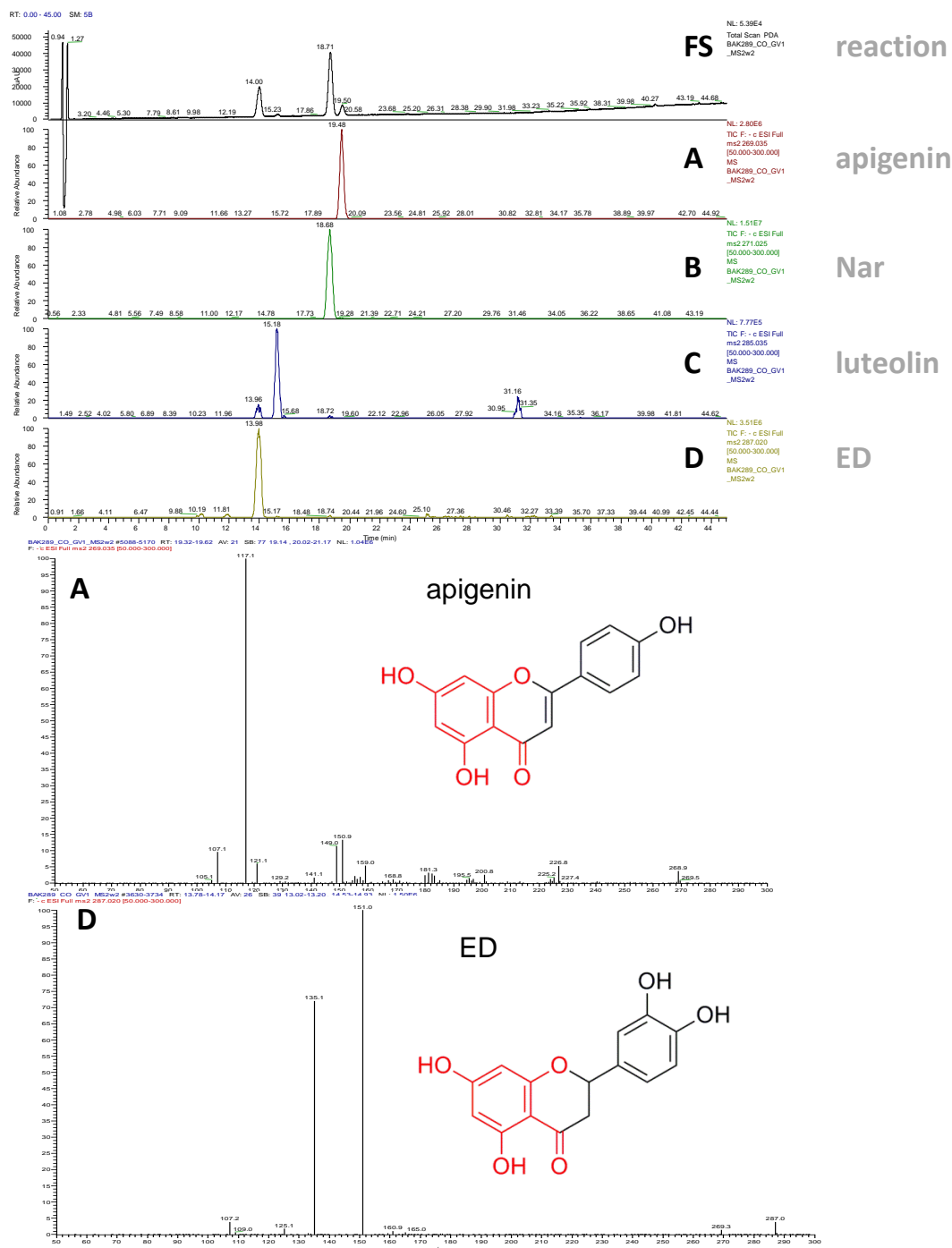


Fig. B 1: UHPLC and MS/MS fragmentation patterns of the products of a BM3-GVQ assay using Nar as a substrate. The signals of the PDA fullscan (FS) were selected using EIC modus for the substrate Nar (18.71 min (B)), the products ED (14.0 min (D)) and apigenin (19.5 min (A)) which were also fragmented via MS/MS confirming the references. The flavonoids are fragmented typically by retro-aldol like fragmentation (highlighted in red). EIC modus for the minor compound luteolin (Signal C (15.2 min)) was also selected, but has no relevance in intensity.

Appendix B

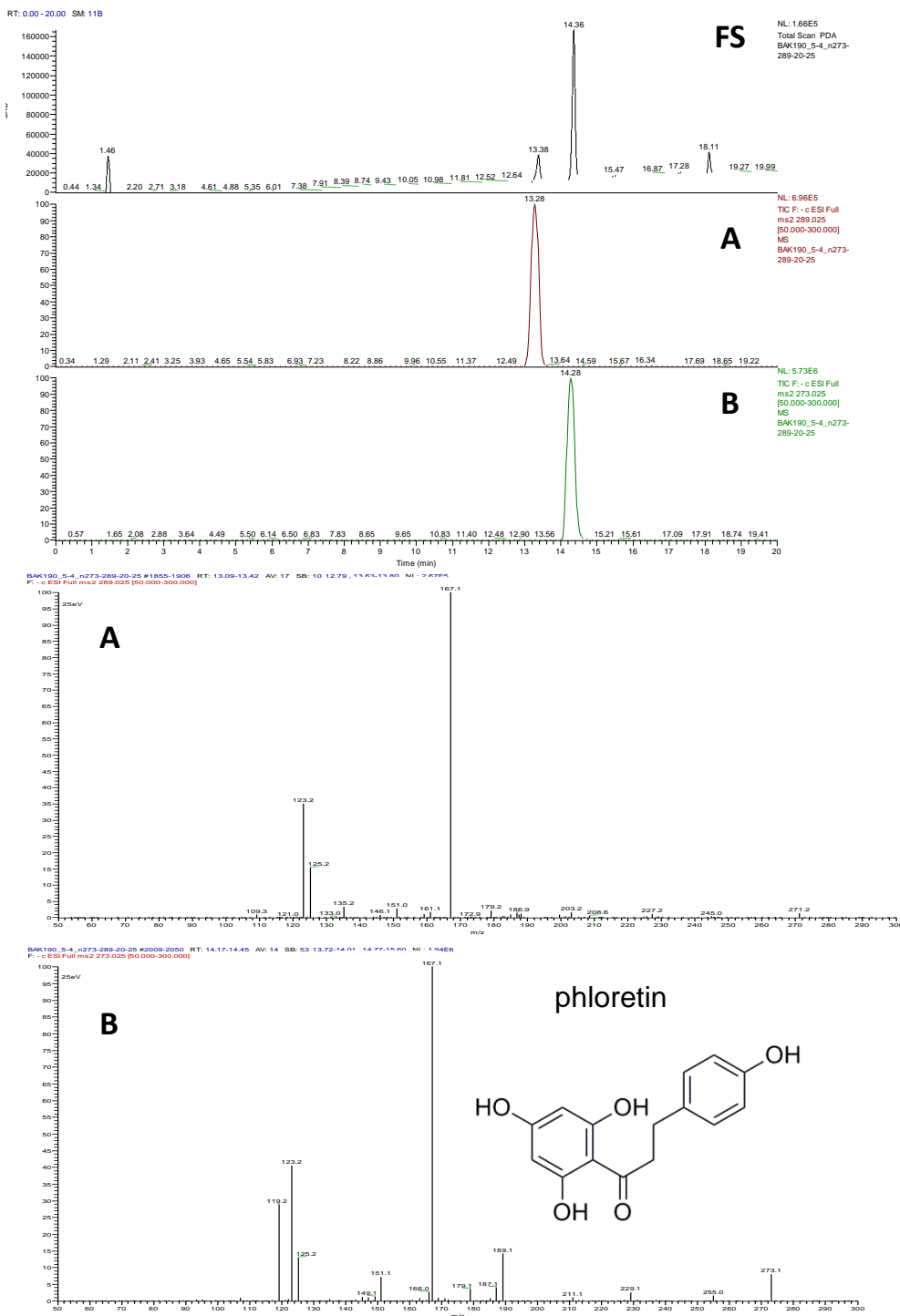


Fig. B 2: UHPLC and MS/MS fragmentation pattern of the products of a BM3-GVQ assay using phloretin as a substrate. The signals of the PDA fullscan (FS) were selected using EIC modus for the substrate phloretin (14.4 min (B)) and the hydroxylated product (13.4 min (A)) which were also fragmented via MS/MS. The exact position of the inserted hydroxyl group was not further localized.

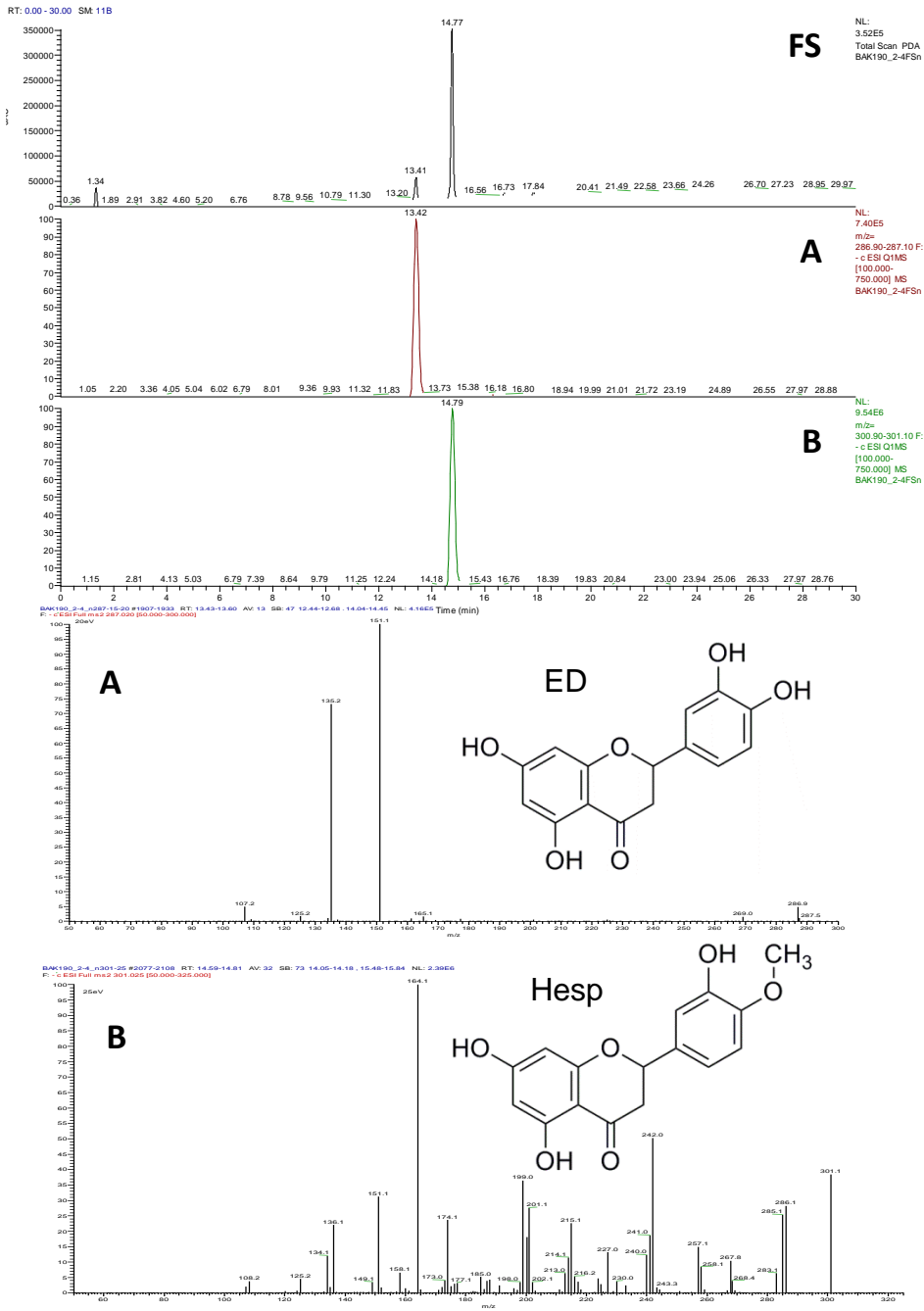
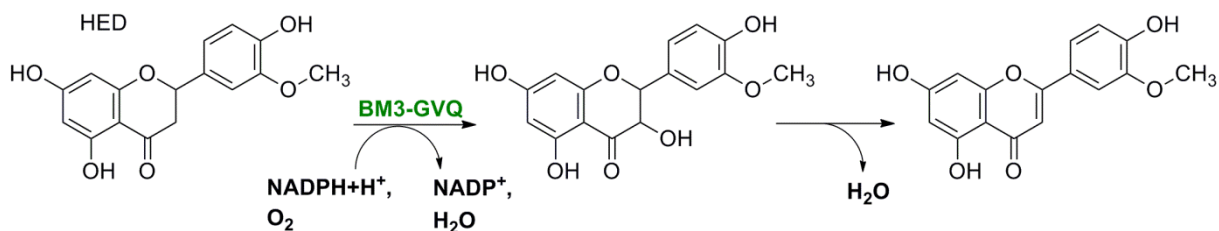


Fig. B 3: UHPLC and MS/MS fragmentation pattern of the products of a BM3-GVQ assay using Hesp as a substrate. The signals of the PDA fullscan (FS) were selected using EIC modus for the substrate Hesp (14.8 min (B)) and the product ED (13.4 min (A)) which were also fragmented via MS/MS confirming the references.

Appendix B



K:\LCMS\BAK274-26_FSp

7/30/2013 2:32:59 PM

RT: 0.00 - 45.00

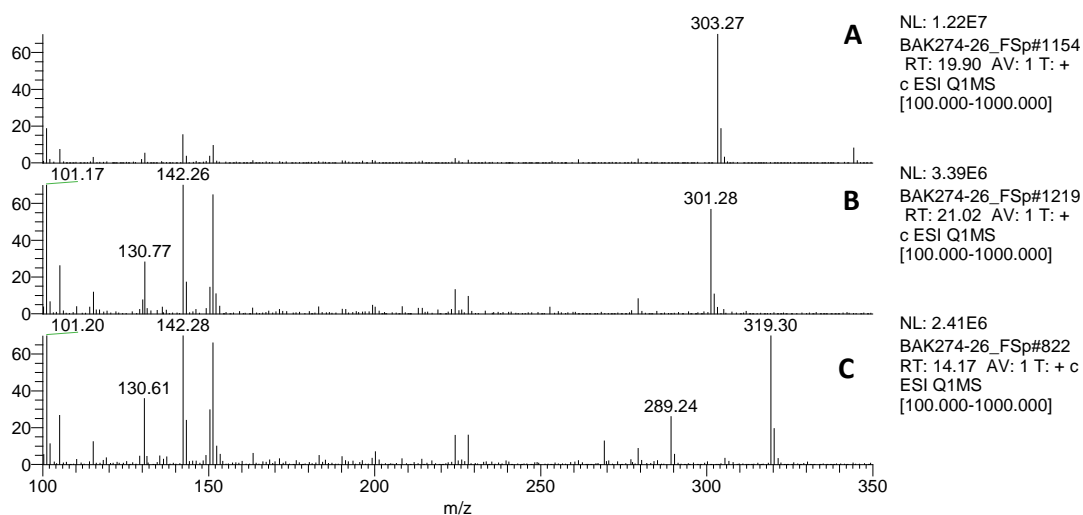
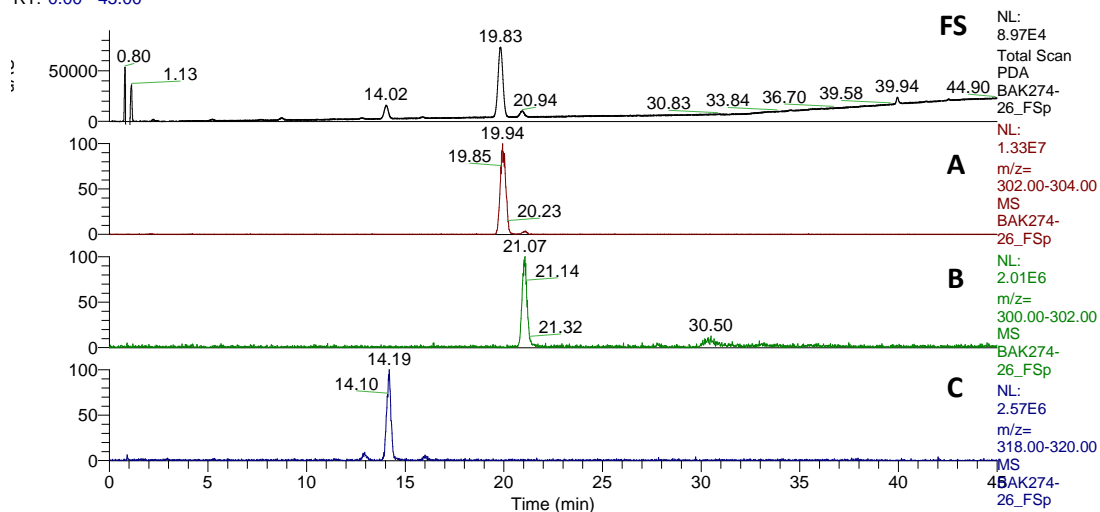


Fig. B 4: Proposed reaction, UHPLC and MS/MS fragmentation pattern of the products of a BM3-GVQ assay using HED as a substrate. The signals of the PDA fullscan (FS) were selected using EIC modus for the substrate HED (19.8 min (A)), the main product 2-OH-HED (14.0 min (C)) and the flavone of HED as a minor product (14.2 min (C)) which were also studied by MS/MS.

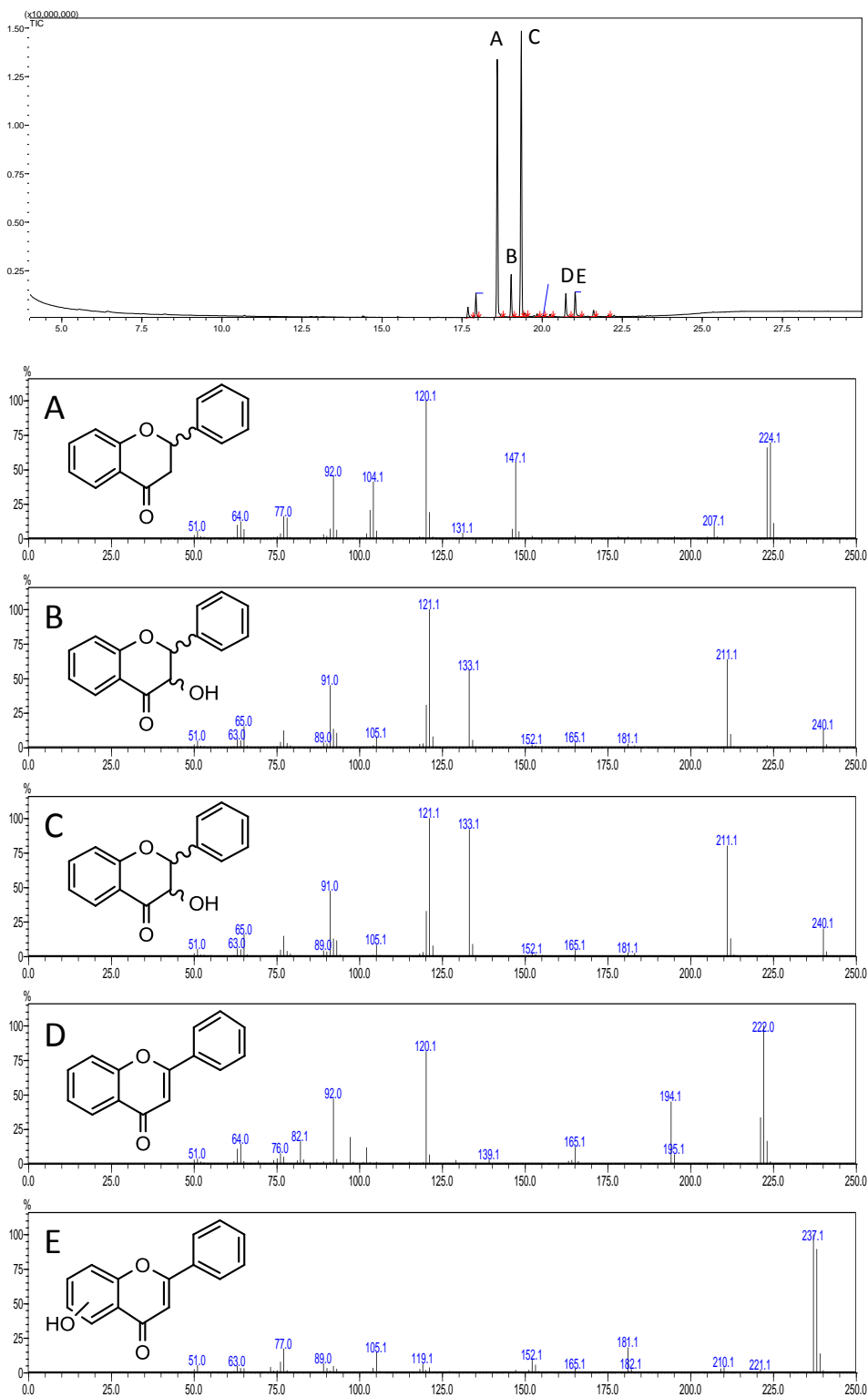


Fig. B 5: Achiral GC-MS chromatogram and fragmentation pattern of a BM3-GVQ assay using flavanone as a substrate. The chromatogram shows the unseparated enantiomers of the substrate flavanone (A, $rt = 18.6$ min), two diastereomers of the 3-hydroxylated products (19.0 min (B); 19.3 min (C)), the resulting flavone (20.7 min (D)) and the mono-hydroxylated flavone (21 min (E)).

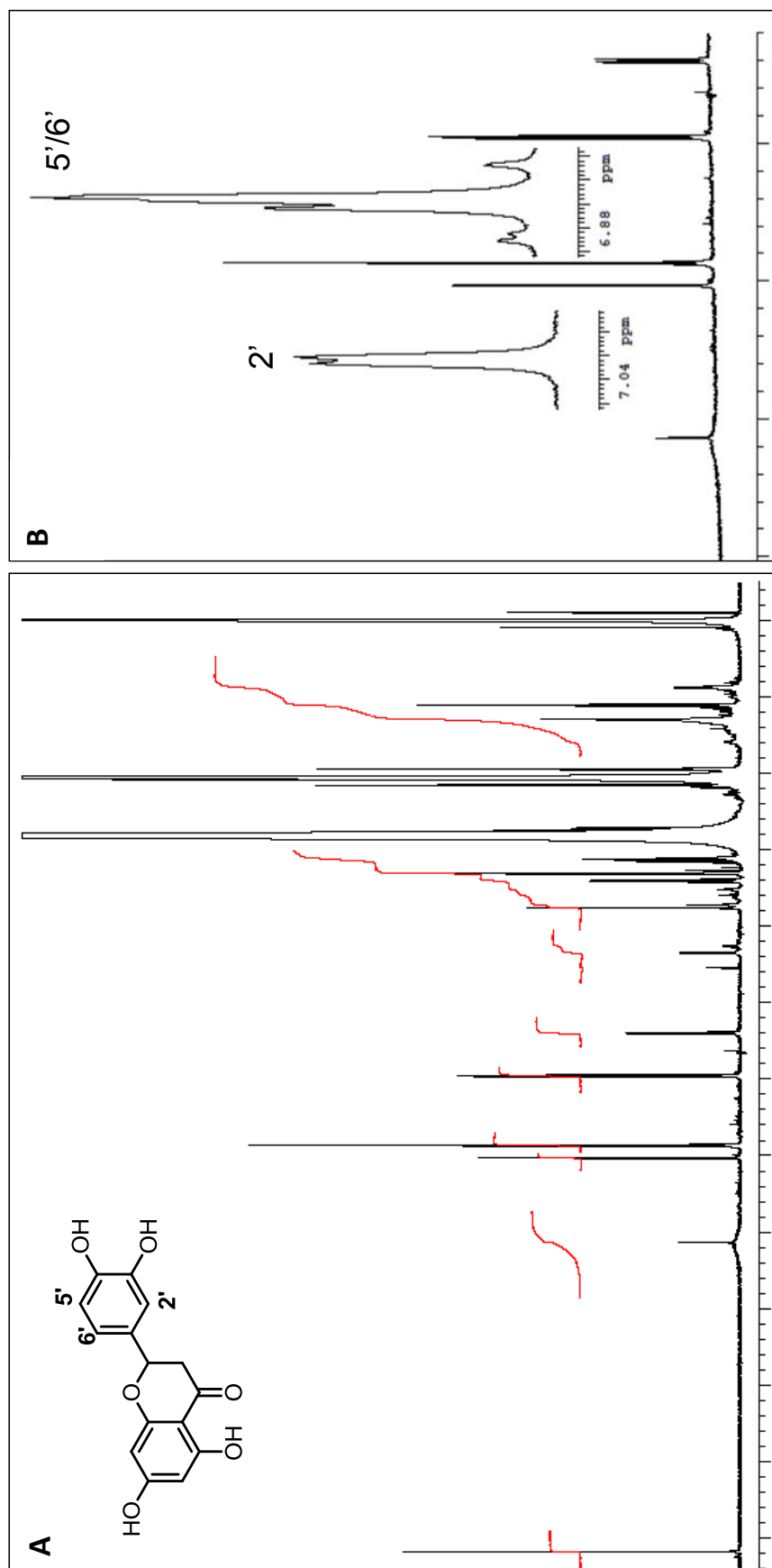
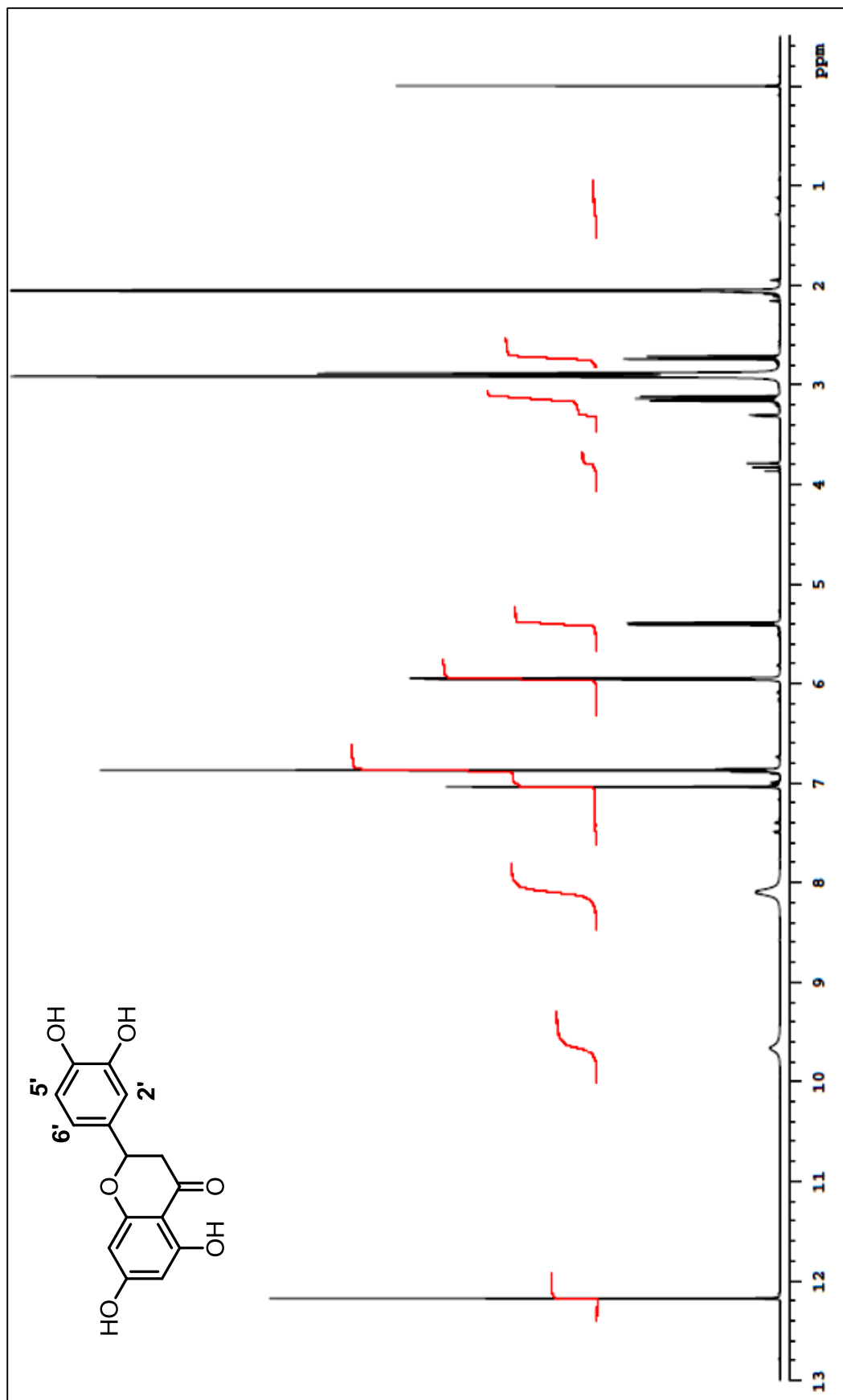


Fig. B 6: (A) $^1\text{H-NMR}$ plot of the main product from the BM3-GVQ assay and (B) relevant section zoomed in the range of 5 and 9 ppm. The plots show the typical signals of ED. The introduction of the hydroxyl group is localized due to the chemical shifts of the protons at position 2', 5' and 6' of ring B.

Fig. B 7 : ¹H-NMR plot of a ED reference.

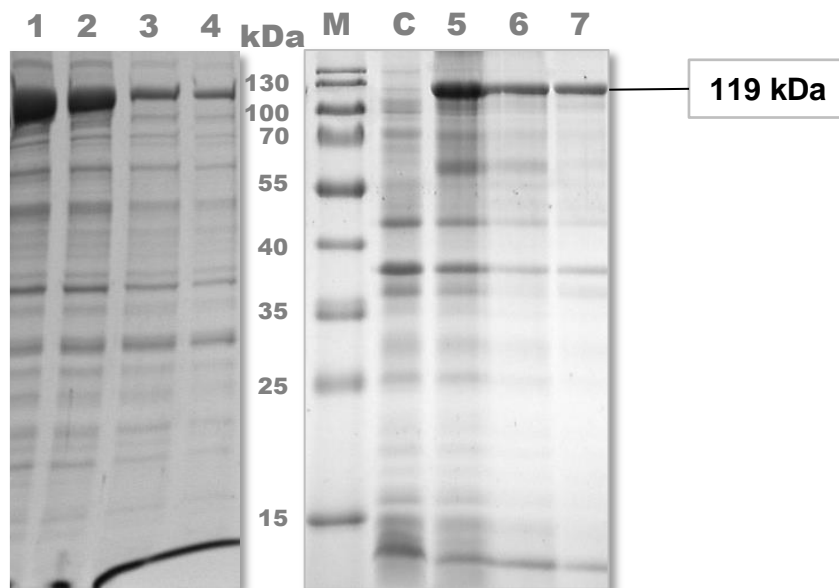


Fig. B 8: SDS-PAGE of the newly designed BM3 variants. The 10 % SDS-PAGE gel shows the crude extract after cell lysis of the inactive variants BM3-GNVQ (1), BM3-GSVQ (2), BM3-NVQ (3) and BM3-SVQ (4) and the active variants BM3-GV (5), BM3-VQ (6) and BM3-GVQS (7). All variants show the crucial protein band for the BM3 enzyme at 119 kDa indicating a successful gene expression. An empty vector was used as a control (C). The marker (M) was used to identify the molecular weight.

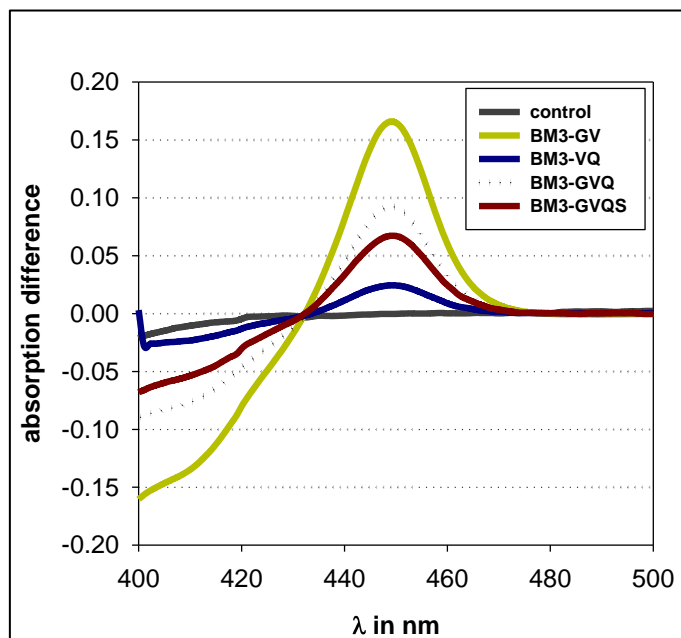


Fig. B 9: CO difference spectra of BM3- variants based on BM3-F87V for BM3-GV and BM3-VQ, and BM3-GVQ for BM3-GVQS containing a further mutation A330S, respectively. The typical Soret band at 450 nm is characteristic for correctly folded P450 enzymes [135]. A similar treated crude extract containing an empty vector (control) was used as a control.

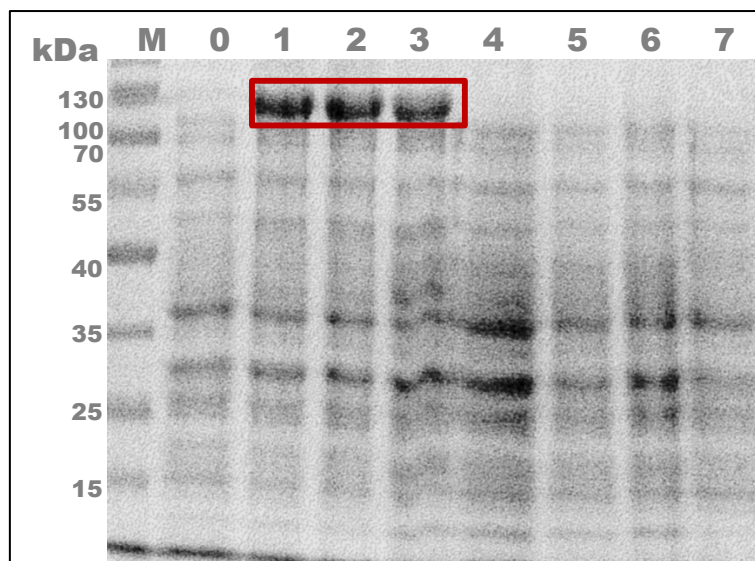


Fig. B 10: SDS-PAGE of *in vivo* biotransformation of Nar in LB/IPTG. The 10 % SDS-PAGE gel shows the crude extract before induction with IPTG (0), before adding the substrate Nar after 1 h of incubation (1), 1 h after adding the substrate Nar to the culture (2) and the culture after 14 h of incubation (3). One hour after induction with IPTG (1) the expected molecular weight of 119 kDa (red framed) of BM3-GVQ is observed indicating the gene expression and enzyme synthesis. The intensity of this protein band does not increase during longer incubation time (2,3). A similar treated control was analyzed analogously in similar sequence (4-7) showing no protein band at the relevant molecular weight during the whole incubation time as expected. The marker (M) was used to identify the molecular weight.

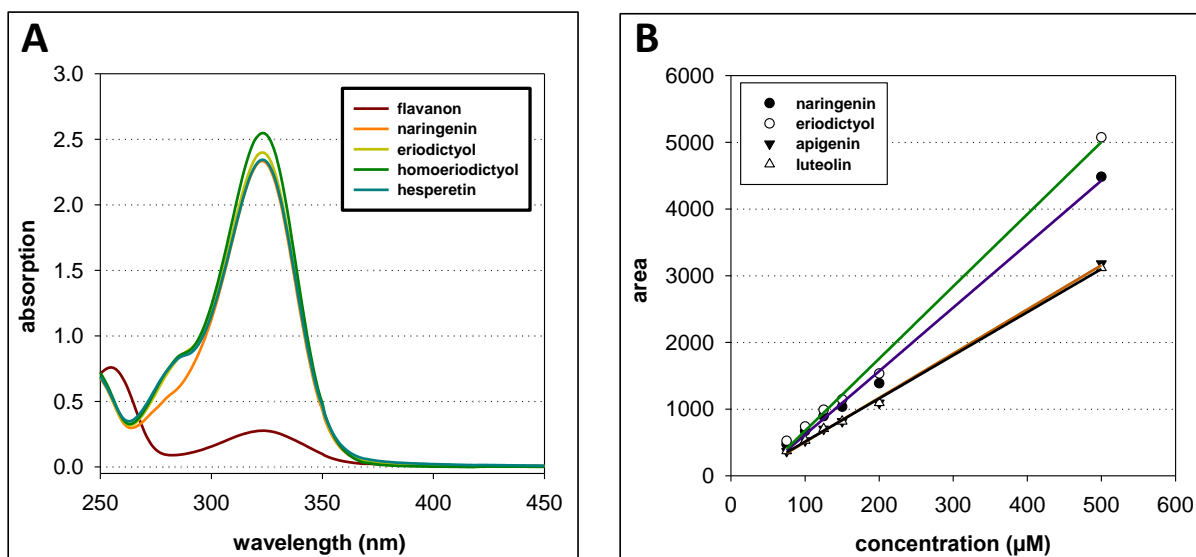


Fig. B 11: UV spectrum of references (A) and external calibration curve of relevant products measured at 280 nm (B) within the BM3-GVQ assay. (A) References were diluted with water to a final concentration of 100 µM from a 10 mM stock solution dissolved in DMSO measured on Jasco V-560 UV/Vis spectrometer. (B) External calibration curves were used to calculate the substrate (Nar) and product concentration (ED, apigenin) of the *in vitro* assay analyzed via HPLC.

Table B 1: BM3 variants with no conversion of Nar and ED after 24 h *in vivo* biotransformation.

	A328I	F87A/A328I	F87I/A328I	F87V/A328I	F87L/A328I
F87A	A328L	F87A/A328L	F87I/A328L	F87V/A328L	F87L/A328L
F87I	A328V	F87A/A328V	F87I/A328V	F87V/A328V	F87L/A328V
F87L	A328F	F87A/A328F	F87I/A328F	F87V/A328F	F87L/A328F

Appendix C

Supplementary information to Chapter III: Methylation of ED – the final step of HED biosynthesis

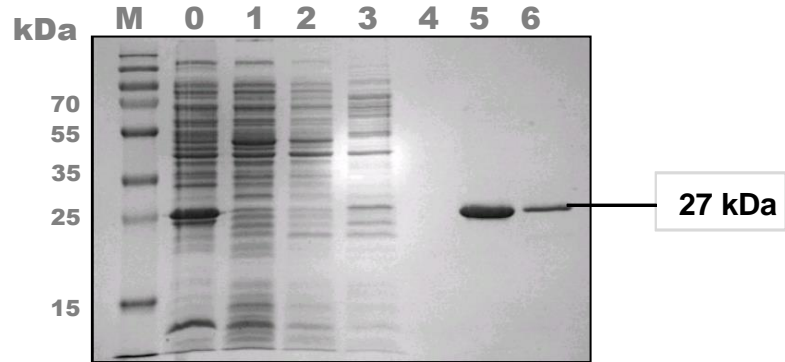


Fig. C 1: SDS-PAGE of the purification of PFOMT. The 14 % SDS-PAGE gel shows the steps of purification after cell lysis of the crude extract (0): the flow-through (1), washing steps (2, 3) and the elution of PFOMT (27 kDa) (4 – 6). The marker (M) was used to identify the molecular weight.

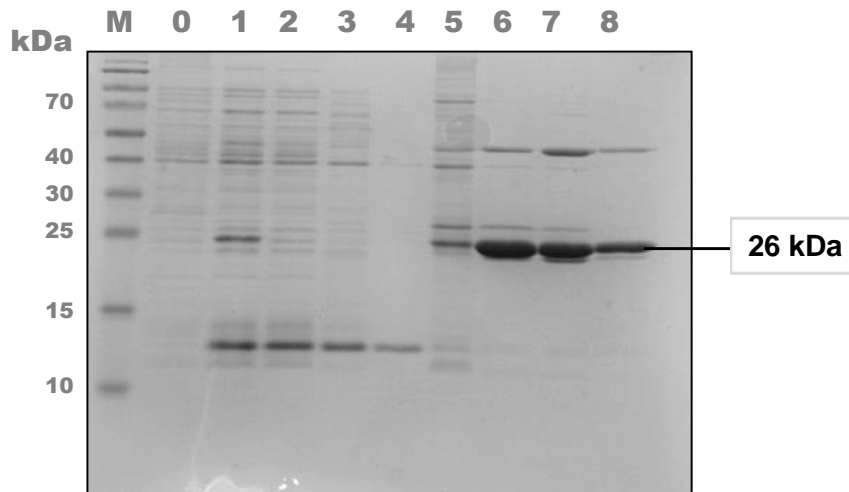


Fig. C 2: SDS-PAGE of the purification of AtTSM1. The 14 % SDS-PAGE gel shows the culture before induction (0) and steps of purification after cell lysis of the crude extract (1): the flow-through (2), washing steps (3, 4) and the elution of AtTSM1 (26 kDa) (4 – 8). The marker (M) was used to identify the molecular weight.

AtTSM1	1	MDGRLPDKGILKSEAL	K	QYIMETTAYPREHELLKELREATIQRYGNLSE	M	MGVVPDESFL
PFOMT	1	-----GLLQSEEL	C	QYILRTSVYPREAGFLKELREANESHPD--	S	YMSTSPLAGQLM
AtTSM1	61	SMLVKIINAKNTIEIGVFTGYSLFTVALALPEDGRITAI	D	T	DQAGYNLGLEFMKKAGVDH	
PFOMT	51	SFVLKLVNAKKTIEVGVFTGYSLLLLTALSIPDDGKITAI	D	F	DREAYEIGLPPFIRKAGVEH	
AtTSM1	121	KINFIQSDAVRGLDQLLNGEKQE--YDFAFVDADKTNVY	F	L	EKLLKLVKVGIIAFDNT	
PFOMT	111	KINFIESDAMLALDNLLQGQSEGSYDFGFVDADKPNY	I	K	YHERLMKLVKVGIVAYDNT	
AtTSM1	179	LWFGTLIQKENEVPGHMRA	Y	R	EALLENFKILARDPRVEIAQISIGDGLTLCRRLIXX	
PFOMT	171	LWGGTVAQPESVDFMKE	N	R	EAVIELNKLLAADPRIIVHLPLGDGITFCRRLYXX	

Fig. C 3: Sequence alignment of PFOMT and AtTSM1. The crucial aa with potential influence for the (non-) acceptance of the sp^3 -hybridised flavonoids are highlighted (cyan).

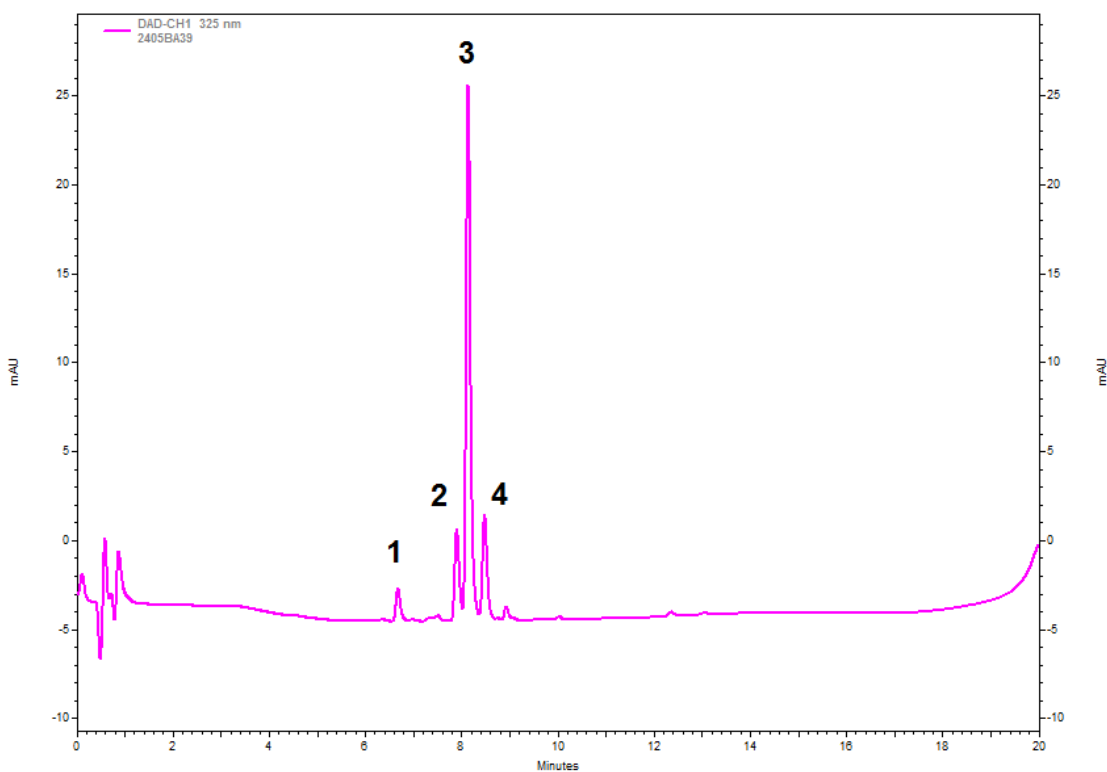


Fig. C 4: HPLC Chromatogram of a product mixture of a standard PFOMT assay using 1,5-dicaffeoylquinic acid as a substrate after 600 min incubation. The chromatogram exemplifies the distribution of the products for the substrates consisting of two catechol groups: 1) the substrate – 4.4 % (Ret. time: 6,683), 2) first single methylated intermediate – 11.8 % (Ret. time: 7.9), 3) second single methylated intermediate – 69.6 % (Ret. time: 8.1) and 4) the double methylated end-product – 14.2 % (Ret. time: 8.5).

RT: 0.00 - 20.01

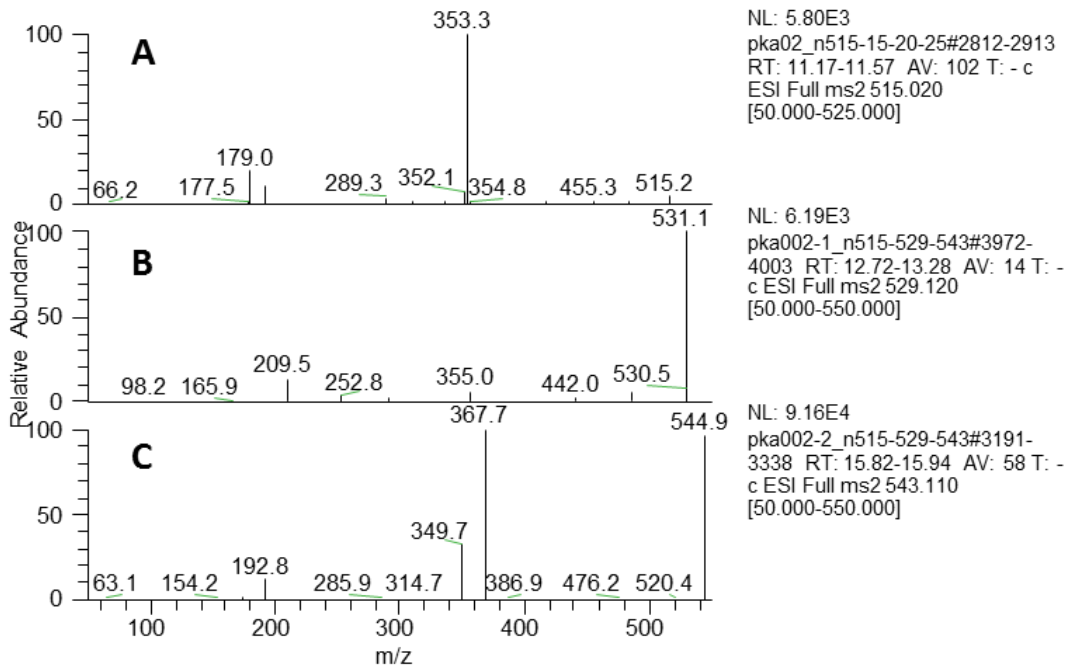
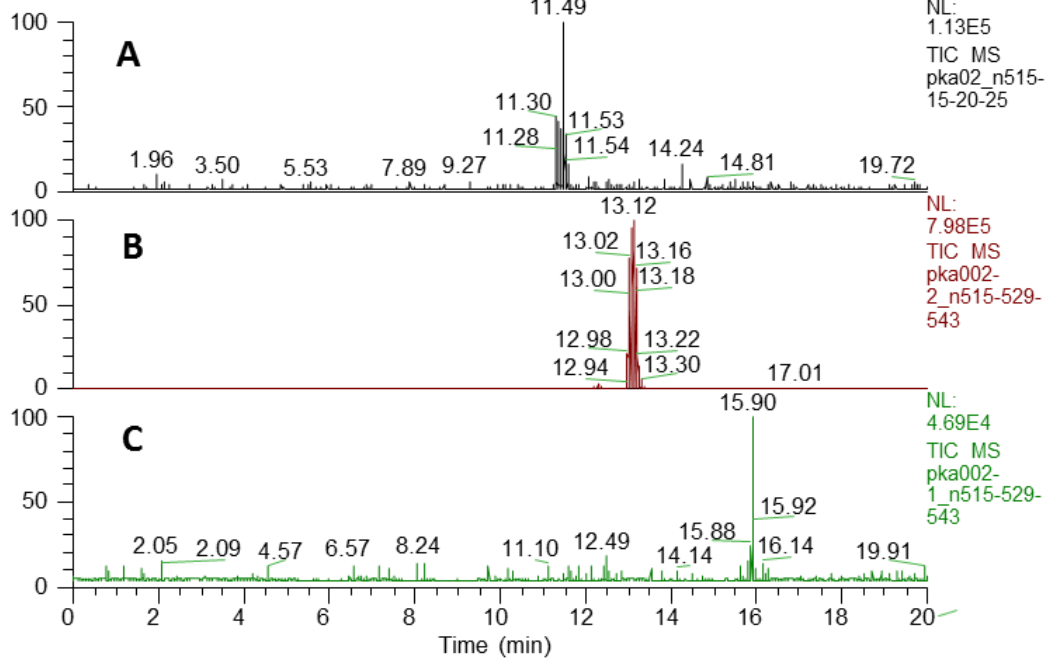


Fig. C 5: UHPLC and MS/MS fragmentation pattern of the products of the PFOMT assay using 1,5-dicaffeoylquinic acid as a substrate. EIC negative modulus and the fragmentation by MS/MS were used to verify the masses and localization of the methyl group of the products within the PFOMT assay detected in the HPLC run: the substrate 1,5 dicaffeoylquinic acid (11.5 min, 515 m/z), the single methylated intermediates (13.0 min, 529 m/z) and (13.2 min, 529 m/z) and the double methylated end product (15.9 min, 543 m/z) were identified. The single methylated intermediates are similar in their fragmentation patterns and could not be distinguished.

References

1. P. A. S. Breslin, "An evolutionary perspective on food and human taste," *Curr. Biol.*, **23**, 9, R409–18 (2013).
2. A. Drewnowski, "Taste preferences and food intake," *Annu. Rev. Nutr.*, **17**, 237–53 (1997).
3. D. W. Haslam and W. P. T. James, "Obesity," *Lancet*, **366**, 9492, 1197–209 (2005).
4. A. Drewnowski and C. Gomez-Carneros, "Bitter taste, phytonutrients, and the consumer: a review," *Am. J. Clin. Nutr.*, **72**, 6, 1424–35 (2000).
5. T. K. Beck, S. Jensen, G. K. Bjoern, and U. Kidmose, "The Masking Effect of Sucrose on Perception of Bitter Compounds in Brassica Vegetables," *J. Sens. Stud.*, **29**, 3, 190–200 (2014).
6. A. Taylor and J. Hort, *Modifying Flavour in Food*, **20**, 1. Woodhead Publishing, 2007.
7. V. J. Breitzkreutz, "Bittere Arzneistoffe gut kaschiert," *Pharm. Ztg.*, **8**, (2008).
8. J. P. Ley, G. Krammer, G. Reinders, I. L. Gatfield, and H.-J. Bertram, "Evaluation of bitter masking flavanones from Herba Santa (*Eriodictyon californicum* (H. and A.) Torr., Hydrophyllaceae)," *J. Agric. Food Chem.*, **53**, 15, 6061–6 (2005).
9. J. P. Ley, "Masking Bitter Taste by Molecules," *Chemosens. Percept.*, **1**, 1, 58–77 (2008).
10. G. M. Roy, "The applications and future implications of bitterness reduction and inhibition in food products," *Crit. Rev. Food Sci. Nutr.*, **29**, 2, 59–71 (1990).
11. N. Chaudhari and S. D. Roper, "The cell biology of taste," *J. Cell Biol.*, **190**, 3, 285–96 (2010).
12. J. Chandrashekar, M. A. Hoon, N. J. P. Ryba, and C. S. Zuker, "The receptors and cells for mammalian taste," *Nature*, **444**, 7117, 288–94 (2006).
13. A. Vandenbeuch and S. C. Kinnamon, "Why do taste cells generate action potentials?," *J. Biol.*, **8**, 4, 42 (2009).
14. C. Cartoni, K. Yasumatsu, T. Ohkuri, N. Shigemura, R. Yoshida, N. Godinot, J. le Coutre, Y. Ninomiya, and S. Damak, "Taste preference for fatty acids is mediated by GPR40 and GPR120," *J. Neurosci.*, **30**, 25, 8376–82 (2010).
15. M. M. Galindo, N. Voigt, J. Stein, J. van Lengerich, J.-D. Raguse, T. Hofmann, W. Meyerhof, and M. Behrens, "G protein-coupled receptors in human fat taste perception," *Chem. Senses*, **37**, 2, 123–39 (2012).
16. P. a S. Breslin and A. C. Spector, "Mammalian taste perception," *Curr. Biol.*, **18**, 4, R148–55 (2008).
17. A. Brockhoff, M. Behrens, N. Roudnitzky, G. Appendino, C. Avonto, and W. Meyerhof, "Receptor agonism and antagonism of dietary bitter compounds," *J. Neurosci.*, **31**, 41, 14775–82 (2011).
18. R. K. Palmer, "The pharmacology and signaling of bitter, sweet, and umami taste sensing," *Mol. Interv.*, **7**, 2, 87–98 (2007).
19. S. Rodgers, J. Busch, H. Peters, and E. Christ-Hazelhof, "Building a tree of knowledge: analysis of bitter molecules," *Chem. Senses*, **30**, 7, 547–57 (2005).

20. J. Suez, T. Korem, D. Zeevi, G. Zilberman-Schapira, C. A. Thaiss, O. Maza, D. Israeli, N. Zmora, S. Gilad, A. Weinberger, Y. Kuperman, A. Harmelin, I. Kolodkin-Gal, H. Shapiro, Z. Halpern, E. Segal, and E. Elinav, "Artificial sweeteners induce glucose intolerance by altering the gut microbiota," *Nature*, **514**, 7521, 181–186 (2014).
21. N. D. Johnson, "Flavonoid aglycones from *Eriodictyon californicum* resin and their implications for herbivory and UV screening," *Biochem. Syst. Ecol.*, **11**, 3, 211–215 (1983).
22. S. Pollastri and M. Tattini, "Flavonols: old compounds for old roles," *Ann. Bot.*, **108**, 7, 1225–33 (2011).
23. G. A. C. Driver and M. Bhattacharya, "Role of phenolics in plant evolution," *Phytochemistry*, **49**, 5, 1165–1174 (1998).
24. W. Steglich, B. Fugmann, and S. Lang-Fugmann, *RÖMPP Encyclopedia Natural Products*, 1st ed. Thieme, 2000.
25. S. Quideau, "Flavonoids. Chemistry, Biochemistry and Applications," in *Angewandte Chemie International Edition*, **45**, 41, Ø. M. Andersen and K. R. Markham (Eds.), 6786–6787, 2006.
26. G. Williamson, G. Plumb, and M. Garcia-Conesa, "Glycosylation, Esterification, and Polymerization of Flavonoids and Hydroxycinnamates: Effects on Antioxidant Properties," in *Plant Polyphenols 2*, **66**, G. Gross, R. Hemingway, T. Yoshida, and S. Branham (Eds.), 483–494, Springer US, 1999.
27. E. Grotewold, "The genetics and biochemistry of floral pigments," *Annu. Rev. Plant Biol.*, **57**, 761–80 (2006).
28. M. L. Falcone Ferreyra, S. P. Rius, and P. Casati, "Flavonoids: biosynthesis, biological functions, and biotechnological applications," *Front. Plant Sci.*, **3**, September, 222 (2012).
29. C. Brunetti, M. Di Ferdinando, A. Fini, S. Pollastri, and M. Tattini, "Flavonoids as antioxidants and developmental regulators: relative significance in plants and humans," *Int. J. Mol. Sci.*, **14**, 2, 3540–55 (2013).
30. A. Y. Chen and Y. C. Chen, "A review of the dietary flavonoid, kaempferol on human health and cancer chemoprevention," *Food Chem.*, **138**, 4, 2099–107 (2013).
31. N. Belaya and A. Nikolaevskii, "Antiradical activity of fruit juices in reactions with diphenylpicrylhydrazyl," *Pharm. Chem.*, **43**, 6, 6–8 (2009).
32. A. Bocco, M. M.-E. Cuvelier, H. Richard, and C. Berset, "Antioxidant activity and phenolic composition of citrus peel and seed extracts," *J. Agric. Food Chem.*, **8561**, 97, 2123–2129 (1998).
33. R. J. Nijveldt, E. van Nood, D. E. van Hoorn, P. G. Boelens, K. van Norren, and P. A. van Leeuwen, "Flavonoids: a review of probable mechanisms of action and potential applications," *Am. J. Clin. Nutr.*, **74**, 4, 418–25 (2001).
34. T. P. T. Cushnie and A. J. Lamb, "Antimicrobial activity of flavonoids," *Int. J. Antimicrob. Agents*, **26**, 5, 343–356 (2005).
35. D. Saslowsky, "Localization of flavonoid enzymes in Arabidopsis roots," *Plant J.*, **27**, December 2000, (2001).
36. E. Wollenweber, "Exkret-Flavonoide bei Höheren Pflanzen arider Gebiete," *Plant Syst.*

- Evol.*, **150**, September 1984, 83–88 (1985).
37. F. A. Tomás-Barberán and E. Wollenweber, "Flavonoid aglycones from the leaf surfaces of some Labiatae species," *Plant Syst. Evol.*, **173**, 3–4, 109–118 (1990).
 38. P. Proksch and E. Rodriguez, "Baja California - Ein Model für chemoökologische Adaptationen von Wüstenpflanzen," *Biol. unserer Zeit*, **15**, 3, 75–80 (1985).
 39. N. Johnson, S. Brain, and P. Ehrlich, "The role of leaf resin in the interaction between *Eriodictyon californicum* (Hydrophyllaceae) and its herbivore, *Trirhabda diducta* (Chrysomelidae)," *Oecologia*, 106–110 (1985).
 40. B. Winkel-Shirley, "Flavonoid biosynthesis. A colorful model for genetics, biochemistry, cell biology, and biotechnology," *Plant Physiol.*, **126**, 2, 485–493 (2001).
 41. H. Berke, "The invention of blue and purple pigments in ancient times," *Chem. Soc. Rev.*, **36**, 1, 15–30 (2007).
 42. J. Miller, "The impact of biotechnology on the chemical industry in the 21st century," *Trends Biotechnol.*, **18**, 5, 190–191 (2000).
 43. R. Hatti-Kaul, U. Törnvall, L. Gustafsson, and P. Börjesson, "Industrial biotechnology for the production of bio-based chemicals--a cradle-to-grave perspective," *Trends Biotechnol.*, **25**, 3, 119–24 (2007).
 44. H. Guzmán-Maldonado and O. Paredes-López, "Amylolytic enzymes and products derived from starch: a review," *Crit. Rev. Food Sci. Nutr.*, **35**, 5, 373–403 (1995).
 45. D. M. Barbano and R. R. Rasmussen, "Cheese Yield Performance of Fermentation-Produced Chymosin and Other Milk Coagulants," *J. Dairy Sci.*, **75**, 1, 1–12 (1992).
 46. T. A. Geissman, "The Isolation of Eriodictyol and Homoeriodictyol. An Improved Procedure," *J. Am. Chem. Soc.*, **62**, 11, 3258–3259 (1940).
 47. J. P. Ley, I. Reiss, M. Blings, P. Hoffmann-Lucke, and J. Herzog, "Technical process for isolating homoeriodictyol," WO Patent 2,004,041,804 (2004).2004.
 48. Lindenbaum, "(D) Organische Chemie," *Chem. Zentralblatt.*, **1**, 16, 1941–1942 (1929).
 49. M. O. Farooq, I. P. Varshney, W. Rahman, and P. C. Gangwar, "The synthesis of chrysoeriol (3'-methyl ether of luteolin) and homoeriodictyol (5,7,4-trihydroxy-3'-methoxy flavanone)," *Naturwissenschaften*, **46**, 2, 76–76 (1959).
 50. N. Shetgiri and L. Rege, "Novel synthesis of 4', 5, 7-trihydroxy-3'-methoxy-flavanone (homoeriodictyol)," *INDIAN J. Chem.*, **42B**, 648–650 (2003).
 51. P. S. Kulkarni, "Novel Synthesis of 4', 5, 7-Trihydroxy-3'-Methoxyflavanone & 3', 4', 5, 7-Tetrahydroxyflavanone," *Asian J. Biochem. Pharm. Res.*, **2**, 2, 227–230 (2012).
 52. N. Kasai, S. Ikushiro, S. Hirose, A. Arisawa, H. Ichinose, H. Wariishi, M. Ohta, and T. Sakaki, "Enzymatic properties of cytochrome P450 catalyzing 3'-hydroxylation of naringenin from the white-rot fungus *Phanerochaete chrysosporium*," *Biochem. Biophys. Res. Commun.*, **387**, 1, 103–8 (2009).
 53. I. L.-B. Amor, A. Hehn, E. Guedone, K. Ghedira, J.-M. Engasser, L. Chekir-Ghedira, and M. Ghoul, "Biotransformation of naringenin to eriodictyol by *Saccharomyces cerevisiae* functionally expressing flavonoid 3' hydroxylase," *Nat. Prod. Commun.*, **5**, 12, 1893–8 (2010).
 54. I. Erlund, "Review of the flavonoids quercetin, hesperetin, and naringenin. Dietary

- sources, bioactivities, bioavailability, and epidemiology," *Nutr. Res.*, **24**, 10, 851–874 (2004).
55. Q. Liu, L. Liu, J. Zhou, H.-D. Shin, R. R. Chen, C. Madzak, J. Li, G. Du, and J. Chen, "Biosynthesis of homoeriodictyol from eriodictyol by flavone 3'-O-methyltransferase from recombinant *Yarrowia lipolytica*: Heterologous expression, biochemical characterization, and optimal transformation," *J. Biotechnol.*, **167**, 4, 472–8 (2013).
 56. R. Ullrich and M. Hofrichter, "Enzymatic hydroxylation of aromatic compounds," *Cell. Mol. Life Sci.*, **64**, 3, 271–93 (2007).
 57. S. G. Burton, "Oxidizing enzymes as biocatalysts," *Trends Biotechnol.*, **21**, 12, 543–9 (2003).
 58. O. Hayaishi, "Mechanism of the pyrocatechase reaction," *J. Am. Chem. Soc.*, **77**, 5450–5451 (1955).
 59. O. Hayaishi, *Oxygenases*, United Kin. London: Academic Press INC., 1962.
 60. L. Wessjohann, M. Dippe, M. Tengg, and M. Gruber-Khadjawi, "Methyltransferases in Biocatalysis," in *Cascade Biocatalysis: Integrating Stereoselective and Environmentally Friendly Reactions*, S. Riva and W.-D. Fessner (Eds.), 393–426, Weinheim, Germany: Wiley-VCH Verlag GmbH & Co. KGaA, 2014.
 61. M.-J. Kim, B.-G. Kim, and J.-H. Ahn, "Biosynthesis of bioactive O-methylated flavonoids in *Escherichia coli*," *Appl. Microbiol. Biotechnol.*, **97**, 16, 7195–204 (2013).
 62. H. Schönherr and T. Cernak, "Ausgeprägte Methyleffekte in der Wirkstoff-Forschung und der Bedarf an neuen C-H-Methylierungsreaktionen," *Angew. Chemie*, **125**, 47, 12480–12492 (2013).
 63. L. A. Wessjohann, J. Keim, B. Weigel, and M. Dippe, "Alkylating enzymes," *Curr. Opin. Chem. Biol.*, **17**, 2, 229–35 (2013).
 64. A. Staniek, H. Bouwmeester, P. D. Fraser, O. Kayser, S. Martens, A. Tissier, S. van der Krol, L. Wessjohann, and H. Warzecha, "Natural products - modifying metabolite pathways in plants," *Biotechnol. J.*, **8**, 10, 1159–71 (2013).
 65. K. Drauz, H. Gröger, and O. May, "Principles of Enzyme Catalysis," in *Enzyme Catalysis in Organic Synthesis; Part I*, 3rd ed., Wiley-VCH Verlag GmbH & Co. KGaA, 2012.
 66. N. Nair, C. Denard, and H. Zhao, "Engineering of enzymes for selective catalysis," *Curr. Org. Chem.*, 217, 1870–1882 (2010).
 67. Z. S. Olempska-Beer, R. I. Merker, M. D. Ditto, and M. J. DiNovi, "Food-processing enzymes from recombinant microorganisms--a review," *Regul. Toxicol. Pharmacol.*, **45**, 2, 144–158 (2006).
 68. Y. Yan, A. Kohli, and M. A. G. M. Koffas, "Biosynthesis of natural flavanones in *Saccharomyces cerevisiae*," *Appl. Environ. Microbiol.*, **71**, 9, 5610–5613 (2005).
 69. S. Horinouchi, "Combinatorial biosynthesis of non-bacterial and unnatural flavonoids, stilbenoids and curcuminoids by microorganisms," *J. Antibiot. (Tokyo)*, **61**, 12, 709–28 (2008).
 70. A.-K. Bauer, "Synthese und Analyse geschmacksmodifizierender Flavonoide," Martin-Luther-Universität Halle-Wittenberg, 2010.

71. H. Inoue, H. Nojima, and H. Okayama, "High efficiency transformation of *Escherichia coli* with plasmids," *Gene*, **96**, 1, 23–8 (1990).
72. M. M. Bradford, "A rapid and sensitive method for the quantitation of microgram quantities of protein utilizing the principle of protein-dye binding," *Anal. Biochem.*, **72**, 248–54 (1976).
73. T. Omura and R. Sato, "The carbon monoxide-binding pigment of liver microsomes: I. evidence for its hemoprotein nature," *J Biol Chem*, **239**, 7, 2370–2378 (1964).
74. U. Laemmli, "Cleavage of structural proteins during the assembly of the head of bacteriophage T4," *Nature*, (1970).
75. H. Meng and W. Campbell, "Facile enzymic synthesis of caffeoyl CoA," *Phytochemistry*, 605–608 (1997).
76. Chemical Computing Group Inc, "Molecular Operating Environment (MOE)," **2012.10**. 2010.
77. E. Krieger, K. Joo, J. Lee, S. Raman, J. Thompson, M. Tyka, D. Baker, and K. Karplus, "Improving physical realism, stereochemistry, and side-chain accuracy in homology modeling: Four approaches that performed well in CASP8," *Proteins*, **77 Suppl 9**, 114–122 (2009).
78. E. Krieger, G. Koraimann, and G. Vriend, "Increasing the precision of comparative models with YASARA NOVA--a self-parameterizing force field," *Proteins*, **47**, 393–402 (2002).
79. R. A. Laskowski, M. W. Macarthur, D. S. Moss, and T. J. M., "Procheck - a program to check the stereochemical quality of protein structures," *J Appl Crystallogr*, **26**, 283–291 (1993).
80. Tripos Inc. 1699 South Hanley Rd., "SYBYL [7.0]." St. Louis, Missouri, 63144, USA, 2006.
81. D. A. Case, T. A. Darden, T. E. Cheatham, C. L. Simmerling, J. Wang, R. E. Duke, R. Luo, R. C. Walker, W. Zhang, K. M. Merz, B. Roberts, S. Hayik, A. Roitberg, G. Seabra, J. Swails, A. W. Goetz, I. Kolossváry, K. F. Wong, F. Paesan, J. Vanicek, R. M. Wolf, J. Liu, X. Wu, S. R. Brozell, T. Steinbrecher, H. Gohlke, Q. Cai, X. Ye, M.-J. Hsieh, G. Cui, D. R. Roe, D. H. Mathews, M. G. Seetin, R. Salomon-Ferrer, C. Sagui, V. Babin, T. Luchko, S. Gusarov, A. Kovalenko, and P. A. Kollman, "AMBER 12." University of California, San Francisco, 2012.
82. M. Wojciechowski and B. Lesyng, "Generalized born model: Analysis, refinement, and applications to proteins," *J Phys Chem B*, **108**, 18368–18376 (2004).
83. T. A. Halgren, "The Merck Force Field," *J Comput Chem*, **17**, 490–641 (1996).
84. M. L. Verdonk, J. C. Cole, M. J. Hartshorn, C. W. Murray, and R. D. Taylor, "Improved protein-ligand docking using GOLD," *Proteins*, **52**, 609–623 (2003).
85. M. J. Hartshorn, M. L. Verdonk, G. Chessari, S. C. Brewerton, W. T. Mooij, P. N. Mortenson, and C. W. Murray, "Diverse, high-quality test set for the validation of protein-ligand docking performance," *J. Med. Chem.*, **50**, 726–741 (2007).
86. J. G. Kopycki, D. Rauh, A. A. Chumanevich, P. Neumann, T. Vogt, and M. T. Stubbs, "Biochemical and Structural Analysis of Substrate Promiscuity in Plant Mg²⁺-Dependent O-Methyltransferases," *J. Mol. Biol.*, **378**, 1, 154–164 (2008).

87. O. Korb, T. Stütze, and T. Exner, "PLANTS: Application of Ant Colony Optimization to Structure-Based Drug Design," in *Ant Colony Optimization and Swarm Intelligence SE - 22*, **4150**, M. Dorigo, L. Gambardella, M. Birattari, A. Martinoli, R. Poli, and T. Stütze (Eds.), 247–258, Springer Berlin Heidelberg, 2006.
88. O. Korb, T. Stütze, and T. E. Exner, "An ant colony optimization approach to flexible protein–ligand docking," *Swarm Intell.*, **1**, 2, 115–134 (2007).
89. A. C. Neish, "Biosynthetic Pathways of Aromatic Compounds," *Annu. Rev. Plant Physiol.*, **11**, 1, 55–80 (1960).
90. H. Stafford and R. Ibrahim, "Phenolic metabolism in plants," *Recent Adv. Phytochem.*, **26**, (1992).
91. R. E. Koes, F. Quattrocchio, and J. N. M. Mol, "The flavonoid biosynthetic pathway in plants: Function and evolution," *BioEssays*, **16**, 2, 123–132 (1994).
92. E. Grotewold, *The Science of Flavonoids*. Ohia, USA: Springer Science+Business Media, New York, 2006.
93. J. L. Ferrer, J. M. Jez, M. E. Bowman, R. a Dixon, and J. P. Noel, "Structure of chalcone synthase and the molecular basis of plant polyketide biosynthesis," *Nat. Struct. Biol.*, **6**, 8, 775–84 (1999).
94. A. B. Christensen, P. L. Gregersen, J. Schröder, and D. B. Collinge, "A chalcone synthase with an unusual substrate preference is expressed in barley leaves in response to UV light and pathogen attack," *Plant Mol. Biol.*, **37**, 5, 849–57 (1998).
95. M. Pietrowska-Borek, H.-P. Stuibler, E. Kombrink, and A. Guranowski, "4-Coumarate:coenzyme A ligase has the catalytic capacity to synthesize and reuse various (di)adenosine polyphosphates," *Plant Physiol.*, **131**, 3, 1401–10 (2003).
96. K. Schneider, K. Hövel, K. Witzel, B. Hamberger, D. Schomburg, E. Kombrink, and H.-P. Stuibler, "The substrate specificity-determining amino acid code of 4-coumarate:CoA ligase," *Proc. Natl. Acad. Sci. U. S. A.*, **100**, 14, 8601–6 (2003).
97. A. Nibbs and K. Scheidt, "Asymmetric methods for the synthesis of flavanones, chromanones, and azaflavanones," *European J. Org. Chem.*, **2012**, 3, 449–462 (2012).
98. L. A. Wessjohann and H. Wilhelm, "An Efficient Synthesis of the Phytoestrogen 8-Prenylnaringenin from Xanthohumol by a Novel Demethylation Process," *Tetrahedron*, **62**, 6961–6966 (2006).
99. M. Wink, "Biochemistry of Plant Secondary Metabolism," in *ANNUAL PLANT REVIEWS VOLUME 40*, 2nd ed., Wiley-VCH Verlag GmbH & Co. KGaA, 2008.
100. M. R. Dyson, S. P. Shadbolt, K. J. Vincent, R. L. Perera, and J. McCafferty, "Production of soluble mammalian proteins in Escherichia coli: identification of protein features that correlate with successful expression," *BMC Biotechnol.*, **4**, 32 (2004).
101. R. D'Ordine, P. Paneth, and V. Anderson, "¹³C NMR and ¹H-¹H NOEs of Coenzyme-A: conformation of the pantoic acid moiety," *Bioorg. Chem.*, **23**, 2, 169–185 (1995).
102. M. Sisa, S. L. Bonnet, D. Ferreira, and J. H. Van der Westhuizen, "Photochemistry of flavonoids," *Molecules*, **15**, 8, 5196–245 (2010).
103. G. L. Ellman, "Tissue sulfhydryl groups," *Arch. Biochem. Biophys.*, **82**, 1, 70–77 (1959).
104. S. Malla, M. a G. Koffas, R. J. Kazlauskas, and B.-G. Kim, "Production of 7-O-methyl

- aromadendrin, a medicinally valuable flavonoid, in *Escherichia coli*,” *Appl. Environ. Microbiol.*, **78**, 3, 684–94 (2012).
105. D. H. Kim, B.-G. Kim, Y. Lee, J. Y. Ryu, Y. Lim, H.-G. Hur, and J.-H. Ahn, “Regiospecific methylation of naringenin to ponciretin by soybean O-methyltransferase expressed in *Escherichia coli*,” *J. Biotechnol.*, **119**, 2, 155–62 (2005).
106. S. Ayabe and T. Akashi, “Cytochrome P450s in flavonoid metabolism,” *Phytochem. Rev.*, **5**, 2–3, 271–282 (2006).
107. F. Hannemann, A. Bichet, K. M. Ewen, and R. Bernhardt, “Cytochrome P450 systems--biological variations of electron transport chains,” *Biochim. Biophys. Acta*, **1770**, 3, 330–44 (2007).
108. P. B. Watkins, “Role of cytochromes P450 in drug metabolism and hepatotoxicity,” *Semin. Liver Dis.*, **10**, 4, 235–250 (1990).
109. R. Bernhardt, “Cytochromes P450 as versatile biocatalysts,” *J. Biotechnol.*, **124**, 1, 128–45 (2006).
110. T. Omura, “Structural diversity of cytochrome P450 enzyme system,” *J. Biochem.*, **147**, 3, 297–306 (2010).
111. M. A. Noble, C. S. Miles, S. K. Chapman, D. A. Lysek, A. C. MacKay, G. A. Reid, R. P. Hanzlik, and A. W. Munro, “Roles of key active-site residues in flavocytochrome P450 BM3,” *Biochem. J.*, **339**, 2, 371 (1999).
112. R. Schmid and V. Urlacher, *Modern Biooxidation*. Weinheim, Germany: Wiley-VCH Verlag GmbH & Co. KGaA, 2007.
113. L. Liu, R. D. Schmid, and V. B. Urlacher, “Cloning, expression, and characterization of a self-sufficient cytochrome P450 monooxygenase from *Rhodococcus ruber* DSM 44319,” *Appl. Microbiol. Biotechnol.*, **72**, 5, 876–82 (2006).
114. H.-K. Chang and G. J. Zylstra, “Examination and expansion of the substrate range of m-hydroxybenzoate hydroxylase,” *Biochem. Biophys. Res. Commun.*, **371**, 1, 149–153 (2008).
115. F. De Matteis, D. P. Ballou, M. J. Coon, R. W. Estabrook, and D. C. Haines, “Peroxidase-like activity of uncoupled cytochrome P450: studies with bilirubin and toxicological implications of uncoupling,” *Biochem. Pharmacol.*, **84**, 3, 374–82 (2012).
116. J. Dordick and A. Klibanov, “Horseradish peroxidase-catalyzed hydroxylations: mechanistic studies,” *Biochemistry*, 2946–2951 (1986).
117. D. Buhler and H. Mason, “Hydroxylation catalyzed by peroxidase,” *Arch. Biochem. Biophys.*, **92**, 424–437 (1961).
118. B. B. Halliwell and S. Ahluwalia, “Hydroxylation of p-coumaric acid by horseradish peroxidase,” *Biochem. J.*, **153**, 513–518 (1976).
119. R. Z. Kazandjian and A. M. Klibanov, “Regioselective oxidation of phenols catalyzed by polyphenol oxidase in chloroform,” *J. Am. Chem. Soc.*, **107**, 19, 5448–5450 (1985).
120. A. Azevedo and V. Martins, “Horseradish peroxidase: a valuable tool in biotechnology,” *Biotechnol. Annu.*, **9**, 03, (2003).
121. E. Leonard, Y. Yan, and M. a G. Koffas, “Functional expression of a P450 flavonoid hydroxylase for the biosynthesis of plant-specific hydroxylated flavonols in *Escherichia*

- coli*," *Metab. Eng.*, **8**, 2, 172–81 (2006).
122. D. E. Torres Pazmiño, M. Winkler, A. Glieder, and M. W. Fraaije, "Monooxygenases as biocatalysts: Classification, mechanistic aspects and biotechnological applications," *J. Biotechnol.*, **146**, 1–2, 9–24 (2010).
 123. M. Patzlaff and W. Barz, "Peroxidatic degradation of flavanones," *Z. Naturforsch.*, **33c**, 675–684 (1978).
 124. M. Jiménez-Atiénzar, J. Escribano, J. Cabanes, F. Gandía-Herrero, and F. García-Carmona, "Oxidation of the flavonoid eriodictyol by tyrosinase," *Plant Physiol. Biochem.*, **43**, 9, 866–73 (2005).
 125. A. M. Azevedo, D. M. F. Prazeres, J. M. S. Cabral, and P. Fonseca, "Stability of free and immobilised peroxidase in aqueous – organic solvents mixtures," **15**, 147–153 (2001).
 126. C. Virus and R. Bernhardt, "Molecular evolution of a steroid hydroxylating cytochrome P450 using a versatile steroid detection system for screening," *Lipids*, **43**, 12, 1133–41 (2008).
 127. Y. Khatri, F. Hannemann, K. M. Ewen, D. Pistorius, O. Perlova, N. Kagawa, A. O. Brachmann, R. Müller, and R. Bernhardt, "The CYPome of *Sorangium cellulosum* So ce56 and identification of CYP109D1 as a new fatty acid hydroxylase," *Chem. Biol.*, **17**, 12, 1295–305 (2010).
 128. W. A. Suske, "Purification and Characterization of 2-Hydroxybiphenyl 3-Monooxygenase, a Novel NADH-dependent, FAD-containing Aromatic Hydroxylase from *Pseudomonas azelaica* HBP1," *J. Biol. Chem.*, **272**, 39, 24257–24265 (1997).
 129. C.-H. Yun, K.-H. Kim, D.-H. Kim, H.-C. Jung, and J.-G. Pan, "The bacterial P450 BM3: a prototype for a biocatalyst with human P450 activities," *Trends Biotechnol.*, **25**, 7, 289–98 (2007).
 130. Y. Lin and Y. Yan, "Biosynthesis of caffeic acid in *Escherichia coli* using its endogenous hydroxylase complex," *Microb. Cell Fact.*, **11**, 42 (2012).
 131. J. M. Berg, J. L. Tymoczko, and L. Stryer, *Biochemistry*, 5th ed. New York: W. H. Freeman, 2002.
 132. H. Doostdar, M. D. Burke, and R. T. Mayer, "Bioflavonoids: selective substrates and inhibitors for cytochrome P450 CYP1A and CYP1B," *Toxicology*, **144**, 2000, 31–38 (2000).
 133. D. Voet and J. G. Voet, *Biochemistry*, 4th ed. John Wiley & Sons, 2011.
 134. E. Hofmann, *Enzyme und Bioenergetik: Dynamische Biochemie Teil II*, 4th ed. Akademie-Verlag Berlin, 1979.
 135. D. Lewis, *Guide to Cytochromes: Structure and Function*. London: Taylor & Francis, 2001.
 136. A. W. Munro, D. G. Leys, K. J. McLean, K. R. Marshall, T. W. B. Ost, S. Daff, C. S. Miles, S. K. Chapman, D. a Lysek, C. C. Moser, C. C. Page, and P. L. Dutton, "P450 BM3: the very model of a modern flavocytochrome," *Trends Biochem. Sci.*, **27**, 5, 250–7 (2002).
 137. J. Yanez and C. Remsberg, "Pharmacokinetics of selected chiral flavonoids: hesperetin, naringenin and eriodictyol in rats and their content in fruit juices,"

- Biopharm. Drug Dispos.*, **82**, April 2007, 63–82 (2008).
138. P. K. Andrews, N. M. Davies, and J. A. Yáñez, “Methods of analysis and separation of chiral flavonoids,” *J. Chromatogr. B*, **848**, 159–181 (2007).
 139. H. Hirakawa, Y. Inazumi, T. Masaki, T. Hirata, and A. Yamaguchi, “Indole induces the expression of multidrug exporter genes in *Escherichia coli*,” *Mol. Microbiol.*, **55**, 4, 1113–26 (2005).
 140. Q. S. Li, U. Schwaneberg, P. Fischer, and R. D. Schmid, “Directed evolution of the fatty-acid hydroxylase P450 BM-3 into an indole-hydroxylating catalyst,” *Chemistry*, **6**, 9, 1531–6 (2000).
 141. O. A. Olaofe, C. J. Fenner, R. K. Gudimichi, M. S. Smit, and S. T. L. Harrison, “The influence of microbial physiology on biocatalyst activity and efficiency in the terminal hydroxylation of n-octane using *Escherichia coli* expressing the alkane hydroxylase, CYP153A6,” *Microb. Cell Fact.*, **12**, 8 (2013).
 142. S. Roje, “S-Adenosyl-L-methionine: beyond the universal methyl group donor,” *Phytochemistry*, **67**, 15, 1686–98 (2006).
 143. G. L. Cantoni, “S-adenosylmethionin; a new intermediate formed enzymatically from l-methionine and adenosinetriphosphate,” *J. Biol. Chem.*, **204**, 1, 403–416 (1953).
 144. R. W. Woodard, M. D. Tsai, H. G. Floss, P. A. Crooks, and J. K. Coward, “Stereochemical course of the transmethylation catalyzed by catechol O-methyltransferase,” *J. Biol. Chem.*, **255**, 19, 9124–7 (1980).
 145. T. L. Grove, J. S. Benner, M. I. Radle, J. H. Ahlum, B. J. Landgraf, C. Krebs, and S. J. Booker, “A radically different mechanism for S-adenosylmethionine-dependent methyltransferases,” *Science*, **332**, 6029, 604–7 (2011).
 146. J. Axelrod, “O-Methylation of Epinephrine and Other Catechols in vitro and in vivo,” *Science*, **126**, 3270, 400–401 (1957).
 147. P. T. Männistö and S. Kaakkola, “Catechol-O-methyltransferase (COMT): biochemistry, molecular biology, pharmacology, and clinical efficacy of the new selective COMT inhibitors,” *Pharmacol. Rev.*, **51**, 4, 593–628 (1999).
 148. A. Alazizi, M.-Y. Liu, F. E. Williams, K. Kurogi, Y. Sakakibara, M. Suiko, and M.-C. Liu, “Identification, characterization, and ontogenic study of a catechol O-methyltransferase from zebrafish,” *Aquat. Toxicol.*, **102**, 1–2, 18–23 (2011).
 149. G. Scalliet, C. Lionnet, M. Le Behec, L. Dutron, J.-L. Magnard, S. Baudino, V. Bergougnoux, F. Jullien, P. Chambrier, P. Vergne, C. Dumas, J. M. Cock, and P. Hugueney, “Role of petal-specific orcinol O-methyltransferases in the evolution of rose scent,” *Plant Physiol.*, **140**, 1, 18–29 (2006).
 150. D. R. Gang, “Evolution of flavors and scents,” *Annu. Rev. Plant Biol.*, **56**, 301–25 (2005).
 151. D. K. Liscombe, G. V Louie, and J. P. Noel, “Architectures, mechanisms and molecular evolution of natural product methyltransferases,” *Nat. Prod. Rep.*, **29**, 10, 1238–50 (2012).
 152. R. K. Ibrahim, A. Bruneau, and B. Bantignies, “Plant O-methyltransferases : molecular analysis , common signature and classification,” *Plant Mol. Biol.*, **36**, 1–10 (1998).
 153. W. Boerjan, J. Ralph, and M. Baucher, “Lignin biosynthesis,” *Annu. Rev. Plant Biol.*,

- 54**, 519–46 (2003).
154. J. P. Noel, R. A. Dixon, E. Pichersky, C. Zubieta, and J.-L. Ferrer, "Chapter two Structural, functional, and evolutionary basis for methylation of plant small molecules," in *Integrative Phytochemistry: from Ethnobotany to Molecular Ecology*, **Volume 37**, 37–58, Elsevier, 2003.
 155. F. Chen, J. C. D'Auria, D. Tholl, J. R. Ross, J. Gershenzon, J. P. Noel, and E. Pichersky, "An *Arabidopsis thaliana* gene for methylsalicylate biosynthesis, identified by a biochemical genomics approach, has a role in defense," *Plant J.*, **36**, 5, 577–588 (2003).
 156. M. Ibdah, X.-H. Zhang, J. Schmidt, and T. Vogt, "A novel Mg(2+)-dependent O-methyltransferase in the phenylpropanoid metabolism of *Mesembryanthemum crystallinum*," *J. Biol. Chem.*, **278**, 45, 43961–72 (2003).
 157. A. Kamaev, "Bestimmung des Substrat- und Produktspektrums natürlicher und mutierter Alkyltransferasen," Martin-Luther-Universität Halle-Wittenberg, 2011.
 158. C. Fellenberg, C. Milkowski, B. Hause, P. Lange, C. Böttcher, J. Schmidt, T. Vogt, and C. Bo, "Tapetum-specific location of a cation-dependent O-methyltransferase in *Arabidopsis thaliana*," *Plant J.*, **56**, 1, 132–45 (2008).
 159. M. Nagy, L. Krizková, P. Mucaji, Z. Kontseková, F. Sersen, and J. Krajcovic, "Antimutagenic activity and radical scavenging activity of water infusions and phenolics from ligustrum plants leaves," *Molecules*, **14**, 1, 509–18 (2009).
 160. C. R. Wils, W. Brandt, K. Manke, and T. Vogt, "A single amino acid determines position specificity of an *Arabidopsis thaliana* CCoAOMT-like O-methyltransferase," *FEBS Lett.*, **587**, 6, 683–689 (2013).
 161. G. Li and K. D. Young, "Indole production by the tryptophanase TnaA in *Escherichia coli* is determined by the amount of exogenous tryptophan," *Microbiology*, **159**, Pt 2, 402–10 (2013).
 162. J. Park, B. Bühler, T. Habicher, B. Hauer, S. Panke, B. Witholt, and A. Schmid, "The efficiency of recombinant *Escherichia coli* as biocatalyst for stereospecific epoxidation," *Biotechnol. Bioeng.*, **95**, 3, 501–12 (2006).
 163. N. H. Tolia and L. Joshua-Tor, "Strategies for protein coexpression in *Escherichia coli*," *Nat. Methods*, **3**, 1, 55–64 (2006).
 164. S. Y. Lee, *Systems Biology and Biotechnology of Escherichia coli*. Dordrecht: Springer Netherlands, 2009.
 165. M. Green and J. Sambrook, *Molecular cloning: a laboratory manual*, 4th ed. Cold Spring Harbor Laboratory, 2012.
 166. R. Novick, "Plasmid incompatibility," *Microbiol. Rev.*, **51**, 4, 381–95 (1987).
 167. I. Miyahisa, N. Funai, Y. Ohnishi, S. Martens, T. Moriguchi, and S. Horinouchi, "Combinatorial biosynthesis of flavones and flavonols in *Escherichia coli*," *Appl. Microbiol. Biotechnol.*, **71**, 1, 53–8 (2006).
 168. Y. Yan, Z. Li, and M. a G. Koffas, "High-yield anthocyanin biosynthesis in engineered *Escherichia coli*," *Biotechnol. Bioeng.*, **100**, 1, 126–40 (2008).
 169. E. Leonard, K.-H. Lim, P.-N. Saw, and M. a G. Koffas, "Engineering central metabolic pathways for high-level flavonoid production in *Escherichia coli*," *Appl. Environ.*

- Microbiol.*, **73**, 12, 3877–86 (2007).
170. S. H. Sung, “Optimization of Rhamnetin Production in *Escherichia coli*,” *J. Microbiol. Biotechnol.*, **21**, 8, 854–857 (2011).
 171. K. Mädje, K. Schmölzer, B. Nidetzky, and R. Kratzer, “Host cell and expression engineering for development of an *E. coli* ketoreductase catalyst: enhancement of formate dehydrogenase activity for regeneration of NADH,” *Microb. Cell Fact.*, **11**, 1, 7 (2012).
 172. W. Zha, S. B. Rubin-Pitel, Z. Shao, and H. Zhao, “Improving cellular malonyl-CoA level in *Escherichia coli* via metabolic engineering,” *Metab. Eng.*, **11**, 3, 192–8 (2009).
 173. E. Petrusa, E. Braidot, M. Zancani, C. Peresson, A. Bertolini, S. Patui, and A. Vianello, “Plant flavonoids--biosynthesis, transport and involvement in stress responses,” *Int. J. Mol. Sci.*, **14**, 7, 14950–73 (2013).
 174. Y. Takamura and G. Nomura, “Changes in the intracellular concentration of acetyl-CoA and malonyl-CoA in relation to the carbon and energy metabolism of *Escherichia coli* K12,” *J. Gen. Microbiol.*, **134**, 8, 2249–53 (1988).
 175. K. T. Watts, P. C. Lee, and C. Schmidt-Dannert, “Exploring recombinant flavonoid biosynthesis in metabolically engineered *Escherichia coli*,” *Chembiochem*, **5**, 4, 500–507 (2004).
 176. M. A. Grillo and S. Colombatto, “S-adenosylmethionine and its products,” *Amino Acids*, **34**, 2, 187–193 (2008).
 177. M. Sauter, B. Moffatt, M. C. Saechao, R. Hell, and M. Wirtz, “Methionine salvage and S-adenosylmethionine: essential links between sulfur, ethylene and polyamine biosynthesis,” *Biochem. J.*, **451**, 2, 145–154 (2013).
 178. H. K. Chenault, E. S. Simon, and G. M. Whitesides, “Cofactor Regeneration for Enzyme-Catalysed Synthesis,” *Biotechnol. Genet. Eng. Rev.*, **6**, 1, 221–270 (1988).
 179. Y. Huang, X. Gou, H. Hu, Q. Xu, Y. Lu, and J. Cheng, “Enhanced S-adenosyl-l-methionine production in *Saccharomyces cerevisiae* by spaceflight culture, overexpressing methionine adenosyltransferase and optimizing cultivation,” *J. Appl. Microbiol.*, **112**, 4, 683–694 (2012).
 180. C. F. Brayton, “Dimethyl sulfoxide (DMSO): a review,” *Cornell Vet.*, **76**, 1, 61–90 (1986).

Presentations and Proceedings

- 03 / 2015 L. Wessjohann, **A.-K. Bauer**, M. Dippe, J. Ley, T. Geissler, "Biocatalytic synthesis of natural products by O-methyltransferases", Book-Chapter in „Applied Biocatalysis - From Fundamental Signs To Industrial Applications". Weinheim, Germany: Wiley-VCH Verlag GmbH & Co. KGaA, ISBN: 9783527336692; *in print*
- 10 / 2014 L. Wessjohann, **A.-K. Bauer**, J. Ley, T. Geißler, K. Geißler, „Verfahren zur biotechnologischen Herstellung von Flavonoiden", European patent application. EP: 14187583.1 – 1501. application date: October 3rd, 2014
- 11 / 2009 C. R. B. Rhoden, D. G. Rivera, O. Kreye, **A. K. Bauer**, B. Westermann, and L. A. Wessjohann, "Rapid Access to N-Substituted Diketopiperazines by One-Pot Ugi-4CR/Deprotection +Activation/Cyclization (UDAC)," *J. Comb. Chem.*, **11**, 6, 1078–1082 (2009).

Oral Presentations

- 04 / 2013 *Enzymatic transformation of polyphenols with taste modifying properties*
Naturstofftreffen: Chemie, Biologie und Ökologie, Würzburg
- 09 / 2012 *Facile and regioselective methylation of aromatic compounds by O-methyltransferases*
PlantEngine COST Action FA 1006: Plant Natural Products – From Science to Bioproducts, Cluj-Napoca, Romania
- 09 / 2012 *P34 – nachhaltige Entwicklung von biosynthetischen Methoden für die Herstellung von methoxylierten Flavanonen und Flavanen als Aromastoffe*
BMBF Clustertreffen: Biokatalyse2021, Hamburg

Poster Presentation

08 / 2011

Methylation of aromatic compounds by O-methyltransferases

Summer school – Biotransformations 2011, Bad Herrenalb

Curriculum vitae

Personal details

Name	Dipl.-LMChem. Anne-Katrin Bauer
Date of Birth	February 17 th , 1984
Place of Birth	Halle (Saale)
Nationality	German

Education

10 / 2010 – 03 / 2014	Ph.D. candidate Leibniz Institute of Plant Biochemistry, Halle (Saale), Germany Thesis title: <i>Biocatalytic synthesis of taste-modifying flavonoids</i> Supervisor: Professor Ludger A. Wessjohann
08 / 2004 – 04 / 2010	Food chemistry studies at the Martin-Luther-University Halle-Wittenberg, Germany
08 / 2003 – 08 / 2004	Agriculture studies at the Martin-Luther-University Halle-Wittenberg, Germany
06 / 2003	Abitur (A-levels, school leaving examination)

Research Experience

09 / 2015 – present	Research Assistant Leibniz Institute of Plant Biochemistry, Halle (Saale), Germany Project: <i>Biocatalytic synthesis of compounds for the phenylpropanoid pathway</i> Supervisor: Professor Dr. Ludger A. Wessjohann
05 / 2014 – 08 / 2015	Maternity and parental leave
07 / 2010 – 03 / 2014	Research Assistant , Doctoral level Leibniz Institute of Plant Biochemistry, Halle (Saale), Germany

Project: *Biosynthetic investigations for the synthesis of methoxylated flavanones and flavanes*

Supervisor: Professor Dr. Ludger A. Wessjohann

11 / 2009 – 04 / 2010

Research Assistant, Diploma level

Leibniz Institute of Plant Biochemistry, Halle (Saale), Germany

Project: *Synthesis and analysis of taste-modifying flavonoids*

Supervisor: Professor Dr. Ludger A. Wessjohann

11 / 2008 – 11 / 2009

Research Assistant, internship

Leibniz Institute of Plant Biochemistry, Halle (Saale), Germany

Project: *Organic synthesis of compounds for peptoids*

Supervisor: Professor Dr. Ludger A. Wessjohann

Halle (Saale), December 17th, 2015

Anne-Katrin Bauer

Eidesstattliche Erklärung

Hiermit erkläre ich an Eides statt, dass ich die vorliegende Arbeit selbständig und ohne fremde Hilfe verfasst habe. Andere als die von mir angegebene Quellen und Hilfsmittel habe ich nicht benutzt und die den benutzten Werken wörtlich oder inhaltlich entnommenen Stellen habe ich als solche kenntlich gemacht. Des Weiteren wurde diese Arbeit an keiner weiteren wissenschaftlichen Einrichtung zur Erlangung des akademischen Grades eingereicht.

Halle (Saale), den 17.12.2015

Anne-Katrin Bauer